MRI Mensuration of the Canine Head: the Effect of Head Conformation on the Shape and Dimensions of the Facial and Cranial Regions and Their Components

Aseel Kamil Hussein

BVMS, MSc

Submitted in fulfilment of the requirements for the

Degree of Doctor of Philosophy

University of Glasgow

School of Veterinary Medicine

June, 2012

Declaration

I declare that the work recorded here is solely mine, except where otherwise stated.

Aseel

The thesis is approved by the supervisors, Professor Jacques Penderis and Professor Martin Sullivan, at School of Veterinary Medicine, College of Medical Veterinary & Life Sciences.

Jacques Penderis

Martin Sullivan

Summary

The selection for specific physical characteristics by dog breeders has resulted in the expression of undesirable phenotypes, either directly or indirectly related to the physical characteristic selected for. One conformation that was considered desirable is extreme brachycephalia, which is associated with secondary physical changes adversely affecting the airways, eyes and central nervous system.

Using a large population of pet dogs having diagnostic magnetic resonance imaging (MRI) studies, I demonstrated that the most commonly used historical head phenotype indices (Stockard and Evans indices) can be determined on MR images. I furthermore conformed that olfactory bulb angulation can be used as an alternate for classification of dog into brachycephalic, mesaticephalic and dolichocephalic head shapes, with similar results to the historical indices. The advantages of olfactory bulb angulation are that it only requires a single midline MR image and inclusion of the entire nose is not required. Using the historical indices and olfactory bulb angulation I then examined the effect of increasing brachycephalia on the appearance and dimensions of the nasal and cranial cavity. I established that progressive ventral rotation of the olfactory bulb (increasing brachycephalia) resulted in an alteration in the shape and a reduction in cross-sectional area of the nasopharynx. Similarly, increasing brachycephalia resulted in a reduction in the dorsal area of the ethmoturbinates and a corresponding reduction in the midline area of the olfactory bulb, providing a potential explanation for reduced olfactory acuity in brachycephalic dogs. Finally, I examined the effect of head phenotype on the structures of the middle fossa, the 3rd ventricle, quadrigeminal cistern and interthalamic adhesion. Head phenotype had a lesser effect on these structures, while brain disease (in particular ventriculomegaly) has a substantial effect, the recognition of which I described.

These results confirm the potential of olfactory bulb angulation and orientation for objectively determining head phenotype using *in vivo* MRI, in particular determining the degree of brachycephalia. The study also quantified the effect of brachycephalia on the nasal cavity and rostral and middle cranial fossae dimensions. The objective quantification of head phenotype provides a useful tool for selection of breeding animals to normalise extreme brachycephalia. This might reduce the incidence of the adverse effects associated with extreme brachycephalia.

Table of Contents

Dedication

To anyone who has, does or will give some attention to animals, orphans and elderly people.

Aseel

Acknowledgements

After thanking The God “Allah the almighty” for giving me such strength to pass all the difficulties during my PhD, I am extremely grateful to my supervisors: Professors Jacques Penderis and Martin Sullivan for providing me with great discussions, comments on manuscripts and help with developing ideas. In particular for the huge support and patience they gave me to produce this thesis. So I want to tell you that I indeed believe without you, I would not be able to achieve half of this work, so thanks from all of my heart.

I am also very indebted to Professor Tomas F. Fletcher [DVM, PhD, College of Veterinary Medicine, University of Minnesota, USA] for being willing unflaggingly to engage in intellectual dialogue that supported, and gave me confidence in, my opinions in the early stages of the project.

Dr. Tim Parkin [BSc, BVSc, PhD, DipECVPH, FHEA, MRCVS, School of Veterinary Medicine, University of Glasgow, UK] who provided valuable statistical advice throughout the study. I am also appreciative to Professor Gheorghe M. Constantinescu [DVM, PhD, College of Veterinary Medicine, University of Missouri-Columbia] and Professor Jack Boyd, Emeritus Professor of Clinical Anatomy, for clarifying points I needed within my work. My thanks also go to the Diagnostic Imaging Unit staff for their assistance. In addition, I would like to give thanks to Dr. Julia Edgar, Mr. Richard Irvine and Mr. Iain McNaught, and all those whose names are not mentioned here, for their direct or indirect assistance. I extend my deepest gratitude and appreciation to all of the above

Last, but by no means least, I must also give my thanks to my sponsor, the Iraqi Higher Ministry, which funded my studies, which has allowed me to develop my career for the future.

Aseel

List of Chapters

List of Tables

List of Figures

1 GENERAL INTRODUCTION

1.1 An introduction to the clinical significance of head phenotype

The selective breeding of specific populations of the domestic dog (*Canis familiaris*), in some cases for well over a century, has resulted in the creation of specific breeds of dogs. The creation of national kennel clubs and the restriction of the breeding population of an individual breed to a defined population of dogs, combined with the adoption of statutory breed standards, have further isolated these sub-populations of dogs and restricted the genetic variability within these populations. There is also a tendency for new dog breeds to be defined and consequently the number of individual breeds recognised by the American and British Kennel Clubs has increased over the years (Evans, 1993; Kennel Club, 1998).

The growth in popularity of pedigree dogs has resulted in larger populations within certain individual dog breeds, but because the breeding populations were originally restricted to a small, defined founding population this has not necessarily increased the genetic diversity within these individual breeds. Of particular concern is the over-emphasis on selection for certain physical phenotypes, where these specific conformational characteristics are perceived as desirable by the breeders. While some of these conformational characteristics are associated with health benefits within a breed (Collins et al 2011), frequently this extreme selection impacts negatively on the health and welfare of subsequent generations. This negative impact may either occur directly in relation to extreme over-expression of a particular phenotype, or indirectly through the over-expression of an unrelated but co-selected phenotype. One such situation where selective breeding has resulted in adverse health effects is the extreme brachycephalic head conformation in certain breeds including the English bulldog, Boston terrier, Pekingese and Pug (Harvey, 2008).

Dogs have historically been classified into dolichocephalic, mesaticephalic and brachycephalic breeds according to head conformation using a variety of cephalic indices, with those of Stockard and Evans being the most widely accepted (Evans, 1993). In some cases the exact demarcation between dolichocephalic, mesaticephalic and brachycephalic head conformations is poorly defined. Within the brachycephalic breeds there is marked shortening of the rostral skull, particularly affecting the facial bones, nasal cavity and frontal sinuses, they display prognathism and the orbits are wide-set and rounded. In conjunction with this, there is dorsal rotation of the rostral aspect of the maxilla (with a canine tooth that is dorsally rotated and approaches a more horizontal position), an altered position of the nasal turbinates, reduction in size of the frontal

sinuses (with complete obliteration of one or more compartments of the frontal sinuses in more extreme brachycephalia) and changes in the angle of the nasolacrimal drainage pathway. The dorsal rotation of the rostral maxilla results in a reduced craniofacial angle. The brachycephalic head characteristics have been attributed to the early fusion of the skull-base in brachycephalic breeds, resulting in shortening of the base of the cranial cavity (Evans, 1993).

A variety of conditions affecting facial morphology, the upper airways, eyes and central nervous system (CNS) are frequently diagnosed in brachycephalic breeds, which in many cases can directly be attributed to the brachycephalic head phenotype. One of these represents a substantive health problem in affected dogs is brachycephalic obstructive airway syndrome (BOAS), where a combination of abnormalities results in obstruction of the upper airways (and which may also extend to affect the lower airways). BOAS tends to occur in brachycephalic breeds with a more marked brachycephalic head phenotype, including the Pug, Pekinese, Shih-tzu, Lhasa apso and Bulldog (1969; Hendricks, 1992). There are a variety of other anatomical variations that may result in obstruction of the upper airways and these are not always directly related to BOAS. Protrusion of the nasoturbinates into the pharynx and stenosis of the nasopharynx are frequently demonstrated in a variety of dog breeds, but brachycephalic breeds have a particularly high incidence (Billen et al. 2006). Other clinical abnormalities, including otitis media, apnoea, hypopnoea, oxygen desaturation, snoring and obstruction sleep apnoea syndrome (OSAS), may also be associated with narrowing of the bony nasopharynx and oropharynx, and thickening of the soft palate. These have been demonstrated in man and animals (Laurikainen et al. 1987; Maw et al. 1991; Ono et al. 1996; Yu et al. 2003; Renko et al. 2007). Choanal atresia (Khoo et al. 2007) and stenosis of the nasopharynx (Mitten, 1988) have also been reported in the cat.

Other diseases also occur more frequently in brachycephalic dog breeds where the correlation between head conformation and the disease predisposition is not immediately apparent. One of these is the increased risk for the development of gliomas in brachycephalic dog breeds (Hayes and Schiefer). In contrast, a higher incidence of nasal disease, including neoplasia, has been reported in mesaticephalic and dolichocephalic breeds (Morgan et al. 1972; Moore et al. 1991).

Congenital hydrocephalus, where there is an abnormal increase in the size of the brain ventricular system in association with raised intracranial pressure, is reported to occur more frequently in small brachycephalic breeds including the Chihuahua, Maltese and Cavalier King Charles Spaniel (CKCS) (Braund, 2003; Bagley, 2005). These breeds are

also more prone to other skull anomalies, such as occipital dysplasia (Watson et al. 1989). Quadrigeminal cistern cysts are furthermore over-represented in brachycephalic breeds, which may be associated with hydrocephalus if there is obstruction of the cerebrospinal fluid (CSF) drainage pathways (Saito et al. 2001). Excessive skin fold, in particular over the head, are reported in breeds with a brachycephalic head phenotype, including the Shar pei, English bulldog and Pug (Asher et al. 2009), and a large head to pelvis ratio in certain brachycephalic breeds leads to an increased risk of dystocia (Johnson, 1986).

1.2 Gross features of the skull

Both the size and shape of the head of dogs vary from one breed to another. The main determinant of head conformation is the shape of the skull, which is also the part of the skeleton that is made up of the largest number of compound bone elements (representing the fusion of bones of more than one embryological origin) (Evans, 1993). The skull is comprised of three main bony structures: the facial, palatal and neural (braincase) portions (Evans, 1993). The facial portion has greater variability compared to the palatal or neural portions. However, both palatal and neural portions still vary between breeds (Stockard, 1941). The facial and palatal portions allow the provision of a large surface area for the upper respiratory tract and for olfactory function. The facial and palatal portions are composed of 21 bones that fuse during development to form a narrower rostral end and a wider caudal end (largely comprising the maxilla) and merge with the third region - the braincase (Evans, 1993). The braincase forms the cranial cavity that is separated from the facial cavity by a perforated bony structure known as the cribriform plate. The caudal border of the braincase is composed of the external occipital protuberance dorso-caudally and foramen magnum caudally. The 21 paired and 8 unpaired bones of the skull are listed in Table 1-1. The skull has three main cavities: the nasal cavity forming the facial respiratory tract, the cranial cavity where the brain with both its coverings and vessels are housed and the sinuses (Evans, 1993).

Skull Regions	Paired bones	Unpaired bones
Braincase	Exoccipital, parietal, frontal and temporal	Supraoccipital, interparietal, basioccipital, basisphenoid, presphenoid and ethmoid
Face and palate	Premaxilla, nasal, maxilla, dorsal concha, ventral concha, zygomatic, palatine, lacrimal, pterygoid and mandible	Vomer
Hyoid apparatus & middle ear	Stylohyoid, epiphyoid, ceratohyoid, thyrohyoid, malleus, incus and stapes	Basihyoid

Table 1-1: Bones of the skull (modified from Evans, 1993)

1.2.1 Facial region

In mammals generally the main area of the facial region is the nasal cavity and is composed of two symmetrical fossae, separated by a midline septum. Rostrally the nasal fossae contain the maxilloturbinates and caudally the ethmoturbinates (Evans, 1993). The nasal septum is comprised of cartilage rostrally, while four bones make up the caudal portion, namely: the septal processes of the nasal and frontal bones, the perpendicular plate of the ethmoidal bone and the sagittal part of the vomer (Evans, 1993). The ethmoidal bone has been described as a series of osseous scrolls (ethmoturbinates), which connect to the cribriform plate caudally and to other bony plates (the external lamina) dorsally and laterally (Adams, 2004). The cribriform plate is the origin of the ethmoturbinates, which terminate rostrally in an expanded body with a slender neck (Negus, 1958). Other researchers have described the osseous scrolls that occupy the nasal fundus as the ethmoidal labyrinth, consisting of four medially situated endoturbinates and six smaller laterally situated ectoturbinates (Evans, 1993). In contrast, Negus defined these turbinates as five large turbinals in the medial aspect of the nasal cavity of domestic dogs, some extending to the frontal and sphenoidal recesses (Negus, 1958).

Embryologically, at the time that conchal differentiation occurs via invagination of the nasal mucous membrane, the spongy bone of the ethmoidal cells (previously formed by ossification of lateral masses) is resorbed, forming the conchae. The conchae then grow laterally to form the ethmoidal labyrinths, including the endoturbinates, ectoturbinates and ethmoidal cells (Anderson et al. 1994). Both endoturbinates and ectoturbinates attach to the external lamina of the ethmoid bone (Evans, 1993; Anderson et al. 1994; Adams, 2004). The external lamina is a thin, papyraceous bone layer that coats the ethmoturbinates. The caudo-ventral part fills the sphenoid sinus, while the caudo-dorsal

part occupies a portion of the frontal sinus (Evans, 1993). In cats, the ethmoidal turbinals are rounded and covered by mucous membrane (Negus, 1958). The shape and the size of these turbinals have been reported to vary substantially in the wallaby and cat but not in Echidna. In primates, like the Macacus, the ethmoidal turbinals are comprised of a single row, compared to the multiple rows of ethmoidal turbinals found in keen-scented animals, such as dogs (Negus, 1958).

The cribriform plate of the ethmoidal bone forms the rostral wall of the cranial cavity (Evans, 1993; Smith, 1999; Constantinescu, 2002; Adams, 2004; Evans and De Lahunta, 2004), separating the caudal part of the nasal cavity from the olfactory bulb of the brain (Evans, 1993; Adams, 2004). In keen-scented animals such as the *Carnivora*, the cribriform plate is large with a high number of perforations, unlike the smaller plate found in weaker smelling species including the lemurs, old and new world monkeys and man (Negus, 1958). The individual branches of the olfactory nerves pass through the cribriform plate foraminae to the olfactory bulb where synapses arise, thence through the olfactory tract to the rest of the mammalian cerebrum (Negus, 1958).

The external lamina (*papyraceous lamina*) lines the inner surfaces of the heavier bones of the nasal fundus, which forms the caudal part of the nasal cavity. The external lamina is divided into three different parts: dorsal (roof or *lamina tectoria*), lateral (side or *lamina orbitalis*) and ventral (floor or *lamina basalis*) (Evans, 1993). At the level of the nasal and frontal bone components of the septum, the external lamina extends dorsally then sweeps laterally over the top of the ethmoidal labyrinth forming the lamina roof and down each side laterally forming its side (Evans, 1993). The basilar lamina of the ethmoidal bone forms the dorsal part of the ventral meatus (Assheuer and Sager, 1997). A sub-ethmoidal shelf, or *lamina transversa*, is made up of the basal plate linking the ethmo-turbinals with the lateral wings of the vomer bone and the processes of the sphenoid, and is found ventral to the ethmoidal turbinals and protects them from direct air currents (Negus, 1958). This lamina is particularly well developed in some carnivore species, including the foxes and African wild dog (also known as the Cape hunting dog or painted dog) (Negus, 1958). The external lamina completely separates the ethmoidal area from the maxillary (respiratory) area (Cook, 1964).

The nasal cavity mucosa is pigmented and in keen-scented species such as the dog, cat and rabbit, it is black or brown. In contrast, the nasal cavity mucosa is yellow in the calf, sheep and man, suggesting that pigmentation of the nasal cavity mucosa plays a role in olfactory perception (Negus, 1958). The olfactory epithelium and sensory nerves develop from the olfactory placode (Evans, 1993). The olfactory epithelium is generally

composed of receptor, supporting and basal cells (Allison, 1953). Specific cells covering the maxilloturbinates are called non-olfactory epithelia, whilst olfactory epithelia cover the ethmoturbinals (Adams, 1972). A correlation has been shown to exist between the area of olfactory epithelium, the number of the olfactory receptors, and thus the acuity of the perception of smell (Negus, 1958). The olfactory receptors are primarily located on the ethmoturbinates situated in the caudal part of the nasal cavity. However the shift from peripheral respiratory epithelium to olfactory epithelium is gradual (Evans, 1993). Smith and Rossie (2008) found that the posterior area of the nasal fossa in lemurs is covered with olfactory mucosa, with the exception of the maxilloturbinal area (Smith and Rossie, 2008). In man, olfactory epithelial cells are identified in a minor olfactory area located in the roof of the nose, comprising part of the superior turbinal and part of the nasal septum (Negus, 1958). When an anatomical and histological study of the more complex turbinals was performed in the Mexican fruit-bat (*Artibeus*), a larger area of olfactory epithelium was found (Bhatnagar and Kallen, 1974a). Each mitral cell (a transmitting or hub cell) is related to a large number of nerve fibres and the plexiform arrangement (Le Gros Clark, 1956), allows some or all glomeruli to receive impulses from different areas of the olfactory epithelium, not necessarily in direct topographical relation to each other, but in some way associated with olfactory discrimination [cited by (Negus, 1958)]. Extension of the ethmoturbinals with olfactory mucosa into surrounding bones has been identified in many animals, chiefly those of a carnivorous habit. This is particularly evident in members of the cat and dog families, in which there is caudal excavation of the sphenoid and frontal bones and their recesses (Negus, 1958). He concluded that a larger area of olfactory epithelium was directly related to a higher acuity of olfaction, and not to the development of refined discrimination of olfaction (Negus, 1958).

1.2.2 Palatal region

The second region of the skull is the palatal, which with the facial region, forms the rostral part of the pharynx called the osseous nasal pharynx illustrated in Figure 1-1 (Evans, 1993). It was defined in the cat by Jayne (1898) (cited by Evans, 1993) as a basipharyngeal canal, and as a choanal region by Evans (Evans, 1993). The sides of the nasal cavity end in right and left caudal choanae (Evans and De Lahunta, 1996; Smith, 1999; Wible, 2008). Each choana was described as having an oblique oval shape (Cinnamond, 1987), through which the two nasopharyngeal meatii continue as the nasopharynx (Evans, 1993). The choanae are located at the caudal end of the hard palate

at the symphysis of the latter with the vomer bone (Evans and De Lahunta, 1996; Smith, 1999; Wible, 2008). The vomer forms the roof and the inner surface of the perpendicular lamina of the palatine bone, giving rise to the elliptical shape of the choanae (Evans, 1993). Rostrally, both the nasal crest of the palatine bone (ventrally) and the sphenoidal crest (dorsally) produce paired orifices, but caudally these are only indentations detracting from a true oval shape to the choanae (Giannini et al. 2006). One of the common congenital anomalies of the human nose is posterior choanal atresia, which is generally bony (90%) but can be membranous (10%) (Cinnamond, 1987). According to Cinnamond, the typical site of choanal atresia was just in front of the posterior end of the nasal septum, and the obstruction was usually a thin layer easily destroyed (Cinnamond, 1987). The definition of the choanal region in dogs was described by Smith as the area extending from the choanae rostrally to the end of the pterygoid bones caudally (Smith, 1999). The width of the choanal region according to Evans was about half its length, while the depth was nearly equal to the width (Evans, 1993).

The nasal pharynx is defined as the last part of the nasal cavity, and as the respiratory portion of the pharynx (Hedlund and Taboada, 2002). It is a cavity lying dorsal to the soft palate and extends rostrally from the nasal choanae to the palatopharygeal arches caudally (Evans and De Lahunta, 1996; Hedlund and Taboada, 2002), and is surprisingly hard to recognise in the embalmed dog (Evans, 1993; Smith, 1999). Evans referred to the nasopharynx as starting at the caudal aspect of the hard palate, but not the caudal nasal spine (Evans, 1993). Billen et al (2006) stated that the nasopharynx was situated caudal to the choanae of the nasal cavity . In man, the nasopharynx was defined as a trapezoid formed by four landmarks that represent the skeletal limits of this region (Handelman and Osborne, 1976), while Bergland (1963) used a triangle based on three anatomic points, pterygomaxillare, hormion and basion to describe the bony nasopharynx.

The middle and the caudal portions of the nasopharynx were described as the deeper part of the nasopharynx that started just caudal to the hard palate and extended until the palatopharyngeal arch (caudal pillar of the soft palate) caudally, while the skull-base with its muscles formed the dorsal edge and the soft palate formed the ventral edge (Evans, 1993). Although dogs have a relatively long soft palate, brachycephalic breeds have the longest soft palate among dogs. Elongation of the soft palate may interfere with the passage of air into the larynx (Evans, 1993). In children with unilateral cleft lip and palatal anomalies, the bony nasopharynx was found to be smaller than in normal children (Satoh et al. 1998).

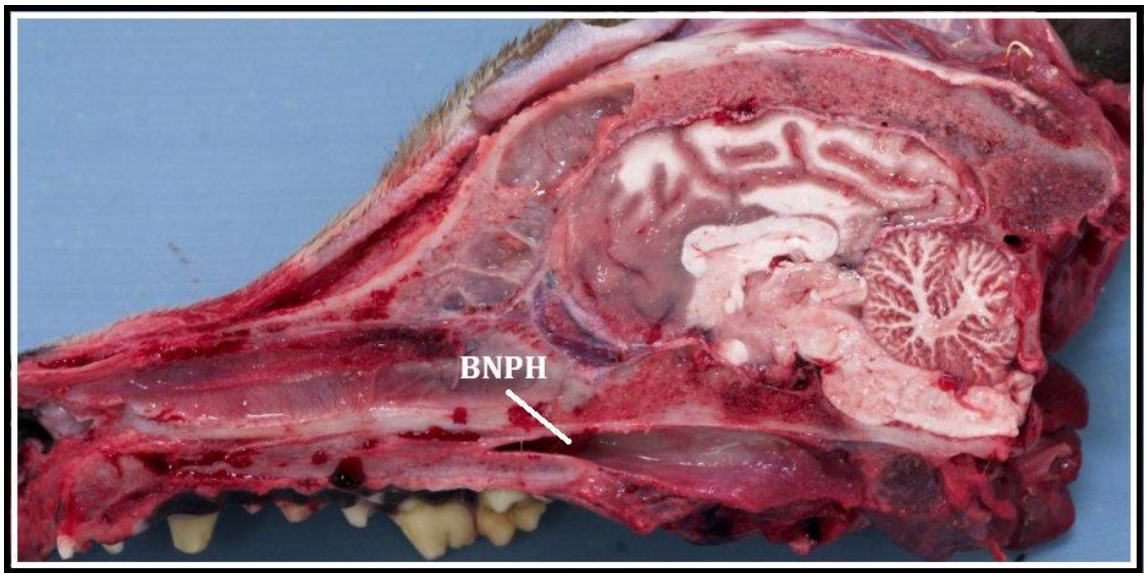

Figure 1-1: Gross fresh midline canine specimen highlighting the bony nasopharynx (BNPH)

1.2.3 Neural region and the related brain components

The third region of the skull is the neural part (braincase) that includes the cranial cavity. The cranial cavity varies in its capacity, more according to body size than skull shape, with a range of between 40 and 140ml. The braincase forms the housing for the brain and associated structures, including the blood vessels, meninges and CSF (Miller and Christensen, 1964; Evans, 1993). The bones forming the braincase are listed (Table 1-1). The base of the cranial cavity can be subdivided into three parts: rostral, middle and caudal fossae, as illustrated in Figure 1-2 (Evans, 1993; Anderson et al. 1994; Smith, 1999; Budras et al. 2002; Constantinescu, 2002; Evans and De Lahunta, 2004). In 1993, Evans stated *"The cranial fossae form the floor of the cranial cavity. The remaining portion of the cranium is marked internally by smooth depressions and elevations that are formed by the gyri and sulci of the brain"*.

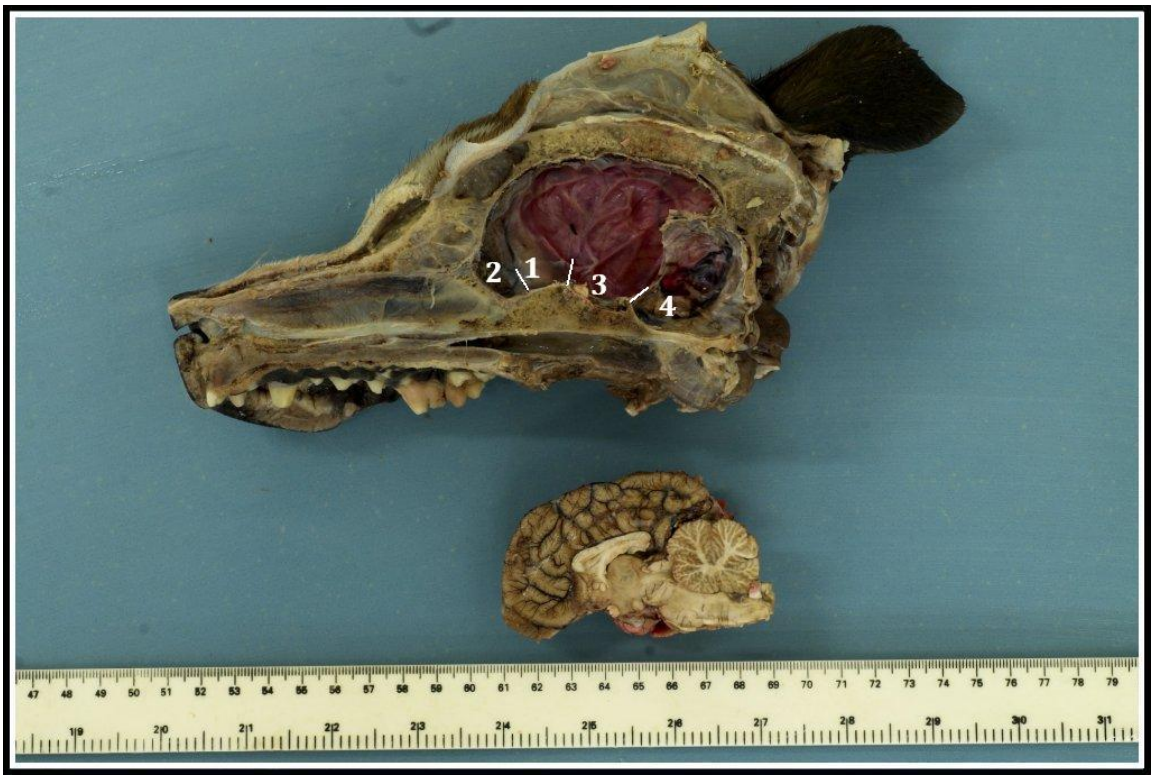

Figure 1-2: Gross appearance of the midline section of the head of a dog (with the brain removed) showing the outline of the cranial fossae along the ventral surface of the floor of the cranial cavity: rostral (1) including the ethmoidal (2), middle (3) and caudal (4)

Generally, the rostral part of the cranial fossa is defined as the area of the cranial cavity that extends from the cribriform plate to the level of the optic canal (Anderson et al. 1994; Smith, 1999; Budras et al. 2002). The rostral cranial fossa extends rostrally to include the ethmoidal fossa and caudally is bounded by the middle cranial fossa (Evans, 1993). The rostral cranial fossa is a much narrower than the middle and caudal parts of the cranial fossa (Anderson et al. 1994; Smith, 1999; Budras et al. 2002). Evans (1993) referred to the ethmoidal fossa as a deep rostral continuity of the rostral parts of the cranial fossa. The rostral fossa supports the olfactory bulb, tract and other parts of the frontal lobes (Evans, 1993; Anderson et al. 1994; Smith, 1999). In 1883, Langley defined the frontal lobe as *"the lobe which includes the sub-orbital lobe and the part of the anterior limb of the sigmoidal gyrus which lies medially of a line drawn in a sagittal direction from the anterior end of the crucial fissure to the supra-orbital fissure"* . Furthermore, Ferrier (1888), (cited by Bianchi 1985), referred to the area rostral to the sigmoid gyrus as the frontal lobes in dogs and cats. On MRI, the frontal cortex was defined as extending from the anterior pole of the olfactory bulb to the anterior cruciate sulcus (Tapp et al. 2004) (Figure 1-3).

The olfactory bulb is described in dogs as the first component of the basal portion of the

rhinencephalon, and as the rostral extension of the olfactory peduncle, where the olfactory nerves terminate. Additionally, the olfactory bulb may be considered to be the most rostral portion of the olfactory region, composed of an accumulation of olfactory nerve fibres adjacent to the inner surface of the cribriform plate (Figure 1-3) (Beitz and Fletcher, 1993). In man, Warwick and Williams (1973) in Gray's Anatomy defined the olfactory bulb as "*a compressed, oval mass which is located upper to the medial margin of the orbital plate of frontal bone near the lateral margin of the cribriform plate".*

Grooves, which separate one or more parts of the olfactory lobe from the rest of the brain, have been reported since the nineteen century. Gervais (1870) described the rhinal fissure as the groove that lies above the olfactory lobe and separates it from the uncinate region [cited by (Langley, 1883)]. Similarly, Krueg, in 1880, defined the anterior extension of the rhinal fissure as the olfactory fissure, which separates the olfactory tract from the brain cortex [cited by (Langley, 1883)]. In 1873, Wilder called this olfactory fissure the ecto-rhinal fissure [cited by (Wilder, 1880)]. Furthermore, following studies based on dissection of cat brains to identify the structures of the brain, the term olfactory fissure was given to the fissure where the olfactory lobe was lodged [cited by (Wilder, 1880)]. De Lahunta (1983) and De Lahunta and Glass (2009) reported that the olfactory nerves (cranial nerve I) penetrated the cribriform plate to reach the olfactory bulb.

The point where the caudal end of the rostral fossa tips ventrally is referred to as the optical canal landmark (Smith, 1999; Budras et al. 2002). The middle fossa of the cranial fossa follows from the rostral fossa and terminates at the dorsum sellae, where the caudal fossa starts. It includes the area of the sella turcica (Budras et al. 2002), with the sella turcica classified as a complex of structures that surrounded the hypophysis by Evans (1993). A different interpretation is that most of the cerebrum occupies the middle fossa, and extends from the optical canal rostrally to the hypophyseal region, which contains the hypophyseal fossa and sella turcica caudally (Smith, 1999). The temporal lobes of the brain mainly pack the lateral parts of the middle fossa (Evans, 1993) (Figure 1-3).

The third part of the cranial fossa is the caudal fossa, which is delineated by the dorsum sellae rostrally and foramen magnum caudally (Evans, 1993; Smith, 1999). The cerebellum, pons and medulla oblongata are all housed within this fossa (Smith, 1999). Budras (2002) referred to the rostral part of the caudal fossa as the area in which the pons is situated, and the caudal portion of caudal fossa as the area in which the medulla oblongata is situated, without reference to the cerebellum. In 1993, Evans assigned the cerebellar fossa to the caudal fossa as in Figure 1-3.

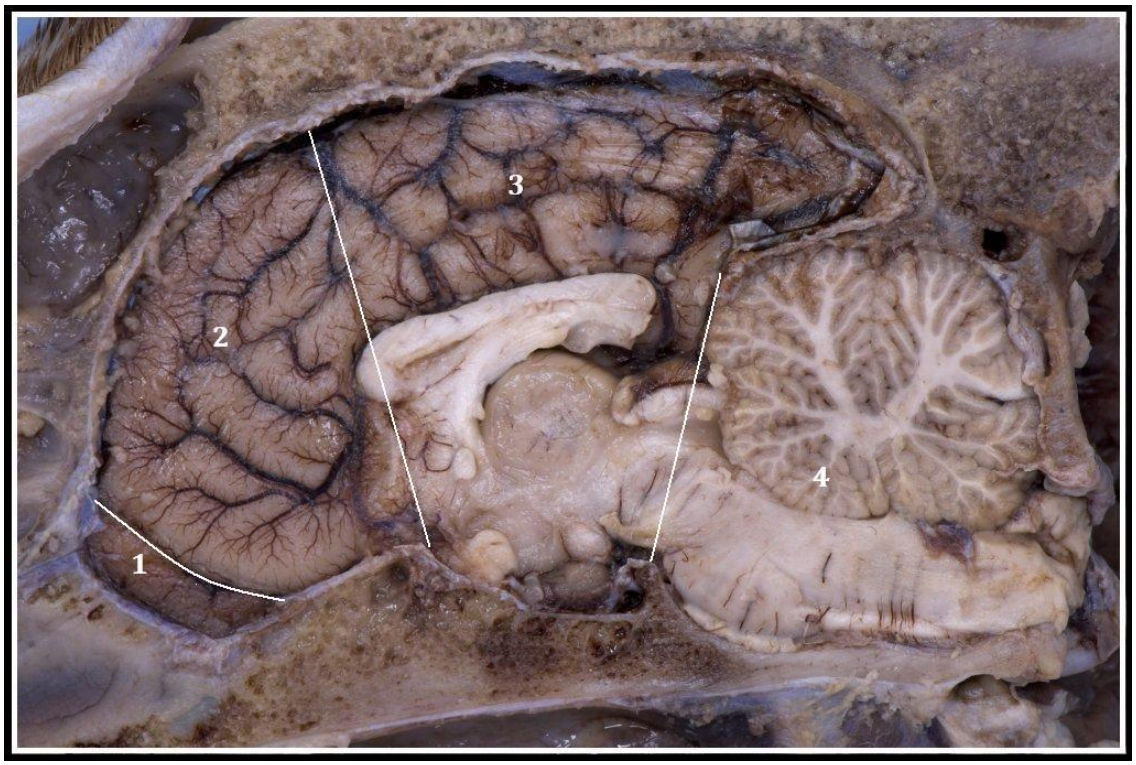

Figure 1-3: Gross midline formalin-fixed specimen. The landmarks of the ethmoidal fossa (1), rostral fossa which includes the ethmoidal fossa (2), middle fossa (3) and caudal fossa

1.3 The ventricular system of the brain

There has been tremendous variation in the anatomical description of ventricular system in the dog. However, the most widely accepted consensus is the division of this system into four ventricles and five foramina (Fitzgerald, 1961; De Lahunta, 1983; Fletcher, 1993). These include: i) two lateral ventricles (left and right) that also represent the largest part of the ventricular system; ii) a pair of interventricular foramina (in man termed the foramina of Monro) through which cerebrospinal fluid (CSF) drains from each lateral ventricle to the 3rd ventricle; iii) the 3rd ventricle is a narrow cleft within the diencephalon, somewhat oval in shape in the lateral view; iv) the 4th ventricle, which is also the last part of the ventricular system and receives the CSF from the 3rd ventricle through the mesencephalic aqueduct (in man termed the aqueduct of Sylvius). In man, CSF drains from the 4th ventricle to the subarachnoid space through three apertures: two lateral apertures (in man termed the foramina of Luschka) and one medial aperture (in man termed the foramen of Magendie) (Barr, 1948; De Lahunta, 1983). Fitzgerald (1961) described the apparent presence of a medial aperture (foramen of Magendie) in dogs, but not in other domestic animals. This has subsequently been refuted by later studies, with no evidence of a medial aperture in dogs, nor in a number of other domestic animals (including cats, goats and rabbits) (Coben, 1967; Martin-Garcia et al. 1995).

These studies demonstrated that drainage of CSF from the 4th ventricle to the subarachnoid space is only through paired lateral foramina in the roof of the lateral recesses of the 4th ventricle.

As the largest part of the brain ventricular system, the lateral ventricles are further subdivided into a number of compartments; however these divisions vary from study to study. Enlargement or asymmetry of the lateral ventricles may also be evident, but is suggested to occur in dogs with increasing age (De Haan et al. 1994; Kii et al. 1997; Vullo et al. 1997; Esteve-Ratsch et al. 2001; González-Soriano et al. 2001). On the other hand, a proposed explanation for the presence of ventricular asymmetry in beagle-type dogs was the prior occurrence of some form of intraventricular haemorrhage in newborn puppies (Hudson et al. 1989). Moulds of the ventricular system of dogs revealed a narrowing (or coarctation) of the lateral ventricles, with most of these lateral ventricle coarctations located at the same place within the temporal horn of the lateral ventricle (González-Soriano et al. 2001). Similar findings have been reported in sheep, with coarctation at the level of the rostral and temporal horns of the lateral ventricles (Rajtová, 2001). The CSF drains from both lateral ventricles to the 3rd ventricle through the interventricular foramina, which are situated at approximately the same position in man and the dog. The interventricular foramina are bordered by the fornix and septum rostrally and dorsally and are much wider and more elongated in dogs than in man (Horodyska and Kreiner, 1962).

The 3rd ventricle, located within the middle fossa, is defined as a narrow chamber that surrounds the interthalamic adhesion, which therefore occupies the centre of the 3rd ventricle (Beitz and Fletcher, 1993). The 3rd ventricle has a roof where the choroid plexus is situated, and a floor which is defined by the optic chiasm rostrally and the pituitary gland caudally (Fitzgerald, 1961; Horodyska and Kreiner, 1962). The rostral border of the 3rd ventricle mainly consists of the lamina terminalis, while the mass of the mesencephalon constitutes its caudal border (Fitzgerald, 1961; Horodyska and Kreiner, 1962; Beitz and Fletcher, 1993). The 3rd ventricle has several recesses; however three recesses are well recognised by anatomists: the optic, infundibular and suprapineal (Beitz and Fletcher, 1993; Anderson et al. 1994; De Lahunta and Glass, 2009). The pineal gland is an unpaired, cream-coloured, wedge-shaped, small excrescence that is called the *epiphysis cerebri* and forms part of the caudal boundary point of the roof of the 3rd ventricle. It extends into the potential space between the cerebellum caudally and the approximation of the two cerebral hemispheres dorsally and laterally (Beitz and Fletcher, 1993).

The 4th ventricle is a cavity of the hind-brain (Horodyska and Kreiner, 1962) that communicates with the central canal and with the lateral recesses, receiving the CSF from the 3rd ventricle via the mesencephalon aqueduct (aqueduct of Sylvius) (Fitzgerald, 1961; Horodyska and Kreiner, 1962). The choroid plexus (*tela choroida*) is found in the floor of the lateral ventricles, roof of the interventricular foramina, 3rd ventricle, mesencephalic aqueduct and the 4th ventricle.

The onset of expansion of the ventricular system was shown to occur at around 3 to 4 weeks in the postnatal period in Beagle-type dogs (Kii et al. 1998). In this study the day that CSF was first visible, unilaterally or bilaterally at the interventricular foramen of the lateral ventricle, was considered to be the point of onset of ventricular expansion. Size and asymmetry of the lateral ventricles are not related to this point of onset. The brain and lateral ventricle volume increases up until 150 and 210 days of age respectively, with the maximal rate of increase in volume evident between 45 and 75 days. The most sensitive area to change in ventricular symmetry and size has been stated to be at the level of the interventricular foramina (Kii et al. 1997).

On the basis of published sizes of the ventricular system (González-Soriano et al. 2001), the length of the different parts of the ventricular system increased when adult dogs (age range 2-5 years) were compared to aged dogs (10 to 12 years) in a population of GSD dogs. The length increased by 3.73% and 3.24% for the left and right lateral ventricles respectively, 0.34% (for 3rd ventricle), 1.23% (for the mesencephalic aqueduct) and 0.99% (for 4th ventricle) in aged dogs. In light of these findings, a normal increase in lateral ventricle, mesencephalic aqueduct and 4th ventricle length occurs with age. Analysis of these values may therefore be less useful for identifying changes in the ventricular system, especially since the 3rd ventricle only demonstrated a weak effect of age on the length (González-Soriano et al. 2001).

In addition to the ventricular system, there are also accumulations of CSF in the cisterns. The brain is surrounded by a set of membranes called the meninges, which are comprised of the dura mater, arachnoid mater and pia mater (Fletcher, 1993). The dura mater is the outer thick fibrous layer that is normally attached to bone. The other two meningeal layers are more delicate [called the leptomeninges] (Fletcher, 1993). The arachnoid membrane is deep to the dura and attaches to the pia mater through trabeculae that traverse a subarachnoid space filled with CSF. In certain areas it widens to form cisterns. The most obvious cisterns in dogs and cat are the cerebellomedullary, intercrural and quadrigeminal cisterns. The third membrane, the pia mater, normally adheres to the surface of the brain (Fletcher, 1993).

1.4 Methods of diagnostic imaging of the canine head

Radiography and computed tomography (CT) are considered the most useful methods for identifying the anatomical features and defining lesions of bony structures *in vivo* (Figure 1-4). As a consequence of significant attenuation of x-ray photons, magentic resonance maging (MRI) is superior to these imaging modalities for imaging soft tissues, particularly when they lie deep to bone (Figure 1-5) (Assheuer and Sager, 1997). Although defining the radiographic features of the skull is complicated due to superimposition, it is considered the simplest and most common technique for examining the skull and the nasal cavity (Farrow, 2003; Lavin, 2003). This hindrance is overcome by CT. Although the whole head can be visualised by MRI, the soft tissues generate the best detail (Gavin and Bagley, 2009). Cortical bone tends to produce a signal void due to the lack of hydrogen on both T1- and T2-weighted squences, while cancellous bone appears bright due to the presence of bone marrow, which is largely fat (Gavin and Bagley, 2009). MRI is used in dogs for investigating the nasal cavity (Assheuer and Sager, 1997; Rycke et al. 2003; Craven et al. 2007). MR images of the cribriform plate and the olfactory bulb have been shown to be of a good quality (Dhaliwal et al. 2004).

Figure 1-4: Lateral radiographs (A-C) and midline sagittal plane computer tomographic images (D-F) of macerated skulls demonstrating the normal appearance of the cranial fossa and cribriform plate (arrows) in different head shapes

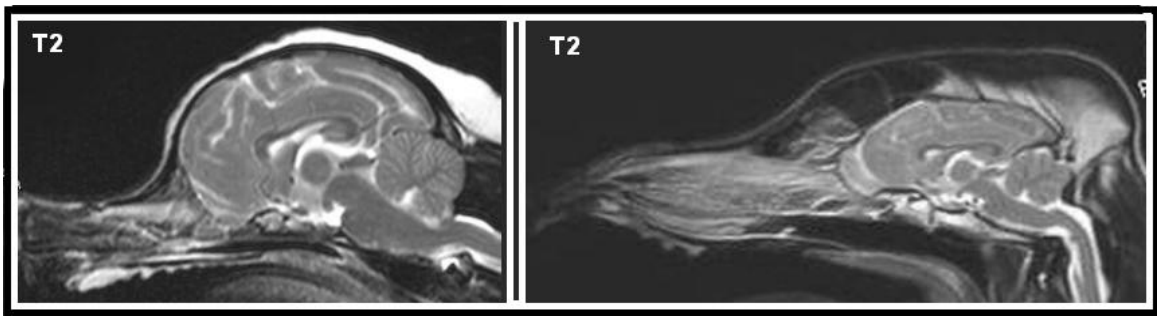

Figure 1-5: The shape of the head on midline sagittal plane T2 weighted MR images, including bony and soft structures

Radiography, ultrasonography, CT and MRI can be used to evaluate the normal and abnormal canine brain (Farrow, 2003). Plain radiography will not image the brain, and lesions are only identifiable when they have a secondary impact on overlying bone such as has been recorded in severe hydrocephalus (Farrow, 2003; Kealy and McAllister, 2005). However, more subtle abnormalities can be identified following contrast studies, such as cerebral angiography, cranial sinus venography and ventriculography (Kealy and McAllister, 2005). Open fontanelles allow ultrasound waves from high-frequency transducers to penetrate the cranial cavity to allow assessment of some brain abnormalities, such as hydrocephalus (Kealy and McAllister, 2005).

CT was the first imaging modality to allow detailed imaging of the brain (Farrow, 2003). CT atlases of the dog head (George and Smallwood, 1992), and brain (Kaufman et al. 1981) have been published. In 1981, Fike et al gave clear information about the brain and its structures using high resolution CT. To evaluate the brain on CT scans, bony landmarks are used including the tentorium osseum, petrosal portion of the temporal bone and tympanic bullae; these are used to identify adjacent brain structures including the cerebellum, medulla oblongata and midbrain (Fike et al. 1981). Quantitative CT scans using iodinated contrast medium have been described to differentiate neoplastic and non-neoplastic lesions in canine brain (Fike et al. 1986). Despite the fact that CT can be used to investigate the brain, it is unable to provide the level of detail that can be obtained from MRI (Kraft et al. 1989; Leigh et al. 2008; Fletcher, 2011).

In 1980, Holland et al published the first report describing human central nervous system lesions identified using MRI (Holland et al. 1980). The first veterinary publication of brain MRI was in 1989 by Kraft et al. Transverse, sagittal and dorsal plane images are used to determine the anatomical features of different parts of the brain and concentrations of CSF (Kraft et al. 1989; Assheuer and Sager, 1997; Leigh et al. 2008). The technique of MRI can be summarised as follows: after positioning the subject in a strong stable magnetic field, radio waves are pulsed into the tissue leading to excitation

of the hydrogen protons in a predictable manner. During the intervals, relaxation occurs and the protons emit radiowaves that are detected by a receiver coil, which are then analysed. Finally, an image is created by Fourier transformation. Two exponential time constants can be produced when the relaxation occurs: a longitudinal relaxation (T1) and a dephasing time (T2). Signal strength will be determined by the relaxation rates of the specific tissues and proton density (Kraft et al. 1989). MRI gives good contrast and spatial resolution for brain tissue and CSF on dorsal, sagittal and transverse planes (Leigh et al. 2008; Fletcher, 2011). The different signal intensities associated with white and grey matter, fat, air, oedema and CSF will allow the normal CNS anatomy to be visualised and abnormalities identified (Kraft et al. 1989). Normally the meninges of the brain, are not detectable on standard T1- and T2-weighted MR images (Gavin and Bagley, 2009). However, the *tela choroida* of the lateral, 3rd and 4th ventricles, and which is considered part of the meninges, is visible on MRI (Fletcher, 2011).

On T1-weighted images, the normal CSF has a hypointense signal, while it is hyperintense on T2-weighted images compared to the surrounding tissue (Gavin and Bagley, 2009). The structure of the surrounding tissues may affect the shape of the ventricular system. For example, the size and shape of the 3rd ventricle alters as a consequence of thalamic neural atrophy or vascular changes (González-Soriano et al. 2001) and the identification of brain atrophy due to senility or dementia can be recognised by measuring the thickness of the interthalamic adhesion (Hasegawa et al. 2005).

1.5 Terminological inexactitude

Anatomical terms are sometimes not coherent. More than one term is often given to a structure, or more than one structure has the same name. For example, in 1883, an *intra*-olfactory fissure was described as a groove that is shallow or missing at the posterior portion of the olfactory lobe (Langley, 1883), yet he used the term *inter*-olfactory fissure in an accompanying diagram to describe the same feature. In 1994, Anderson et al. named the olfactory sulcus as the groove separating the olfactory lobe from the rest of the brain on the lateral aspect in dogs . This definition has also been used in man (Gottfried and Zald, 2005). In addition, in man olfactory fissure was used to describe the groove between the middle turbinate and the septum in the nasal cavity (Lee et al. 2007). The olfactory recess was considered part of the cranial cavity by Weidenreich (1941). However, it was also described as being located outside the cranium, in the nasal

cavity (Craven et al. 2010). The groove between the olfactory peduncle and the olfactory bulb was termed the *sulcus limitans bulbi olfactorii* in *Nomina Anatomica Veterinaria* (Schaller, 1992).

There is also considerable variation regarding which skull bones are thought to comprise the calvarium (also termed the skull-cap or calva), including i) the frontal, parietal and part of the interparietal process of the occipital bone (Evans, 1993; König et al. 2010), ii) the same but including the temporal bone in the human calvarium (Warwick and Williams, 1973), and iii) only the paired parietal and frontal bones are included by others (Smith, 1999; Constantinescu, 2002; Evans and De Lahunta, 2004). The caudal third of the cranial-base is formed by the basilar part of the occipital bone (Evans, 1993), while the rostral two-thirds of the basilar part of the neurocranium is formed by presphenoid and basisphenoid bones (Miller and Christensen, 1964; Evans, 1993; Smith, 1999). It has also been proposed that the caudal part of the cranial-base is formed by the occipital and temporal bones (Evans and De Lahunta, 2004).

Dorso-laterally, the cranium is formed by the parietal bone. Medially, hidden from external view, the frontal bone articulates with the ethmoidal bone. Caudally, the internal surface of the frontal bone forms part of the braincase and rostrally, it forms a small part of the nasal cavity (Miller and Christensen, 1964; Evans, 1993). The cribriform plate of the ethmoidal bone forms the rostral wall of the cranial cavity; the occipital bone the caudal wall. The lateral walls are formed by: temporal, parietal, frontal and sphenoidal bones (Smith, 1999; Constantinescu, 2002; Evans and De Lahunta, 2004). In contrast, König & Liebich (2004) used the same anatomical structures for defining the cranial and caudal walls of the cranial cavity, but described the lateral walls of the cranial cavity as composed of the paired temporal bones.

Moving to the ventricular system, the rostral part of the lateral ventricle has variably been defined as the rostral horn (De Lahunta, 1983; De Haan et al. 1994; Kii et al. 1997; Kii et al. 1998), or frontal area (Vullo et al. 1997). In man it is named the frontal horn (González-Soriano et al. 2001; Duffner et al. 2003). Equally, the last part of the lateral ventricle has variously been termed the temporal horn (De Lahunta, 1983; De Haan et al. 1994; Kii et al. 1997; Vullo et al. 1997; González-Soriano et al. 2001) (presumably because this part of the lateral ventricle is located within the temporal lobe of the cerebral hemisphere), ventral horn (De Lahunta, 1983) (presumably because of the anatomical orientation rather than anatomical location) and caudal horn (Hudson et al. 1991) (which is less acceptable anatomically). In man, the caudal part of the lateral ventricle is known as the occipital or posterior horn (Cardoza et al. 1988; Duffner et al.

2003) on the basis of its anatomical location and orientation. In veterinary species this portion of the lateral ventricle is variously termed the body of the lateral ventricle (Fitzgerald, 1961; González-Soriano et al. 2001) or parietal horn (Vullo et al. 1997). The reason for referring to this portion of the lateral ventricle as the parietal portion, rather than occipital portion, may be related to its anatomical location, as in dogs it appears to primarily be located within the parietal lobe, rather than in the occipital lobe as is the case in man.

In the dog, the evagination of the caudo-dorsal border of the 3rd ventricle was called the suprahabenular recess (Reiter, 1981), but termed the suprapineal recess by others (Fletcher, 1993; Anderson et al. 1994; De Lahunta and Glass, 2009). In man, a suprapineal recess of variable size was identified in about two thirds of the total number of ventricular moulds created (Last and Tompsett, 1953). However, McLone (2004) referred to it as the pineal recess instead of the suprapineal recess. In 1961, Fitzgerald defined the recess at a level above the caudal border of pineal gland and caudal commissure, which extends into a stalk of the epiphysis, as a pineal recess, when casts of the ventricular system were studied. A rostral diverticulum of the 3rd ventricle above the optic chiasm was called the preoptic recess by Horodyska and Kreiner (1962). Yet in the same publication this diverticulum was also termed the optic recess, as do others (Fletcher, 1993; Anderson et al. 1994; De Lahunta and Glass, 2009), or the supraoptic recess (Last and Tompsett, 1953). A recess at the level of the ventro-caudal portion of the 3rd ventricle was defined as the infundibular recess, because of its relationship to infundibulum of the pituitary gland (Fletcher, 1993; Anderson et al. 1994; De Lahunta and Glass, 2009), and as pituitary recess in man by McLone (2004), while in 1900 Retzius used the term post-mammillary recess to identify an area in front of/or behind the mammillary body [cited by Last and Thompsett (1953)]. In conclusion, there appears to be a lack of consensus on the application of anatomical terms in relation to the skull and brain.

1.6 Skull indices

A number of different indices are used to classify head shape in the dog, including, the skull, cranial, facial, palatal and snout indices. These indices all characterise, head shape on the basis of a ratio calculated from two measurements. The majority of these indices are used to classify dogs into dolichocephalic, mesaticephalic and brachycephalic breeds (Evans 1993), or short and long nosed (Stockard 1941). Another use of the head indices

is to determine the gender of dogs, in particular a ratio based on the breadth (width) and the length of the skull (Trouth et al. 1977). In this index the width is the distance between the most lateral point of the temporo-occipital fissures, while the length is the distance between the basion and the centre of a line that joins the most medial points of the jugular foramina.

The most accepted, well-known and historical formulae are the Stockard and Evans indices (Stockard, 1941; Evans, 1993). In his formula, Stockard used the interzygomatic arche width and the skull-base length (length), the latter defined as a straight distance between the prosthion rostrally and the basion caudally (Figure 1-6), to divide dogs into short-nose and long-nose groups. The same width was used in the formula by Evans. However, length was defined as the straight line distance between the prosthion rostrally and the inion caudally (Figure 1-7). According to this formula, Evans classified dogs into brachycephalic, mesaticephalic and dolichocephalic groups (Evans, 1993).

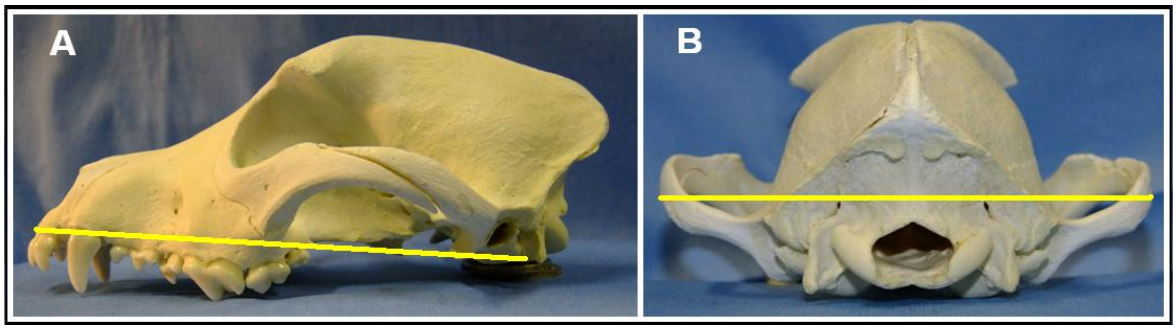

Figure 1-6: Stockard index is defined by dividing the product of the width (B) x100 by the length, which is defined as skull-base length (A)

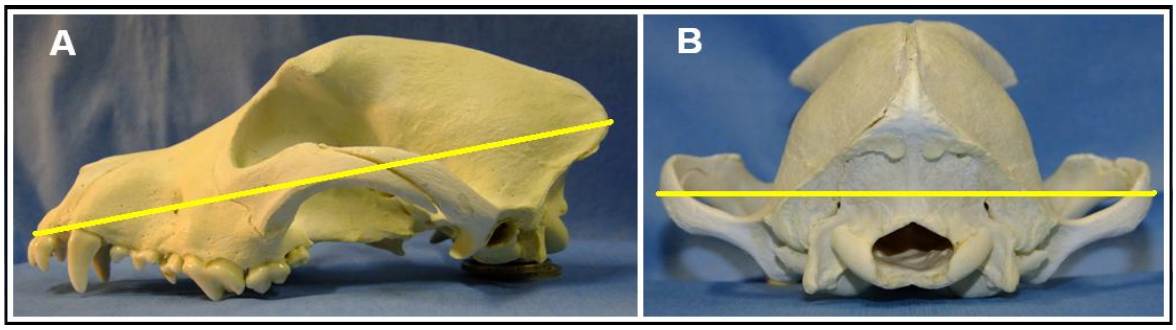

Figure 1-7: Evans index is defined by dividing the width (B) by the length (A), the landmarks being the prosthion rostrally and the inion caudally

1.6.1 Classification of dogs according to the skull shape

Dogs are classified into dolichocephalic, mesaticephalic and brachycephalic breeds according to the indices described above (Miller and Christensen, 1964; Evans, 1993;

Smith, 1999). Within the three groups of dogs, there are certain skull shape characteristics that are broadly common to the group.

Dolichocephalic breeds: In general these dogs tend to have a lower jaw (mandible) that is shorter than the upper jaw (maxilla) and the head tends to be longer and narrower than mesaticephalic breeds (Smith, 1999), with a ratio of about 0.39 between the width and the length of the skull (Evans, 1993). *Collie* dogs have been proposed as typical of dolichocephalic dog breeds (Miller and Christensen, 1964; Hardy et al. 1967; Niebauer and Evans, 1988; Evans, 1993; Onar, 1999; Hasegawa et al. 2005). GSDs have been categorised as dolichocephalic in a number of studies (Hardy et al. 1967; Onar, 1999; Schwarz et al. 2000; Hasegawa et al. 2005). However, there is some debate, with some studies classifying GSDs as mesaticephalic (Miller and Christensen, 1964; Evans, 1993; Smith, 1999). In addition to the GSD, Smith (1999) classified the Collie and Dobermann pinscher as mesaticephalic breeds, whereas Hardy et al. (1967) in studying the Dobermann pinscher and the Collies cross assigned them as dolichocephalic.

The Dachshund has been described as dolichocephalic (Hardy et al. 1967), but with the Miniature dachshund classified as mesaticephalic (Hasegawa et al. 2005). Other breeds defined as dolichocephalic include the Saluki (Stockard, 1941; Smith, 1999), Greyhound (Sisson, 1975; Smith, 1999), Shetland sheepdog (Niebauer and Evans, 1988; Hasegawa et al. 2005) and Setter dog (Miller and Christensen, 1964; Evans, 1993), Afghan hound (Smith, 1999), Russian wolfhound or Borzoi (Miller and Christensen, 1964; Evans, 1993) and Fox hound (Stockard, 1941). However, perhaps indecisively, the Rottweiler has been described as intermediate mesati-dolichocephalic (Schwarz et al. 2000). The skull shape of the Yorkshire terrier has been described as consistent with a dolichocephalic skull shape, while the cranial cavity is more consistent with brachycephalic breeds (Esteve-Ratsch et al. 2001).

Mesaticephalic breeds: In general mesaticephalic dogs are characterised by having a similar facial and cranial region length, equal length of the upper and lower jaws (Smith, 1999) and having a ratio between the width and the length of the head of about 0.52 (Evans, 1993). A large number of breeds are included under the mesaticephalic heading, including the Labrador retriever (Hardy et al. 1967; Smith, 1999; Glass et al. 2000; Hasegawa et al. 2005; Carrera et al. 2009), Beagle (Miller and Christensen, 1964; Evans, 1993; Smith, 1999; Hasegawa et al. 2005), Great Dane (Hardy et al. 1967), Cocker spaniel (Glass et al. 2000; Schwarz et al. 2000; Hasegawa et al. 2005; Carrera et al. 2009), Fox terrier (Hardy et al. 1967; Sisson, 1975), Husky (Smith, 1999; Hasegawa et al. 2005), Giant schnauzer, German shorthaired pointer and Dalmatian

(Hardy et al. 1967), Pomeranian and Alaskan malamute (Sisson, 1975), Pointers and Terriers (Smith, 1999), Springer spaniel (Carrera et al. 2009), Toy poodle (Glass et al. 2000), Tibetan terrier and Caucasian shepherd (Schwarz et al. 2000), Inu Shiba, Basset hound, Miniature schnauzer and Welsh corgi (Hasegawa et al. 2005).

Brachycephalic breeds: In general these are characterised by a shorter and wider cranium than the mesaticephalic breeds with an upper jaw that is usually shorter than the lower jaw (Smith, 1999). According to Evans, dogs should be considered as typical brachycephalic breeds when the ratio between the width and the length of the skull is equal or greater than 0.81(Evans, 1993). The following breeds have been classified as brachycephalic: Boston terrier (Stockard, 1941; Hardy et al. 1967; Smith, 1999), Boxer (Hardy et al. 1967; Niebauer and Evans, 1988), Pekingese (Miller and Christensen, 1964; Niebauer and Evans, 1988; Evans, 1993; Smith, 1999), Chihuahua (Smith, 1999; Hasegawa et al. 2005), Pug and Shi-tzu (Niebauer and Evans, 1988; Hasegawa et al. 2005), CKCS (Hasegawa et al. 2005), Bull mastiff (Hardy et al. 1967), Shar pei (Niebauer and Evans, 1988) and French bulldog (Stockard, 1941). The Maltese, Yorkshire terrier, Papillon, Pomeranian (Hasegawa et al. 2005) and English bulldog were also classified as brachycephalic (Stockard, 1941; Smith, 1999). However, in a separate study on the cribriform plate, the CKCS, Miniature poodle and West highland white terrier (WHWT) were described as brachy-mesaticephalic (Schwarz et al. 2000).

1.7 Aim of the current work

The primary objectives of this work were, to use MRI to investigate the possibility of establishing a new parameter for defining the skull shape in dogs, which could readily be performed on MRI images that did not include the entire head, and to assess the influence of these various skull shapes on the facial, palatal and neural regions of the head and their constitutive components.

2 GENERAL MATERIALS & METHODS

2.1 Introduction

The experimental studies undertaken within this thesis attempted to examine the effects of head conformation (brachycephalic, mesaticephalic and dolichocephalic) on aspects of brain and skull anatomy in the dog using MRI. The studies looked at the effect of head conformation on the entire cranial fossa (rostral, middle and caudal fossae), but concentrated in more detail on the components of the rostral and middle fossae (including the olfactory bulb, 3rd ventricle, interthalamic adhesion and quadrigeminal cistern) and their related skull structures, namely the nasal cavity, ethmoturbinates and nasopharynx. The following chapter details the materials and techniques used in this thesis.

2.2 Animals

The animals included in this study were all client-owned pet dogs presented to the Small Animal Hospital, University of Glasgow between 2007 and 2011. For inclusion in the study dogs were required to have a full MRI study performed of the head region. The information gained from each animal and the MRI were all part of the normal clinical investigation in that particular animal and no additional procedures were performed for the purposes of this study. Informed consent for the use of clinical data from each animal was included as part of the hospital owner consent form. Ethical approval was granted through the local Ethics and Welfare Committee. The case history and MR images were reviewed in each dog prior to inclusion in different parts of this study.

2.3 Magnetic Resonance Imaging

MRI was performed using a 1.5 Tesla MRI unit (Siemens Magnetom Essenza, Siemens Medical Solutions, Camberley, UK). Sequences included T2- and T1-weighted dorsal, sagittal and transverse plane images with additional post-contrast T1-weighted images. In the majority of smaller dogs, the routine sequences described above included the relevant parts of the head required for the purposes of this study. In larger and in small dogs where the routine sequences did not include the required parts of the head in order to calculate cephalic indices (detailed in 2.7), additional whole head MRI sequences were included as part of the MRI study. These comprised sagittal, dorsal and transverse plane T2-weighted images that were obtained without prolonging the duration of the general anaesthesia or the MRI study, by sandwiching the scans between the immediate post-

contrast T1-weighted transverse plane sequence and a routine second, delayed post-contrast, T1-weighted transverse plane sequence. The field of view varied according to the individual clinical study on the basis of the area of interest, but in all cases included the entire brain in dorsal, sagittal and transverse planes.

2.3.1 T1 sequence

A T1 sequence is called spin-lattice relaxation time and is acquired using short (timing) echo time (TE) and repetition time (TR) values. This sequence highlights anatomical detail because it shows the boundaries between different tissues well. In this sequence, fat is bright/hyperintense and free fluid dark/hypointense. Other soft tissues show a range of intensities between these two extremes. In addition, as with all common MRI sequences, compact bone and air show signal voids and are therefore black on displays. T1-weighted sequences were performed with a TR within the range of 360-870 and a TE within the range of 10-15 (REF).

2.3.2 T1 sequence with contrast

As small blood vessels are not highlighted by either T1 or T2 sequences, the addition of contrast delivered intravenously highlights tissues with high vascularity or where the blood-brain barrier is disrupted. Such contrast also increases the signal to noise ratio so that image quality is improved and better resolution is achieved. The most common contrast agent is based on gadolinium. T1-weighted sequences with contrast were performed following intravenous administration of gadopentetate dimeglumine at $94 mgkg^{-1}$ (Magnevist, Bayer plc, Newbury, UK).

2.3.3 T2 sequence

A T2 sequence is called spin-spin relaxation time and is acquired using a short TE value, but long TR value. Pathological features are highlighted with this sequence when the pathological lesion has significantly more fluid content than the normal surrounding tissue or where there is peri-lesional oedema. T2-weighted sequences were performed with a TR within the range of 2160-5890 and a TE within the range of 86-130.

2.3.4 Sagittal plane

The sagittal plane is that which runs head to tail parallel to the dorso-ventral plane. The midline sagittal plane on MRI was defined as the slice which bisects the interthalamic adhesion and both rostral and caudal commissures (Assheuer and Sager, 1997).

This plane was used to delineate the head length, angulation and orientation of the olfactory bulb, height of the nasopharynx, and the midline areas of the nasal cavity, cranial fossae, olfactory bulb, 3rd ventricle, interthalamic adhesion, quadrigeminal cistern, and the brain area.

2.3.5 Transverse plane

The transverse plane is that which is perpendicular to the long axis of the body. Two parameters were measured in this plane: the width of the skull and the transverse nasopharyngeal area and shape.

2.3.6 Dorsal plane

The dorsal plane corresponds to the coronal plane in man. In both the skull and spine, the dorsal plane is perpendicular to both the transverse and sagittal planes. The measurements performed in this plane were dorsal ethmoturbinate area, and both length and width of the olfactory bulb.

2.4 Software

2.4.1 Image Storage

Data acquired by the MRI machine were initially manipulated on the local dedicated PC workstation running Windows XP using bespoke Siemens software (NUMARIS/4 version syngo MR C13). From this computer DICOM files were exported to a PACS (see below).

2.4.1.1 DICOM

Digital Imaging and Communications in Medicine is a standard used for the electronic transfer of digital image data from and to medical imaging equipment. (This was initially developed by a joint committee of the American College of Radiology and the National Electronics Manufacturers' Association. The standard included a set of protocols for devices communicating over a network, a syntax and semantics of

commands and associated information that could be exchanged using these protocols, a set of media storage services and devices claiming conformance to the standard, as well as a file format and a medical directory structure to facilitate access to the images and related information stored on media that allowed sharing of information.)

2.4.1.2 PACS

PACS is a Picture Archiving and Communications System (PACS). (This is a server/s used to provide an archive for storage of multimodality images, to integrate images with patient database information, to facilitate laser printing of images, and to display images at work stations throughout a network. PACS also allows inspection of images in remote locations using DICOM viewers.)

2.5 eFilm Workstation™ 3.0

eFilm Workstation 3.0 is a widely used DICOM viewer, and is a trademark of Merge Healthcare (www.mergehealthcare.com). All images were examined using eFilm. The linear parameters for the studies and the orientation and angulation of the olfactory bulb were determined with electronic calipers.

2.5.1 ImageJ 1.42q

ImageJ 1.42q is public domain open source software (http://rsb.info.nih.gov/ij/index.html), created by Wayne Rasband at the National Institute of Health, USA. The areas of the following regions were outlined using imageJ software calipers: the nasal cavity, ethmoturbinates, nasopharynx, brain area, olfactory bulb, cranial fossae, 3rd ventricle, interthalamic adhesion and quadrigeminal cistern. Each image was calibrated for scale followed by measurement of the area of interest. The individual areas were corrected for bodyweight by expressing them as a ratio relative to midline sagittal brain area, or as a ratio relative to bodyweight, further details are presented in relevant sections.

2.5.2 Image editing

Image editing was performed using Microsoft Office Picture Manager (http://office.microsoft.com/) and IrfanView 3.98 (http://www.irfanview.com/). Figures were generated using Microsoft Office Picture Manager and Corel Draw 10 (Corel Corporation, Ottawa, Canada).

2.6 Statistical analysis

Statistical analysis was performed using GraphPad Prism 5 software (GraphPad Software Inc., La Jolla, USA) in all studies. The main elements of the data were reported using descriptive statistics (mean, standard deviation and range). The normality of the data was examined using the D'Agostino and Pearson Omnibus normality test. If the data passed the normality test (Gaussian distribution test), then statistical analysis was performed using the two tailed unpaired t-test or the one-way ANOVA with Bonferroni post multiple comparison test (alpha level was set to 0.05). If the data did not pass a Gaussian distribution test then statistical analysis was done using a non-parametric test, either the Mann-Whitney or Kruskal-Wallis tests with Dunns post multiple comparison test (at a significant level of 95%). Frequency distribution, the ROC curve test for defining the best cut-off point between two groups, and both linear and non-linear regression analyses were also performed where appropriate. The choice of statistical method utilised in each study is discussed in more detail in the individual chapters.

2.7 Measurements of objective quantification of the canine head phenotype

Only dogs with no disease affecting the skull (normal skull anatomy) and of a pure breed were recruited to this part of the study.

2.7.1 Defining breeds as brachycephalic, mesaticephalic and dolichocephalic

2.7.1.1 Evans index

The Evans index for each dog was calculated from the MR images of the skull. The Evans index (Table 2-1) is defined as the ratio between the widest distance between the interzygomatic arches (Width) and the distance from the prosthion rostrally to the inion caudally (Length).

Evans index = width * 100/length	Width = widest distance between the interzygomatic arches
	Length = distance between the prosthion and the inion

Table 2-1: The Evans index for classification of dog head shape on the basis of skull width and length (Evans, 1993)

2.7.1.2 Stockard index

The Stockard index for each dog was calculated from MR images on the basis of skull-base length and skull width as defined in Table 2-2.

Stockard index= width * 100/length	Width= widest distance between the interzygomatic arches
	Length= distance between the prosthion and the basion

Table 2-2: The Stockard index for classification of dog head shape on the basis of skull width and skull-base length (Stockard, 1941)

2.7.2 Determination of olfactory bulb angulation and orientation

In Chapter 3, olfactory bulb angulation and orientation were assessed and validated as an alternative measure of head phenotype as it did not require MR imaging of the whole head, but just the cranial cavity including the hard palate on the midline sagittal plane. This alternative measure was then used in Chapters 4 and 5 to determine head phenotype. The dogs selected for inclusion in studies where olfactory bulb angulation and orientation were determined had no apparent clinical abnormalities affecting the anatomy of the skull or the olfactory bulb region.

2.7.2.1 Identification and definition of the olfactory bulb fissure

The olfactory bulb fissure was identified and defined on fresh and formalin fixed heads as well as on T1-weighted and T2-weighted MR images in the midline sagittal and dorsal planes.

2.7.2.2 Olfactory bulb angulation and orientation

The olfactory bulb position in relation to the skull was determined as follows: a baseline

was defined as the straight line passing through the intercondylar notch caudally and oral aspect of the hard palate rostrally. This baseline was then used as the reference line for determination of the olfactory bulb angulation and its orientation in midline sagittal plane MR images (Figure 2-1A).

To define the angulation of the olfactory bulb, a straight line was drawn from the most dorsal to the most ventral points of the olfactory bulb fissure to intersect the baseline. The angulation of the olfactory bulb was measured as the angle between this line and the baseline (Figure 2-1B).

Olfactory bulb orientation was determined as follows: a line was drawn perpendicular to the baseline to touch the rostral most portion of the olfactory bulb. The olfactory bulb was divided into four quarters, named from the ventral aspect of the olfactory bulb fissure to the dorsal aspect as 1, 2, 3 and 4 respectively. Depending on which quarter of the olfactory bulb the line perpendicular to the baseline touched, the olfactory bulb orientation was defined as type 1, 2, 3 or 4. If the olfactory bulb was ventrally orientated and the perpendicular line contacted the frontal squama of the frontal bone then this was defined as type-5 (Figure 2-2).

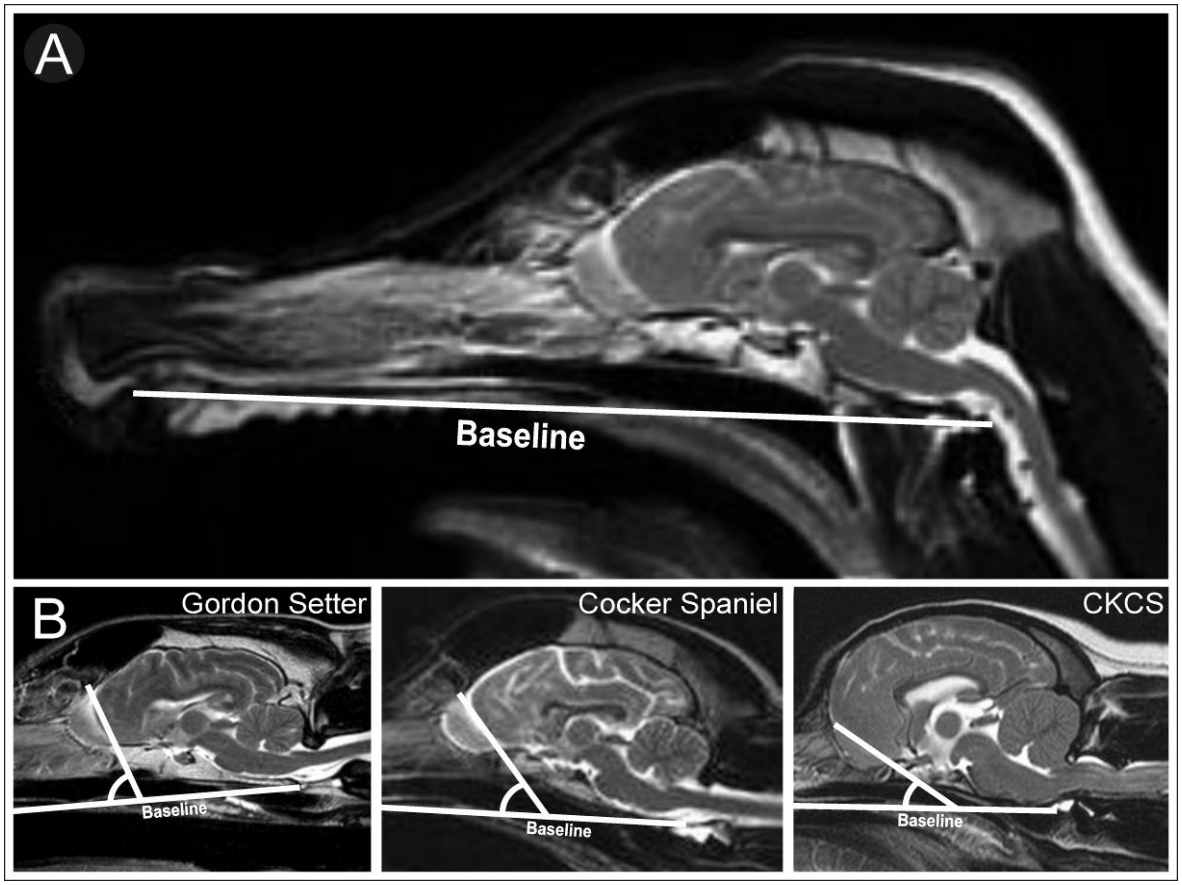

Figure 2-1: Determination of olfactory bulb angulation. (A) The baseline was defined as the line extending from the oral aspect of the hard palate rostrally to the intercondylar notch of the foramen magnum

caudally. The baseline was used to establish the angulation and the orientation of the olfactory bulb. (B) The angulation of the olfactory bulb was defined as the angle where the baseline intersected a straight line drawn from the most dorsal to the most ventral points of the olfactory bulb fissure

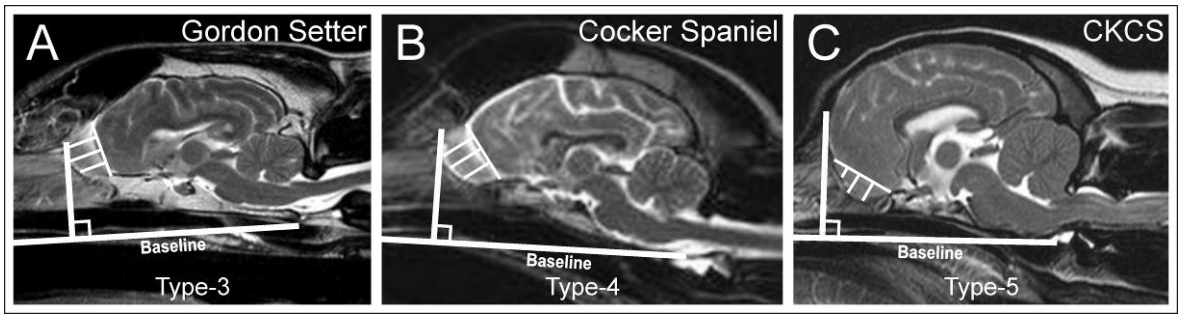

Figure 2-2: Determination of olfactory bulb orientation. The olfactory bulb was divided into four quarters, named from the ventral aspect of the olfactory bulb fissure to the dorsal aspect as 1, 2, 3 and 4 respectively. A line perpendicular to the baseline was drawn to touch the rostral most portion of the olfactory bulb. Depending on which quarter of the olfactory bulb this line touched, the orientation was defined as types 1-4 [e.g. types-3 (A) and 4 (B)]. If the olfactory bulb was ventrally orientated and the perpendicular line contacted the frontal squama of the frontal bone then this was defined as a type-5 (C)

2.8 Defining the boundaries of the fossae of the cranial cavity (Chapter 3)

The cranial cavity is divided into three fossae: the rostral, middle and caudal fossae (Figure 2-3). The midline areas of the different cranial fossae were determined on midline sagittal T2w MR images as follows:

- The midline area of the rostral fossa was defined as the area of the cranial cavity that extended from the cribriform plate rostrally to the cruciate sulcus dorso-caudally and the optical canal ventro-caudally. The rostral fossa includes the ethmoidal fossa, which occupies the rostral most portion of the fossa. The ethmoidal fossa extends from the cribiform plate rostrally to the olfactory bulb fissure caudally.
- The midline area of the middle fossa was defined as the area of the central portion of the cranial cavity, bordered by the rostral fossa rostrally and the caudal fossa caudally.
- The midline area of the caudal fossa was defined as the area of the cranial cavity bordered by the osseous tentorium cerebelli rostro-dorsally, the dorsum sellae rostro-ventrally and the foramen magnum caudally (including the intercondylar notch ventrally and the internuchal notch dorsally).

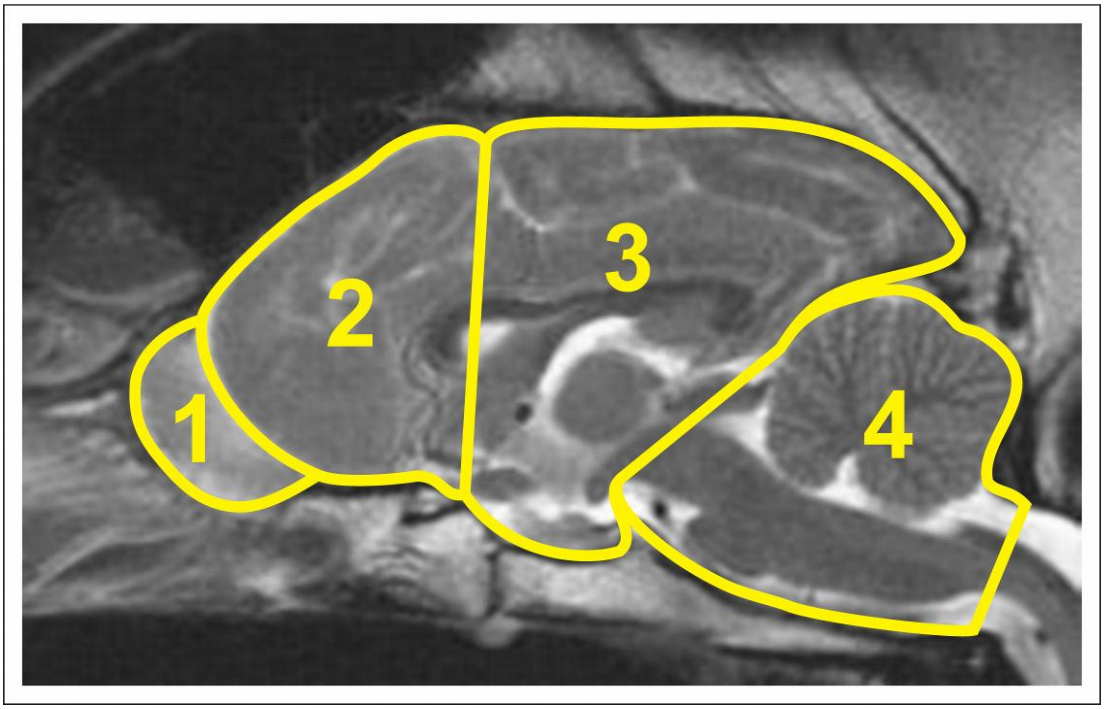

Figure 2-3: The different compartments of the cranial cavity: ethmoidal fossa (1), rostral fossa (1 and 2 – the rostral fossa includes the ethmoidal fossa), middle fossa (3 – which includes the hypophyseal fossa) and the caudal fossa (Evans, 1993)

2.9 Measurements of the dimensions of the olfactory bulb (Chapter 3)

The dimensions of the olfactory bulb were determined on dorsal plane T1w & T2w MR images at the level of the colliculi and on midline sagittal plane MR images. The individual measurements are listed in (Table 2-3) and detailed in (Figure 2-4). The dimensions of the olfactory bulb were then compared between dogs of different age, gender and head phenotype (using the new parameter olfactory bulb angulation).

MR Plane	Measurement	Description
Dorsal	Olfactory bulb width	Greatest width of the olfactory bulb
Dorsal	Olfactory bulb length 1	Greatest distance between the cribriform plate and the olfactory bulb fissure
Midline sagittal	Olfactory bulb length 2	Greatest distance between the cribriform plate and the olfactory bulb fissure

Midline sagittal	Olfactory bulb length 3	Distance from the mid point of olfactory bulb fissure to the cribriform plate
Midline sagittal	Olfactory bulb height	Distance from the dorsal (frontal) to the ventral (episphenoidal) aspect of the olfactory bulb fissure

Table 2-3: Landmarks and MR imaging planes used to define the linear dimensions of the olfactory bulb

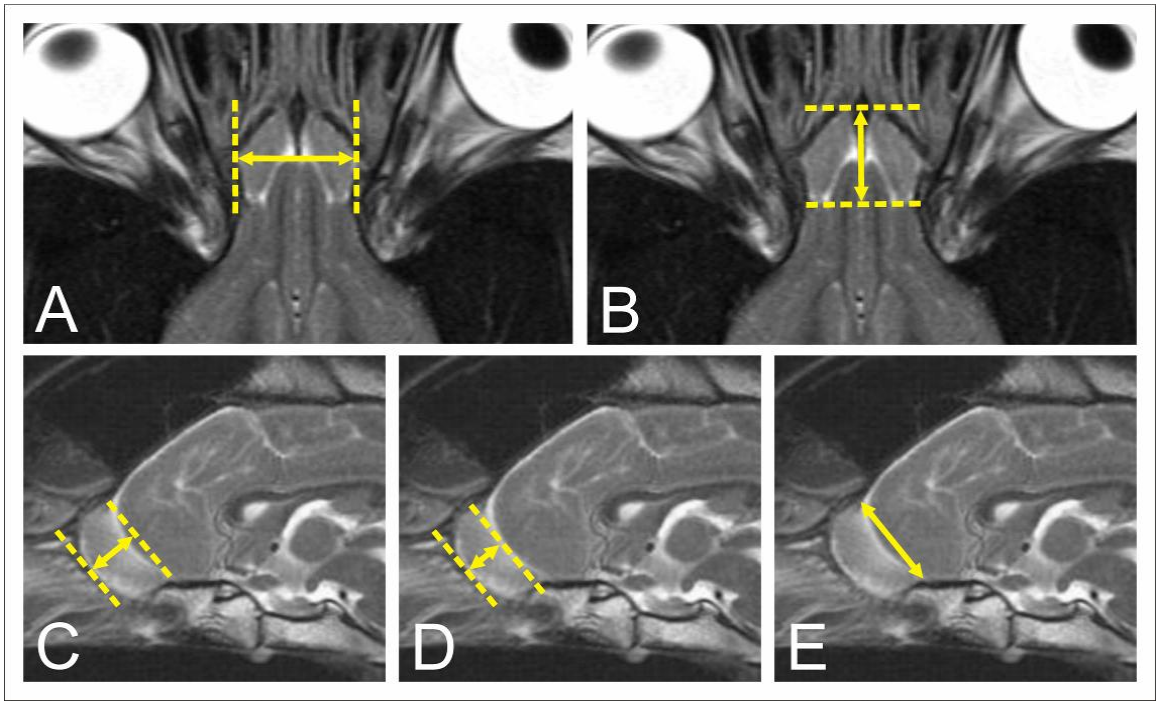

Figure 2-4: Methods of measurement of the olfactory bulb. A) Width in the dorsal plane. B) Length 1 in the dorsal plane. C) Length 2 in the midline sagittal plane. D) Length 3 in the midline sagittal plane. E) Height in the midline sagittal plane

2.10 Measurement of nasal cavity, ethmoid turbinates and olfactory bulb areas (Chapter 4)

The nasal cavity area was measured on midline sagittal plane T1w & T2w MR images (Figure 2-5). It was bounded rostrally by the alar fold and caudally by the cribriform plate.

The ethmoturbinate area was measured on dorsal plane T1w & T2w MR images (Figure 2-5). It was located within the right and left sides of the nasal cavity, bounded caudally by the cribriform plate and the external lamina rostrally and laterally. The inner surface

of the bones of the nasal cavity was used to define the position of the external lamina on MR images, as the external lamina is apposed to the inner surface of the nasal bones.

The brain and the olfactory bulb areas were measured on midline sagittal plane T1w & T2w MR images (Figure 2-6). The boundaries of the latter were defined as the inner surface of the cribriform plate rostrally and the olfactory bulb fissure caudally (Figure 2-6). The midline area included the olfactory bulb area.

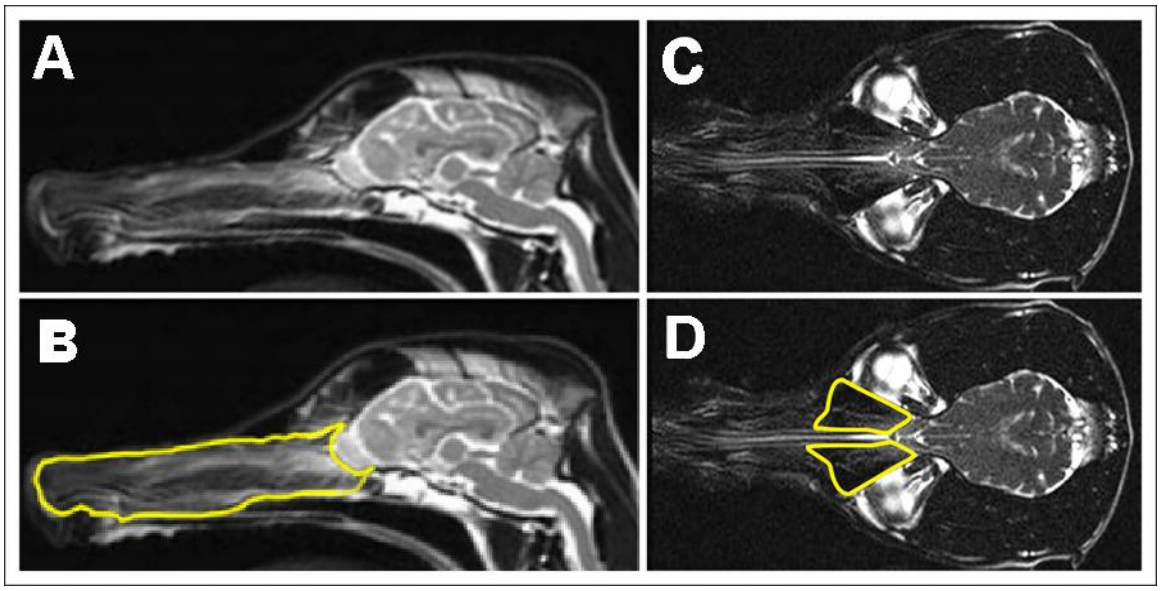

Figure 2-5: Measurements of the nasal cavity area on midline sagittal plane T2w MR images (A & B), and ethmoturbinate area on dorsal plane T2w MR images (C & D)

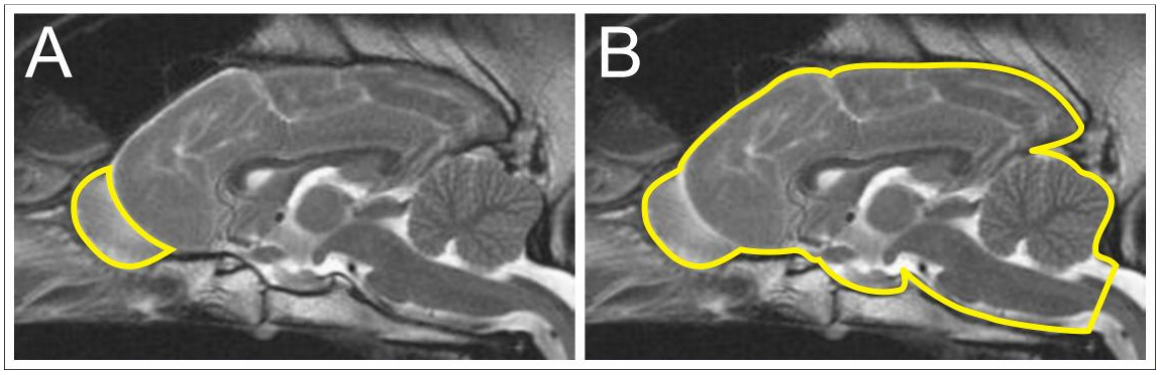

Figure 2-6: Measurement of the olfactory bulb (A) and brain (B) areas on midline sagittal plane T2w MR images. Note: The midline brain area includes the olfactory bulb

2.11 Measurements of the bony nasopharynx (Chapter 4)

In all animals, T2-weighted MR images were used. The height of the nasopharynx was measured on a midline sagittal plane MR image by drawing a line perpendicular to the baseline as defined in section 2.7 to intersect the centre of the olfactory bulb. The height of the nasopharynx was defined as the portion of this perpendicular line that traversed the

air-filled nasopharynx, from the inner surface of the roof of the bony nasopharynx dorsally to the nasal surface of the hard palate ventrally (Figure 2-7). The transverse area and shape of the nasopharynx were determined on a transverse MR image at the level of the caudal border of the bony nasopharynx, immediately dorsal to the caudal point of the nasal spine of the palatine bone (Figure 2-8). In all animals, the Evans and Stockard indices were calculated and the olfactory bulb area, orientation and angulation were measured as described in sections 2.7 & 2.8.

Figure 2-7: The height of nasopharynx (arrow) was measured on a line perpendicular to the baseline, that intersected the centre point of the olfactory bulb, using a midline sagittal plane T2w MR image

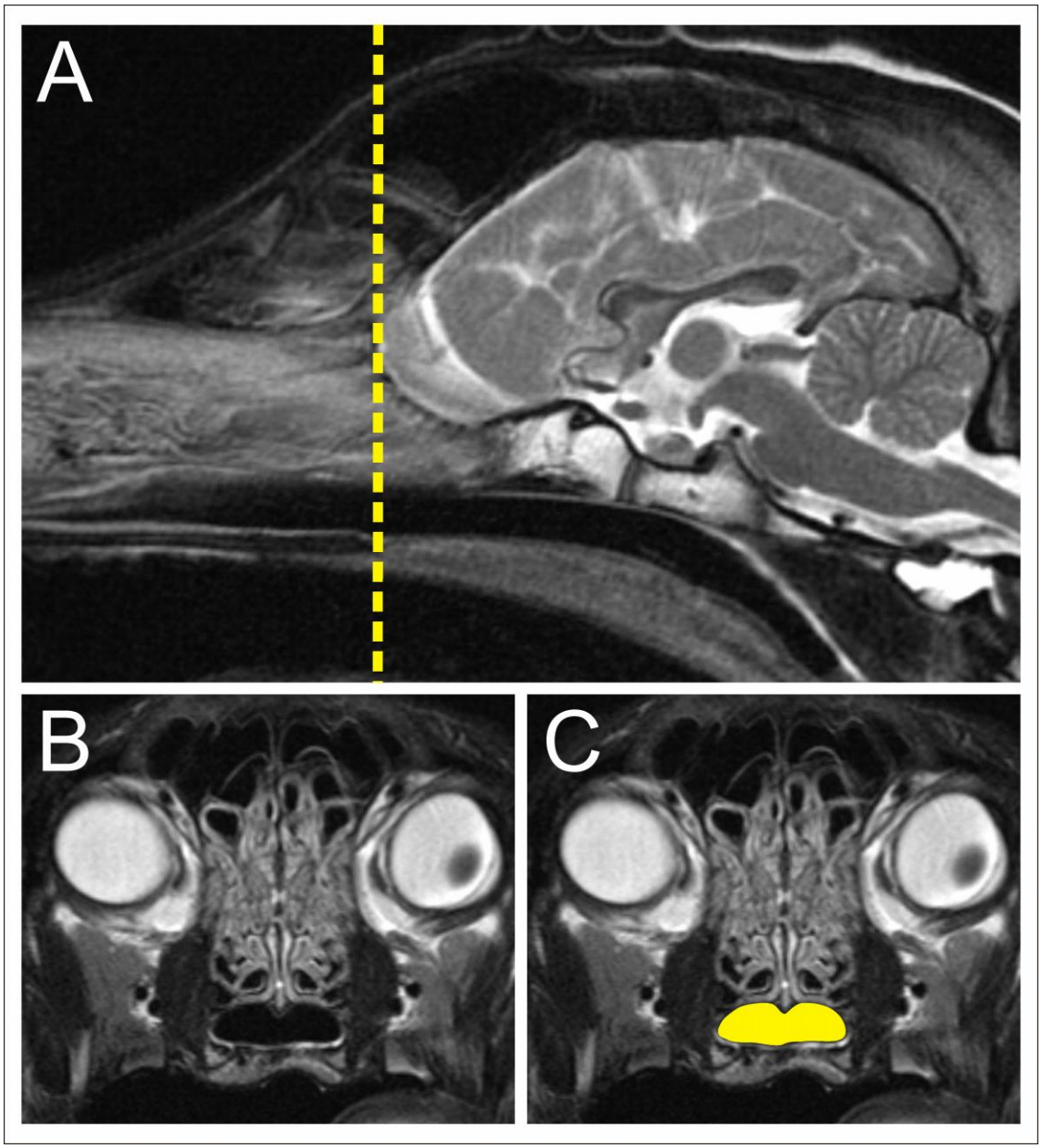

Figure 2-8: Determination of the transverse area and shape of the nasopharynx on transverse T2w MR images, at the level of the caudal border of the bony nasopharynx, immediately dorsal to the caudal point of the nasal spine of the palatine bone (reference line in A). The area of the air-filled nasopharynx was measured (B) and its shape was defined (yellow) (C)

2.12 MRI anatomy of the structures of the middle fossa

Structures within the middle fossa were examined in five different populations of dogs. Dogs were grouped according to the final clinical diagnosis (more detail is presented in chapter 5).

In all dogs included in this part of the study measurements from midline sagittal plane T2w MR images through the brain included: olfactory bulb angulation and orientation, and the areas of the following structures, brain (as defined by the inner surface of the

bones of the cranial cavity), interthalamic adhesion, quadrigeminal cistern and 3rd ventricle. The borders of the 3rd ventricle were defined as the *lamina terminalis* (including the rostral commissure) rostrally, *tela choroidae* dorsally, quadrigeminal cistern and mesencephalon caudally, and the optic chiasm and pituitary gland ventrally. The interthalamic adhesion area was defined as a hypointense round shape bordered by the hyperintense 3rd ventricle. The quadrigeminal cistern area was defined as a cerebrospinal fluid-filled cistern bordered by the arachnoid membrane rostrally and dorsally, the tectum ventrally, and mainly the cerebellum caudally (Figure 2-9).

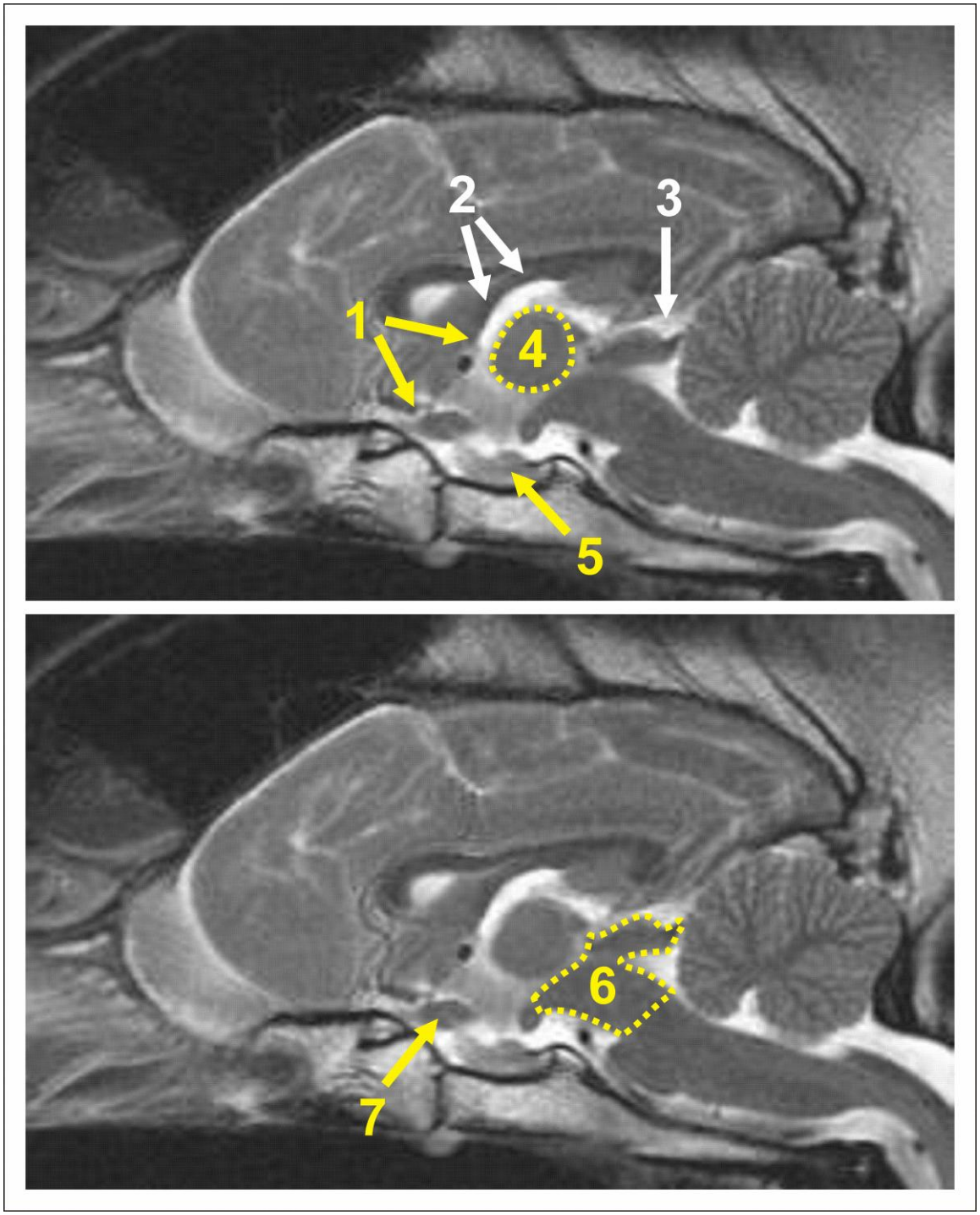

Figure 2-9: Middle fossa landmarks on T2-weighted midline sagittal MR images. 1) Lamina terminalis, 2) tela choroidae, 3) quadrigeminal cistern, 4) interthalamic adhesion, 5) pituitary gland, 6) mesencephalon, 7) optic chiasm

3 OBJECTIVE QUANTIFICATION OF HEAD PHENOTYPE

3.1 Introduction

The Evans index is generally accepted (on the basis of citations in textbooks and journals) to be the most commonly used reference index to classify dog heads into dolichocephalic, mesaticephalic and brachycephalic (Evans, 1993). For his formula, Evans defined the index as multiplying the width of the skull by 100 then dividing the product by the length of the skull. The width of the skull was defined as the widest interzygomatic arch distance. The length of the skull was defined as the distance between the prosthion (rostral end of the interincisive suture that is located between the roots of the upper central incisor teeth), and the inion (the central surface point on the external occipital protuberance).

Although Evans was not the first to use these parameters, it is believed that he was the first to employ these to classify dog heads into brachycephalic, mesaticephalic and dolichocephalic. Stockard (1941) separated dogs into long-skull and short-skull types, using the same width. However, this index differs in that the length of the skull-base is used to define skull width instead. The length of the skull-base was defined as the distance from the prosthion to the basion.

Breeds such as the Boston terrier and Pekingese were described as typical brachycephalic or short-skull type breeds according to both of the above workers, while other breeds like the GSD were ascribed to the long-skull type or mesaticephalic breeds according to Stockard and Evans respectively.

A number of other indices have also been used to classify head shape in dogs, including among others, the cranial, facial, palatal and snout indices. These all characterise different head shapes on the basis of a ratio calculated from two measurements. Another use of skull indices is in the determination of the gender of dogs. In particular, a ratio based on the width and length of the skull can be used for gender determination (Trouth et al. 1977). In this index the skull width was defined as the distance between the most lateral points of the temporo-occipital fissure, while skull length was defined as the distance between the basion and the centre of a line that joins the medial most points of the jugular foramina. Unfortunately, the different indices used a variety of start and end points for defining skull width and length.

Evans (1993) also described the early fusion between the spheno-occipital synchondrosis, the intersphenoidal synchondrosis or both in brachycephalic breeds, resulting in limited basicranial axis growth. At least one study suggested that the ventral rotation of the olfactory bulb observed in these breeds may have been influenced by that fusion, and lead to

antero-posterior (rostro-caudal)compression of the rostral aspect of the frontal lobes within the cranial cavity (Lyras, 2009). The cranial cavity of dogs is divided into the rostral, middle and caudal fossae, which are formed by the floor of the cranial cavity and are therefore affected by the basicranial axis. It has been stated that the cranial cavity volume is predominantly affected by bodyweight, but that an effect of skull shape could not be excluded (Evans, 1993).

A limitation of the Evans and Stockard indices are that they define the average values that allow identification of different breeds as brachycephalic, mesaticephalic or dolichocephalic.

The objectives of this part of the study were to:

- Define the Evans index values and head phenotypes associated with brachycephalic, mesaticephalic and dolichocephalic breeds of dogs on the basis of MRI
- Investigate using olfactory bulb angulation to define head phenotype from a single MR image
- Investigate the effect of head phenotype (defined using the Evans index and angulation of the olfactory bulb) on the midline sagittal area of the rostral, middle and caudal fossae of the cranial cavity from MR images
- Using MR images to determine the dimensions of the olfactory bulb and investigate the influence of head shape, gender and age on the olfactory bulb.

3.2 Materials and Methods

Within this chapter, the head indices of a population of normal dogs, representing a range of different pure breeds and head conformations, were measured on MRI. On the basis of those results the classification of dogs into brachycephalic, mesaticephalic and dolichocephalic groups was tested and refined (Figure 3-1):

Control Breeds were defined as brachycephalic, mesaticephalic or dolichocephalic on the basis of their accepted historical classification in previous publications, where these publications used the Evans index (Evans 1993).

Method 1 The Evans index values and olfactory bulb angle measurements that best defined brachycephalic, mesaticephalic and dolichocephalic head phenotypes were calculated for the control group on the basis of the Lower and Upper 95% CI of the Mean values for each.

Method 2 The Evans index values and olfactory bulb angle measurements that best defined brachycephalic, mesaticephalic and dolichocephalic head phenotypes were calculated for the control group on the basis of the best cut-off point values determined using the ROC curve test.

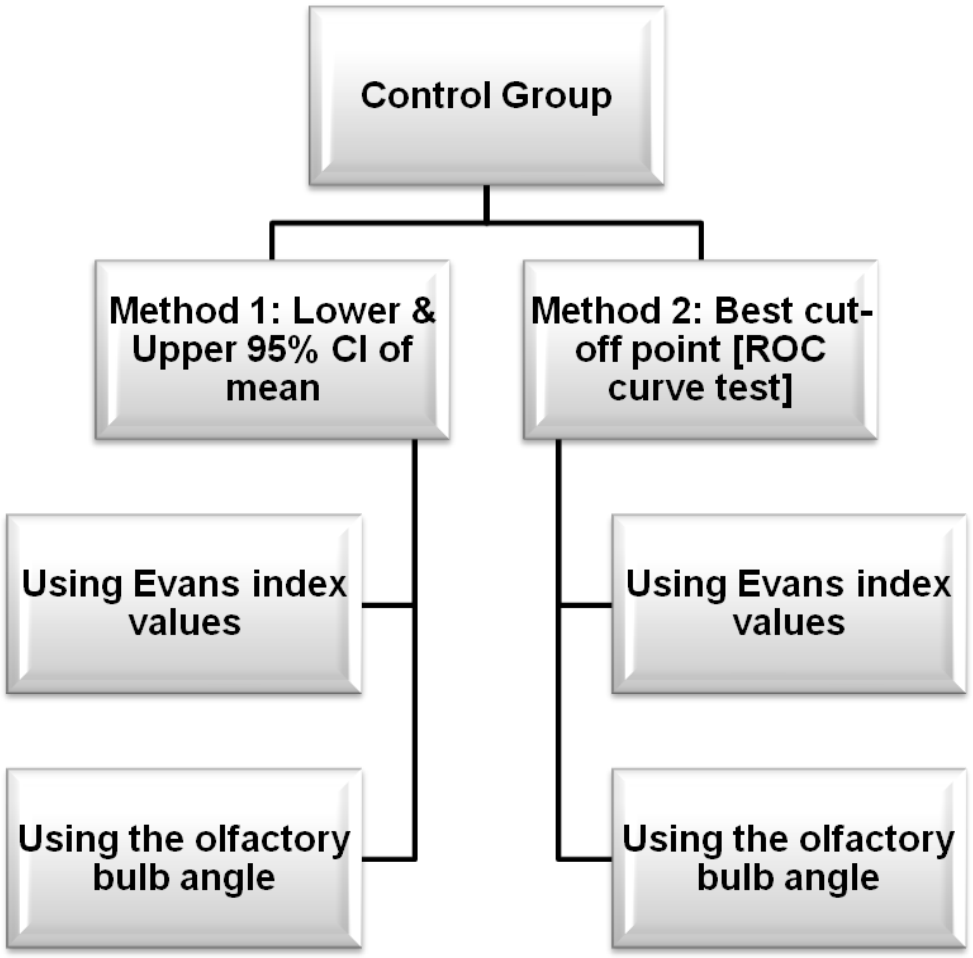

Figure 3-1: Diagram showing the structure of the proposed work

3.2.1 Determining head phenotype using the head indices

Arbitrary Control: head phenotype was defined in 48 dogs of 20 pure breeds, including 36 brachycephalic dogs [13 female, 23 male]; 8 mesaticephalic dogs [1 female, 7 male] and 4 dolichocephalic dogs [3 female, 1 male], using the Evans & Stockard indices as defined in Chapter 2.

The breeds were grouped arbitrarily as follows:

Brachycephalic group: 15 CKCS, 4 boxers, 4 Shih-tzus, 3 Lhasa apsos, 2 Chihuahuas, 2 Pugs, 2 WHWT and one each of the following breeds: bichon frise, Boston terrier, mastiff and Staffordshire bull terrier. Age ranged from 1.6-16.7 years [M±STDEV=5.5±3.4], and bodyweight from 2.7-90 kg [M±STDEV=11.7±15.5].

Mesaticephalic group: 4 Labrador retrievers and one each of the following breeds: English springer spaniel, Giant schnauzer, Miniature schnauzer and Pointer. Age ranged from 1.6-11.8 years [M±STDEV=5.6±3.4] and bodyweight from 6.8-36 kg [M±STDEV=28.0±9.8].

Dolichocephalic group: 1 each of the following breeds: Belgian shepherd (12.6 years, female), Scottish deerhound (4 years, male), GSD (3.5 years, female) and Greyhound (9.5 years, female).

3.2.2 Establishing a new parameter for defining head phenotype

In order to validate olfactory bulb angulation and orientation as a new parameter for defining head phenotype, the following steps needed to be performed first:

- Establishing what the olfactory bulb fissure is
- Defining the technique to determine angulation and orientation of the olfactory bulb

3.2.2.1 Identification of the olfactory bulb fissure

639 images from 261 individual dogs representing a wide spectrum of different breeds were evaluated to identify the olfactory bulb fissure. This included 328 midline sagittal and 311 dorsal plane images. The olfactory bulb fissure was subsequently described and defined as the groove that separated the olfactory bulb from the rest of the brain.

3.2.2.2 Defining the angulation and orientation of the olfactory bulb

To establish whether the angulation and orientation of the olfactory bulb could be measured, 37 dogs from three breeds according to the arbitrary control classification as being representative of brachy-, mesati- and dolicephalic head shapes: (15 CKCSs, 14 Cocker spaniels and 8 GSDs). These dogs were aged between 1.6-17 years [M±STDEV=5.4±3.8], each group contained female and male dogs [female = 11 and male = 26], and bodyweight was between 4-43kg [M±STDEV=20.2±16.7]. The methodology to define the angulation and the orientation of the olfactory bulb are described in Chapter 2.

Following this, two studies were then performed to define the angle of the olfactory bulb associated with each head type.

Study OB1:

Using the 48 dogs from the control classification (Section 3.2.1) the angulation and the orientation of the olfactory bulb were measured [see Chapter 2 for further details] and tested using Methods 1 and 2.

Study OB2:

Once the methodology was validated in Study OB1, the same criteria were measured in a larger cohort of dogs. Eighty-two dogs were grouped using the arbitrary control classification into the following head phenotypes: brachycephalic, 19 dogs (4 female and 15 male); mesaticephalic, 38 dogs (18 female and 20 male); and dolichocephalic, 25 dogs (13 female and 12 male).

Brachycephalic group: 9 boxers, 4 Yorkshire terriers, 2 Shih-tzus and one each of the following breeds: Border terrier, Boston terrier, Maltese terrier and CKCS. Age ranged from 1.1-10.8 years [M±STDEV=5.5±2.9], bodyweight from 2.7-32kg [M±STDEV=18±13.4].

Mesaticephalic group: 13 Labrador retrievers, 6 springer spaniels, 5 Golden retrievers, 2 German shorthaired pointers, 2 Huskies, 2 Miniature schnauzers, 2 Pointers, 2 Poodles and one each of the following breeds: Alaskan malamute, Beagle, Hungarian vizsla and Giant schnauzer. Age ranged from 1-13.8 years [M±STDEV=6.7±3.7], bodyweight from 6.8-57kg [M±STDEV=26.5±8.9].

Dolichocephalic group: Including 8 Border collies, 7 GSDs, 4 Dalmatians, 2 Gordon setters and one each of the following breeds: Basset hound, Greyhound, Dobermann pincher and Rough collie. Age ranged from 1.11-17 years [M±STDEV=6.3±4.3], bodyweight from 13.5 to 43kg [M±STDEV=27.2±9.4].

3.2.3 Effect of head phenotype on the rostral, middle and caudal fossae areas of the cranial cavity

Once the head phenotype was defined using the Evans index and olfactory bulb angulation, two studies were performed to investigate the effect of the head phenotype on the cranial fossae:

Study F1: Are the midline areas of the cranial fossae influenced by head phenotype (as determined using the Evans index)?

The control group of 48 dogs were used to determine if there was a correlation between the Evans index and the midline area of the entire cranial fossa and its different parts (see Chapter 2 for further details of the techniques used). Using Method 2 [the best cut-off points of the Evans index, as defined on the basis of the results of Section 3.2.1]; the dogs were classified as brachycephalic, mesaticephalic or dolichocephalic.

Study F2: Are the midline areas of the cranial fossae influenced by head phenotype (as determined by angulation of the olfactory bulb)?

To examine if there was a relationship between olfactory bulb angulation and the midline area of the cranial fossae, the OB1 and OB2 groups were combined to give a total population of 130 dogs and the results were tested using Method 2.

3.2.4 Olfactory bulb linear dimensions

The olfactory bulb width, length (1-3) and height were measured then corrected for brain area and the olfactory bulb index was also defined [as a ratio between the width and the length of the olfactory bulb on dorsal plane of MRI]. The corrected olfactory bulb dimensions and index were compared according to head conformation, age and gender as described below:

3.2.4.1 Effect of head conformation

MR images in two planes were required for evaluation. 102 dogs were included, representing a variety of breeds.

Study OD1 (arbitrary classification):

Brachycephalic: 28 dogs [8 female and 20 male], bodyweight ranged from 4-32kg [M±STDEV=15.2±12.2], age ranged from 0.3-15.9 years [M±STDEV=5.4±4.1]. The group was composed of the following breeds: 15 CKCS, 9 Boxers, 3 Bichon frises and one American bulldog.

Mesaticephalic: 45 dogs [19 female and 26 male], bodyweight ranged from 13.3-33kg [M±STDEV=24.8±7.7], age range 0.8-15.3 years [M±STDEV=6.6±3.8]. The following breeds were included: 16 Labrador retrievers, 14 Cocker spaniels, 6 Golden retrievers, 3 Alaskan malamutes, 2 Beagles, 2 Hungarian viszlas and 2 Huskies.

Dolichocephalic: 29 dogs [12 female and 17 male], bodyweight ranged from 13.5-43kg [M±STDEV=26.2±11.1], age ranged from 0.7-17 years [M±STDEV=6.8±4.7]. The following breeds were included: 16 Border collies, 9 GSDs, 2 Gordon setters, 1 Greyhound and 1 Doberman pincher.

Study OD2:

The same dogs as were included in study OD1 were reclassified into brachycephalic, mesaticephalic and dolichocephalic groups using Method 2.

3.2.4.2 Effect of age

Study OD3:

This sought to evaluate the effect of age on the corrected linear dimensions of the olfactory bulb and the olfactory bulb index in three sentinel breeds, selected to represent three head phenotypes. 38 dogs were included, comprising 15 CKCS, 14 Cocker spaniels and 9 GSDs. Age ranged from 0.25-17years. Each group contained female and male dogs.

3.2.4.3 Effect of gender

Study OD4:

To examine the influence of gender on the corrected linear dimensions of the olfactory bulb and the olfactory bulb index in 47 dogs from three sentinel breeds selected to represent the three head phenotypes: CKCS, 15 dogs (6 female and 9 male), age [M±STDEV=5.2 years ±4.3], bodyweight [M±STDEV=6.4kg ±2.03]; Labrador retriever, 16 dogs (7 female and 9 male), age [M±STDEV=7.7 years ±3.8], bodyweight [M= 31.03kg ±2.3]; Border collie, 16 dogs (7 female and 9 male) age [M±STDEV=7.3 years ±4.9], bodyweight of [M±STDEV=17.4kg ±3.6].

3.3 Results

3.3.1 Defining head phenotype using the Evans index

Control: Due to the small numbers in the dolichocephalic group, the data did not pass the normality test so a non-parametric ANOVA test was used for comparison among the three head phenotypes. The results of the non-parameteric ANOVA test of the Evans index values demonstrated a highly significant difference (P<0.0001) between the three different head phenotype (Figure 3-2), however by using a post comparison test the real difference was shown to only be apparent between the brachycephalic group and both the mesaticephalic and dolichocephalic groups. Using the Stockard index to define brachycephalic, mesaticephalic and dolichocephalic head phenotypes, a similar significant difference was demonstrated as had been shown using the Evans index (Figure 3-2). These breeds were then redistributed according to Evans index *average* published in 1964 (Figure 3-3A and Table 3-1) and according to the arbitrary grouping (Figure 3-3B).

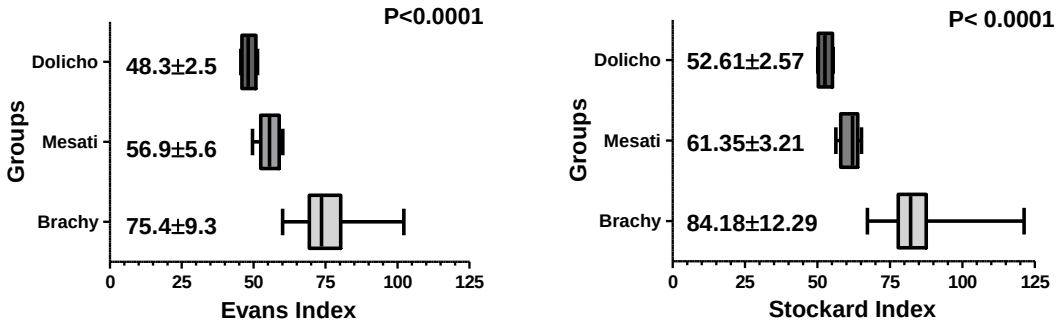

Figure 3-2: A horizontal Box and Whiskers plot (min-max) demonstrating the average with the standard deviation a significant difference in the Evans and Stockard index values for the arbitrary control brachycephalic (n=36), mesaticephalic (n=8) and dolichocephalic (n=4) groups, and showing the average and the standard deviation of each group as determined on the basis of MR images

Evans index	**Brachycephalic (≥81)**	**Mesaticephalic**		**Dolichocephalic (≤39)**
		(80-52)	**(51-40)**	
Breed				
Pug	▌▌			
Chihuahua	▌▌			
Boston terrier	▌			
Shih-tzu	▌▌▌	▌		
CKCSs		▌▌▌▌▌▌▌▌▌▌▌▌▌		
Lhasa apso		▌▌▌		
Boxer		▌▌▌▌		
Bichon frise		▌		
Staffordshire bull terrier		▌		
Mastiff		▌		
WHWT		▌▌		
Labrador retriever		▌▌▌▌		
Miniature schnauzer		▌		
English springer spaniel		▌		
Pointer		▌		
Scottish deerhound			▌	
Greyhound			▌	
Giant schnauzer			▌	
GSD			▌	
Belgian shepherd			▌	

Table 3-1: Classification of individual dogs into brachycephalic, mesaticephalic and dolichocephalic groups according to the published average Evans index (1964)

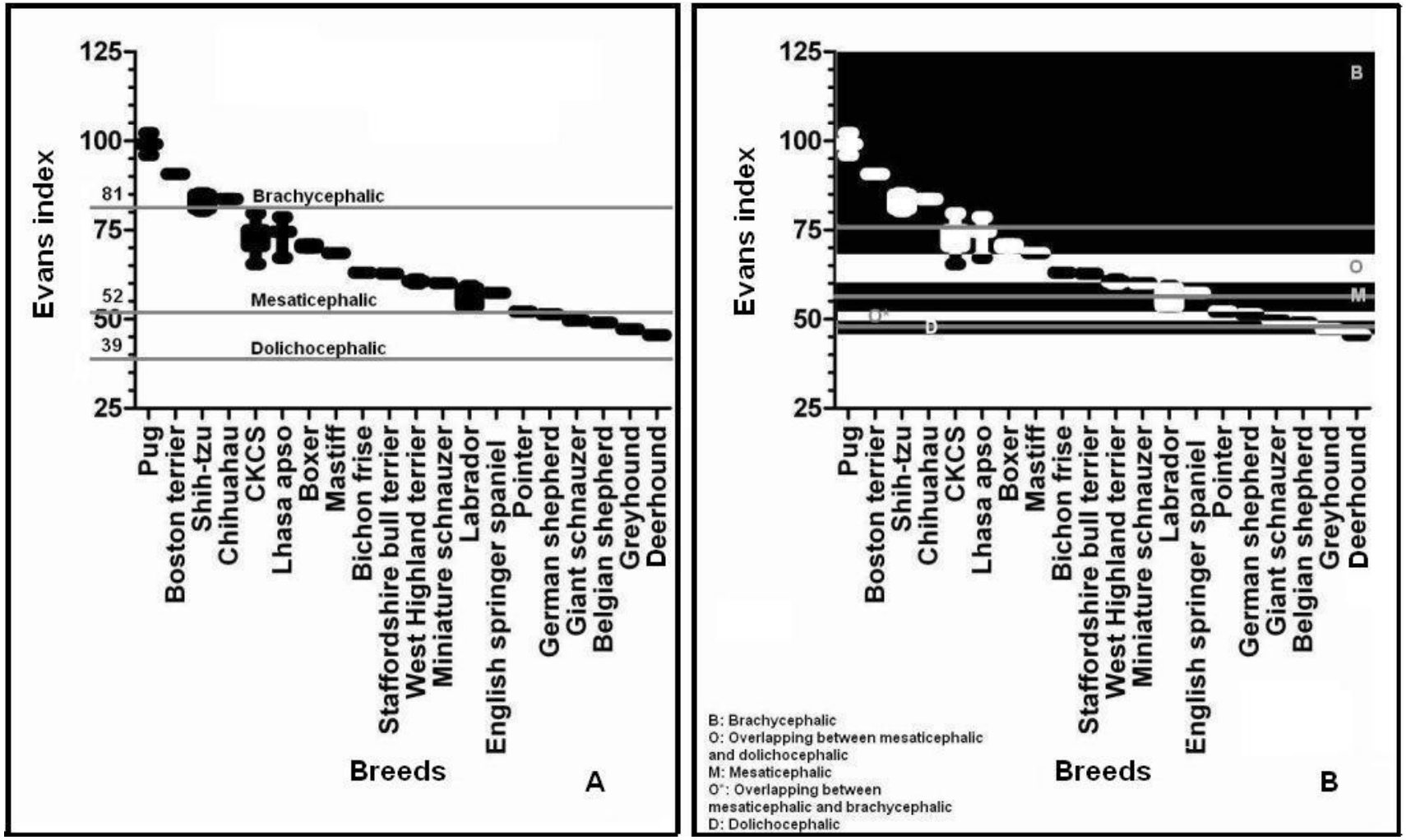

Figure 3-3: Two scatter graphs (with average index and standard deviation of each breed) revealing the distribution of dog breeds according to (A) Evans index average values published in 1964 and (B) control - arbitrary assignment

Method 1: The range of Evans index values for each group was then defined according to the Lower & Upper 95% confidence interval (CI) of the mean (in Table 3-2). Based on the Lower & Upper 95% CI of the mean for each group, dogs with an Evans index ≥72.17 were considered more likely to be brachycephalic, while mesaticephalic and dolichocephalic Evans index values were defined as 52.58-61.14 and ≤52.26 respectively. The control breeds were then re-distributed into brachycephalic, mesaticephalic and dolichocephalic groups, and an *in-between 1* group situated between the brachycephalic (≥72.17) and mesaticephalic (≤61.14) groups (Table 3-3).

	Brachycephalic	**Mesaticephalic**	**Dolichocephalic**
Lower 95% CI of mean	72.17	52.58	44.27
Upper 95% CI of mean	78.59	61.14	52.26

Table 3-2: The Lower & Upper 95% CI of the mean Evans index values for the brachycephalic, mesaticephalic and dolichocephalic groups

Dog breed	Brachycephalic	*In-between 1*	Mesaticephalic	Dolichocephalic
Chihuahua	▌▌			
Shih-tzu	▌▌▌			
Pug	▌▌			
Boston terrier	▌			
Lhasa apso	▌▌	▌		
CKCS	▌▌▌▌▌▌▌▌▌▌	▌▌▌▌		
Boxer		▌▌▌▌		
Staffordshire bull terrier		▌		
Bichon frise		▌		
Mastiff		▌		
WHWT		▌▌		
Labrador retriever			▌▌▌▌	
English springer spaniel			▌	
Miniature schnauzer			▌	
Giant schnauzer				▌
Pointer				▌
Belgian shepherd				▌
GSD				▌
Greyhound				▌
Scottish deerhound				▌

Table 3-3: Classification of breeds according to the Lower & Upper 95% CI of the mean Evans index values into brachycephalic, mesaticephalic and dolichocephalic groups and a further group (the *in-between 1* group) representing the range of values between the brachycephalic and mesaticephalic groups

Method 2: The second method for determining the ranges of Evans index values that defined brachycephalic, mesaticephalic and dolichocephalic head phenotypes was to examine the Evans index values of each group using a ROC curve test. The ideal cut-off point of the Evans index between each two adjacent groups was chosen to provide the highest probable sensitivity and specificity. The best cut-off value between the brachycephalic and mesaticephalic groups using this method was defined as <60.7; i.e. an Evans index value equal to or greater than 60.7 would indicate that a dog was more likely to fall within the brachycephalic group (Table 3-4 & Figure 3-4A). The best cut-off point between the mesaticephalic and dolichocephalic groups was <51.7; i.e. a dog with an Evans

index value of <51.7 was more likely to fall within the dolichocephalic group (Table 3-4 & Figure 3-4B). According to these cut-off points, the mesaticephalic group had an Evans index value range of 51.7-60.6. On the basis of these defined best cut-off points the different breeds were reclassified again according to their measured Evans index values as brachycephalic, mesaticephalic and dolichocephalic in order to define the actual head shape (Table 3-5).

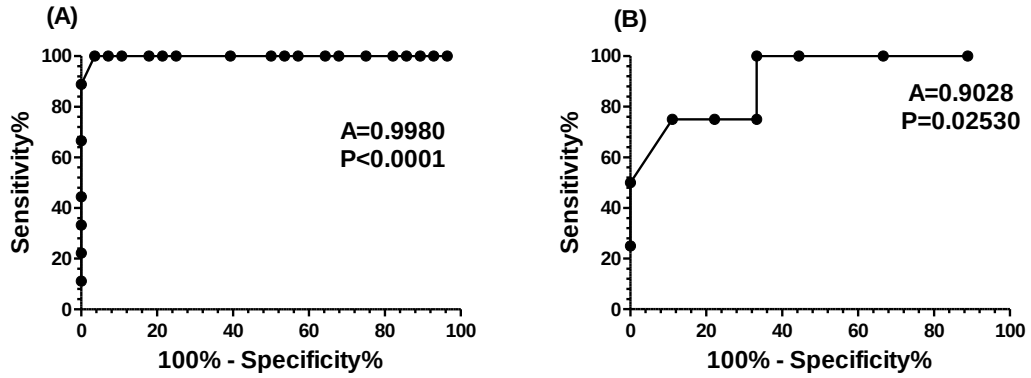

Figure 3-4: Non linear regression graphs representing the ROC curve findings of the Evans index values between the (A) brachycephalic and mesaticephalic, and (B) mesaticephalic and dolichocephalic groups

The cut-off point of the Evans index values between the brachycephalic and mesaticephalic groups			
<60.7	Brachycephalic	Mesaticephalic	Total
Brachycephalic	35	1	36
Mesaticephalic	0	8	8
Total	35	9	44
The cut-off point of the Evans index values between the mesaticephalic and dolichocephalic groups			
<51.7	Mesaticephalic	Dolichocephalic	Total
Mesaticephalic	7	1	8
Dolichocephalic	0	4	4
Total	7	5	12

Table 3-4: The best cut-off point for the Evans index in order to differentiate between the brachycephalic and mesaticephalic groups, and between the mesaticephalic and dolichocephalic groups, originating from the arbitrary control classification

Dog breed	Brachycephalic	Mesaticephalic	Dolichocephalic
CKCS	▌▌▌▌▌▌▌▌▌▌▌▌▌		
Boxer	▌▌▌▌		
Shih-tzu	▌▌▌▌		
Lhasa apso	▌▌		
Chihuahua	▌▌		
Pug	▌▌		
Bichon frise	▌		
Staffordshire bull terrier	▌		
Boston terrier	▌		
Mastiff	▌		
WHWT	▌	▌	
Labrador retriever		▌▌▌▌	
Miniature schnauzer		▌	
English springer spaniel		▌	
Pointer		▌	
Belgian shepherd			▌
Scottish deerhound			▌
Greyhound			▌
Giant schnauzer			▌
GSD			▌

Table 3-5: Reclassification of individual breeds based on the best cut-off points between brachycephalic (<60.5) and mesaticephalic and between mesaticephalic and dolichocephalic (<51.7) groups determined using ROC curve test

The Evans index demonstrated no overlap in the range of values defining brachycephalic, mesaticephalic or dolichocephalic when Method 1 was applied [the Lower and Upper 95% CI of the mean], while overlap was evident when the Evans index values of arbitrary control and Method 2 were used (Figures 3-5 & 3-6).

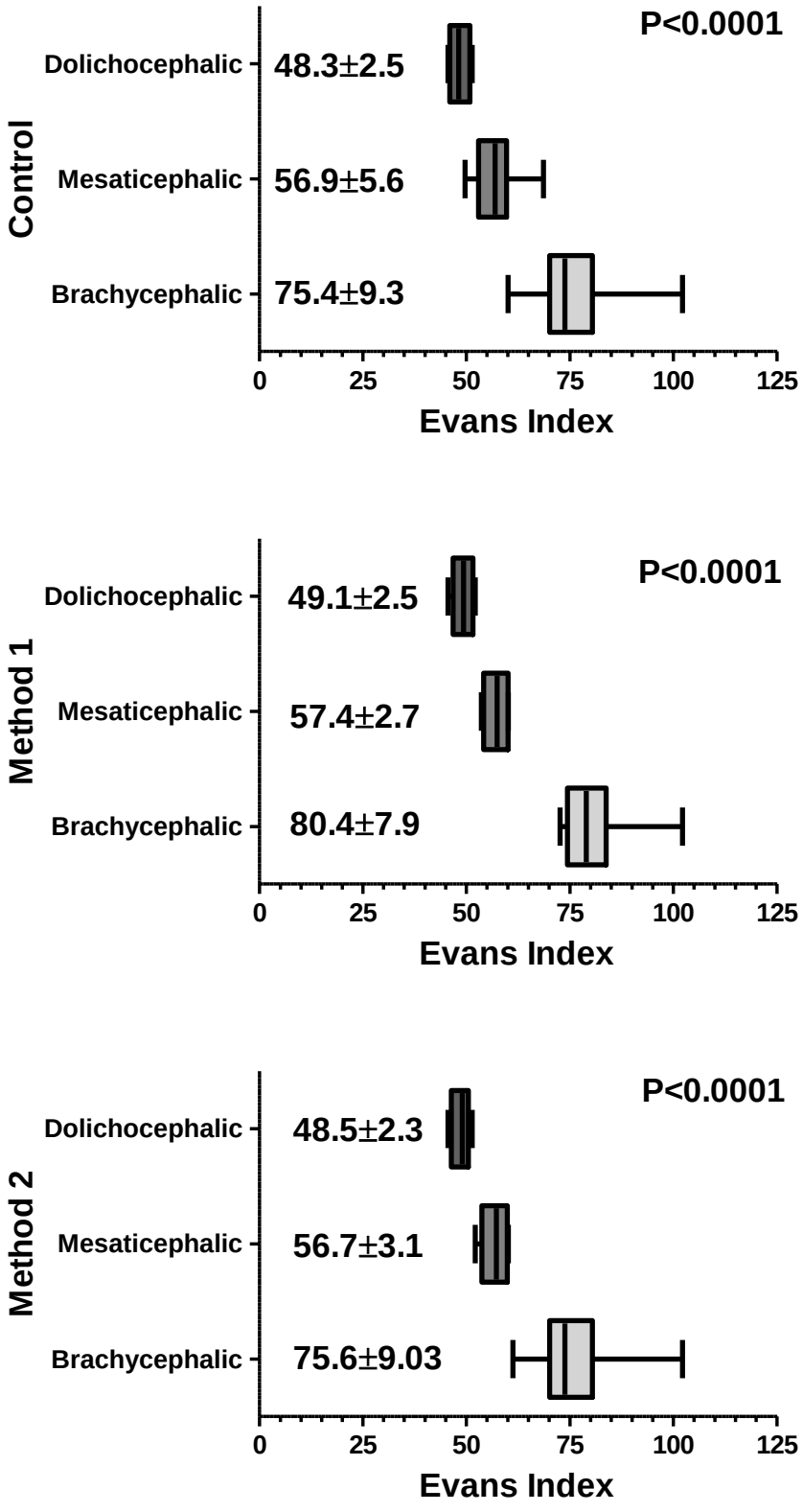

Figure 3-5: Horizontal box and whiskers plots demonstrating the Evans index (M±SDEV) values for brachycephalic, mesaticephalic and dolichocephalic dogs, classified according to the three different methods: arbitrary control and Methods 1 & 2 of Evan index values

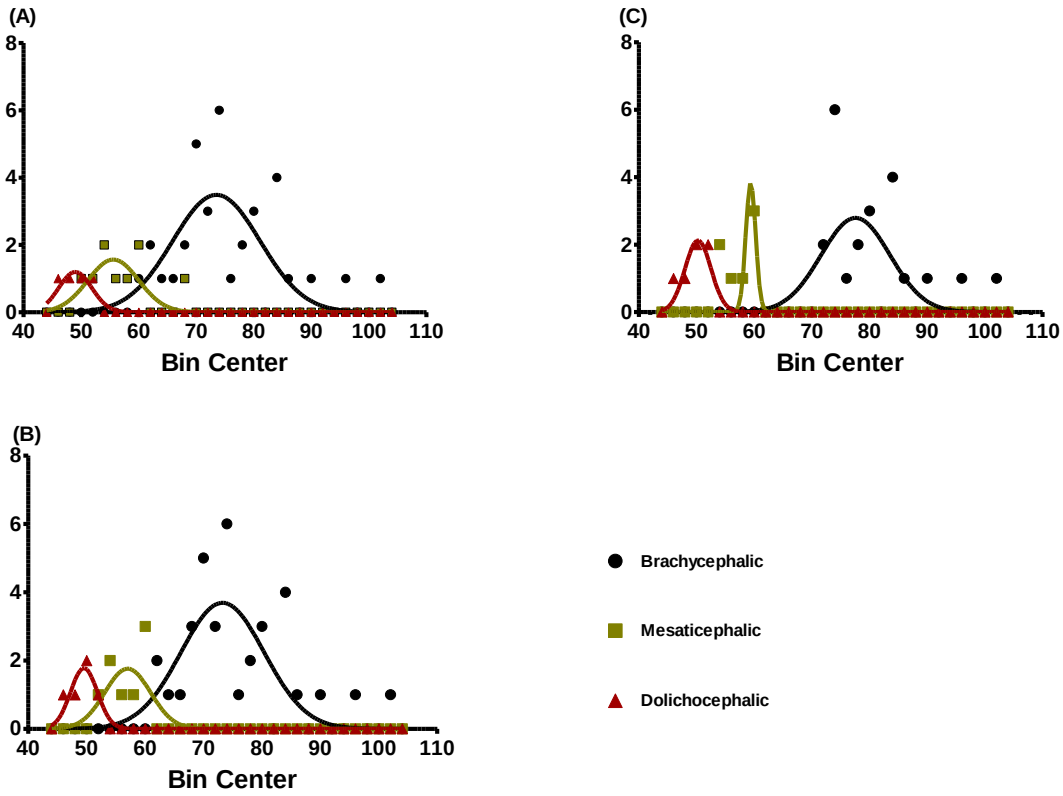

Figure 3-6: Three non-linear regression graphs representing the distribution of Evans index values for brachycephalic, mesaticephalic and dolichocephalic groups of dogs, classified using the arbitrary control (A), Methods 1 (B) & Method 2 (B)

3.3.2 Olfactory bulb angulation and orientation parameters for defining head phenotype

3.3.2.1 Identification and descriptive appearance of the olfactory bulb fissure

The olfactory bulb fissure was identified grossly (Figures 3-7 & 3-8) and on MRI (Figures 3-9 & 3-10), as defined in 3.2.2.2. 328 T1 and T2-weighted midline sagittal images were available for review and from these the olfactory bulb was identified in 309 images (94%). It appears as a hypointense line on T1w and hyperintense line on T2w. Within this group of 309 midline sagittal images, the olfactory bulb fissure was recognised in 97% of the T2-weighted images, and in 83% the T1-weighted images. The olfactory bulb fissure was identified in 282 images from the total 311 dorsal plane images available (91%). Within these 282 plane images, the olfactory bulb fissure was identified in 86% of the available T1-weighted images and 95% of the T2-weighted images.

The olfactory bulb fissure was more readily identified on T2-weighted than T1-weighted MR images (96% and 85% respectively. (Table 3-6 and Figures 3-9 & 3-10).

	Midline sagittal	Dorsal	Total
T1	83% (59/71)	86% (127/147)	85% (186/218)
T2	97% (250/257)	95% (155/164)	96% (405/421)
Total	94% (309/328)	91% (282/311)	93% (591/639)

Table 3-6: The total number of MR images reviewed and the proportion and percentage of these where the olfactory bulb fissure could be recognised on T1 and T2-weighted images in the midline sagittal and dorsal planes

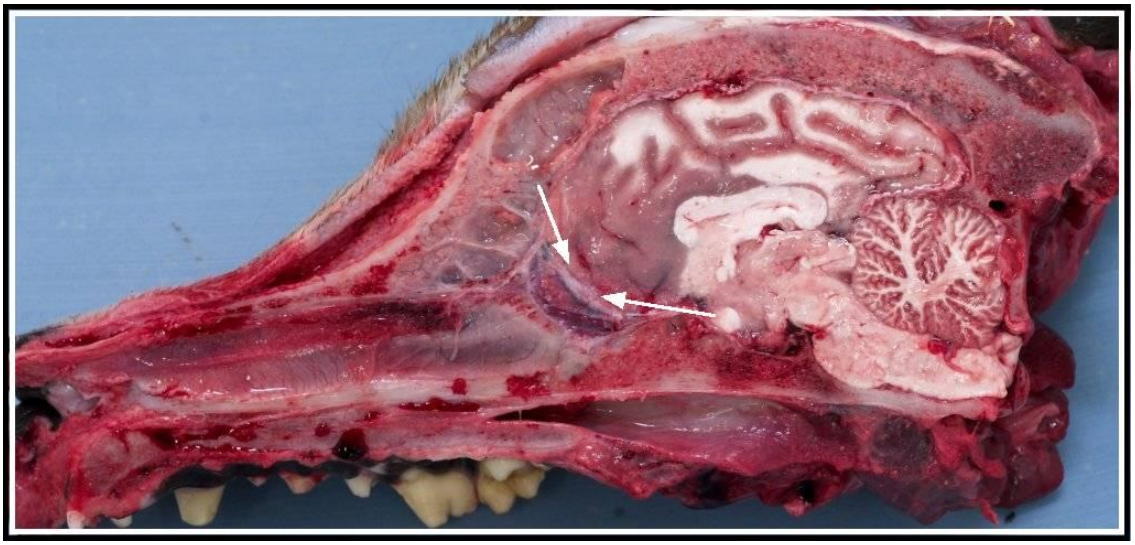

Figure 3-7: Fresh gross midline section through the canine head allowing identification of the olfactory bulb fissure (white arrows) following gross dissection

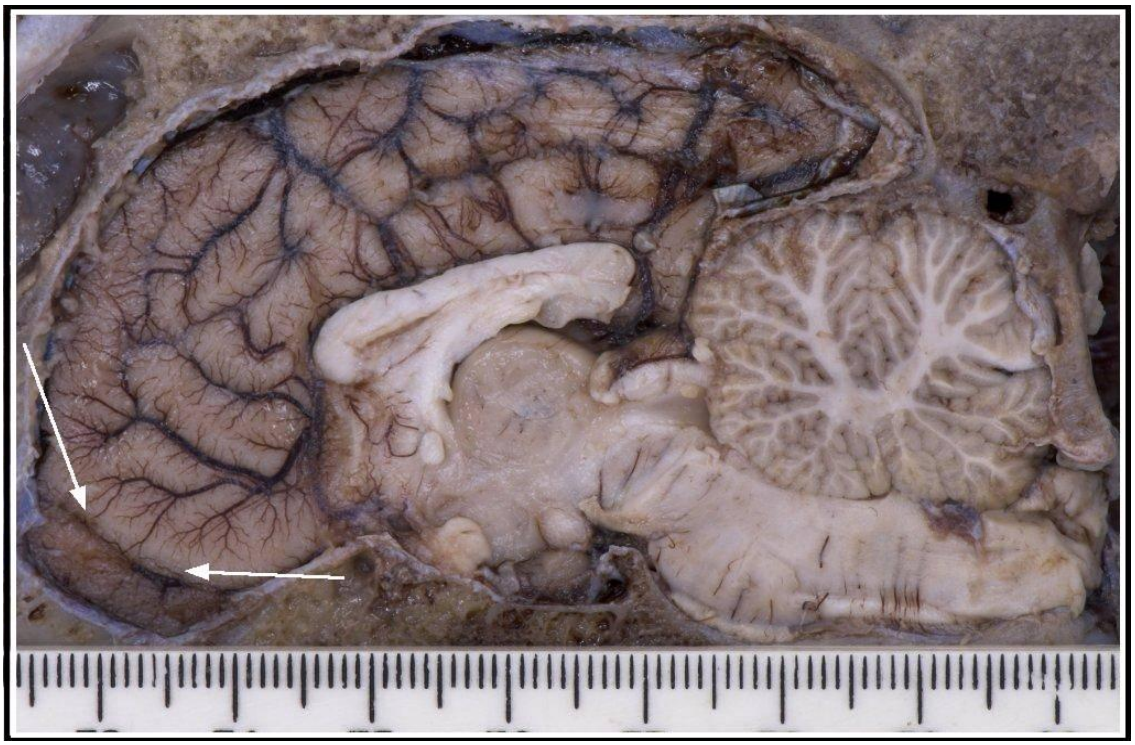

Figure 3-8: Gross midline formalin fixed section through the canine head identifying the olfactory bulb fissure (white arrows) following immersion in 10% formalin for seven days

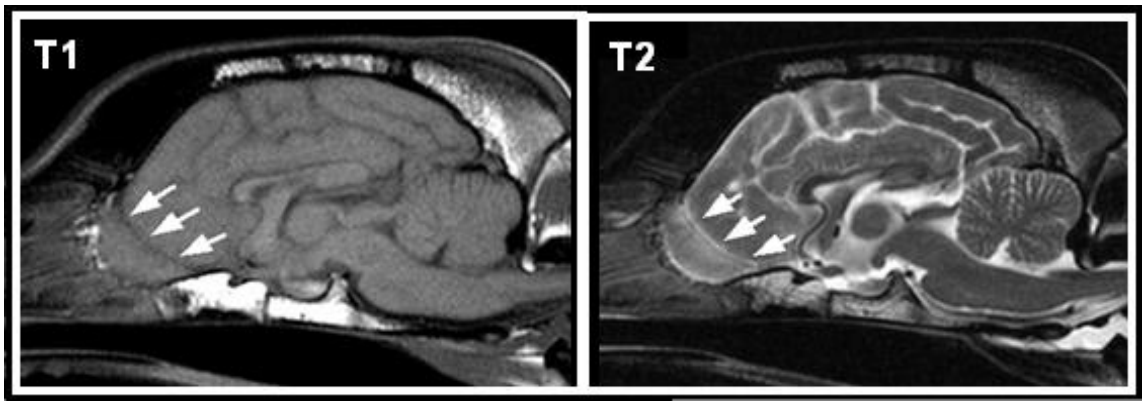

Figure 3-9: The olfactory bulb fissure (arrows), defined as the fissure that separates the olfactory bulb from the rest of the brain, as seen on midline sagittal plane T1 and T2-weighted MR images

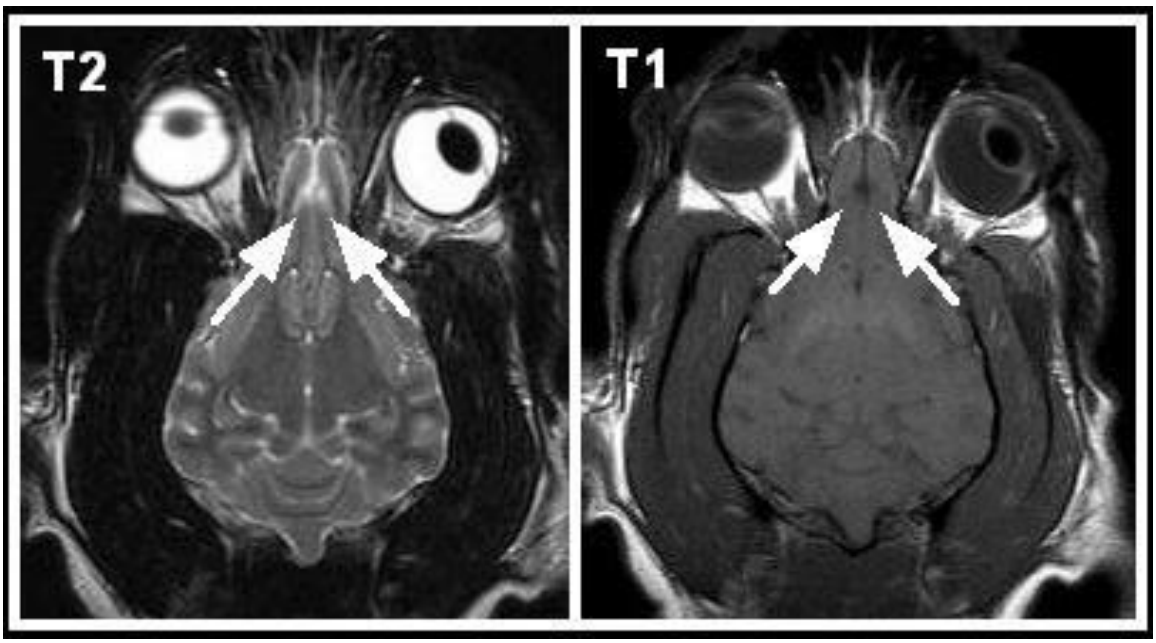

Figure 3-10: Dorsal plane T2 and T1-weighted MR images demonstrating the appearance of the olfactory bulb fissure, defined as a groove separating the olfactory bulb from the rest of the brain (arrows)

3.3.2.2 Validation of olfactory bulb angulation and orientation for determination of head phenotype

Comparison of the olfactory bulb angulation between the brachycephalic, mesaticephalic and dolichocephalic groups using one-way analysis of variance (ANOVA) demonstrated a significant difference ($P<0.0001$). The olfactory bulb orientation was also found to be more ventral (moving towards type-5) in the brachycephalic group (Figure 3-11), which was correlated with a smaller olfactory bulb angle. In the mesaticephalic and dolichocephalic groups, the olfactory bulb was more rostro-dorsally orientated (moving toward type-1) with a larger olfactory bulb angle (Table 3-7 and Figure 3-12).

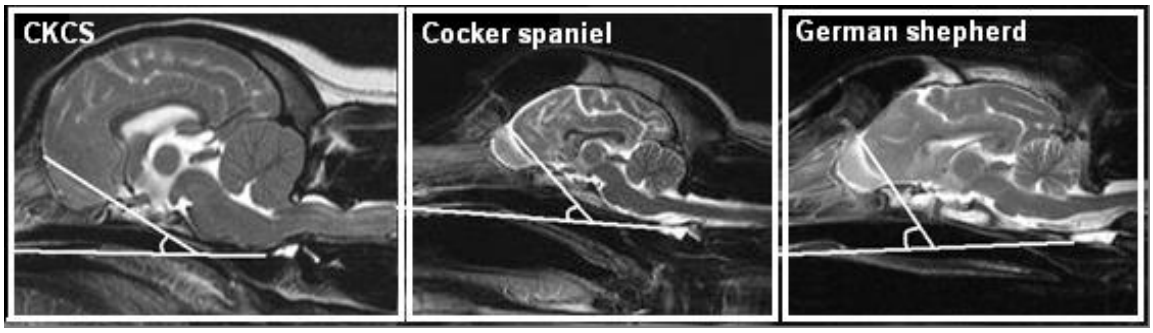

Figure 3-11: Midline sagittal T2 weighted MR images demonstrating the measurement of the olfactory bulb angle in the dog [the angle defined as the angle between the intersection of a straight line touching the dorsal and ventral points of the olfactory bulb fissure and the baseline- the line passing through the oral aspect of the hard palate rostrally and the intercondylar notch of the foramen magnum caudally]. The angle increases as the nose becomes longer, from the smallest angle on the left (CKCS) to the largest angle on the right in the German shepherd

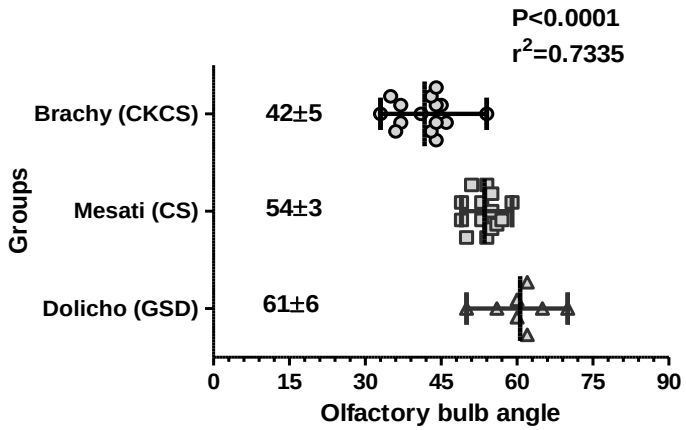

Figure 3-12: A horizontal scatter graph (with range) showing the average olfactory bulb angulation values and the standard deviation for the 3 groups of head phenotype

Dog type	No	Olfactory bulb angle range	Olfactory bulb angle (M±STDEV)	Orientation
Brachycephalic (CKCS)	15	30-54	42±5	Typ-5 & 4
Mesaticephalic (Cocker spaniel)	14	49-59	54±3	Type-4 & 3
Dolichocephalic (GSD)	8	50-70	61±6	Type-4 & 3

Table 3-7: The olfactory bulb angle range, mean & standard deviation and olfactory bulb orientation for the three groups of head phenotype

3.3.2.3 Olfactory bulb angulation as a new index for defining head phenotype

Study OB1:

When the Evans index values and the olfactory bulb angle values for the arbitrary control brachycephalic, mesaticephalic and dolichocephalic groups were compared, a significant negative correlation (P<0.0001) was identified (Figure 3-13). In other words, olfactory bulb angulation decreased with increasing degree of brachycephalia. Analysis to exclude the confounding effect of bodyweight (as brachycephalic breeds tended to be smaller breeds) demonstrated that the degree of olfactory bulb angulation was less affected by bodyweight than the head conformation (Figure 3-14).

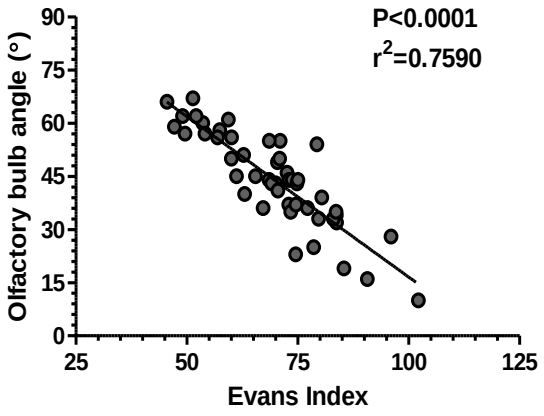

Figure 3-13: Linear regression plot demonstrating a significant negative correlation between olfactory bulb angulation and the Evans index in the arbitrary control group

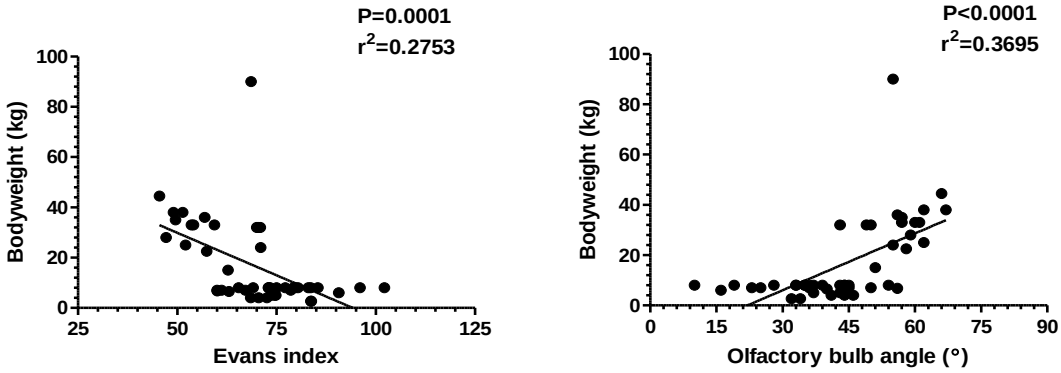

Figure 3-14: Linear regression plots showing a negative correlation between body weight and Evans index, and positive correlation between body weight and olfactory bulb angle in arbitrary control group

In order to assess the validity of olfactory bulb angulation for determining the head phenotype for each group when defined by the arbitrary control and Methods 1 & 2), it was first necessary to compare the measured olfactory bulb angles to actual Evans index values (Section 3.3.1). The purpose of this was to determine if the degree of brachycephalia was also associated with the degree of the olfactory bulb angulation for the range of Evans index values in each group. The range of olfactory bulb angle values was associated for the brachycephalic, mesaticephalic and dolichocephalic groups as defined using the arbitrary control group and the Evans index values according to Methods 1&2 (Table 3-8 and Figures 3-15-18).

	Dog type	**No. of dogs**	**Evans index**	**Olfactory bulb angle**
Control	Brachycephalic	36	M±STDEV= 75.2±9.3 R= 60-102	M±STDEV= 39±11 R= 10-55
	Mesaticephalic	8	M±STDEV= 55.4±3.7 R= 49.6-60.1	M±STDEV=58±2 R= 56-62
	Dolichocephalic	4	M±STDEV= 48.3±2.5 R= 45.5-51.4	M±STDEV= 64±4 R= 59-67
Method 1	Brachycephalic	22	≤ 72.17	M±STDEV=34±11 R= 10-54
	Mesaticephalic	7	R= 52.58-61.14	M±STDEV=57±4 R= 50-61
	Dolichocephalic	6	≥ 52.26	M±STDEV= 62±4 R= 57-67
Method 2	Brachycephalic	35	≤ 60.8	M±STDEV=38±11 R= 10-55
	Mesaticephalic	8	R=51.7-60.7	M±STDEV= 58±4 R= 50-62
	Dolichocephalic	5	≥ 51.6	M±STDEV= 62±4 R= 57-67

Table 3-8: The average, standard deviation and range of the olfactory bulb angles in dogs classified as brachycephalic, mesaticephalic and dolichocephalic according to arbitrary control and Methods 1 and 2

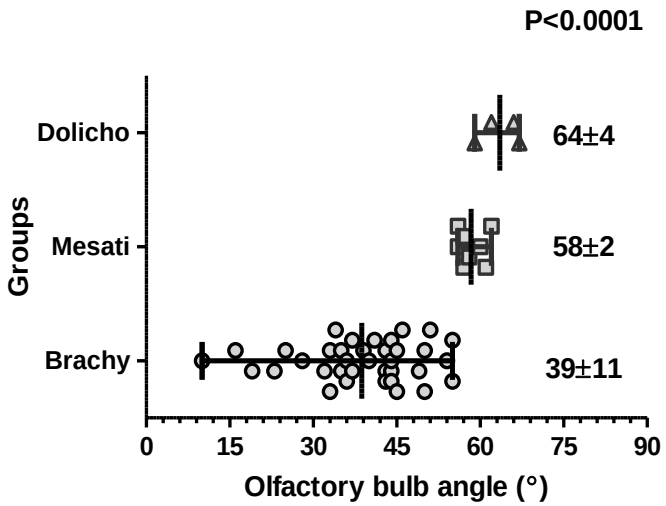

Figure 3-15: A horizontal scatter plot showing the range of olfactory bulb angle values (with M±STDEV) for each of the three head phenotypes within the arbitrary control group

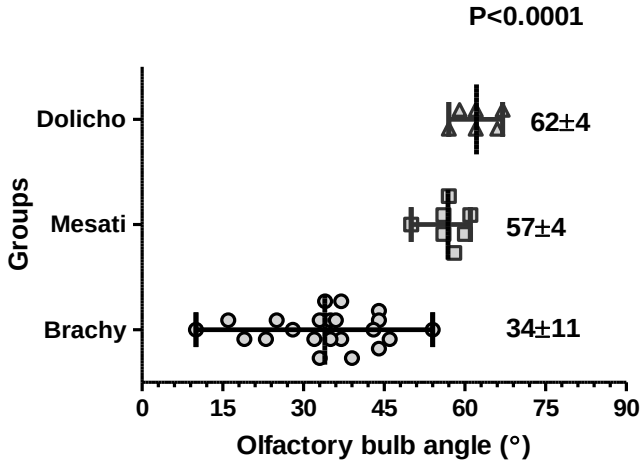

Figure 3-16: A horizontal scatter plot showing range of the olfactory bulb angles values (with M±STDEV) for each of the three head phenotypes: brachycephalic using the Lower & Upper 95% CI of the mean of the Evans index values (Method 1)

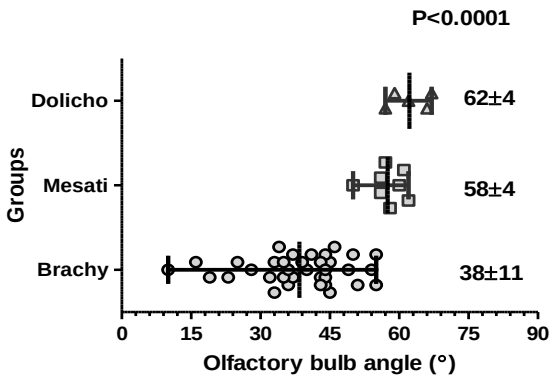

Figure 3-17: A horizontal scatter plot showing range of the olfactory bulb angles values (with M±STDEV) for each of the three head phenotypes defined using the best cut-off point of the Evans index values (Method 2)

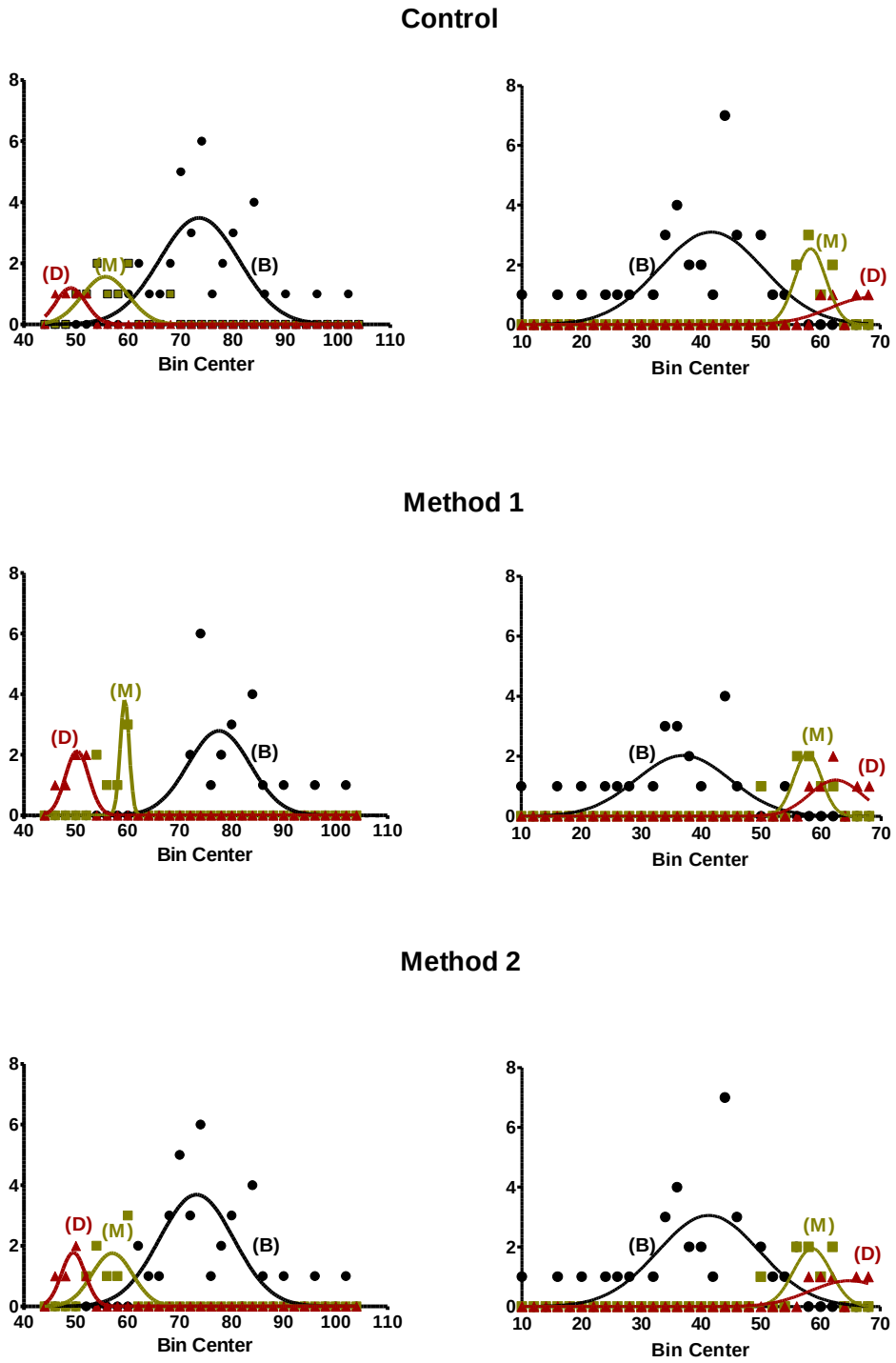

Figure 3-18: Non-linear regression graphs (frequency distribution histograms) representing the distribution of the values of the Evans index (left column) and the angulation of the olfactory bulb (right column) for the three head groups as defined using arbitrary control, Methods 1&2 [B-brachycephalic, M-mesaticephalic and D-dolichocephalic]

The Lower & Upper 95% CI of the mean of the olfactory bulb angles was then calculated (Table 3-9) for the arbitrary control group (Method 1) demonstrated that dogs with an olfactory bulb angle of ≤42° could be defined as brachycephalic. The mesaticephalic group

fell into the range of 56-60°, while the dolichocephalic group was ≥58°. An overlap was evident between the values for the mesaticephalic and dolichocephalic groups for olfactory bulb angulation at the first pass.

	Brachycephalic	Mesaticephalic	Dolichocephalic
Lower 95% CI of mean	39°	56°	58°
Upper 95% CI of mean	42°	60°	69°

Table 3-9: The Lower & Upper 95% CI of the Mean for olfactory bulb angulation for the brachycephalic, mesaticephalic and dolichocephalic groups in the arbitrary control group

To obviate the overlap, the range of each group was adjusted so that the following data could be used to define head phenotype:

1. Brachycephalic ≤42°
2. Mesaticephalic 56-57°
3. Dolichocephalic ≥61°

The dogs that fell between brachycephalic and mesaticephalic were grouped as ***In-between 1***, while those that fell between mesaticephalic and dolichocephalic were named ***In-between 2***.

Based on these ranges calculated using Method 1, dogs were re-distributed according to their olfactory bulb angulations into brachycephalic, mesaticephalic and dolichocephalic groups (Figure 3-19 and Table 3-10).

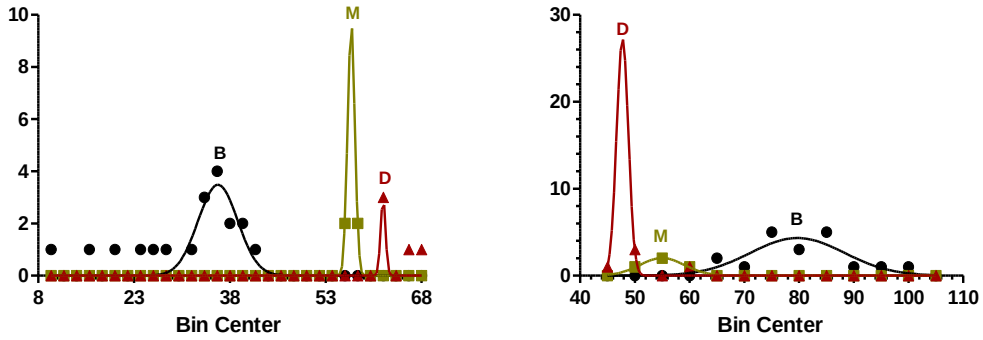

Figure 3-19: Non-linear regression graphs (frequency distribution histograms) demonstrating the distribution of olfactory bulb angulation values in three head phenotypes as defined using Lower & Upper 95% CI of mean for the olfactory bulb angulation (left) and then on the right, the Evans index values of these animals using the olfactory bulb angulation grouping (Method 1)

Dog breed	Brachy-	*In-between 1*	Mesati-	*In-between 2*	Dolicho-
Shih-tzu	▌▌▌▌				
Lhasa apso	▌▌▌				
Chihuahua	▌▌				
Pug	▌▌				
Boston terrier	▌				
Bichon frise	▌				
CKCS	▌▌▌▌▌▌	▌▌▌▌▌▌▌▌▌			
Boxer		▌▌▌▌			
WHWT		▌▌			
Mastiff		▌			
Staffordshire bull terrier		▌			
Miniature schnauzer			▌		
Giant schnauzer			▌		
Labrador retriever			▌▌	▌	▌
English springer spaniel				▌	
Greyhound				▌	
Belgian shepherd					▌
Pointer					▌
GSD					▌
Scottish deerhound					▌

Table 3-10: The distribution of breeds according to the Lower & Upper 95% CI of the Mean for olfactory bulb angulation values into brachycephalic (≤42°), *In-between 1* (43-55°), mesaticephalic (56-57°), *In-between 2* (58-60°) and dolichocephalic (≥61°) groups

Selection of the best cut-off points (Method 2) for the probable highest sensitivity and specificity (Figure 3-20 & Table 3-11), resulted in the following range of values for each head phenotype group:

1. Brachycephalic group ≤55°
2. Mesaticephalic group 56-61°
3. Dolichocephalic group ≥62°

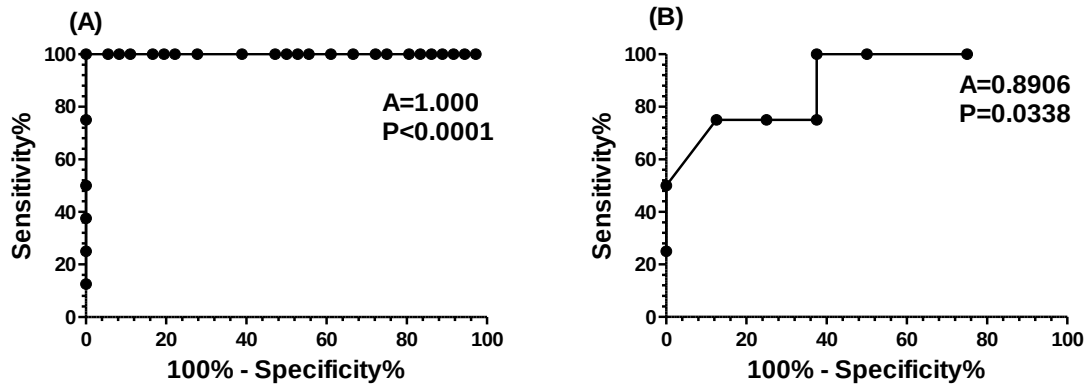

Figure 3-20: Non-linear regression graphs showing the sensitivity and specificity of the angulation of the olfactory bulb using a ROC curve test to determine the best cut-off point between (A) brachycephalic and mesaticephalic, and (B) mesaticephalic and dolichocephalic

The cut-off point of the olfactory bulb angle between brachycephalic and mesaticephalic			
> 56°	Brachycephalic	Mesaticephalic	Total
Brachycephalic	36	0	36
Mesaticephalic	0	8	8
Total	36	8	44
The cut-off point of the olfactory bulb angle between mesaticephalic and dolichocephalic			
> 62°	Mesaticephalic	Dolichocephalic	Total
Mesaticephalic	7	1	8
Dolichocephalic	1	3	4
Total	8	4	12

Table 3-11: The best cut-off point for olfactory bulb angulation in order to differentiate between the brachycephalic and mesaticephalic groups, and between the mesaticephalic and dolichocephalic groups

Based on these olfactory bulb ranges calculated using Method 2, dogs were re-distributed according to their calculated olfactory bulb angulations into brachycephalic, dolichocephalic and mesaticephalic groups (Table 3-12 and Figure 3-21).

Dog breeds	Brachycephalic	Mesaticephalic	Dolichocephalic
CKCS	▌▌▌▌▌▌▌▌▌▌▌▌		
Boxer	▌▌▌▌		
Shih-tzu	▌▌▌▌		
Lhasa apso	▌▌▌		
Pug	▌▌		
Chihuahua	▌▌		
WHWT	▌▌		
Boston terrier	▌		
Bichon frise	▌		
Mastiff	▌		
Staffordshire bull terrier	▌		
Labrador retriever		▌▌▌▌	
Greyhound		▌	
Giant schnauzer		▌	
Miniature schnauzer		▌	
English springer spaniel		▌	
Belgian shepherd			▌
GSD			▌
Pointer			▌
Scottish deerhound			▌

Table 3-12: The distribution of the dog breeds with brachycephalic, mesaticephalic and dolichocephalic groups according to the best cut-off point values for olfactory bulb angulation

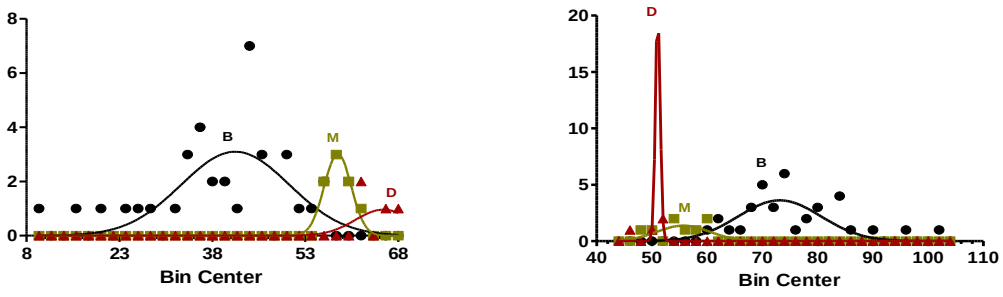

Figure 3-21: Non-linear regression plots (frequency distribution histograms) showing the distribution of the olfactory bulb angles (left) and Evans index values (right)in three head groups using Method 2

Dogs were also classified according to olfactory bulb orientation into Type-3, 4 and 5 to define the effect of the orientation of the olfactory bulb on the Evans index and olfactory bulb angulation values. A highly significant correlation (P<0.0001 for both) was evident when olfactory bulb orientation was compared with the Evans index and olfactory bulb angulation values (Figure 3-22 and Table 3-13).

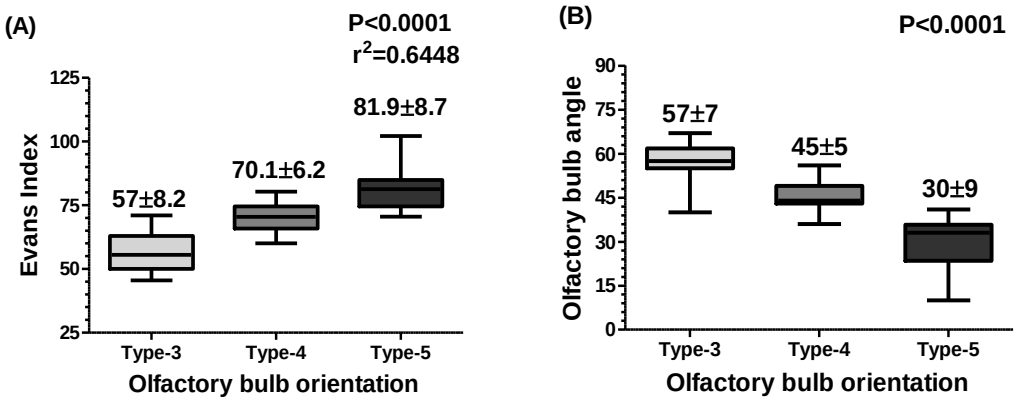

Figure 3-22: Vertical box and whiskers plots (with min-max values) revealing the differences between Evans index values (A) and olfactory bulb angulation values (B) for Type-3, 4 and 5 olfactory bulb orientation (n=16 for all three)

Olfactory bulb orientation	No. of dogs	Evans index values	Olfactory bulb angle values
Type-3	16	57±8.2	57±7°
Type-4	16	70.1±6.2	45±5°
Type-5	16	81.9±8.7	30±9°

Table 3-13: The correlation between the orientation of the olfactory bulb, Evans index values and the olfactory bulb angle in the arbitrary control group

Study OB2:

In this part of the study, the methodology developed in the previous part of the study (Study OB1) was evaluated in a larger cohort of dogs in order to refine the findings of the study. Dogs were classified into head phenotype groups using the arbitrary control and compared to olfactory bulb angulation and a significant difference (P<0.0001) was evident. However, consistent with the findings of Study OB1, the difference was only apparent between the brachycephalic group and the other two groups (Figure 3-23 & 3-24).

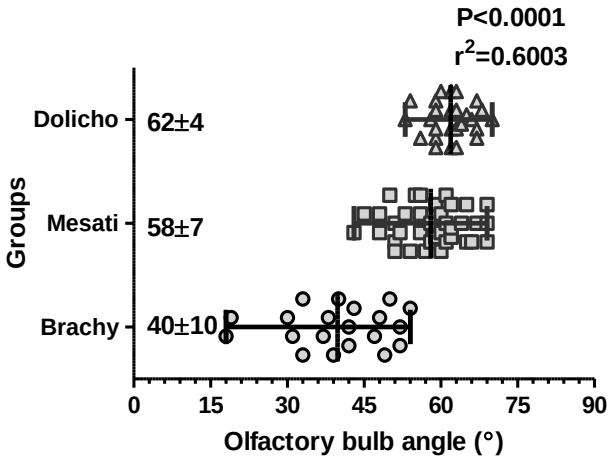

Figure 3-23: A horizontal scatter graph (with mean, range and standard deviation) demonstrating the difference in olfactory bulb angulation for the three head phenotype defined arbitrarily

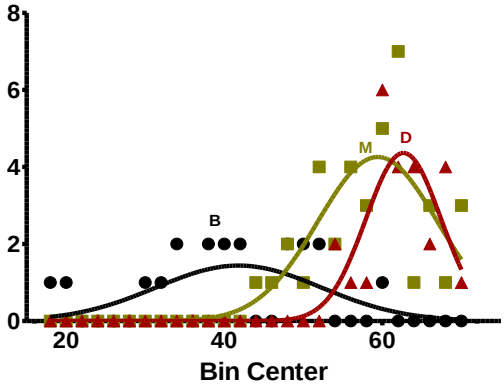

Figure 3-24: Non-linear regression graph (frequency distribution histogram) representing the distribution of olfactory bulb angle values for head phenotypes. Groups defined arbitrarily [B-brachycephalic, M-mesaticephaic and D-dolichocephalic]

Following this the Lower & Upper 95% CI of the Mean of the olfactory bulb was defined for each arbitrary group (Table 3-14, Figure 3-25). The brachycephalic group was found to have an olfactory bulb angle of ≤45°, the mesaticephalic group 56-60° and the dolichocephalic group ≥60°. As can be seen, an overlap was still present between the mesaticephalic and dolichocephalic groups. To reduce the overlap the range for these two groups was adjusted as follows (Table 3-14 & Figure 3-25):

1. Brachycephalic ≤ 45°
2. Mesaticephalic 56-59°
3. Dolichocephalic ≥ 61°

	Brachycephalic	Mesaticephalic	Dolichocephalic
Lower 95% CI of mean	35.03~35°	55.83-56°	60.09~60°
Upper 95% CI of mean	44.67~45°	60.22~60°	63.67~64°

Table 3-14: The Lower & Upper 95% CI of the Mean olfactory bulb angles (Method 1) for the three head phenotype defined arbitrarily

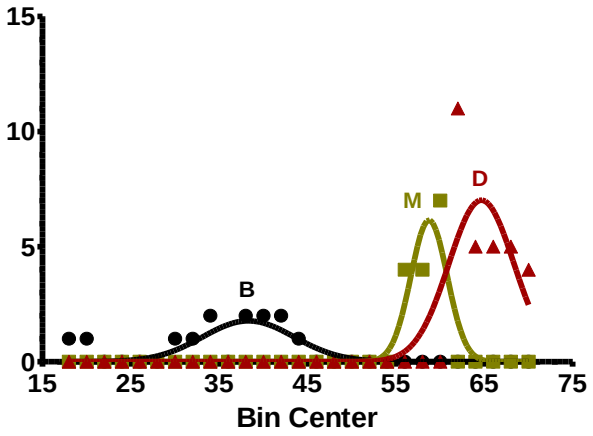

Figure 3-25: Non-linear regression graph (frequency distribution histogram) representing the distribution arbitrarily for brachycephalic (B), mesaticephalic (M) and dolichocephalic (D) head phenotypes classified according to the Lower & Upper 95% CI of the Mean of olfactory bulb angle values (Method 1)

Dog breeds were then redistributed using these results (Method 1) into brachycephalic, mesaticephalic and dolichocephalic groups, while dogs having olfactory bulb angle values outwith these ranges were defined as *in-between groups 1 and 2* (Table 3-15 & Figure 3-26).

Dog breed	Brachy	In-between 1	Mesati	In-between 2	Dolicho
Yorkshire terrier	▌▌▌▌				
Shih-tzu	▌▌				
Boston terrier	▌				
Maltese terrier	▌				
Border terrier	▌				
Poodle	▌		▌		
CKCSs	▌				
Boxer	▌▌	▌▌▌▌▌	▌		
Springer spaniel		▌▌▌▌			▌▌
Beagle		▌			
Greyhound		▌			
Miniature schnauzer		▌	▌		
Golden retriever		▌▌		▌	▌▌
GSD		▌			▌▌▌▌▌
Labrador retriever		▌▌▌	▌▌▌▌▌	▌	▌▌▌
Rough collie			▌		
Border collie			▌▌▌▌▌		▌▌
Husky				▌	▌
Dalmatian				▌	▌▌▌
German shorthair pointer					▌▌
Pointer					▌▌
Gordon setter					▌▌
Giant schnauzer					▌
Dobermann pincher					▌
Alaskan malamute					▌
Basset hound					▌
Hungarian vizsla					▌

Table 3-15: Dogs breeds classified according to the Lower & Upper 95% CI of the Mean of the olfactory bulb angle (Method 1) into brachycephalic (≤ 45°), *In-between 1* (46-55°), mesaticephalic (56-59°), *In-between* 2 (60°) & dolichocephalic (≥ 61°) groups

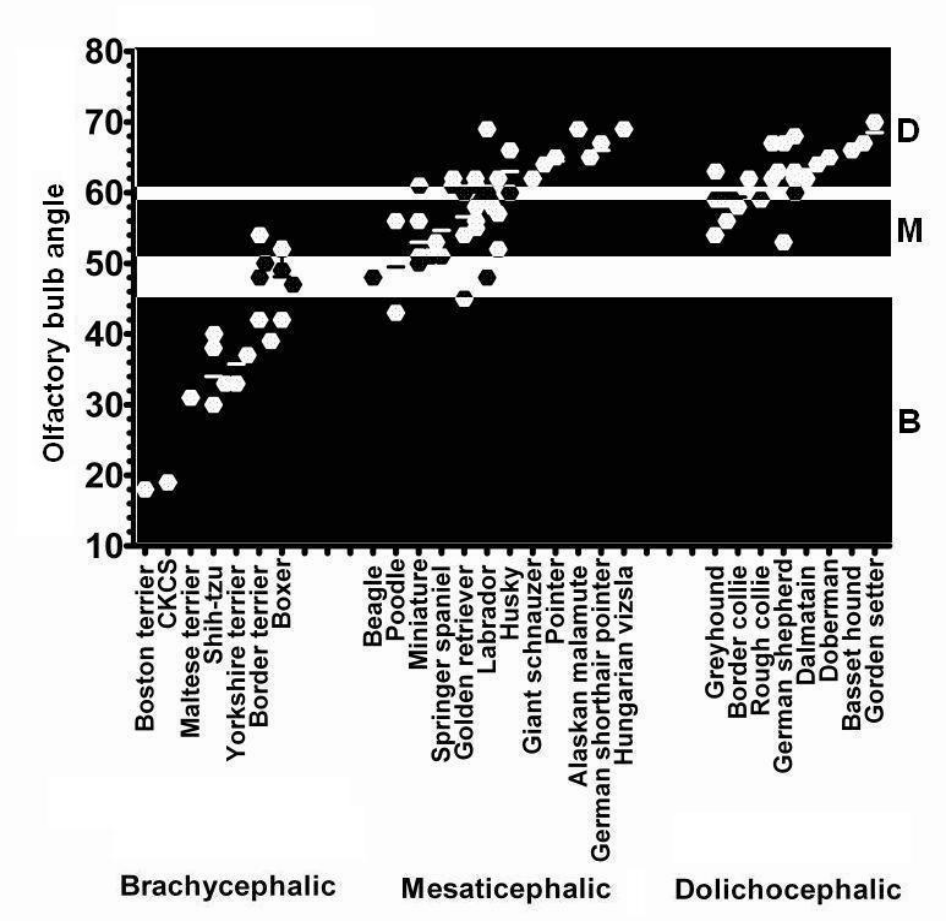

Figure 3-26: A scattered dot plot (mean) showing the distribution of breeds classified as brachycephalic, mesaticephalic and dolichocephalic arbitrarily (X-axis) and according to olfactory bulb angle Method 1 (Y-axis)

The third step was to define the best cut-off points for olfactory bulb angulation within arbitrary group, using a ROC curve test (Method 2) (Table 3-16 & Figure 3-27). The results demonstrated that the best cut-off point between brachycephalic & mesaticephalic was 51°, while the best cut-off point between mesaticephalic & dolichocephalic was 62°. On this basis dogs were classified as:

1. Brachycephalic ≤50°
2. Mesaticephalic 51-61°
3. Dolichocephalic ≥62°

Cut-off point for olfactory bulb angulation to differentiate between brachycephalic and mesaticephalic			
<50.5~51°	Brachycephalic	Mesaticephalic	Total
Brachycephalic	16	3	19
Mesaticephalic	4	34	38
Total	20	37	57
Cut-off point for olfactory bulb angulation to differentiate between mesaticephalic and dolichocephalic			
<61.5~62°	Mesaticephalic	Dolichocephalic	Total
Mesaticephalic	26	12	38
Dolichocephalic	10	16	26
Total	36	28	64

Table 3-16: The best cut-off point for olfactory bulb angulation in order to differentiate between the brachycephalic and mesaticephalic groups. The values were defined using a ROC curve test

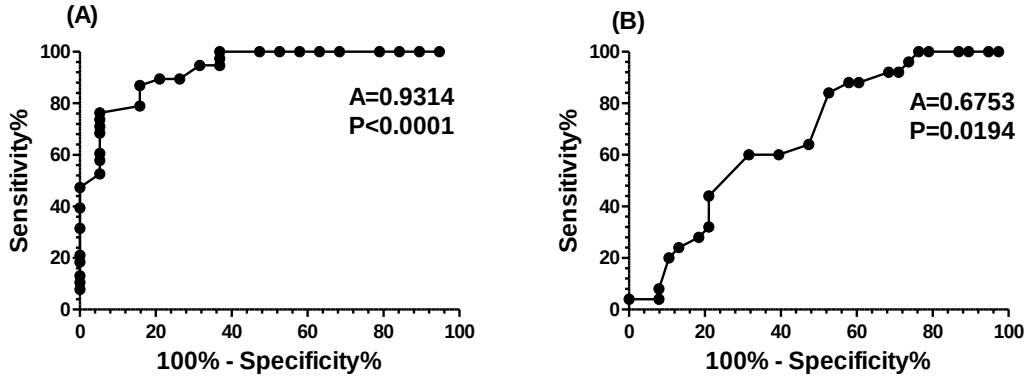

Figure 3-27: Non-linear regression graphs revealing the best cut-off points for olfactory bulb angulation to deliver the highest probable sensitivity and specificity values using a ROC curve test between (A) brachycephalic and mesaticephalic, and (B) mesaticephalic and dolichocephalic groups

Following the definition of these cut-off points, individual dogs were redistributed according to the best cut-off points (Table 3-17 & Figures 3-28 & 3-29).

Dog breeds	Brachycephalic	Mesaticephalic	Dolichocephalic
Shih-tzu	▌▌		
Yorkshire terrier	▌▌▌▌		
Border terrier	▌		
Boston terrier	▌		
Maltese terrier	▌		
CKCS	▌		
Beagle	▌		
Boxer	▌▌▌▌▌▌	▌▌▌	
Poodle	▌	▌	
Miniature schnauzer		▌▌	
Greyhound		▌	
Rough collie		▌	
Springer spaniel		▌▌▌▌▌	
Golden retriever		▌▌▌	▌▌
Husky		▌	▌
Labrador retriever		▌▌▌▌▌▌▌▌▌	▌▌
Border collie		▌▌▌▌▌	▌▌
Dalmatian		▌	▌▌▌
GSD		▌	▌▌▌▌▌
German shorthair pointer			▌▌
Pointer			▌▌
Gordon setter			▌▌
Basset hound			▌
Alaskan malamute			▌
Hungarian vizsla			
Giant schnauzer			▌
Dobermann pincher			▌

Table 3-17: The distribution of dog breeds using the best cut-off points for olfactory bulb angulation values as follows: brachycephalic (≤50°), mesaticephalic (51-61°) & dolichocephalic (≥62°) groups

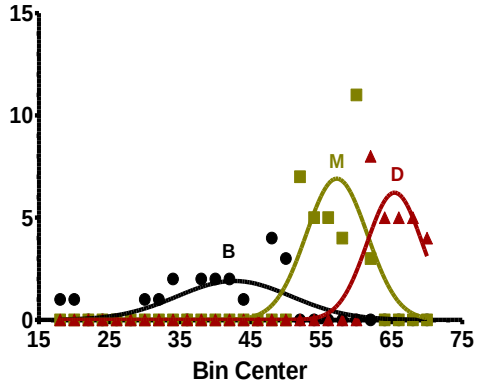

Figure 3-28: Non-linear regression graph (frequency distribution histogram) representing the distribution of olfactory bulb angle values for brachycephalic (B), mesaticephalic (M) and dolichocephalic (D) head phenotypes classified according to best cut off point of the olfactory bulb angle values (Method 2)

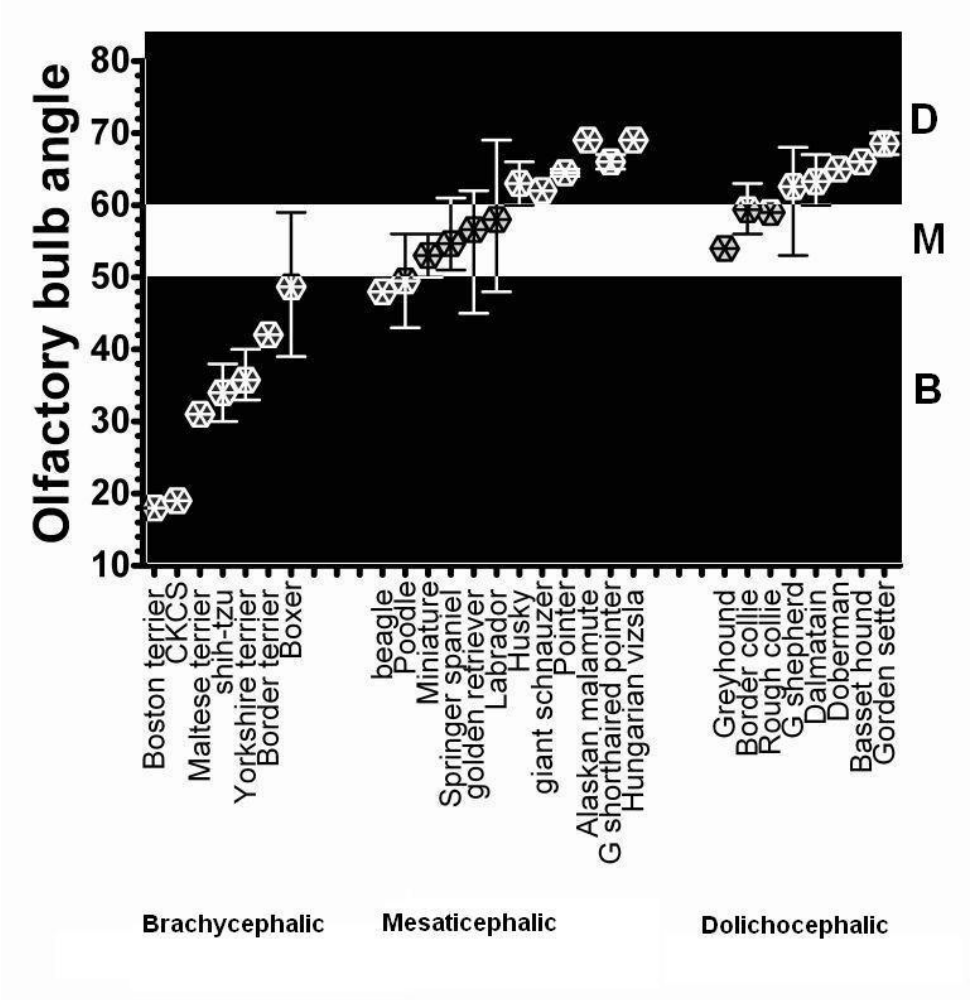

Figure 3-29: A scattered dot plot (mean) showing the distribution of breeds classified as brachycephalic, mesaticephalic and dolichocephalic arbitrarily (X-axis) and according to olfactory bulb angle (Method 2) (Y-axis)

The results demonstrated a significant difference (P<0.0001) between the arbitrary groups when olfactory bulb angulation was compared with olfactory bulb orientation [M±STDEV=30±9, 47±5 & 59±8 for Type-3, 4 and 5] (Figure 3-30).

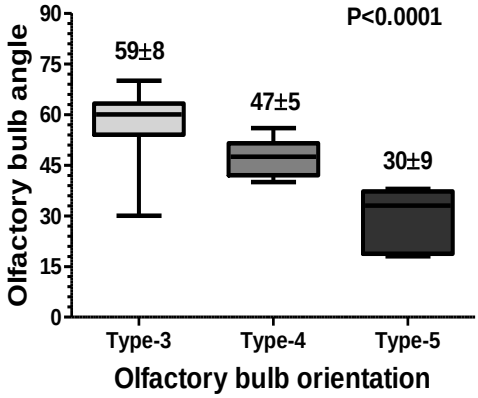

Figure 3-30: Vertical box and whiskers plot (with min-max values) revealing the (M±SDEV) differences between olfactory bulb angulation values for Type-3, 4 and 5 olfactory bulb orientation

In the last part of this portion of the study, the dogs of Study OB1 and OB2 were merged and re-evaluated. The statistical analysis demonstrated a significant difference (P<0.0001) between head phenotypes when olfactory bulb angulation was compared (Figure 3-31). Using the combined results, the best ranges for defining brachycephalic, mesaticephalic and dolichocephalic head phenotypes on the basis of olfactory bulb angulation were (Figure 3-32):

1. Brachycephalic group ≤45°
2. Mesaticephalic group 57-60°
3. Dolichocephalic group ≥61°

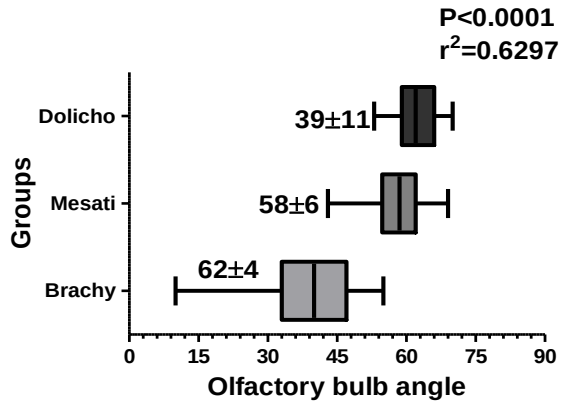

Figure 3-31: A horizontal box and whiskers plot (with min-max values) (with mean, and standard deviation) demonstrating the difference in olfactory bulb angulation for brachycephalic (Brachy) (n=55), mesaticephalic (Mesati) (n=46) and dolichocephalic (Dolicho) (n=29) head phenotypes as defined arbitrarily

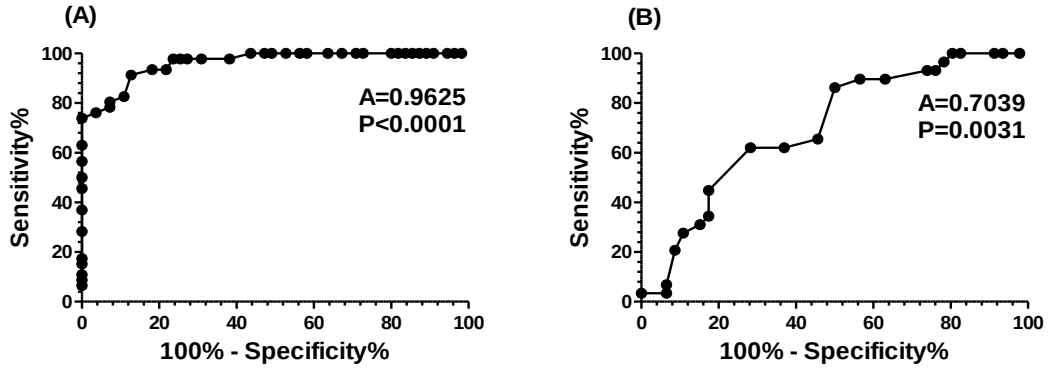

Figure 3-32: Non-linear regression (ROC curves) representing the best cut-off points for olfactory bulb angulation between (A) brachycephalic and mesaticephalic and (B) mesaticephalic and dolichocephalic head phenotypes

Finally, the Lower & Upper 95% CI of the Mean of the olfactory bulb angle and the best cut-off points between the arbitrary as brachycephalic, mesaticephalic and dolichocephalic groups were compared in a merged data table (Table 3-18).

	Dog group	Study OB1	Study OB2	Merged
Control	Brachycephalic	34 ± 11°	40 ± 10	39 ±11°
	Mesaticephalic	57 ± 4°	58 ± 7°	58 ± 6°
	Dolichocephalic	62 ± 4°	62 ± 2°	62 ±4°
Method 1	Brachycephalic	≤ 42°	≤ 45°	≤ 42°
	Mesaticephalic	56-57°	56-59°	57-60°
	Dolichocephalic	≥ 61°	≥ 61°	≥ 61°
Method 2	Brachycephalic	≤ 55°	≤ 50°	≤ 51°
	Mesaticephalic	56-61°	51-61°	52-61°
	Dolichocephalic	≥ 62°	≥ 62°	≥ 62°

Table 3-18: Olfactory bulb angles for defining dogs as brachycephalic, mesaticephalic and dolichocephalic from the Control and Methods 1 & 2 for Studies OB1 and OB2 and the merged groups

Accordingly the individual dogs were reclassified on the basis of this merged data into new brachycephalic, mesaticephalic and dolichocephalic groupings (Table 3-19).

Based on the best cut-off points to differentiate between the groups, the following values were derived (Table 3-20):

1. Brachycephalic group ≤51°
2. Mesaticephalic group 52-61°
3. Dolichocephalic group ≥62°

Dog breed	**Brachy-**	***In-between 1***	**Mesati-**	**Dolicho-**
Shih-tzu	▌▌▌▌▌▌			
Yorkshire terrier	▌▌▌▌			
Lhasa apso	▌▌▌			
Chihuahua	▌▌			
Boston terrier	▌▌			
Pug	▌▌			
Maltese terrier	▌			
Border terrier	▌			
Bichon frise	▌			
CKCS	▌▌▌▌▌▌▌	▌▌▌▌▌▌▌▌▌		
Boxer	▌▌	▌▌▌▌▌▌▌▌▌▌▌		
Staffordshire terrier		▌		
Beagle		▌		
WHWT		▌▌		
Mastiff		▌		
Poodle		▌▌		
Miniature schnauzer		▌▌▌		
Golden retriever		▌▌	▌	▌▌
Husky			▌	▌
Labrador retriever		▌▌▌▌▌	▌▌▌▌▌▌▌▌	▌▌▌▌
German & Belgian shepherds		▌		▌▌▌▌▌▌▌▌
Springer spaniel		▌▌▌▌	▌	▌▌
Greyhound		▌	▌	
Giant schnauzer			▌	
Collies		▌	▌▌▌▌▌▌	▌▌
Dalmatian			▌	▌▌▌
Scottish deerhound				▌
Basset hound				▌
Alaskan Malamute				▌
German shorthair pointer				▌▌
Dobermann pincher				▌
Pointer				▌▌▌
Gordon setter				▌▌
Hungarian vizsla				▌

Table 3-19: The distribution of dog breeds according to the classification of dogs into brachycephalic mesaticephalic and dolichocephalic using olfactory bulb angle (Method 1)

Dog breed	Brachycephalic	Mesaticephalic	Dolichocephalic
Shih-tzu	▌▌▌▌▌▌		
Yorkshire terrier	▌▌▌▌		
Lhasa apso	▌▌▌		
Chihuahua	▌▌		
Boston terrier	▌▌		
Pug	▌▌		
WHWT	▌▌		
Border terrier	▌		
Bichon frise	▌		
Maltese terrier	▌		
Staffordshire terrier	▌		
Beagle	▌		
CKCS	▌▌▌▌▌▌▌▌▌▌▌▌▌	▌	
Boxer	▌▌▌▌▌▌▌▌	▌▌▌▌	
Poodle	▌	▌	
Miniature schnauzer	▌	▌▌	
Mastiff		▌	
Golden retriever		▌▌	▌▌
Husky		▌	▌
Labrador retriever		▌▌▌▌▌▌▌▌▌▌	▌
German and Belgian shepherds		▌	▌▌▌▌▌▌▌
Springer spaniel		▌▌▌▌	
Greyhound		▌▌	
Giant schnauzer		▌	▌
Collies		▌▌▌▌▌▌▌	▌▌
Dalmatian		▌	▌▌▌
Scottish deerhound			▌
Basset hound			▌
Alaskan Malamute			▌
German shorthair pointer			▌▌
Dobermann pincher			▌
Pointer			▌▌▌
Gordon setter			▌▌
Hungarian vizsla			▌

Table 3-20: The distribution of dog breeds according to the classification of dogs into brachycephalic mesaticephalic and dolichocephalic based on the best olfactory bulb angulation cut-off points (Method 2)

3.3.3 The midline areas of the cranial fossae in relation to head phenotype

In this part of the study, the area of the rostral (including the ethmoidal), middle and caudal fossae were examined using the Evans index (Study F1) and the angulation of the olfactory bulb (Study F2).

Study F1: The area of the cranial fossa is partially determined by the head phenotype [Evans index]

On midline sagittal plane, the midline area of the cranial fossa was compared to bodyweight using the square root of the cranial fossa area, and the cube root of the bodyweight to allow assessment in a single dimension. A significant correlation ($P<0.0001$) was found between the midline area of the entire cranial fossa and bodyweight when considered in a single dimension (Figure 3-33A). There was also a significant correlation ($P<0.0001$) between the corrected area of the cranial fossa for the bodyweight and the head phenotype as defined using Evans index values (Figure 3-33B).

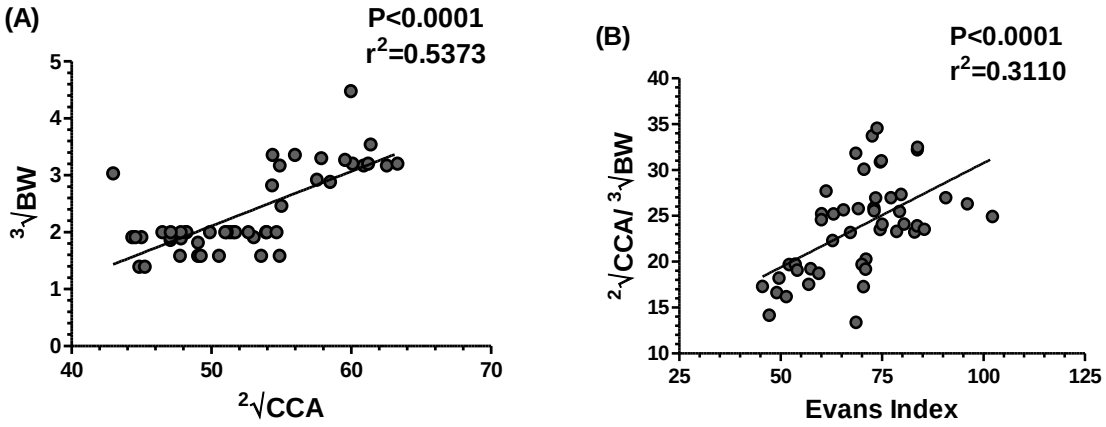

Figure 3-33: Linear regression plots representing the correlation between (A) the square root of the cranial fossa area ($^2\sqrt{}$CCA) and the cube root of the bodyweight ($^3\sqrt{}$BW) and (B) Evans index values and the corrected area of the cranial fossa for bodyweight ($^2\sqrt{}$CCA/ $^3\sqrt{}$BW)

The midline areas of the rostral, middle and caudal fossae were examined separately to determine the effect of head conformation (Evans index). Significant correlations (Figure 3-34) were evident between the Evans index and the corrected areas of the rostral and middle fossae ($P<0.0001$), but a weaker correlation was evident for the caudal fossa ($P=0.0229$).

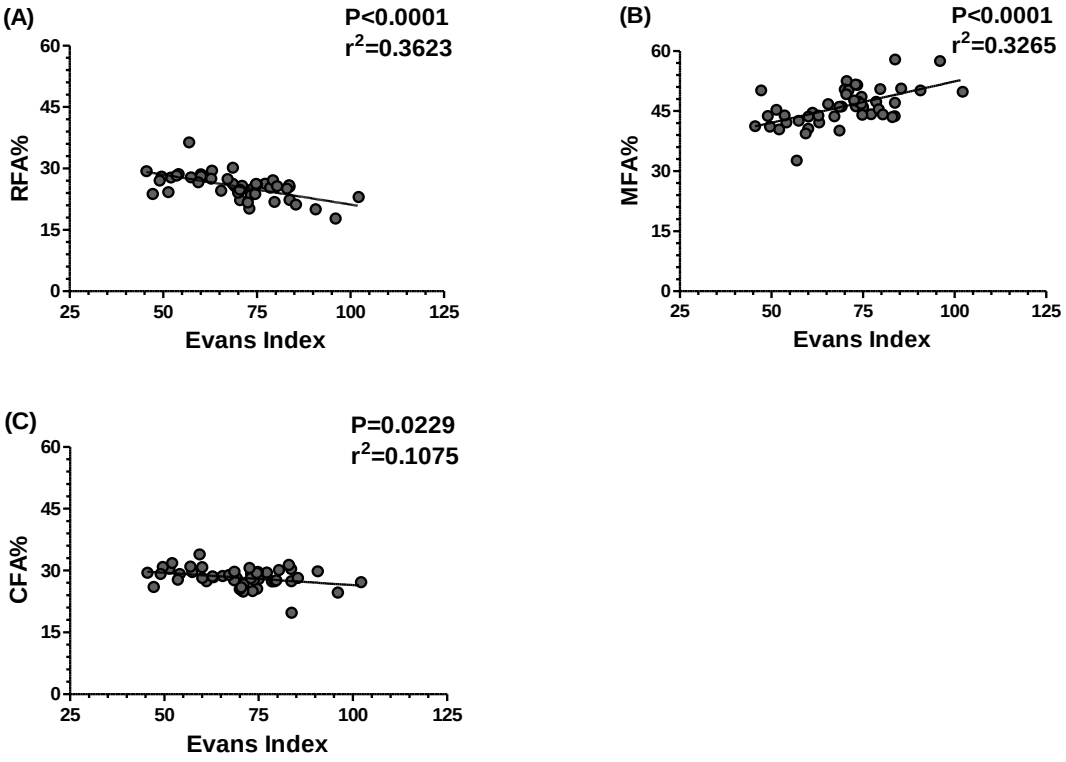

Figure 3-34: Linear regression plots representing the correlation between Evans index values and the corrected midline areas (expressed as a % of the midline area of the cranial fossa) of the (A) rostral fossa (RFA%), (B) middle fossa (MFA%), and (C) caudal fossa (CFA%), which were examined on midline sagittal plane MR images

To tease out which part of the rostral fossa was impacted most by the head phenotype (Evans index); the ethmoidal fossa area was analysed separately. The correlation persisted for the ethmoidal fossa ($P<0.0001$) but not for the remainder of the rostral fossa (RRFA) ($P=0.0931$) (Figure 3-35).

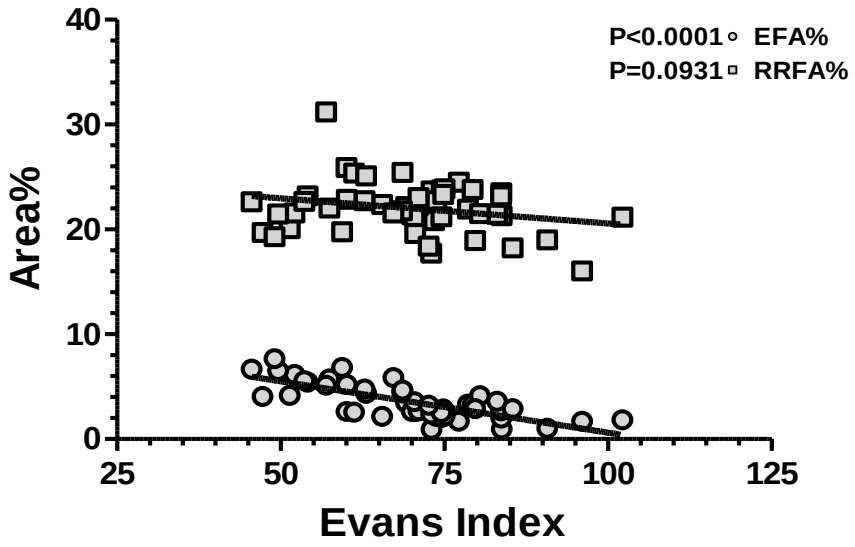

Figure 3-35: Linear regression plot demonstrating a significant correlation between Evans index values and the corrected midline area of the ethmoidal fossa (EFA %), but not the corrected midline area of the rest of the rostral fossa (RRFA %)

When the corrected midline ethmoidal, middle and caudal fossae areas were compared between the three groups of head phenotype, the results demonstrated that head shape had a stronger effect on the midline area of the ethmoidal fossa than bodyweight. However, the results for the other fossae demonstrated no clear correlation with head shape or bodyweight (Figures 3-36 & 3-37 and Table 3-21).

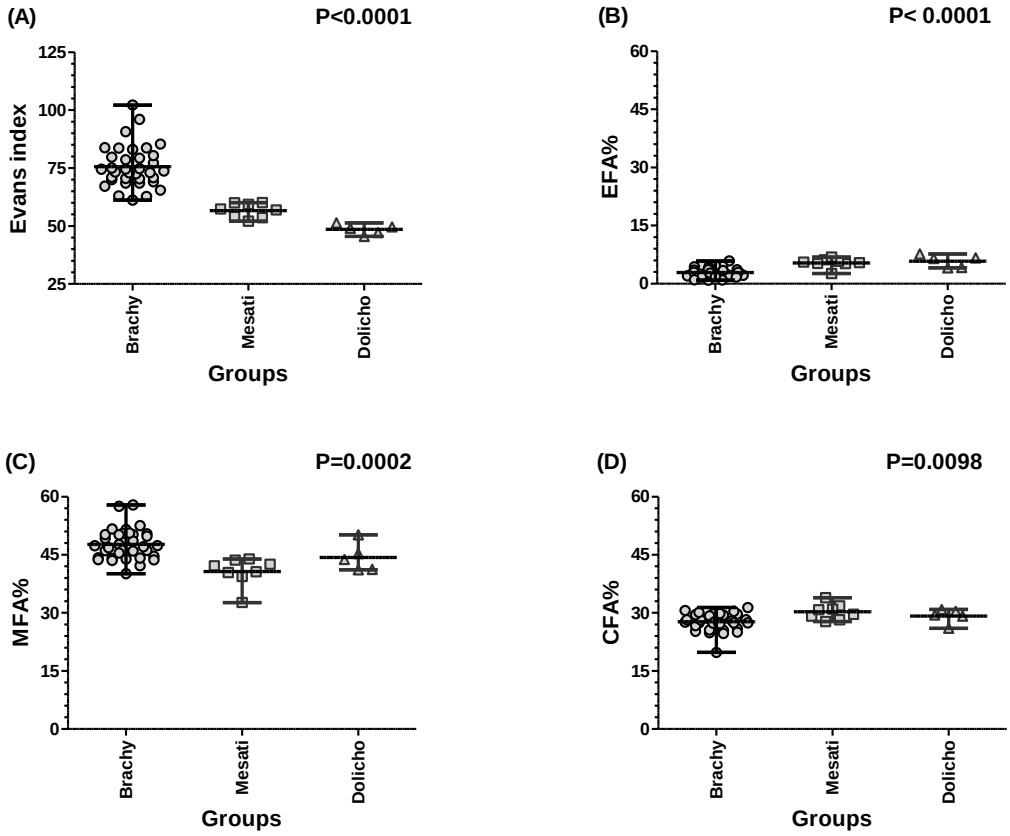

Figure 3-36: Vertical scatter plots (with range and mean) comparing (A) the Evans index, (B) the corrected midline ethmoidal fossa area (EFA %), (C) the corrected midline middle fossa area (MFA %), and (D) the corrected midline caudal fossa area (CFA %) within brachycephalic, mesaticephalic and dolichocephalic head phenotypes according to Evans index Method 2

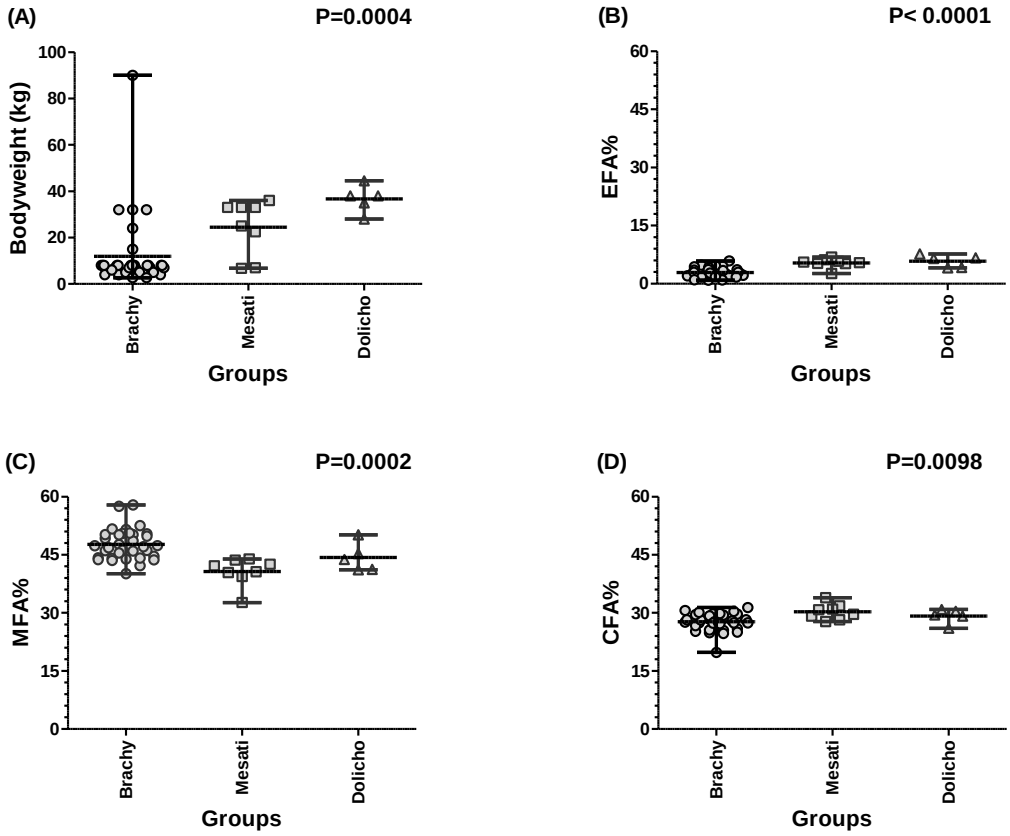

Figure 3-37: Vertical scatter plots (with range and mean) comparing (A) bodyweight, (B) the corrected midline ethmoidal fossa area (EFA), (C) the corrected midline middle fossa area(MFA %), and (D) the corrected midline caudal fossa area (CFA %) within brachycephalic, mesaticephalic and dolichocephalic head phenotypes according to Evans index Method 2

	Evans index	**Bodyweight**	**EFA%**	**MFA%**	**CFA%**
Brachy vs. Mesaticephalic	Yes	No	Yes	Yes	Yes
Brachy vs. Dolichocephalic	Yes	Yes	Yes	No	No
Mesati vs. Dolichocephalic	No	No	No	No	No

Table 3-21: The presence or absence of significant differences between brachycephalic, mesaticephalic and dolichocephalic groups in ethmoidal fossa area (EFA %), middle fossa area (MFA %), caudal fossa area (CFA %), Evans index and bodyweight

Study F2: The midline area of the cranial fossa is partially determined by head phenotype [as defined by angulation of the olfactory bulb]

On the midline sagittal plane, the correlation between the cranial fossa area and bodyweight was tested first, then the correlation between cranial fossa area and head conformation (as defined by the angulation of the olfactory bulb- Method 2) was tested next. The results demonstrated significant correlations between the bodyweight and midline cranial fossa area ($P<0.0001$) (Figure 3-38A) and between the midline cranial fossa area and head conformation ($P<0.0001$) (Figure 3-38B).

A significant correlation ($P<0.0001$) was also found between the angulation of the olfactory bulb and the midline areas of the rostral, middle and caudal fossae (Figure 3-39). When the ethmoidal fossa was examined independently from the rostral fossa the results demonstrated that a significant correlation only existed between the midline area of the ethmoidal fossa (expressed as a percentage of the midline cranial fossa area) ($P<0.0001$), and not for the rest of the rostral fossa ($P=0.0820$) (Figure 3-40).

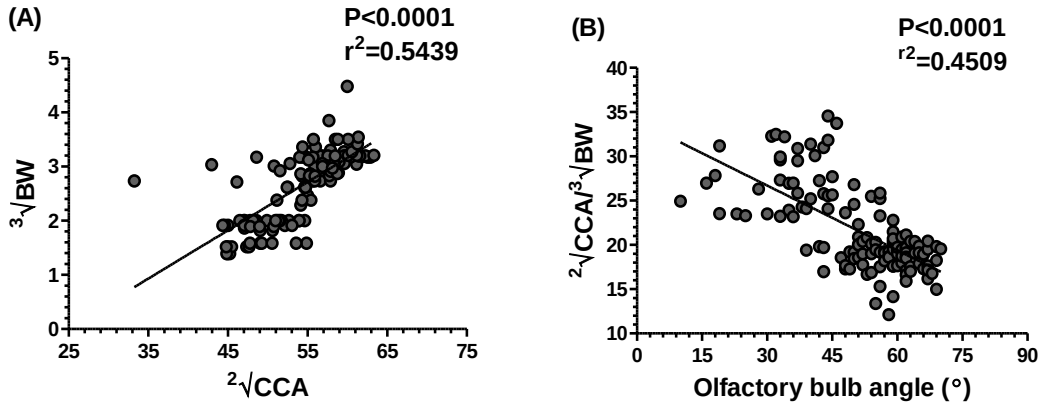

Figure 3-38: Linear regression plots demonstrating the correlation between (A) the square root of the area of the cranial fossa ($^{2}\sqrt{CCA}$) and the cube root of bodyweight ($^{3}\sqrt{BW}$) and (B) the corrected area of the cranial fossa ($^{2}\sqrt{CCA}/^{3}\sqrt{BW}$) and head conformation [using olfactory bulb angle Method 2]

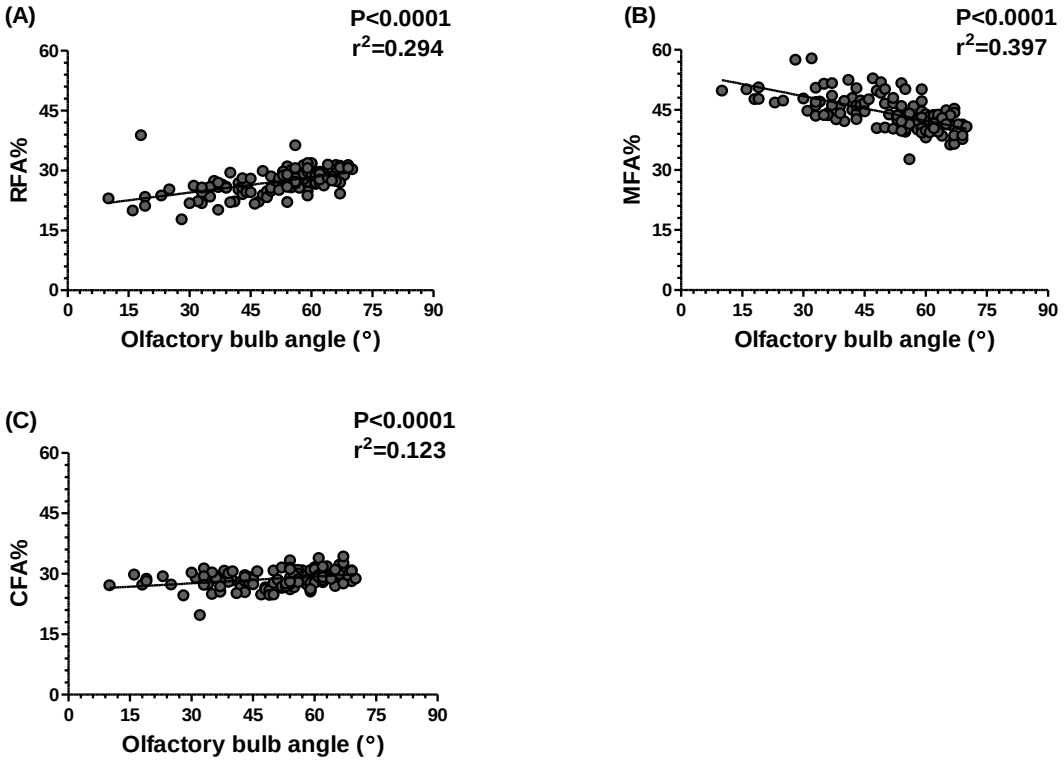

Figure 3-39: Linear regression graphs demonstrating the correlation between olfactory bulb angle and the corrected midline areas of the (A) rostral fossa (RFA %), (B) middle fossa (MFA %) and (C) caudal fossa (CFA%), on midline sagittal plane MR images

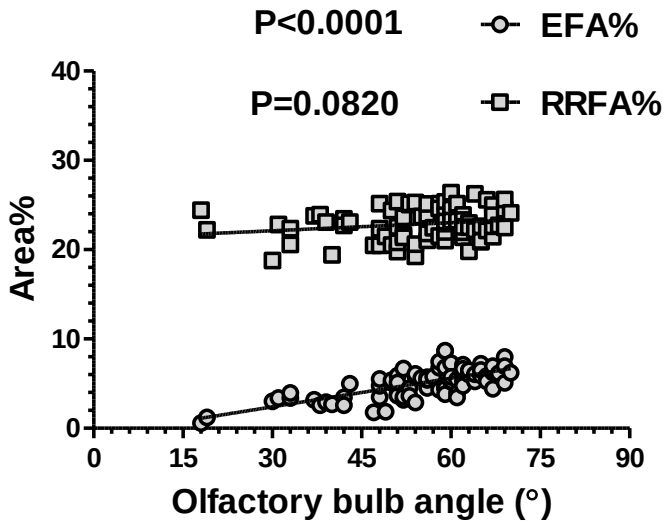

Figure 3-40: Linear regression plot demonstrating the correlation between the angulation of the olfactory bulb and the corrected midline area of the ethmoidal fossa (EFA %) and the midline area of the rest of the rostral fossa (RRFA%)

The ethmoidal, middle and caudal fossae were compared between the three groups of head phenotype and head conformation had a stronger influence on the ethmoidal fossa than on

the other fossae, while bodyweight had a greater influence on the middle fossa than head phenotype (Table 3-22 and Figures 3-41 & 3-42).

	Olfactory bulb angle	Bodyweight	EFA%	MFA%	CFA%
Brachy vs. Mesaticephalic	Yes	Yes	Yes	Yes	No
Brachy vs. Dolichocephalic	Yes	Yes	Yes	Yes	Yes
Mesati vs. Dolichocephalic	Yes	No	Yes	No	No

Table 3-22: The presence or absence of significant differences between brachycephalic, mesaticephalic and dolichocephalic groups in olfactory bulb angulation, bodyweight and the corrected areas of the ethmoidal (EFA%), middle (MFA %) and caudal fossae (CFA %)

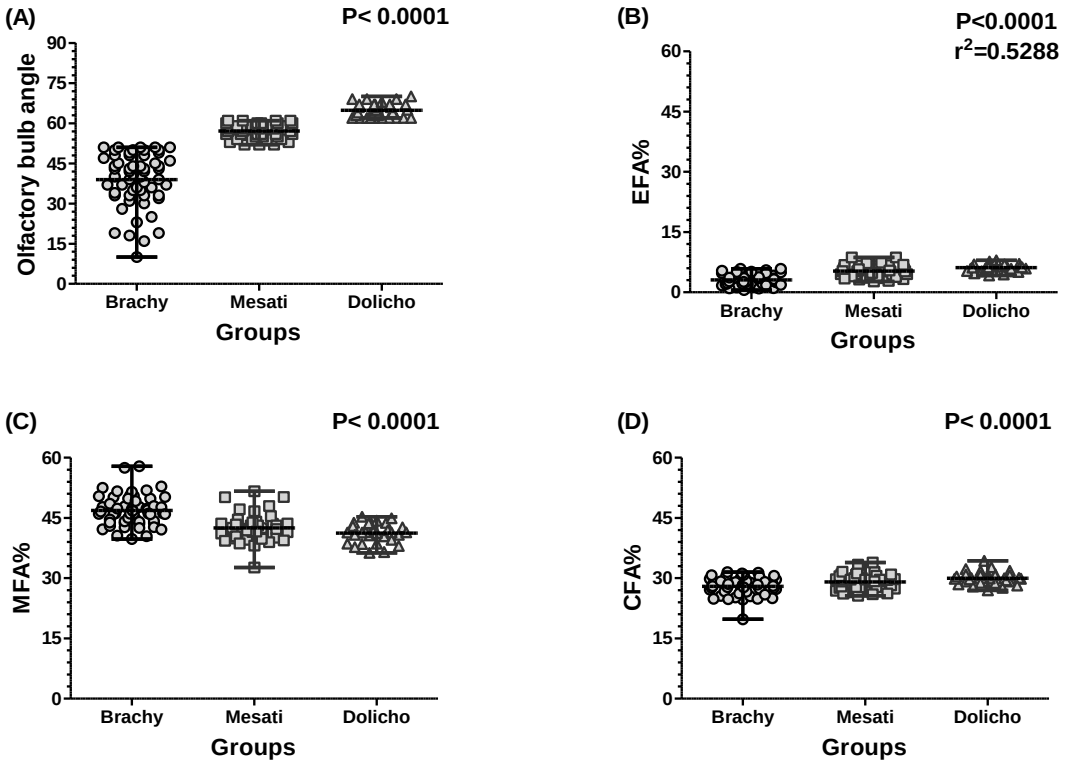

Figure 3-41**:** Vertical scatter plots (with range and mean) comparing (A) olfactory bulb angulation, (B) the corrected midline ethmoidal fossa area (EFA%), (C) the corrected midline middle fossa area (MFA%), and (D) the corrected midline caudal fossa area (CFA%) within brachycephalic, mesaticephalic and dolichocephalic head phenotypes defined according to olfactory bulb angulation (Method 2)

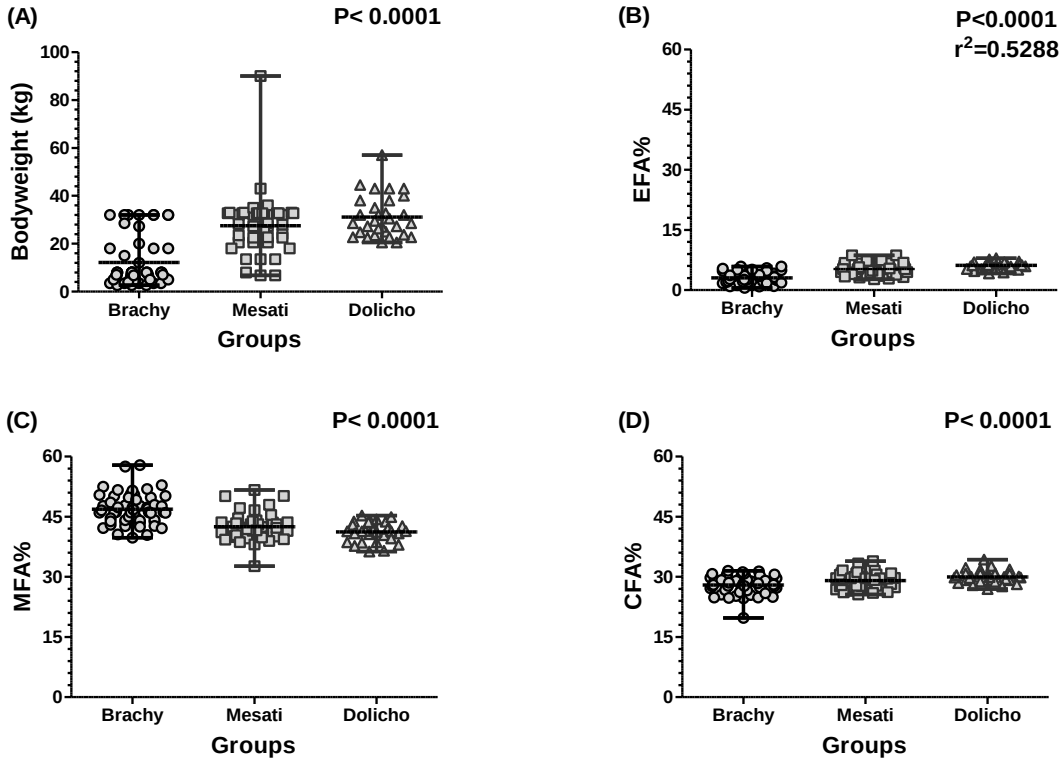

Figure 3-42: Vertical scatter plots (with range and mean) comparing (A) bodyweight, (B) the corrected midline ethmoidal fossa area (EFA%), (C) the corrected midline middle fossa area (MFA%), and (D) the corrected midline caudal fossa area (CFA%) within brachycephalic, mesaticephalic and dolichocephalic head phenotypes defined according to olfactory bulb angle (Method 2)

Finally, the two studies (F1 and F2) were compared in Table 3-23 to illustration the impact of both factors (head conformation and bodyweight) on the corrected midline area of the fossae (ethmoidal, middle and caudal). The effect of head conformation was found to be stronger than bodyweight as an influence on the ethmoidal fossa area in the midline sagittal plane, but not for the other fossae.

	Head phenotype		Bodyweight (kg)		EFA%		MFA%		CFA%	
	Evans index	OB angle								
	F1	F2	F1	F2	F1	F2	F1	F2	F1	F2
Brachy vs. Mesaticephalic	Yes	Yes	No	Yes	Yes	Yes	Yes	Yes	Yes	No
Brachy vs. Dolichocephalic	Yes	Yes	Yes	Yes	Yes	Yes	No	Yes	No	Yes
Mesati vs. Dolichocephalic	No	Yes	No	No	No	Yes	No	No	No	No

Table 3-23: Combining the results of studies F1 and F2 to show the presence or absence of head conformation (Evans index values and olfactory bulb angulation – Method 2) and bodyweight on the cranial fossae: the ethmoidal fossa (EFA%), middle fossa (MFA%) and caudal fossa (CFA%). The data was expressed as a % of the cranial fossa area, measured in the midline sagittal plane on MR images

3.3.4 Linear dimensions of the olfactory bulb are more influenced by head conformation than bodyweight

3.3.4.1 Effect of skull type

Study OD1: The mean and standard deviation values of each of the corrected olfactory bulb measurements of the three arbitrary head phenotypes classified are presented in Table 3.24. Statistical analysis showed no significant differences for either the corrected width or the height of the olfactory bulb when correlated with head conformation (Figure 3-43). L1 (length of the olfactory bulb on the dorsal plane) did, however, demonstrate a significant difference between the brachycephalic head phenotype and the other 2 phenotypes ($P<0.0001$, $r^2 = 06138$: ANOVA). The other two length measurements of the olfactory bulb also demonstrated a similar difference between the brachycephalic head phenotype and the other 2 head phenotypes (Figure 3-44 & Table 3-24).

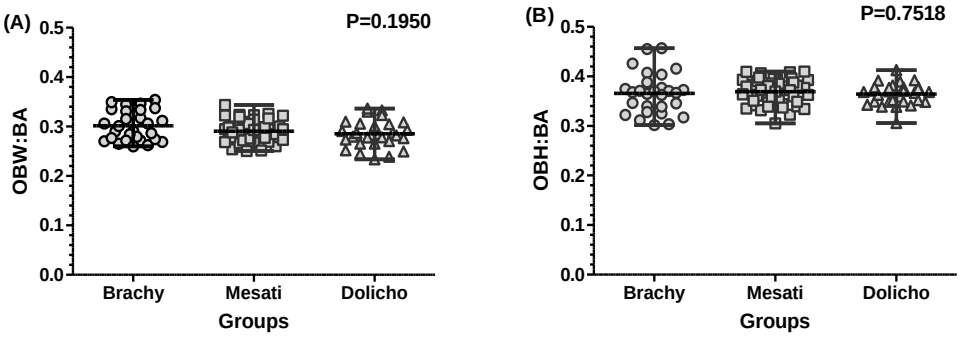

Figure 3-43: Vertical scatter plots (with range and mean) representing (A) the corrected olfactory bulb width (OBW: BA), and (B) the corrected olfactory bulb height (OBH: BA) for the brachycephalic (Brachy), mesaticephalic (Mesati) and dolichocephalic (Dolicho) groups, classified arbitrarily

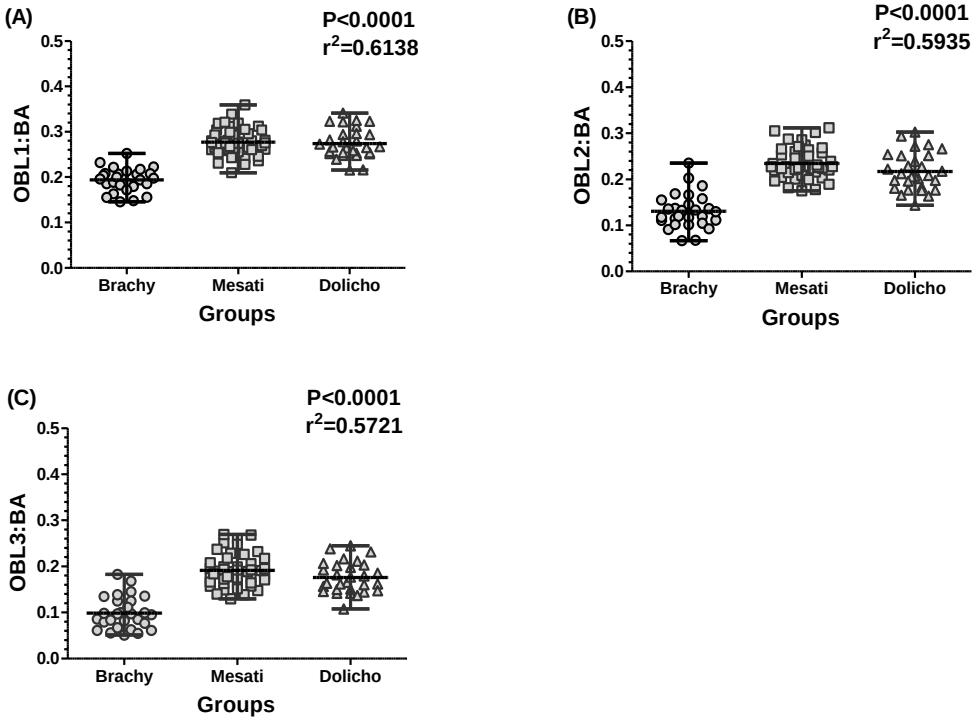

Figure 3-44: Vertical scatter plots (with range and mean) demonstrating the differences in corrected olfactory bulb length (A) OBL1:BA, (B) OBL2:BA & (C) OBL3:BA between dogs arbitrarily defined as brachycephalic (Brachy), mesatiscephalic (Mesati), and dolicocephalic (Dolicho)

Group	No	OBH:BA	OBW:BA	OBL1:BA	OBL2:BA	OBL3:BA
Brachycephalic	28	M±STDEV= 0.37±0.04 R= 0.30-0.46	M±STDEV= 0.30±0.03 R= 0.26-0.35	M±STDEV= 0.19±0.03 R= 0.15-0.25	M±STDEV= 0.13±0.04 R= 0.07-0.24	M±STDEV=0.10±0.04 R= 0.05-0.18
Mesaticephalic	45	M±STDEV= 0.37±0.03 R= 0.31-0.41	M±STDEV= 0.29±0.2 R= 0.25-0.34	M±STDEV= 0.28±0.03 R= 0.21-0.36	M±STDEV= 0.24±0.03 R= 0.18-0.31	M±STDEV= 0.19±0.04 R= 0.13-0.27
Dolichocephalic	29	M±STDEV= 0.36±0.02 R= 0.31-0.41	M±STDEV= 0.29±0.03 R= 0.23-0.34	M±STDEV= 0.27±0.03 R= 0.22-0.34	M±STDEV= 0.21±0.04 R= 0.14-0.30	M±STDEV=0.18±0.04 R= 0.11-0.25

Table 3-24: Corrected olfactory bulb height (OBH: BA), olfactory bulb width (OBW: BA) and olfactory bulb lengths (OBL1: BA, OBL2: BA & OBL3: BA) in dogs arbitrarily classified into the three head phenotype groups

98

Following compensation for the effect of bodyweight on the linear dimensions an olfactory bulb index was created (see details of the methods in Chapter 2), the ANOVA and multiple comparison test only showed significant differences between the brachycephalic group and the other two groups (Figure 3-45).

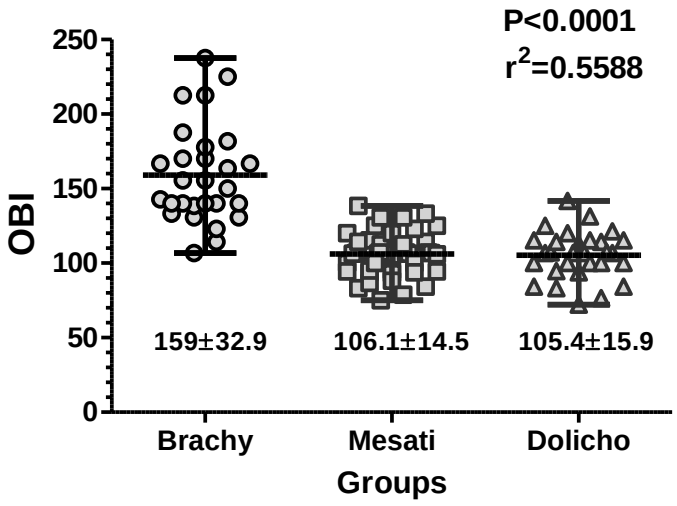

Figure 3-45: Vertical scatter plot (with range) demonstrating a significant difference between the olfactory bulb index (OBI) values (M±STDEV) for the arbitrary brachycephalic (Brachy) group as compared to the other 2 head phenotypes [mesaticephalic (Mesati) and dolichocephalic (Dolicho)

Study OD2:

Significant differences (P<0.0001) were evident for all three corrected olfactory bulb lengths when the brachycephalic group and the other 2 head phenotype groups as defined using olfactory bulb angle (Method 2) were compared in this part of the study (Figure 3-46). For olfactory bulb width, the only difference that was evident was between the brachycephalic and mesaticephalic groups (P=0.0255) (Figure 3-47A). No differences (P=0.5122) were evident between any of the three groups for corrected olfactory bulb height (Figure 3-47B). Although the statistical analysis revealed a significant difference between the three groups (P<0.0001) for olfactory bulb index, this difference was not significant between the mesaticephalic and dolichocephalic groups when the post comparison test was applied (Figure 3-48 & Table 3-24).

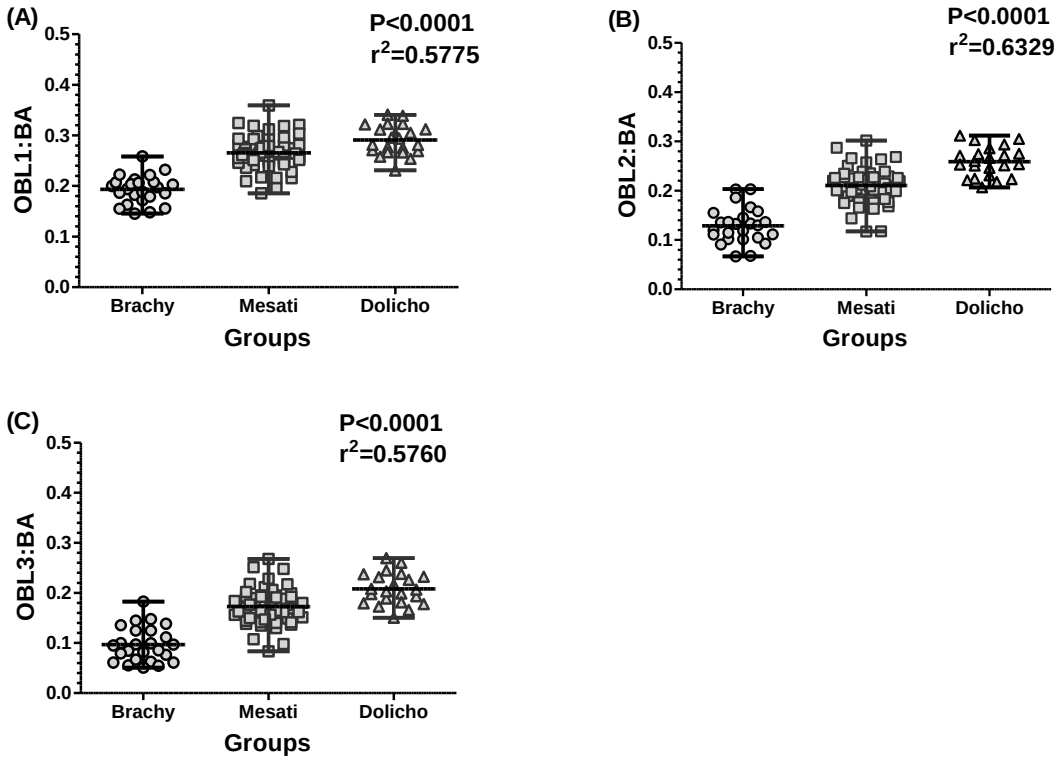

Figure 3-46: Vertical scatter plots (with range and mean) revealing significant differences in corrected olfactory bulb lengths (OBL1: BA, OBL2: BA & OBL3: BA) between brachycephalic (Brachy), mesaticephalic (Mesati) and dolichocephalic (Dolicho) groups as defined using olfactory bulb angle (Method 1)

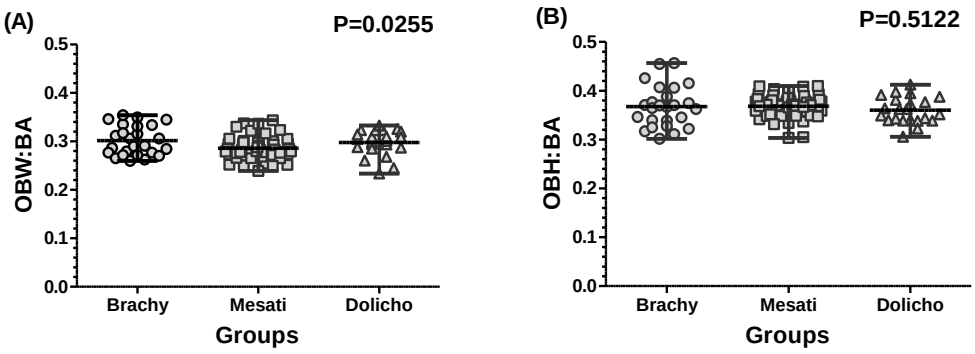

Figure 3-47: Vertical scatter plots (with range and mean) illustrating the effect of the head conformation: as defined using olfactory bulb angle (Method 2) brachycephalic (Brach), mesaticephalic (Mesati) and dolichocephalic (Dolicho) groups (A) OBW: BA and (B) OBH: BA

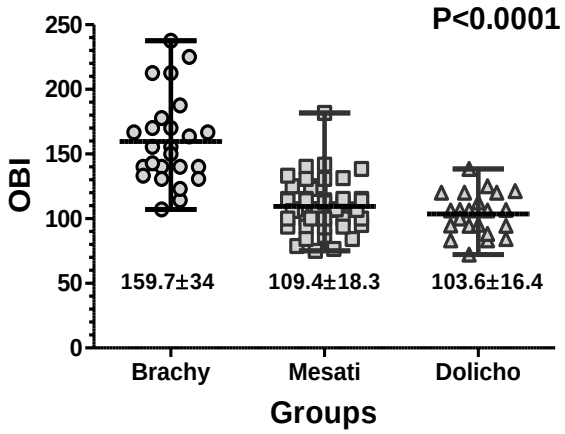

Figure 3-48: Vertical scatter plot (with range, mean & standard deviation) representing the differences in olfactory bulb indices (OBI) between brachycephalic (Brachy), mesaticephalic (Mesati) and dolichocephalic (Dolicho) head phenotypes as defined using olfactory bulb angle (Method 1)

Group	Brachycephalic	Mesaticephalic	Dolichocephalic
Dog No.	25	54	22
Age	M±STDEV= 5.4±4.2	M±STDEV=6.4±4.4	M±STDEV=7.1±3.4
Bodyweight	M±STDEV= 6±1.7	M±STDEV=15.9±1.6	M±STDEV=17.1±1.7
OBW:BA	M±STDEV=0.3±0.03 R= 0.26-0.35	M±STDEV=0.29±0.02 R= 0.24-0.334	M±STDEV=0.3±0.03 R= 0.23-0.33
OBH:BA	M±STDEV=0.37±0.04 R= 0.30-0.46	M±STDEV=0.37±0.02 R= 0.3-0.41	M±STDEV=0.36±0.03 R= 0.31-0.41
OBL1:BA	M±STDEV=0.19±0.03 R= 0.15-0.26	M±STDEV=0.27±0.03 R= 0.19-0.36	M±STDEV=0.29±0.03 R= 0.23-0.34
OBL2:BA	M±STDEV=0.13±0.04 R= 0.06-0.2	M±STDEV=0.21±0.04 R= 0.12-0.3	M±STDEV=0.26±0.03 R= 0.21-0.31
OBL3:BA	M±STDEV=0.10±0.04 R= 0.05-0.18	M±STDEV=0.17±0.04 R= 0.08-0.27	M±STDEV=0.21±0.03 R= 0.15-0.27

Table 3-25: Comparison between the mean, standard deviation & range values in brachycephalic, mesaticephalic and dolichocephalic groups classified according to the olfactory bulb angulation (Method 2) for: (OBW:BA) - the corrected width of the olfactory bulb, (OBH:BA) - the corrected height of the olfactory bulb and (OBL1:BA, OBL2:BA & OBL3:BA) - the corrected lengths of the olfactory bulb

3.3.4.2 Effect of age

Study OD3:

In order to demonstrate that a representative population for each head conformation had been selected on the basis of age, the age of the three breeds (CKCS, Cocker spaniel and GSD) were compared to head conformation defined using angulation of the olfactory bulb (Method 2). No significant correlation (P=0.0668) was found (Figure 3-49) between age and olfactory bulb angle in 38 dogs of three different head phenotypes as defined using olfactory bulb angle (Method 2).

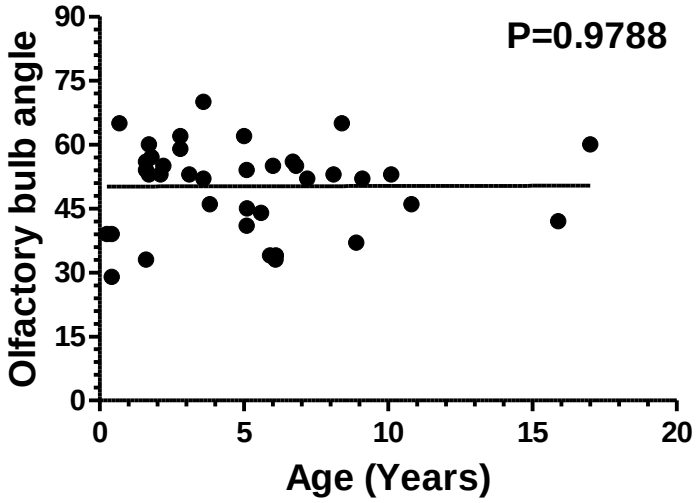

Figure 3-49: Linear regression graph demonstrating a lack of correlation between the olfactory bulb angle and age in a representative population selected from three breeds representing three different head phenotypes

None of the linear dimensions of the olfactory bulb were correlated to age in any of the 3 representative breeds, with the exception of the corrected olfactory bulb length (OBL2: BA) for the CKCS, which increased with age (P=0.0326) (Figures 3-50 to 3-55).

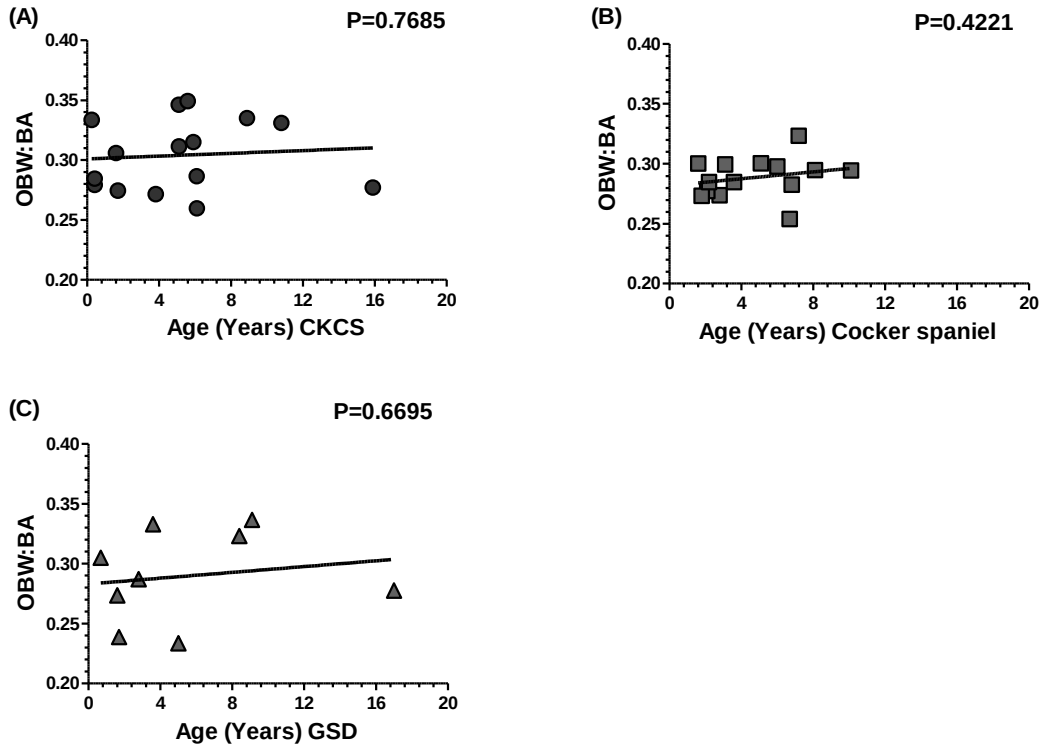

Figure 3-50: Linear regression graphs illustrated the lack of significant correlation between the age of CKCS (A), Cocker spaniels (B) and GSDs (C), and corrected olfactory bulb width (OBW: BA), measured on dorsal plane MR images

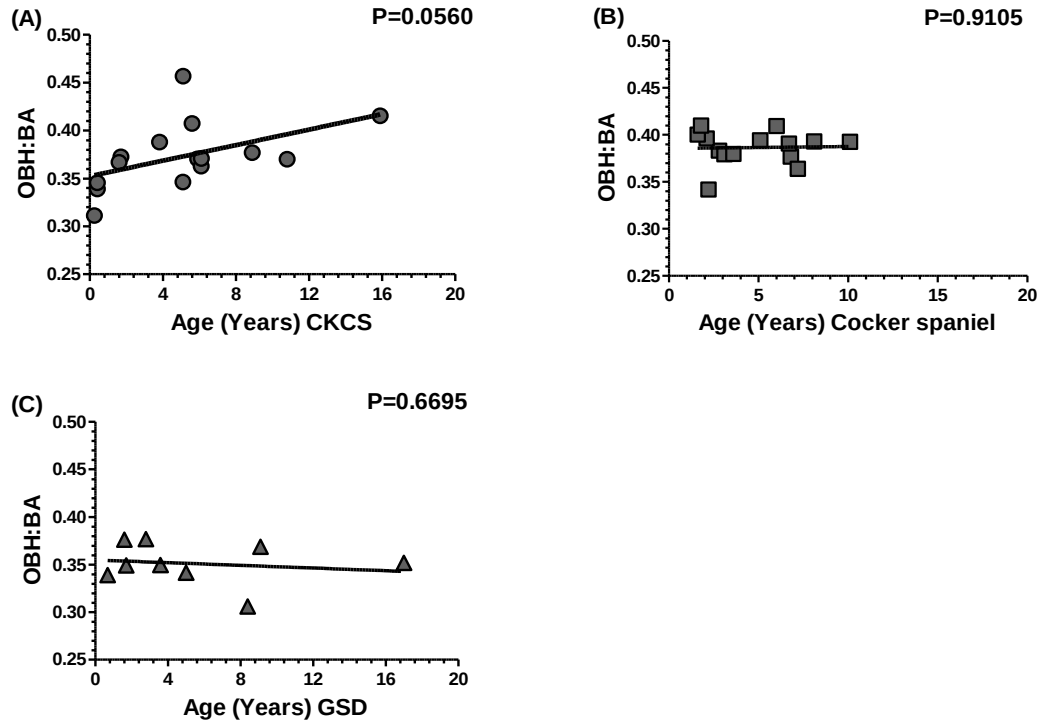

Figure 3-51: Linear regression plots representing the lack of significant correlation between age and corrected olfactory bulb height (OBH: BA) on midline sagittal plane MR images from CKCS (A), Cocker spaniels (B) and GSDs (C)

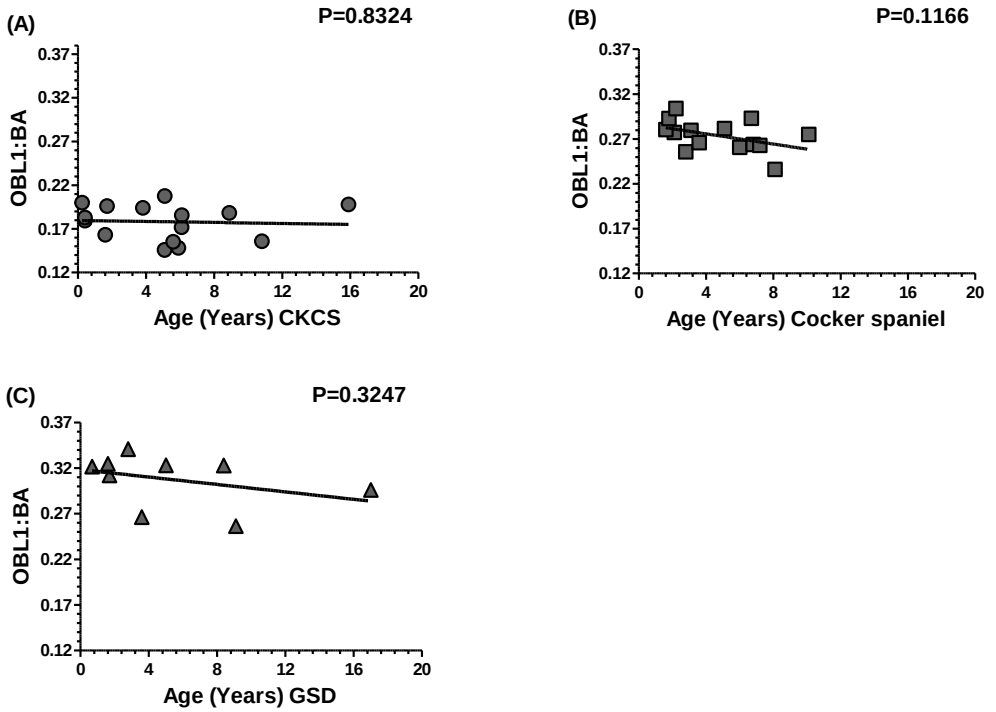

Figure 3-52: Linear regression plots representing the lack of significant correlation between age and corrected olfactory bulb length (OBL1: BA) on dorsal plane MR images from CKCS (A), Cocker spaniels (B) and GSDs (C)

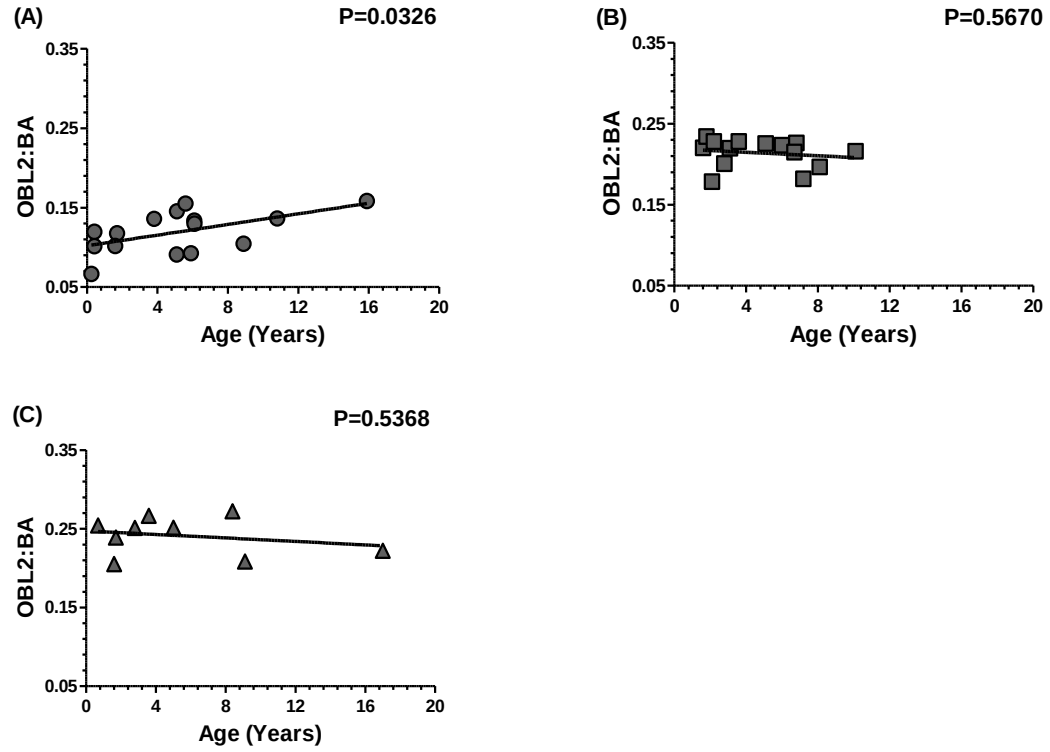

Figure 3-53: Linear regression plots representing the correlation between age and olfactory bulb length corrected for brain area (OBL2: BA) on midline sagittal plane MR images from CKCS (A), Cocker spaniels (B) and GSDs (C)

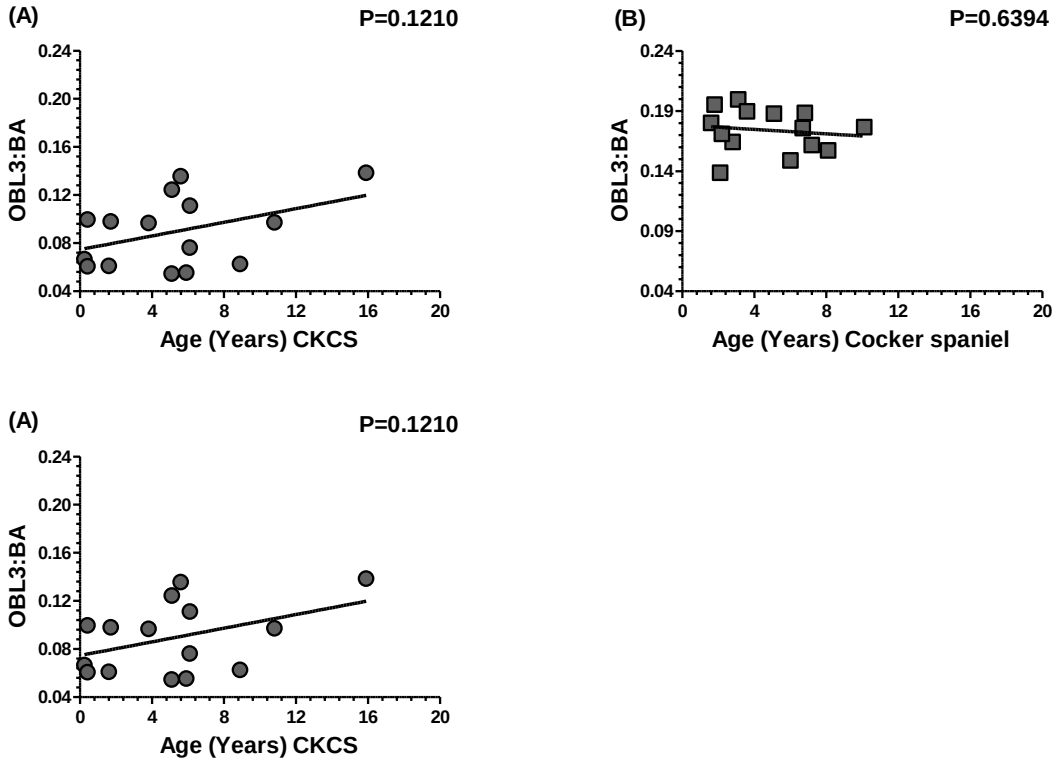

Figure 3-54: Linear regression plots representing the lack of significant correlation between age and corrected olfactory bulb length (OBL3: BA) on midline sagittal plane MR images from CKCS (A), Cocker spaniels (B) and GSDs (C)

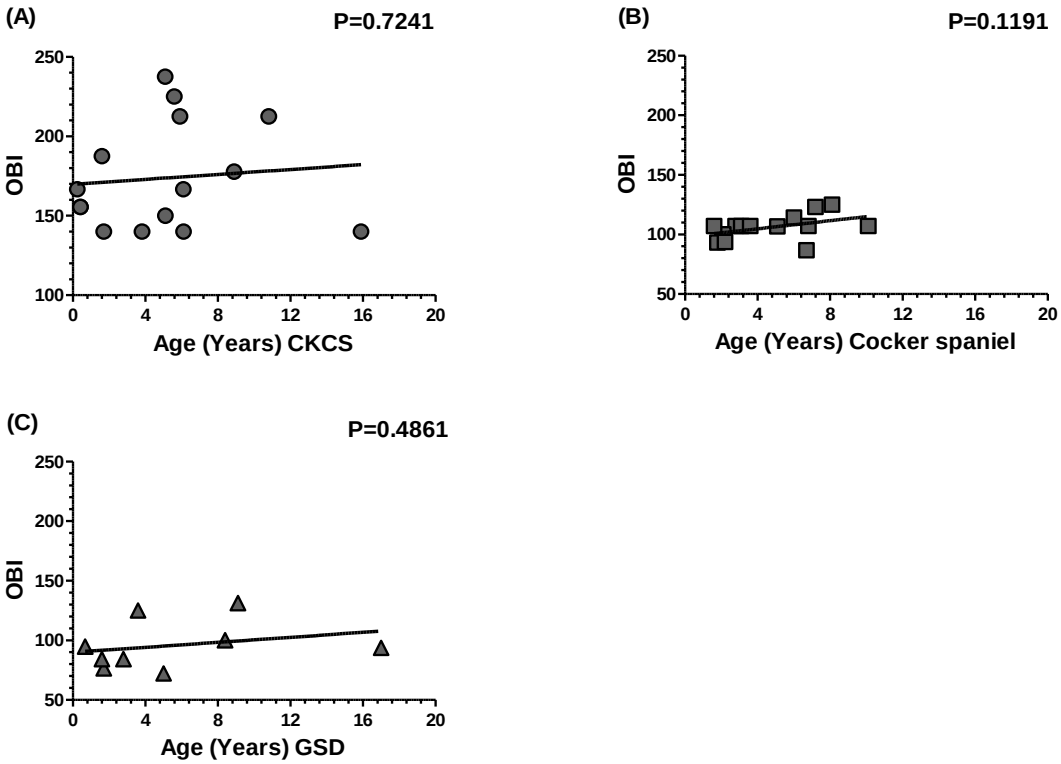

Figure 3-55: Linear regression plots representing the lack of significant correlation between age and olfactory bulb index (OBI) (= olfactory bulb width x 100/length [L1] as measured on dorsal plane MR images) from CKCS (A), Cocker spaniels (B) and GSDs (C)

3.3.4.3 Effect of gender

Study OD4:

No significant effect of gender on any of the corrected olfactory bulb linear dimensions or olfactory bulb index could be demonstrated in the CKCS, Labrador retriever or Border (Figures 3-56 to 3-58).

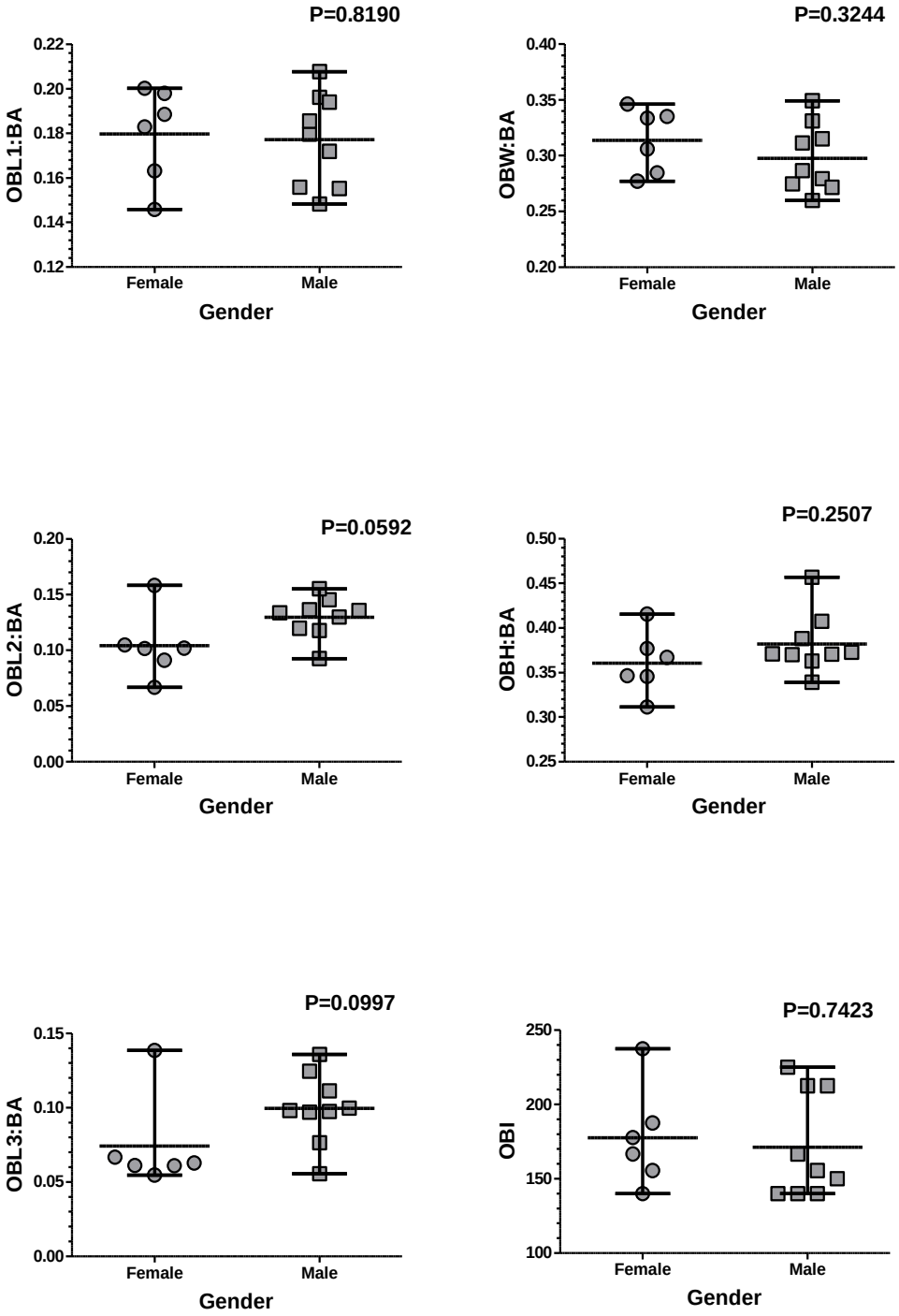

Figure 3-56: Vertical scatter plots (with range and mean) investigating the effect of gender in CKCS on corrected olfactory bulb lengths (OBL1: BA), (OBL2: BA) & (OBL3: BA); corrected olfactory bulb width (OBW: BA); corrected olfactory bulb height (OBH: BA) and olfactory bulb index (OBI)

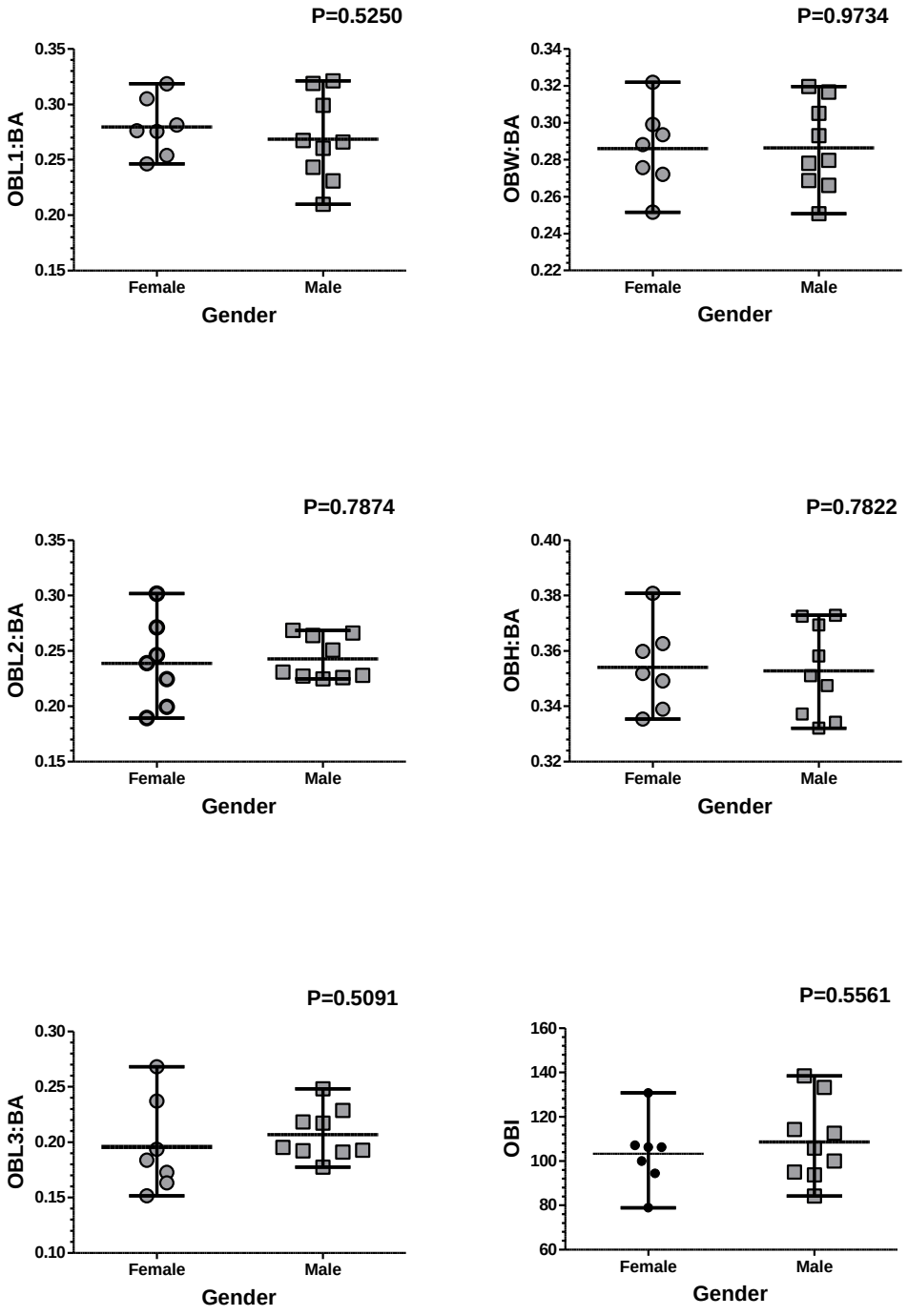

Figure 3-57: Vertical scatter plots (with range and mean) investigating the effect of gender in Labrador retrievers on corrected olfactory bulb lengths (OBL1: BA), (OBL2: BA) & (OBL3: BA); corrected olfactory bulb width (OBW: BA); corrected olfactory bulb height (OBH: BA) and olfactory bulb index (OBI)

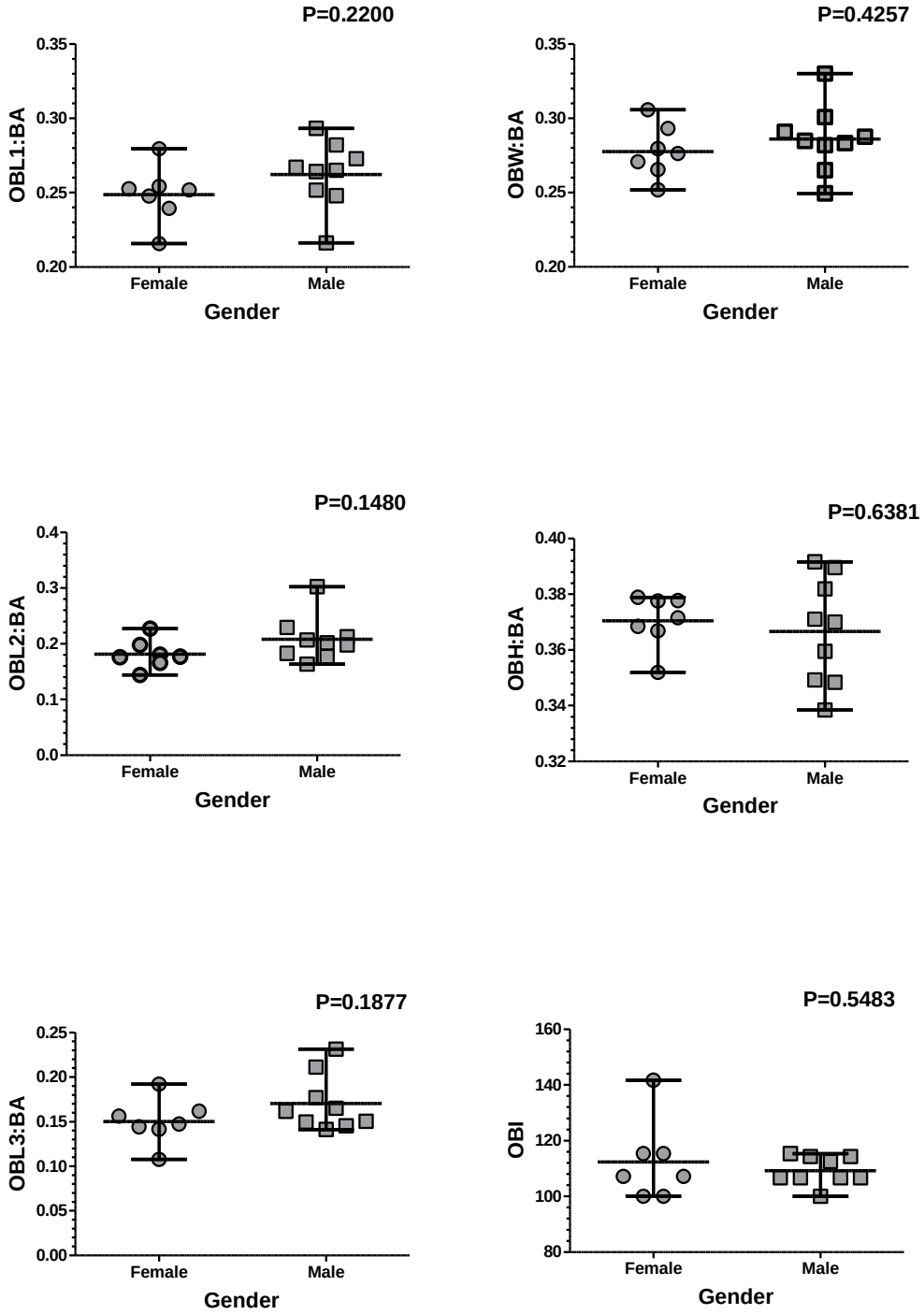

Figure 3-58: Vertical scatter plots (with range and mean) investigating the effect of gender in Border collies on corrected olfactory bulb lengths (OBL1: BA), (OBL2: BA) & (OBL3: BA); corrected olfactory bulb width (OBW: BA); corrected olfactory bulb height (OBH: BA) and olfactory bulb index (OBI)

3.4 Discussion

The dog head varies more, in both size and shape, than in other mammals and is generally considered to consist of two parts: the facial and the cranial part (that includes the brain) (Evans, 1993). Due to this diversity, dogs have been divided into long-skull

and short-skull types (Stockard, 1941). Later, Evans created a classification of brachycephalic, mesaticephalic and dolichocephalic breeds that had average skull indices of 81, 52 and 39 respectively (Miller and Christensen, 1964).

Other workers have classified dogs into brachycephalic, mesaticephalic and dolichocephalic based on either actual measurement (Onar, 1999; Smith, 1999; Schwarz et al. 2000), or simply based on anatomical experience (Pugliese et al. 2010). In the present study dogs such as the Scottish deerhound and Greyhound had Evans skull indices of 45.5 and 47.2 respectively, while the GSD was found to be 51.36. The Scottish deerhound and Greyhound have been described as dolichocephalic (Sisson, 1975; Smith, 1999; Drake and Klingenberg, 2010). However, the GSD was described as a typical long-skull dog (Stockard, 1941), but not by Evans, who defined it as a typical mesaticephalic (Miller and Christensen, 1964).

Other breeds, such as the English springer spaniel and Giant schnauzer were assigned to the dolichocephalic group by some, and mesaticephalic by others (Stockard, 1941; Miller and Christensen, 1964; Hardy et al. 1967; Evans, 1993; Drake and Klingenberg, 2010; Pugliese et al. 2010). Somewhat surprisingly, the Yorkshire terrier was described as a breed that has a dolichocephalic head shape, but with brachycephalic brain cavity features (Esteve-Ratsch et al. 2001). Using the standard Evans index, the results of this study showed that the English springer spaniel and Giant schnauzer had Evans skull index values of 57.4 and 49.6 respectively, which would imply that these breeds were actually mesaticephalic.

Stockard (1941) used seven GSDs to define the skull-base index in the breed (M±STDEV=56 ±1.51). Onar (1999) stated the average Evans index for the breed was 51.44±1.79 (n=12 and age range 2-3.5 months). However, the investigation presented here using MRI returned Stockard skull-base and Evans indices of 55.39 and 51.36 respectively for one dog. Schwarz et al. (2000) named this breed an intermediate mesati-dolichocephalic based on an Evans skull index of 50-52.27 (n=3).

The GSD is not the only breed to throw up variations in the skull-base index. The Pointer has a skull-base index of 63 according to Stockard, while measurements of MRI data in this study produced indices of 57 and 52.1 for Stockard and Evans indices.

Based on Evans' definition of typical brachycephalic breeds, the Chihuahua, Pug and Shih-tzu are typically brachycephalic. In the present study these breeds were found to have Evans skull index values ranging from 83.02 to 102.2. The Boston terrier is a typical brachycephalic breed according to Evans, with a Stockard value of 105.2±4.07.

Here a single example had a Stockard value of 106.2 and an Evans value of 90.72, meaning that this dog had values that clearly described it as a typical brachycephalic breed.

Clinically, breeds such as the CKCS, Lhasa apso, Boxer and WHWT are usually considered as brachycephalic (Hardy et al. 1967; Niebauer and Evans, 1988; Hasegawa et al. 2005). However, the CKCS and WHWT have been termed as intermediate brachy-mesaticephalics with an Evans index range of 65.25-75.74 (Schwarz et al. 2000). Yet the CKCS was found to have skull index range of 65.47-79.67 in this study using MRI data.

At least three factors may play a role in the inconsistent classification of some breeds. First, the stated breed name may be somewhat generic. For example the ***Collie***, described as a typical dolichocephalic breed (Miller and Christensen, 1964; Hardy et al. 1967; Onar, 1999), has numerous types, e.g. the Bearded collie, Border collie, Rough collie and Smooth collie, which are recorded by British Kennel Club as all belonging to the Collie family. These dogs have slightly different head shapes (Figure 3-59), so using the general term of Collie may be to some extent misleading. Second, individual variations between dogs of the same breed may in reality mean that the skull dimensions are not the same in individual dogs within the breed. Third, anatomists may classify the breed based on casual observation of the shape of the head, but not based on the skull dimensions themselves.

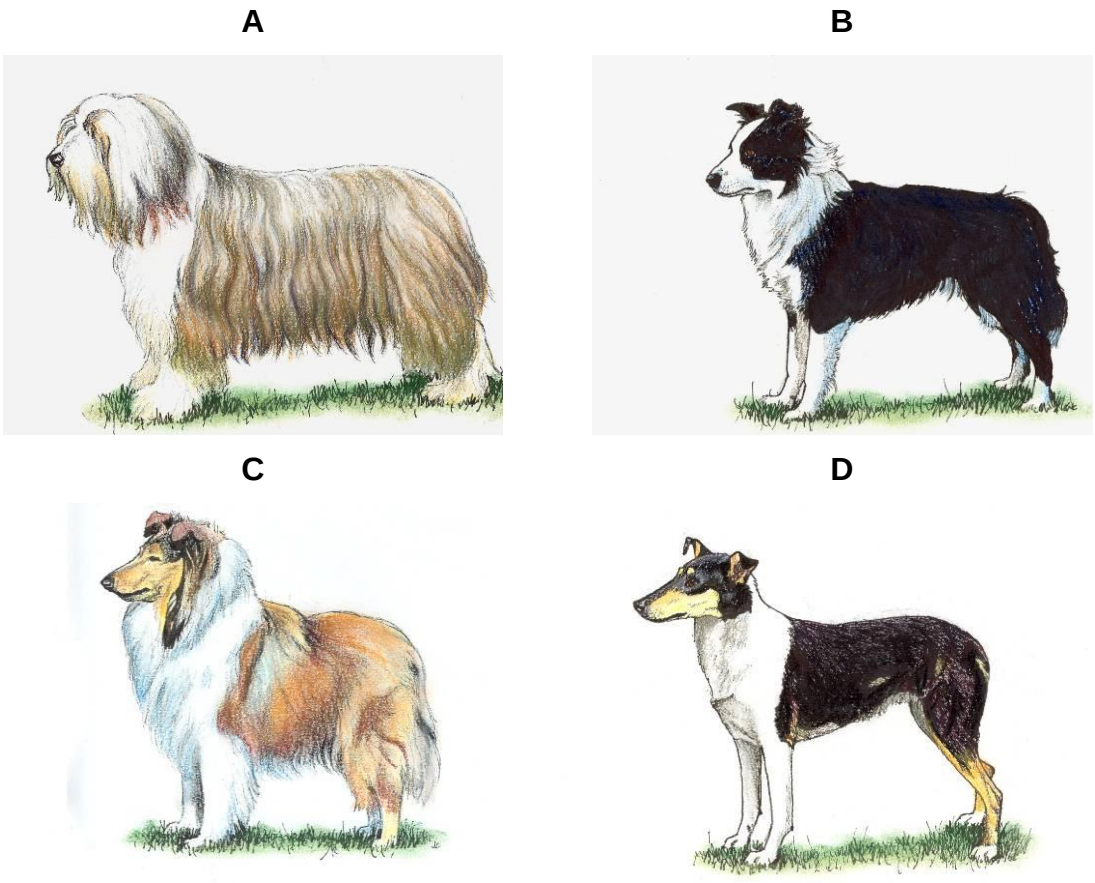

Figure 3-59: Four different types within the Collie family: (A) Bearded collie, (B) Border collie, (C) Rough collie and (D) Smooth collie (with permission of the Kennel Club)

Employing Evans index values, but applying the Lower & Upper 95% CI of the Mean of each group (Method 1) or best cut-off points between two groups (Method 2) might help to resolve the issues of breed and individual dog classification by either skull or skull-base indices.

Evans used, as explained above, the average index valued for each group, leaving investigators to suggest or interpret what the correct range might be. For example, Schwarz et al. (2000) re-defined the skull index of extreme dolichocephalic and brachycephalic as ≤ 44.25 and ≥ 75.75 respectively. Using the same approach to re-define the ranges of Evans values for the different head phenotype groups according to Method 1 and 2, it was hypothesised that a better understanding might be gained of the classification of breeds to an individual head phenotype.

In doing so breeds like German and Belgian shepherds, Scottish deerhound, Greyhound and Giant schnauzer still fell within dolichocephalic group when both new methods were applied. However, for breeds like the CKCS, Boxer, Staffordshire bull terrier, Bichon frise, Mastiff and WHWT such distinction was not achieved and these breeds were

classified at the border of two head phenotypes, with some individuals in the one head phenotype group and other individuals in a different head phenotype group (Tables 3-3 & 3-5).

It was hoped that Method 1 might deliver a higher degree of accuracy due to reduced overlapping, but had the statistical effect of excluding breeds, which would not be particularly helpful in the clinical setting. The CKCS were still seen to be scattered between the clear brachycephalic and *In-between 1* group (Table 3-3). By applying Method 2 (which had the effect of widening the range of each group), the CKCS breed became defined categorically as brachycephalic (Table 3-5). Method 1 also produced the same uncertainty for the Boxer breed as it was defined as within the *in-between 1* group (Table 3-3), whereas applying Method 2 forced it into the brachycephalic group (Table 3-5). As was illustrated in Figure 3-4, significant differences were always evident ($P<0.0001$) between brachycephalic and the non-brachycephalic groups (mesaticephalic and dolichocephalic).

The mesaticephalic group was found to have a range of 52.58-61.14 by Method 1 and 51.7-60.6 by Method 2. These ranges were not too dissimilar to the results obtained from a study measuring the skull width and length from radiographs to define a skull index range of 54.75-65.24 (Schwarz et al. 2000).

Using one dimension to classify head shape as brachycephalic, mesaticephalic or dolichocephalic was one stated goal in this part of the study. Thus a parameter had to be found that would represent anatomical variation and be statistically valid. Lyras (2009) reported a relationship between brain shape and the length of the rostrum, as the posterior border of the palate was drawn more caudally in shorter *rostra* breeds, pulling the cribriform plate backwards and taking the olfactory bulb with it. Independently in this study, and subsequently confirmed in another study (Roberts et al. 2010), an objective measure of olfactory bulb rotation was established.

Searching through anatomical studies that described the brain features from 1881 to 2010, different names for the various grooves separating the olfactory bulb from parts of the brain have been used. However, the groove that separates the olfactory bulb from the rest of the brain does not appear to have been named. Therefore the term olfactory bulb fissure was applied to this groove which could be identified grossly and also in 93% of T1 and T2-weighted dorsal and midline sagittal plane MR images. Accuracy was found to be better on midline sagittal plane images (94%) than dorsal plane images (91%). In seven dogs it was not possible to identify the olfactory bulb fissure due to abnormalities

affecting this part of the brain. Similarly it was not possible to identify this fissure on the dorsal plane if the appropriate section was not imaged. Surprisingly, delineation of the border of the olfactory bulb has been demonstrated to be clearer in the dorsal plane than sagittal images in a group of terriers and working dogs (Drees et al. 2009). Using the most dorsal and ventral points of this olfactory bulb fissure as landmarks, a line intersecting the baseline allowed determination of the degree of olfactory bulb angulation.

Early fusion of one or more of the basicranial joints, which has been observed in brachycephalic skull types, leads to growth limitation of the basicranial axis of the skull (Evans, 1993). Anatomically, the olfactory bulb is housed in the ethmoidal fossa of the cribriform plate. Thus the growth limitation of the basicranial axis causes the cribriform plate to be dragged ventrally and appears to be associated with smaller olfactory bulbs. This appears to provide an acceptable explanation for a reduced angle between the cranial axis and the olfactory bulb fissure in brachycephalic breeds. Further evidence for such translation of structures comes from a study of the palatine bone of fossil and living canids, which showed that caudal migration of the palatine bone and the cribriform plate eventually led to frontal lobe rotation and anterior-dorsal movement (Lyras, 2009).

The average and standard deviation of the olfactory bulb angle of the CKCS, Cocker spaniel and GSD were 42±5, 54±3 & 61±6 respectively, which were statistically different ($P<0.0001$). Roberts et al. (2010) (using a slightly different methodology, measuring an angle produced by intersecting the longitudinal axis of the brain and the hard palate), found that this angle gave a good indication of skull shape as brachycephalic or non-brachycephalic.

Not only the angulation but also the orientation of these angles was shown to be important, where a more ventral (Type-5) to more rostral (Type-3) orientation exemplified the differences between brachycephalic through to dolichocephalic head conformation. This result is supported by et al. (2010) who found that the position of the olfactory bulb was correlated to the skull index in individual dogs, and a more ventrally positioned olfactory bulb was associated with more extreme brachycephalia. When the angulation of the olfactory bulb measured here was compared to the Evans index value, a signification relationship was also evident ($P<0.0001$, $r^2=0.7590$). The relation between the angle of the olfactory bulb or the Evans index value had a weaker but significant correlation with bodyweight ($P<0.0001$, $r^2=0.3695$ & $P=0.0001$, $r^2= 0.2753$). The differences seen between refined groups according to Methods 1 & 2 based on the Evans index values, were also repeated when olfactory bulb angulation was used (Table 3-8).

When the olfactory bulb angles of the arbitrary control groupings were recalculated using Methods 1 & 2 to re-define the significance of the olfactory bulb angle as far as skull phenotype was concerned; a significant difference was established between brachycephalic and mesaticephalic and dolichocephalic head conformations. Using Method 1 to test the distribution of breeds classified on the basis of Evans index values, a similar distribution of breeds was also evident when olfactory bulb angulation was used. For example, the CKCS, Boxer, WHWT, mastiff and Staffordshire bull terrier were distributed across two columns, typical brachycephalic and *in-between 1* (Tables 3-3 & 10), regardless of whether the Evans index or olfactory bulb angle was applied. Interestingly, some Labrador retrievers shifted toward dolichocephalia, while the solitary Greyhound moved toward the *In-between 2* group (Tables 3-3 & 3-10), when the olfactory bulb angle was employed as the discriminator However, this change needs to be tempered by the fact that only relatively small numbers of mesaticephalic and dolichocephalic dogs were available.

Method 2 did deliver a more homogenous distribution for brachycephalic breeds when either the Evans index values or olfactory bulb angle were used; with only the WHWT failing to sit neatly as a brachycephalic. In a similar fashion to the outcome of Method 1, the Giant schnauzer and Greyhound moved toward the mesaticephalic group using the olfactory bulb angle parameter, while the Pointer drifted to be the dolichocephalic group (Tables 3-5 & 3-12). Surprisingly, the sole Beagle moved from the *In-between 1* group to the typical brachycephalic group according to the best cut-off points for the olfactory bulb angle. Skull index values are reported to be more brachycephalic in Beagles that have a dorsal notch in their foramen magnum than Beagles that do not (Watson et al. 1989).

The cranial fossa area in the midline sagittal plane had a significant correlation ($P<0.0001$, $r^2= 0.3110$; $P<0.0001$, $r^2=0.4509$ & $P<0.0001$, $r^2=0.5373$) with skull shape parameters [Evans index and olfactory bulb angle] and bodyweight respectively. Using MR images, it was also found that in dogs, the cranial cavity area calculated on the midline sagittal plane gave a good representation of the cranial cavity volume when all sagittal sections are used to generate a volume (Garcia-Real et al. 2004). Evans stated that the cranial cavity volume was more affected by bodyweight than by head shape (Evans, 1993). The head shape parameter [Evans index values] also had significant correlations ($P<0.0001$, $r^2=0.3623$; $P<0.0001$, $r^2= 0.3265$ & $P=0.0229$, $r^2=0.1075$) with the rostral, middle and caudal fossae midline areas respectively, however the bodyweight may play a role. When the ethmoidal fossa was picked out, it was the only part of the

rostral fossa apparently affected by head conformation as measured by the parameters used ($P<0.0001$). Evans implied that early fusion of the skull-base lead to brachycephalisation of the skull shape. As in man, reduction in the cranial-base leads to a dished deformity within the middle third of the facial skeleton and brachycephalisation of the neurocranium, as seen in Downs syndrome and achondroplasias (Mooney and Siegel, 2002).

When the midline ethmoidal, middle and caudal fossae areas corrected for brain area were compared between groups, it appeared that the only strong correlation was between the ethmoidal fossa and head shape. Bodyweight also appeared to be correlated with the ethmoidal fossa midline area (corrected for brain area), however this correlation was weaker and only evident in brachycephalic breeds compared to the other two head conformation groups using the post comparison test. These results would appear to be supported by work done by Garcia-Real et al (2004) who reported that dogs with the same range of bodyweight had variable cranial cavity volumes.

From the dog population used in this study, the relationship between head phenotype and the corrected area of the ethmoidal fossa appeared to be due to the effect of the skull-base on the direction of the cribriform plate, where flattening led to an increasing degree of brachycephalia. The length of the sphenoid body in man and chimpanzees is believed to have an affect on the degree of the facial projection in relation to the anterior cranial fossa, which ultimately impacts on the cranial shape (Lieberman, 1998). While the actual physical presence of the brain is believed to determine the subsequent development of the craniofacial appearance, so brain absence (anencephaly) results in acalveria in man (Mooney and Siegel, 2002). In primates, increasing size of the brain, especially the neocortex, may lead to increased cranial vault size (Calvaria), basicranial flexion and both forward and downward rotation of the face, while, reduction in body size may lead to reduction in the size of the maxillae (Mooney and Siegel, 2002).

Looking to exemplar breeds, as opposed to groups, the olfactory bulb appeared to be breed related and may change according to the cranial cavity shape e.g. in dome-like heads, the frontal bone and consequently the frontal lobe extend rostrally leaving the cribriform plate and the olfactory bulb caudal and ventral to them. In 1941, Weidenreich mentioned that "*the olfactory recess, completely missing in dwarf dogs but very pronounced in large ones, appears as a median prolongation of the cranial cavity which extends in the direction of the nasion*".

No substantial differences were found between the mesaticephalic and dolichocephalic skull types when the olfactory bulb dimensions were analysed statistically. However, significant differences were seen between olfactory bulb lengths of the brachycephalic and the other two groups. Because the ethmoidal fossa of the cribriform plate forms the cavity where the olfactory bulb of the rhinencephalon is situated, this may suggest that the olfactory bulb dimensions shape the dimensions of the cribriform plate. If this were the case then this leads to speculation that the shape of the cranial cavity at the level of the ethmoidal fossa may have the same width, but different lengths depending on skull shape. This is not supported by work in mice where different strains had no effect on the olfactory bulb size grossly (Mirich et al. 2002). In contrast reduction in the size of the olfactory organs resulted in a generalised reduction of the snout in primates (Mooney and Siegel, 2002).

Total size of the different layers of the olfactory bulb increased in rats with age (3-24 months), but then decreased between 24-30 months of age (Hinds and McNelly, 1977). The effect of age on olfactory bulb length in the midline sagittal plane (OBL2:BA) of the CKCS breed is in agreement with the previous study. This might be due to the postnatal changes in the brachycephalic skull. Yet in mice Mirich et al. 2002) found no effect of age on the size of the olfactory bulb.

In contrast, Cocker spaniels and GSDs (as representatives of the mesaticephalic and dolichocephalic head conformations) demonstrated no correlation with age in all measurements of the olfactory bulb. In man, statistical analysis demonstrated no significant differences in the total volume of the olfactory bulb with age (Bhatnagar et al. 1987). Increasing length of the olfactory bulb (OBL2:BA) in the CKCS may suggest that the shape of the ethmoidal fossa and consequently of the olfactory bulb may change with age, while remain unchanged in Cocker spaniels and GSDs.

In summary, using one dimensional MR images the skull phenotype can be defined on the basis of olfactory bulb angulation, instead of the two dimensions and whole head imaging required for calculation of the Evans and Stockard indices. Olfactory bulb angulation allowed classification of dogs into brachycephalic, mesaticephalic and dolichocephalic groups. The above classification also indicated that head phenotype had a substantive effect on the position of the olfactory bulb and the anatomy of the ethmoidal fossa of the cranial cavity. While dogs can be classified according to head phenotype generally, no definitive range for each group exists and a spectrum of head phenotypes appears to occur within individual breeds. However this provides evidence

that mighth support the use of skull indices for selection of breeding animals in order to reduce extreme brachycephalia.

4 EFFECT OF HEAD CONFORMATION ON THE ETHMOTURBINATES AND NASOPHARYNX

4.1 Introduction

The smell sense is described as well developed in macrosomatic animals, including the dog and cat (Negus, 1958; Venker-van-Haagen, 2005). However, the utility of dogs for scent work varies between different breeds, with brachycephalic dogs typically described as having a poor sense of smell relative to other dogs. One potential explanation for this has being crowding of the ethmoturbinates and altered positioning of the olfactory bulb (Roberts et al. 2010). A direct relationship between the area of the olfactory epithelium and the acuity of the sense of smell has been identified (Negus, 1958), a finding supported by later work in a variety of mammalian species (Gurtovoi, 1966 cited by Adams, 1972).

Alteration in olfactory acuity is not the only change associated with differences in nasal anatomy. Apnoea, hypopnoea, desaturation, otitis media, snoring and obstructive sleep apnoea syndrome (OSAS) have all been associated with a narrowed bony nasopharynx and oropharynx, and also soft palate lesions in man and animals, with these changes being more frequent or more severe in dogs with a brachycephalic head shape (Laurikainen et al. 1987; Ono et al. 1996; Yu et al. 2003; Renko et al. 2007). Nasopharyngeal disorders such as stenosis of the nasopharynx are frequently identified in dogs, with examples including compromise of the choanal area due to protrusion of the nasoturbinates into the nasopharynx and a choanal mass (Billen et al. 2006). Choanal atresia (Khoo et al. 2007) and stenosis of the nasopharynx (Mitten, 1988) have been reported in cats.

Gross examination (Negus, 1958; Schreider and Raabe, 1981) and MRI techniques (Assheuer and Sager, 1997; Rycke et al. 2003; Craven et al. 2007) have been used to describe the anatomical features of the nasal airway in the dog, including the ethmoturbinates and the nasopharynx. MRI would seem a useful technique to allow simultaneous classification of head phenotype and examination of the nasal airways.

The objectives of the study were therefore to:

1. Determine if there was an effect of head conformation on the area of the ethmoturbinates
2. Examine whether the reduction in olfactory bulb area seen in association with increasing brachycephalia was correlated with a similar change in ethmoturbinate area
3. Determine if the dimensions and shape of the bony nasopharynx are influenced by head conformation.

4.2 Materials and Methods

4.2.1 Ethmoturbinate study group

Magnetic resonance data from 39 dogs representing a spectrum of different breeds, which had been shown to lack evidence of disease of the cranial cavity, nasal area and olfactory region were analysed. The breeds included 10 CKCSs, 4 WHWTs, 3 Boxers, 3 Cross breeds, 3 Labrador retrievers, 3 Shih-tzus, 2 Lhasa apsos, and one each of the following breeds: Bichon frise, Chihuahua, Cocker spaniel, Scottish deerhound, English springer spaniel, Mastiff, Miniature schnauzer, Papillon, Pointer, Pug and Staffordshire bull terrier. Both female (13) and male (26) dogs were included, having an age range of 0.8-10.9 years [M±STDEV=5.3±2.9] and bodyweight ranging from 2.7 to 44.3kg [M±STDEV=13.8±11.3].

The following measurements were performed according to the procedures explained in chapter 2:

- Evans and Stockard indices (Tables 2-1 and 2-2)
- Olfactory bulb angulation and orientation (Figures 2-1 and 2-2)
- Olfactory bulb area (Figure 2-6A)
- Brain area (Figure 2-6B)
- Nasal cavity area (Figure 2-5B)
- Ethmoturbinate area (Figure 2-5D)

To establish if there was an effect of bodyweight on the ethmoturbinate area, the cube root of the bodyweight and the square root of the ethmoturbinate area were compared. To diminish the effect of the bodyweight, the data was corrected for midline brain area where stated. This was done by dividing the ethmoturbinate area on the dorsal by the brain area at the midline sagittal plane

4.2.2 Bony nasopharynx study group

The same group in 4.2.1 was used in this part of the study, supplemented by an additional 5 dogs, to define the shape of the bony nasopharynx. These included 2 CKCSs, 1 Boxer, 1 Chihuahua and 1 Giant schnauzer. This gave a total of 44 animals aged between 0.8-16.7 years [M±STDEV=5.3±3.3], 15 were female and 29 were male and the range of the bodyweight became 2.7-44.3 kg [M±STDEV=14.4±11.4].

The following parameters were measured as detailed in chapter 2:

- Evans index (Table 2-1)
- Olfactory bulb angulation and orientation (Figures 2-1 and 2-2)
- Transverse area and shape of the nasopharynx [corrected for bodyweight and brain area] (Figure 2-8)
- Height of the nasopharynx [corrected for brain area] (Figure 2-7)

4.3 Results

4.3.1 The areas of the ethmoturbinates and olfactory bulb decreased with increasing brachycephalia

There was a significant reduction in the corrected ethmoturbinate area in the dorsal plane with increasing brachycephalia (P<0.0001), as determined by the Evans and Stockard indices and by olfactory bulb angulation (Figure 4-1 A to C).

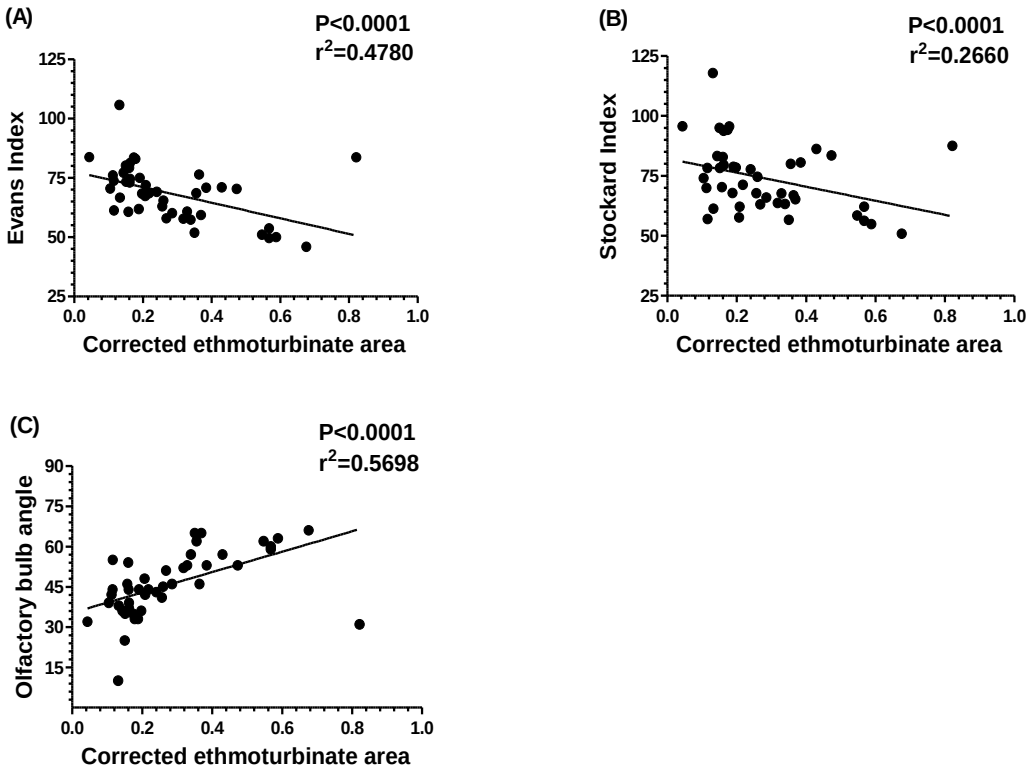

Figure 4-1: Linear regression plots demonstrating that increasing brachycephalic (higher Evans and Stockard index values or a lower olfactory bulb angle) was significantly correlated with a reduction in the corrected ethmoturbinate area. (A) Evans index, (B) Stockard index and (C) the olfactory bulb angulation as determined by MRI

In addition to the correlation noted above, the corrected olfactory bulb area in the midline sagittal plane also demonstrated a significant correlation (P<0.0001) with head conformation, with a reduction in olfactory bulb area with increasing brachycephalia, as determined by the Evans and Stockard indices and olfactory bulb angulation (Figure 4-2).

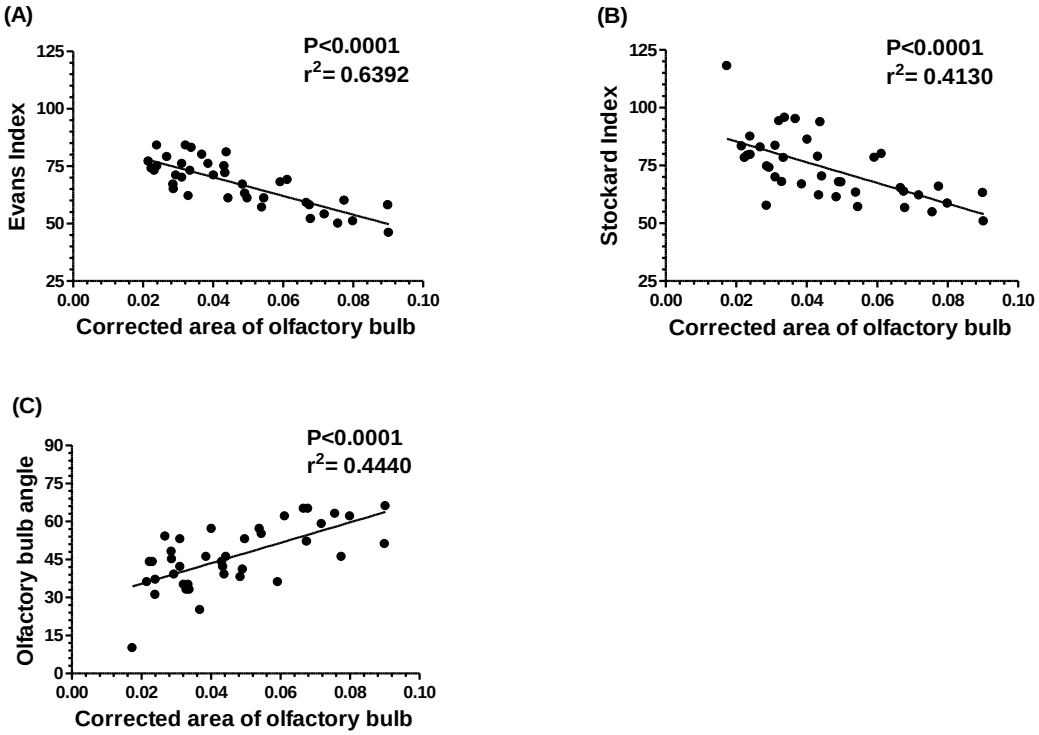

Figure 4-2: Linear regression graphs showing that increasing brachycephalic (higher Evans and Stockard index values or a lower olfactory bulb angle) was significantly correlated with a reduction in the corrected area of the olfactory bulb (A) Evans index, (B) Stockard index and (C) the olfactory bulb angulation as determined by MRI

Examination of olfactory bulb orientation (Types 1 to 5) revealed that ventral orientation of the olfactory bulb (Type-5) correlated with a significant (P<0.0001) reduction in ethmoturbinate area (Figure 4-3).

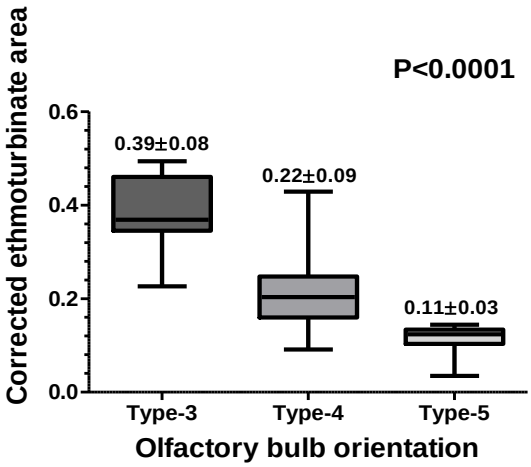

Figure 4-3: Box and whisker plots (range, mean & standard deviation) showing the correlation between olfactory bulb orientation (Types 3-5) and corrected ethmoturbinate area

4.3.2 An increase in ethmoturbinate area was correlated with an increase in nasal cavity area and olfactory bulb area

Examination of the effect of bodyweight on the ethmoturbinate area corrected for the brain area revealed that as bodyweight increased so to did the relative ethmoturbinate area (P<0.0001) (Figure 4-4). However, in general the proportion of dogs with a brachycephalic head phenotype was higher in the lower bodyweight.

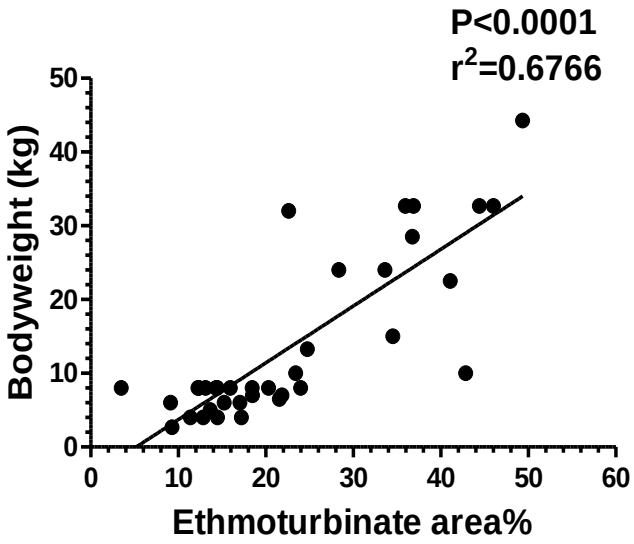

Figure 4-4: Linear regression plot revealing that the increasing bodyweight was correlated with an increase in the relative area of the ethmoturbinates

Comparison of the absolute ethmoturbinate area (dorsal plane) with the absolute area of the nasal cavity (sagittal plane) revealed a strong correlation between both; and also between the latter and the olfactory bulb area (P<0.0001) (Figure 4-5).

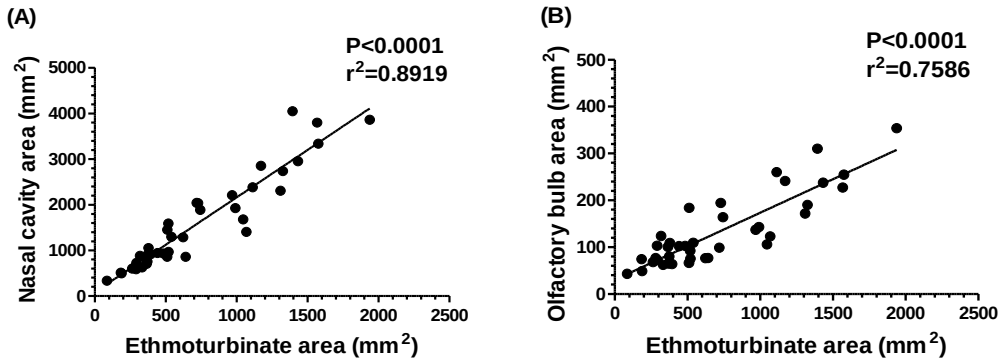

Figure 4-5: Linear regression plots revealing that (A) increasing area of the nasal cavity was directly correlated with an increase in the area of the ethmoturbinates, and (B) similarly an increase in ethmoturbinate area was correlated with an increase in the area of the olfactory bulb

4.3.3 The cross-sectional area of the bony nasopharynx decreased with increasing brachycephalia

The relationship between the cross-sectional area of the bony nasopharynx (corrected for brain area) at the level of caudal nasal spine of the palatine bone on transverse MR images and head phenotype was examined in this part of the study. Head phenotype was quantified according to the Evans and Stockard indices and angulation of the olfactory bulb. The results revealed that increasing brachycephalia was correlated with a decrease in the cross-sectional area of the bony nasopharynx ($P<0.0001$ for Evans index and olfactory bulb angulation, $P=0.0003$ for Stockard index) (Figure 4-6).

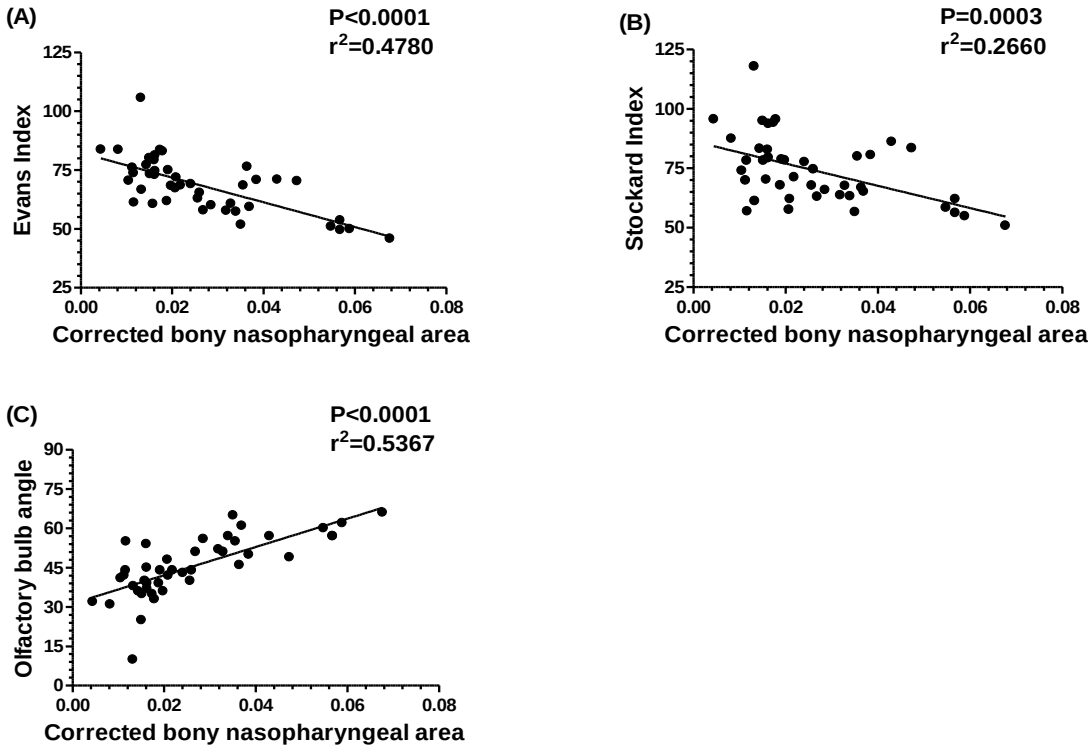

Figure 4-6: Linear regression plots demonstrating that increasing brachycephalia (higher Evans/Stockard indices, lower olfactory bulb angle) resulted in a concomitant decrease in the cross-sectional area of the bony nasopharynx (corrected for midline brain area); (A) Evans index, (B) Stockard index, and (C) olfactory bulb angulation

To diminish the confounding effect of bodyweight, the analysis was repeated with the corrected bony nasopharyngeal area corrected for bodyweight (Figure 4-7). This revealed similar results to the analysis where cross sectional nasopharyngeal area was corrected for midline brain area (Figure 4-6).

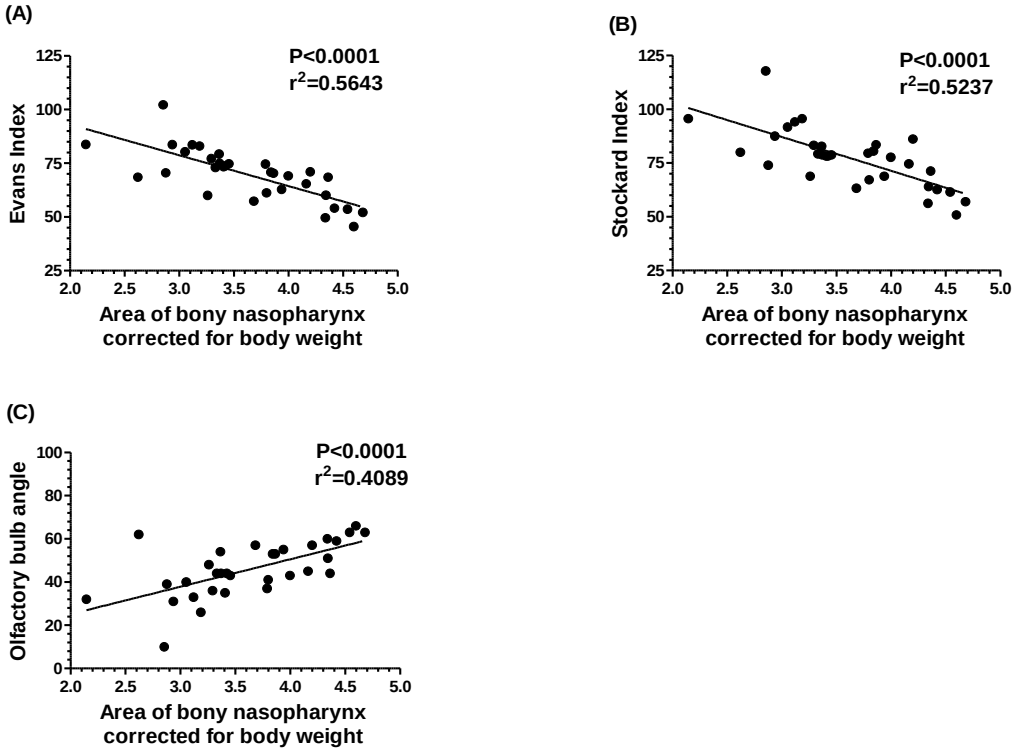

Figure 4-7: Linear regression plots revealing that increasing brachycephalia (higher Evans/Stockard indices values, lower olfactory bulb angulation) resulted in a concomitant decrease in the cross-sectional area of the bony nasopharynx (corrected for bodyweight). The figure demonstrates similar results to Figure 4-6, but following correction for bodyweight instead of brain area; (A) Evans index, (B) Stockard index, and (C) olfactory bulb angulation

4.3.4 The cross sectional area of the bony nasopharynx decreased with increasing brachycephalia

The area of the bony nasopharynx in the transverse plane corrected for brain area demonstrated a significant correlation ($P<0.0001$) with olfactory bulb orientation, with a more ventral olfactory bulb orientation (increasing brachycephalia) associated with a reduction in the midline area of the nasopharynx. This indicated a significant effect of head phenotype on the midline area of the nasopharynx. The mean transverse nasopharyngeal area relative to brain area was 0.01, 0.02 and 0.05 for olfactory bulb orientation type-5, 4 and 3 respectively (Figure 4-8).0.3

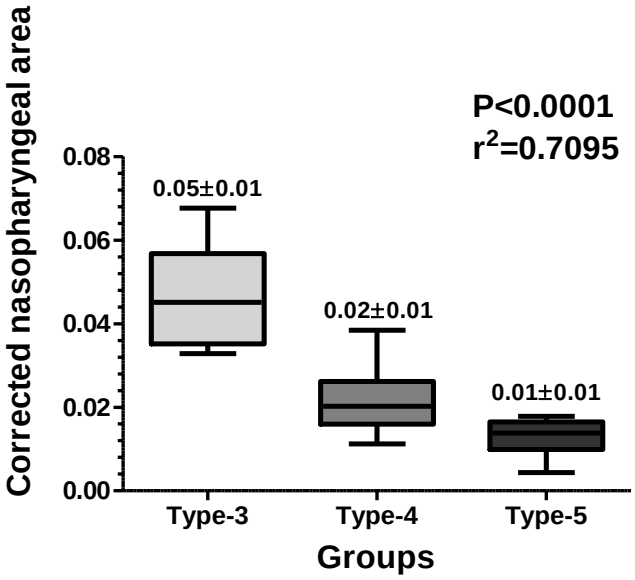

Figure 4-8: Box and whiskers plot (1-99 percentile) with mean and standard deviation showing the correlation between olfactory bulb orientation (Type 3-5) and corrected nasopharyngeal area

4.3.5 The height of the bony nasopharynx decreased with increasing brachycephalia

Similarly, a correlation was evident when the relationship between the height of the nasopharynx (corrected for brain area) and head conformation (using the Evans and Stockard indices and the angulation of the olfactory bulb; P=0.0002, 0.0362 and <0.0001 respectively) was examined (Figure 4-9).

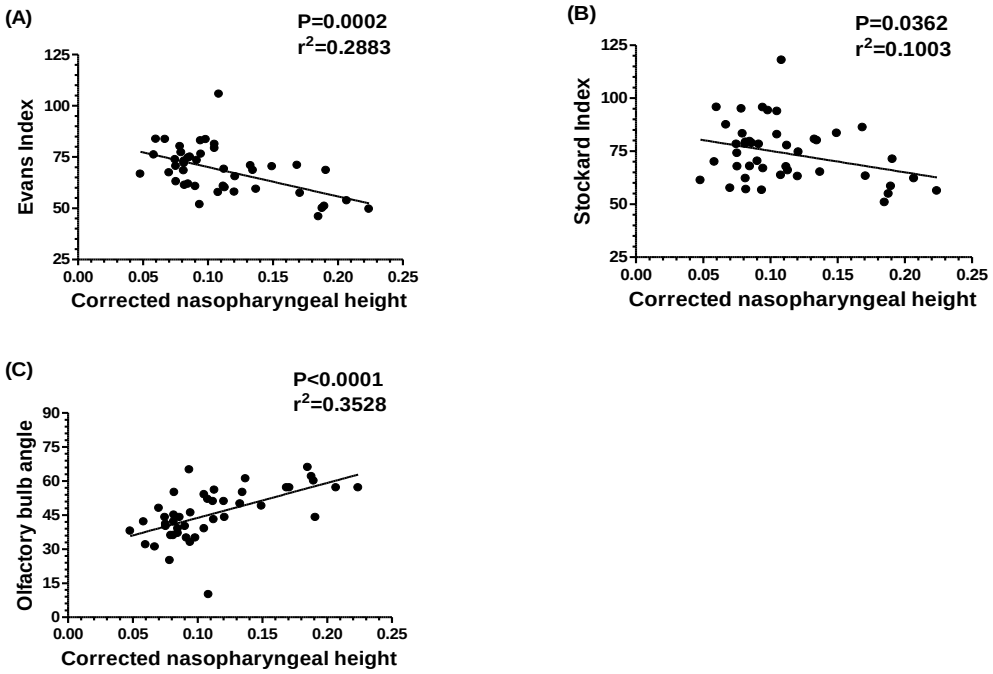

Figure 4-9: Linear regression plots demonstrating the relationship between bony nasopharyngeal height corrected for brain area and head conformation as determined by the (A) Evans index, (B) Stockard index, and (C) olfactory bulb angulation. Bony nasopharyngeal height decreased with increasing brachycephalia

Examination of the effect of olfactory bulb orientation demonstrated a similar correlation between more ventral olfactory bulb orientation and a reduction in the midline height of the bony nasopharynx at the level of the mid-point of the olfactory bulb ($P<0.0001$). However, no significant difference was evident when the analysis was restricted to only dogs with Type-4 and Type-5 olfactory bulb orientation (Figure 4-10).

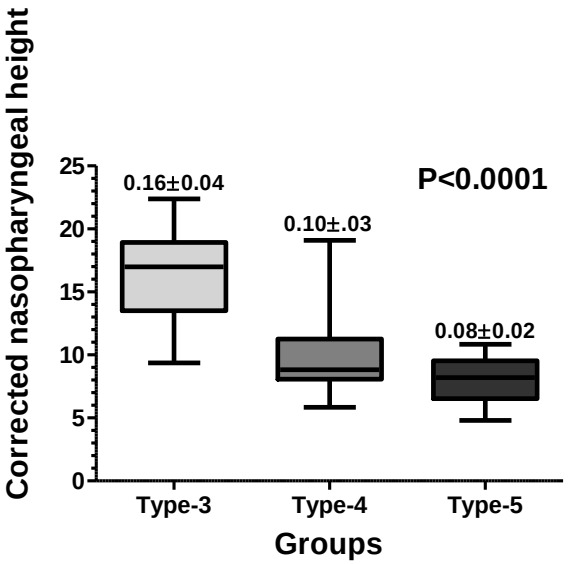

Figure 4-10:. Box and whisker (1-99 percentile) plot demonstrating the relationship between olfactory bulb orientation (Type 3-5) and corrected nasopharyngeal height. Bony nasopharyngeal height decreased with increasing brachycephalia

4.3.6 The cross-sectional shape of the bony nasopharynx changed with increasing brachycephalia and this shape change was correlated with a decrease in the cross-sectional area

Examination of the shape of the bony nasopharynx on MR images in the transverse plane at the level of the caudal nasal spine of the palatine bone revealed three main shapes to the bony nasopharynx in transverse section: oval, mouth and peanut shaped (Figure 4-11). **Oval shaped** was self-explanatory; **mouth shaped** was when there was an invagination into the dorsal OR ventral aspect of the lumen of the nasopharynx; **peanut shaped** was when there was a dorsal AND ventral invagination into the lumen of the nasopharynx.

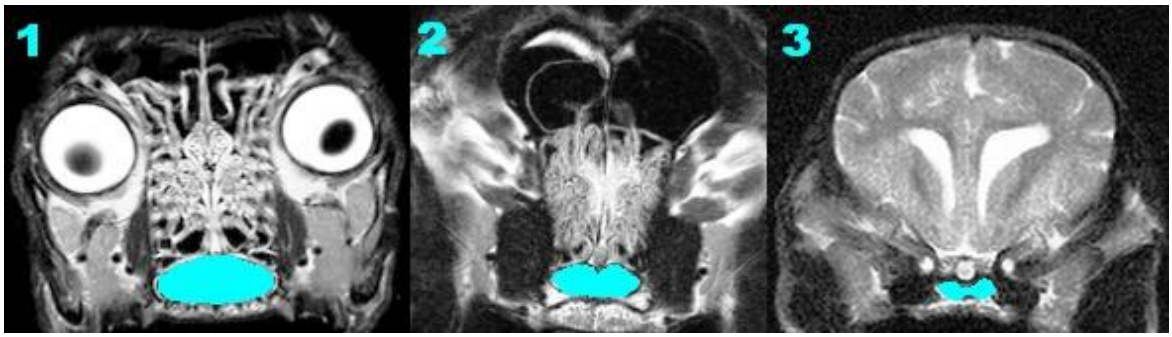

Figure 4-11: The three main shapes of the bony nasopharynx in transverse section identified on T2w MR images at the level of the caudal nasal spine of the palatine bone: (1) oval shaped, (2) mouth shaped, and (3) peanut shaped

Examination of the relationship between the shape and area of the nasopharynx in transverse section at the level of the caudal nasal spine of the palatine bone revealed a highly significant difference in the corrected cross-sectional area between the three different shapes ($P<0.0001$), with the corrected cross-sectional area decreasing from oval, to mouth, to peanut shaped (Figure 4-12A). Examination of the correlation between head phenotype as determined by the Evans index and olfactory bulb angulation demonstrated a similar correlation between head conformation and the shape of the nasopharynx in transverse section, with a tendency for greater brachycephalia as the shape changed from oval, to mouth, to peanut shaped (Figure 4-12B and C).

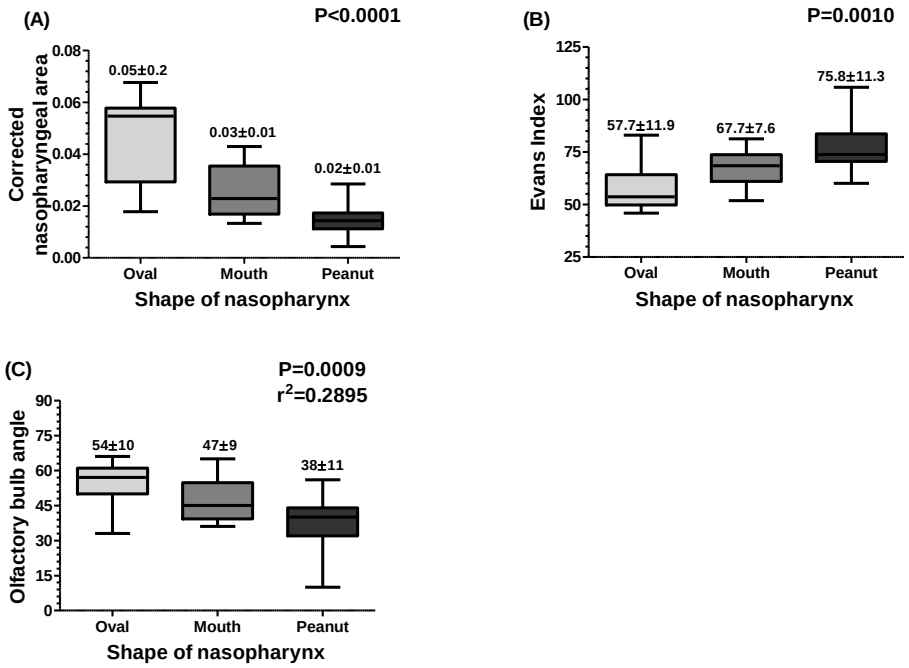

Figure 4-12: Box and whisker (1-99 percentile) plot demonstrating the relationship between the cross-sectional shape of the bony nasopharynx and the corrected area of the bony nasopharynx (A), Evans index (B), and olfactory bulb angulation (C). The area (corrected for brain area) decreased as the shape changed from oval, to mouth to peanut shaped (A). Similarly, the shape changed from oval, to mouth to peanut shaped as the head conformation changed from dolichocephalic to brachycephalic as determined by increasing Evans index (B) and decreasing olfactory bulb angulation (C).

Examination of the specific head phenotype associated with each different shape of the nasopharynx revealed the following pattern of occurrence (summarised in Tables 4-1 and 4-2):

- **Oval shaped**: 9 dogs were classified as having an oval nasopharyngeal shape representing 21% of the total population, including 6 animals classified as Type-3 olfactory bulb orientation, 2 animals classified as Type-4 olfactory bulb orientation and 1 classified as Type-5 olfactory bulb orientation (Table 4-1 and 4-2). The mean corrected nasopharyngeal area was 0.05 ± 0.02 (Figure 4-12A).
- **Mouth shaped:** 20 dogs were classified as having a mouth shaped nasopharynx representing 46% of the total population. The majority of these dogs (12/20) were classified as Type-4 olfactory bulb orientation, followed by Type-3 (6/20) and Type-5 (2/20) (Table 4-1 and 4-2). The mean corrected nasopharyngeal area was 0.03 ± 0.01 (Figure 4-12A).
- **Peanut shape:** 15 dogs were classified as having a peanut shaped nasopharynx representing 33% of the total population. These dogs were all classified as Type-4

(8/15) or Type-5 (7/15) olfactory bulb orientation (Table 4-1 and 4-2). The mean corrected nasopharyngeal area was 0.02±0.01 (Figure 4-12A).

OB orientation	No of dogs	Oval shape	Mouth shape	Peanut shape
Type-3	12	6	6	0
Type-4	22	2	12	8
Type-5	10	1	2	7
Total	44	9	20	15

Table 4-1: The frequency of occurrence for each individual shape classification of the cross-sectional appearance of the nasopharynx relative to the olfactory bulb (OB) orientation, expressed as the absolute number of cases

OB orientation	Oval shape	Mouth shape	Peanut shape
Type-3	50%	50%	0
Type-4	9%	55%	36%
Type-5	10%	20%	70%
Proportion of total population	21%	46%	33%

Table 4-2: The frequency of occurrence for each individual shape classification of the cross-sectional appearance of the nasopharynx relative to the olfactory bulb (OB) orientation, expressed as a percentage. The last row represents the proportion of the total population of dogs for each individual shape

Examination of the frequency of occurrence of each individual cross-sectional shape of the nasopharynx revealed that the pattern of distribution of each shape was also determined by the orientation of the olfactory bulb (Figure 4-13). The more ventrally rotated the olfactory bulb (type-5), the more the nasopharynx adopted a peanut shape, while the more dorsally orientated the olfactory bulb the more likely the nasopharynx was to adopt an oval shape. The mouth shape of the nasopharynx, where there was an invagination on just the dorsal or ventral aspect, was an intermediate shape between the oval and peanut shapes.

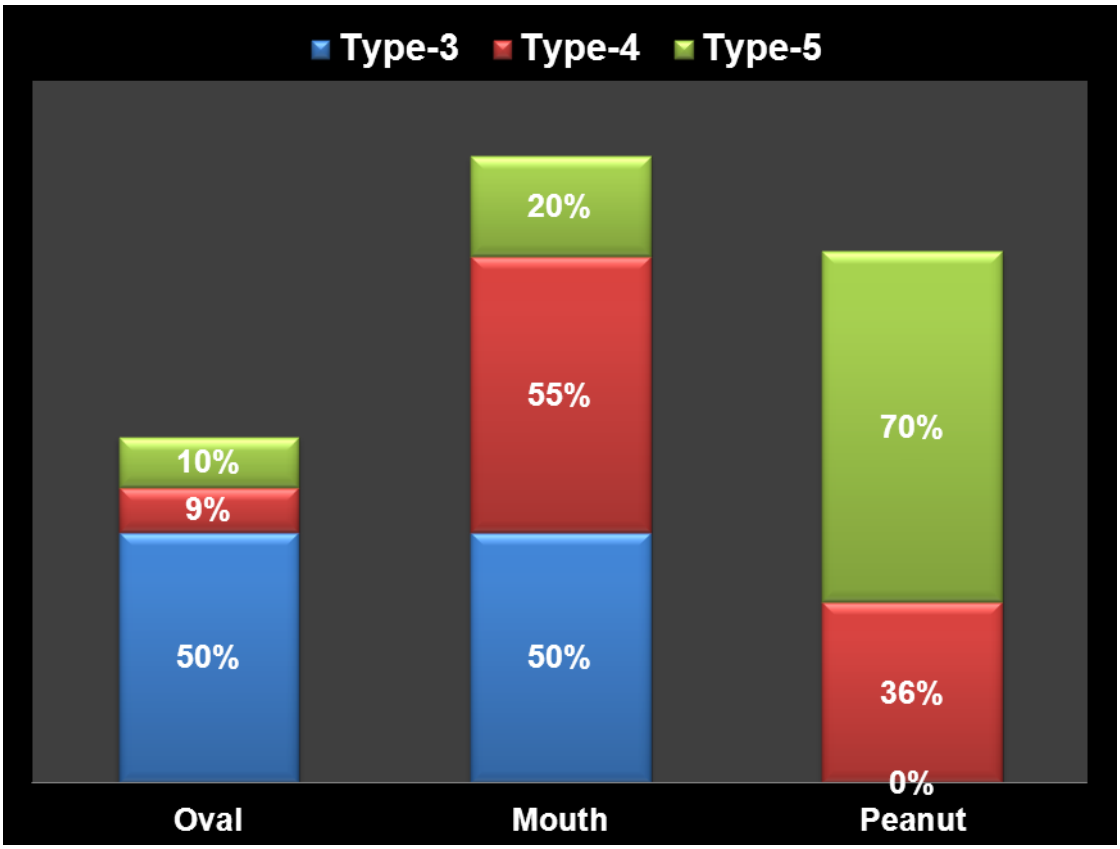

Figure 4-13: Clustered column chart with three types of olfactory bulb orientation groups according to their associated with nasopharyngeal shape (n=44). The peanut shape was more frequent in dogs with a Type 5 (or brachycephalic) olfactory bulb orientation, while the oval shape was more frequent in dogs with a Type 3 (or dolichocephalic) olfactory bulb orientation

4.3.7 The reduction in the transverse area and height of the bony nasopharynx was related to a decrease in the size of the olfactory bulb and the ethmoidal turbinates

The relationship between the olfactory bulb area and both the nasopharyngeal area and height was examined. Additionally, the correlation of the corrected ethmoturbinate area to the corrected nasopharyngeal and height was examined. Previous results had demonstrated a correlation between olfactory bulb area and ethmoidal turbinates area. The results demonstrated a strong positive correlation between olfactory bulb area and nasopharyngeal area ($P<0.0001$) and height ($P<0.0001$). Similarly there was a strong positive correlation between ethmoidal turbinate area and nasopharyngeal area ($P<0.0001$) and height ($P<0.0001$), indicating that the reduction in area and height of the nasopharynx was not due to occlusion of the nasopharynx by a larger olfactory bulb and ethmoidal turbinates (Figures 4-14 and 4-15).

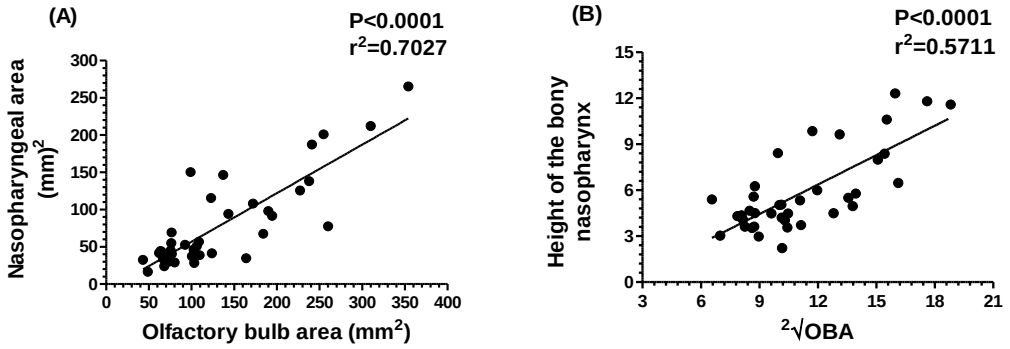

Figure 4-14: Linear regression graphs demonstrating the relationship between the olfactory bulb area and nasopharyngeal area and height. Olfactory bulb area was positively correlated with the area (A) and height (B) of the nasopharynx [$^{2}\sqrt{}$OBA= the square root of the olfactory bulb area]

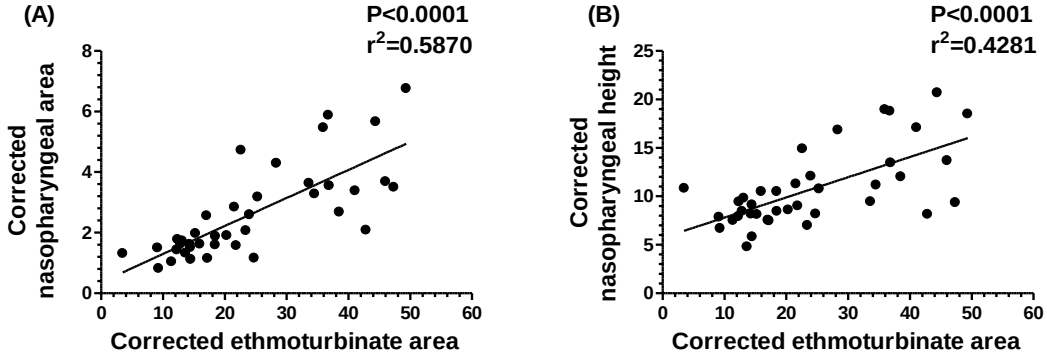

Figure 4-15: Linear regression graphs demonstrating the relationship between ethmoturbinate area and nasopharyngeal area and height. Ethmoturbinate area (corrected for brain area) was positively correlated with the area (A) and height (B) of the nasopharynx (corrected for brain area)

4.4 Discussion

The facial part of the upper respiratory tract is the nasal cavity, which contains the ethmoturbinates at its caudal end (Evans, 1993). Ventral to the ethmoturbinates is the nasal part of the pharynx, which is bounded rostrally by the caudal choanae and extends caudally up to the level of the termination of the soft palate (Budras et al. 2002). The ethmoturbinates are important for olfaction, which is intimately associated with other functions such as feeding behaviour, social interaction and reproduction (Venker-van-Haagen, 2005). The olfactory mucosa has been defined on the basis of the ethmoturbinate area of the nasal cavity in dogs (Craven et al. 2010) and is usually located in the caudal recess of the nasal region (Cook, 1964).

The results of the present study demonstrated a significant correlation between the area of the ethmoturbinates as measured on dorsal plane MR images and head phenotype as

determined by the Evans and Stockard indices and the angulation of the olfactory bulb ($P<0.0001$ for all). There was a reduction in ethmoturbinate area (and therefore the area of the olfactory mucosa) with increasing brachycephalia. Increasing brachycephalia is therefore likely to have an adverse effect on the acuity of sense of smell. Consistent with this finding, it has previously been reported that brachycephalic dogs are not usually selected for tasks that require a high degree of olfaction as there is crowding of the ethmoturbinate bones (Roberts et al. 2010). In a separate study, the smell sense in Boxers (brachycephalic) was thought to be weaker than in poodles (mesaticephalic) (Tacher et al. 2005). Examination of the relationship between the area of the olfactory epithelium (on the basis of anatomical examinations) and the acuity of the sense of smell demonstrated a direct relationship between the two (Negus, 1958), a finding supported by later work demonstrating a better sense of smell in subjects with a larger olfactory epithelium area [(Gurtovoi, 1966) cited by (Adams, 1972)]. However histological and anatomical examination of the nasal cavity of two types of bats, *Artibeus* (shorter nosed) and *Myotis* (longer nosed), found that the complexity of the surface of ethmoturbinates had a greater effect on the development of olfaction than the volume of the nasal cavity may have (Bhatnagar and Kallen, 1974b).

The present study also demonstrated a positive correlation between bodyweight and the ethmoturbinate area, a finding that is in keeping with a previous study which demonstrated a correlation between the epithelial surface of the nasal cavity (including the respiratory and olfactory areas) and bodyweight, and a correlation between nasal cavity length, volume and bodyweight in mice (Adams, 1972).

Differences between species also exist and dogs have a larger olfactory bulb than man (Allison, 1953). Genetic studies have also shown that dogs have about 31% more different olfactory receptors (a larger repertoire) than man, but less pseudogene receptors. The pseudogene receptors are believed to contribute less to the smell of sense (Quignon et al. 2003). In birds a positive correlation has also been suggested between an improved sense of smell and increased diameter of the olfactory bulbs and the cerebral hemispheres (Bang and Cobb, 1968). In the present study the increase in the ethmoturbinate area was accompanied by an increase in olfactory bulb area, which may be argued as further evidence of potential for an enhanced sense of smell.

The nerve connections (or axons) from the olfactory receptors pass through the cribriform lamina (plate) before synapsing within the olfactory bulb. Examination of the area of the cribriform lamina in lemurs, old and new world monkeys and man, demonstrated that a reduction in the area of the cribriform lamina was associated with a

weakened sense of smell (Negus, 1958). In mice, an increase in the area of the cribriform plate was correlated with an increase in the total area of the olfactory bulb (Bhatnagar and Kallen, 1974a). As demonstrated in this chapter, olfactory bulb area was decreased in brachycephalic dogs. The previous chapter demonstrated flattening of the cribriform plate and a decrease in olfactory bulb angulation, in brachycephalic group which suggests that a reduction in the area of the cribriform plate was likely in brachycephalic dogs, although this was not determined as part of the present study. An anatomical, but not functional, correlation between the shape of the nasal pharynx and the olfactory bulb has been demonstrated in living and fossil canids (Lyras, 2009). In that study, the caudal border of the palate was more caudally situated in shorter nosed animals than the relatively longer nosed animals, and this may influence the position of the cribriform plate and therefore the olfactory bulb. The effect of olfactory bulb size on the sense of smell is likely to be due to a reduction in the numbers of receptors within the nasal cavity and reduced cell populations within the olfactory bulb. Consistent with this, the size of the glomeruli (one of the olfactory bulb layers) appeared to vary in nearly direct proportion to the size of the olfactory bulb in a number of different mammals, including the rabbit, rat, monkey, man and dog (with the dog having the largest absolute diameter) (Allison, 1953).

Studies describing the gross (Negus, 1958; Schreider and Raabe, 1981) and MRI (Assheuer and Sager, 1997; Rycke et al. 2003; Craven et al. 2007) features of the nasal airways have been published in dogs. Similar work has been performed describing the nasopharynx in man (Bergland, 1963; Handelman and Osborne, 1976; Laurikainen et al. 1987). However, few studies have focussed on the bony (osseous) portion of the nasopharynx and that makes up the rostral part of the nasopharynx in dogs (Evans, 1993). It has been reported that visual assessment of the area of the nasal cavity on rostro-caudal radiographs (and which most likely represents the osseous nasopharynx) provides a good indirect measure of the nasal airflow volume in man (Holmberg and Linder-Aronson, 1979). It has also been suggested that the shape and diameter of the nasopharynx and of the nose determined the volume of air passing through the nasopharynx and nose (Wong et al. 2005).

A strong correlation between the area of the nasopharynx (corrected for brain area or bodyweight) and head conformation was evident, with increasing brachycephalia correlated with a reduction in the area of the nasopharynx ($P<0.0001$). In man, a smaller width of the bony nasopharynx has been associated with a posterior position of the maxilla and, in combination with enlargement of the soft palate, may contribute to upper

airway narrowing. This may increase the risk of developing OSAS, even in non-obese patients (Yu et al. 2003). A relationship between the adequacy of the airway and morphology of the craniofacial part of the head has been reported with moderate statistical significance (Solow et al. 1984). Furthermore, deeper and narrower nasopharyngeal dimensions were observed in association with obtuse and acute cranial base angles respectively in man (cranial base angle = Nasion-Sella-Basion) (Ricketts, 1960).

Decreasing bodyweight was associated with a reduction in nasopharyngeal area on transverse section in this study. In man, obesity had no effect on the cross-sectional area of the nasopharynx on the basis of radiography in normal subjects and patients with OSAS (Ono et al. 1996). However, this absence of a correlation may result from radiographs only being able to identify the bony boundaries of the nasopharynx. Using pharyngeal endoscopy, the nasopharynx in patients with sleep apnoea was reported to have a smaller cross-sectional area than normal subjects (Isono et al. 1997). The anterior-posterior dimensions of the bony nasopharynx of non-obese people were found to be statistically smaller than both snorers and obese patients (Yu et al. 2003). Whereas, snoring was considered to be the only symptom that had a significant correlation with a smaller size of the nasopharyngeal airway lumen (Sorensen et al. 1980).

Based on the results of the present study, the mean corrected transverse area of the bony nasopharynx (expressed as a ratio relative to brain area) at the level of caudal nasal spine of the palatine bone for oval, mouth and peanut shapes were 0.05, 0.03, and 0.02 respectively. On the basis of these findings it is likely that the oval shape identified in the mesaticephalic and dolichocephalic groups represents the normal appearance, and that the mouth and peanut shapes represent an alteration in the shape with progressive brachycephalia. The change in the cross-sectional shape may well be due to malformation/buckling/bending of the vomer (potentially including the presphenoid bone as well) and/or the hard palate, which leads to the reduction in cross-sectional area and the alteration in shape. The impingement of the ethmoturbinates into the bony nasopharynx may also contribute to this shape change and reduction in cross-sectional area. In human subjects, a reduction in the width of the bony nasopharynx was also associated with more posterior positioning of the maxilla (Yu et al. 2003). The majority of these changes which impact on the bony nasopharynx dimensions appear to be developmental and there is a large amount of evidence to support this, with the correlation between the spheno-occipital synchondrosis being essential for longitudinal

growth and alterations in the shape of the cranial base and the nasopharynx (Bergland, 1963). There is also a strong relationship between the craniofacial and the upper airway structures and functions (Cistulla, 1996), with the adequacy of the airways and the morphology of the craniofacial structures influenced by each other (Solow et al. 1984).

One of the major outcomes of the present study was the recognition and definition on the basis of MRI imaging studies of an extreme variant of olfactory bulb orientation (type-5), found in brachycephalic dogs and the correlation of this change in olfactory bulb orientation with other head conformation changes. The irregular shape of the bony nasopharynx on transverse section was also identified more frequently in brachycephalic dogs, which may be the result of bending of the roof or the floor of the nasopharynx, but may be exacerbated by the presence of nasoturbinates within the bony bounded portion of the nasopharynx. The presence of nasopharyngeal turbinates has been significantly associated with upper respiratory disease in brachycephalic dogs and cats (Ginn et al. 2008). Consequently, breeding away from extreme ventral olfactory bulb orientation may help reduce the incidence of nasopharyngeal turbinates and increase the cross-sectional area of the nasopharynx, and thereby reduce upper respiratory diseases in brachycephalic dogs and cats.

In man, it has been suggested that airway obstruction, the mode of breathing and nasopharynx obstruction were correlated with head posture and the height of the lower jaw, but not the height of the upper face (Woodside and Linder-Aronson, 1979). In contrast, a separate study suggested that decreased nasal airway resistance was not associated with an extended head posture (Weber et al. 1981). In addition, linear regression analysis for the tongue, soft palate, nasopharynx, oropharynx and hypopharynx demonstrated a significant linear relationship between the two-dimensional cross-sectional area and three-dimensional volume of the tongue, soft palate, and nasopharynx (Ono et al. 1996). The same study demonstrated a correlation between the shape of the nasopharynx and the shape of the cranial-base in man, when examined in the sagittal plane. From the age of six years to maturity the bony nasopharynx volume increased by 80% in human patients (due to increasing width and height but not depth of the bony nasopharynx) (Bergland, 1963). The larger nasopharyngeal capacity was associated with a higher nasopharynx, the growth of which was believed to cease with the onset of maturity. In the data presented in the current study, brachycephalic dogs had a smaller area, different shape and smaller height of the bony nasopharynx as compared to mesaticephalic and dolichocephalic dog. These results are supported in man by previous work which identified a correlation between nasopharyngeal area and the

descent of the hard palate from the sphenoid bone, giving a positive correlation with its height (Handelman and Osborne, 1976).

The findings of the current study, particularly when considered in light of the reported literature, not only demonstrated a correlation between head conformation and the area of the ethmoturbinates and nasopharynx ($P<0.0001$), but also that the anatomical arrangement of these components influenced each other. The proposal that early fusion of the ethmo-sphenoid joint occurs in brachycephalic dogs (Evans, 1993), may suggest an explanation for the changes associated with the brachycephalic skull shape that were identified as part of the current study. In particular, retraction of the bones attached to the cranial-base, including the cribriform lamina, would modify head shape by causing rotation of the cribriform plate ventrally, resulting in a reduction in the size of the nasal cavity, crowding of the ethmoidal turbinates, and in some individuals causing displacement of these turbinates into adjacent sinuses. Movement of the cribriform plate caudally would indirectly result in the hard palate being dragged caudally, leading to changes in the area of the bony nasopharynx due to deviation of the bony nasopharynx roof or floor or both.

5 EFFECT OF HEAD CONFORMATION ON THE 3RD VENTRICLE, INTERTHALAMIC ADHESION AND QUADRIGEMINAL CISTERN

5.1 Introduction

The 3rd ventricle has been defined (Figure 5-1) as a CSF filled chamber connecting the left and the right lateral ventricles with the 4th ventricle (Fitzgerald, 1961; Horodyska and Kreiner, 1962). It is comprised of a body and a number of recesses (Fitzgerald, 1961; Horodyska and Kreiner, 1962; Anderson et al. 1994; De Lahunta and Glass, 2009). The body of the 3rd ventricle surrounds the circular interthalamic adhesion, which unites the left and right halves of the thalamus (Beitz and Fletcher, 1993; Anderson et al. 1994; De Lahunta and Glass, 2009). The quadrigeminal cistern is located caudal to the suprapineal recess of the 3rd ventricle and overlain by the cerebrum dorsally, the cerebellum caudally and the midbrain ventrally (Leigh et al. 2008).

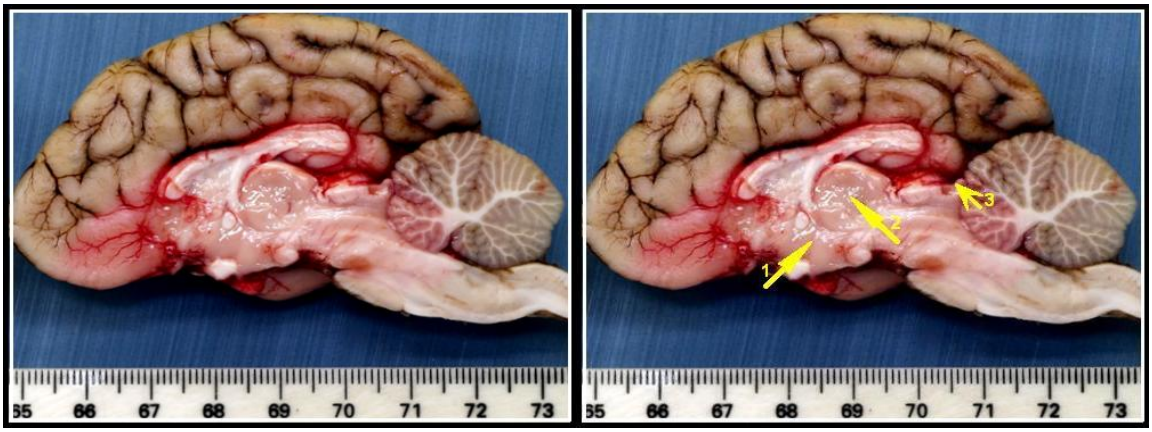

Figure 5-1: Midline sagittal section through a fresh canine brain demonstrating the 3rd ventricle (1), the interthalamic adhesion (2) and the quadrigeminal cistern

Radiography, ultrasonography, CT and MR imaging have all been applied to the investigation of the ventricular system, the interthalamic adhesion and the quadrigeminal cistern in dogs (Assheuer and Sager, 1997; Kealy and McAllister, 2005; Leigh et al. 2008). Radiographic contrast ventriculography has also been used to define the ventricular system shape and position to aid in the detection of abnormalities (Kealy and McAllister, 2005). In addition, ultrasonography has been found to be a safe non-invasive method for examining the ventricular system where an open fontanelle is present (Hudson et al. 1989), and for identifying abnormalities of the quadrigeminal cistern (Saito et al. 2001). MR imaging has revolutionised the *in vivo* study of the brain due to its ability to distinguish different types of soft tissue and fluid, both normal and pathological (Kraft et al. 1989; Assheuer and Sager, 1997; Leigh et al. 2008).

The 3rd ventricle, interthalamic adhesion and quadrigeminal cistern are frequently implicated in, or affected by, disease of the brain; however our understanding of the

normal anatomy of these structures is limited, making interpretation of normality and abnormality difficult. In particular, brachycephalic dogs have a reported higher incidence of quadrigeminal cistern cysts (Saito et al. 2001) and it has not been established if there is a difference in these structures related to head conformation.

The aims of this chapter were therefore to:

1. Describe the normal anatomical appearance and dimensions of the 3rd ventricle, interthalamic adhesion and quadrigeminal cistern, and detail the changes in these structures with disease in the following 3 groups of dogs:
    - Group 1 dogs with a normal brain MRI
    - Group 2 dogs with brain disease resulting in gross pathological ventriculomegaly
    - Group 3 dogs with brain conditions other than gross ventriculomegaly
    - Group 4 dogs with Chiari- like syndrome
2. Determine the effect of skull phenotype on the dimensions of these structures in group 1.
3. Determine the influence of bodyweight on these structures in group 1.
4. Investigate whether age and gender influenced the dimensions of these structures in group 1.
5. Investigate the effect of Chiari-like malformation syndrome on these structures in group 4.

5.2 Materials and Methods

5.2.1 Animals

Dogs were classified according to the final clinical diagnosis into the following groups:

1. **NAD:** No MRI abnormalities affecting the cranial cavity or brain detected. Nineteen dogs [11 female and 8 male] had a clinical diagnosis of idiopathic vestibular syndrome, degenerative myelopathy, otitis media, intervertebral disc extrusion, degenerative disc disease and vagal mediated bradycardia. This group included 12 breeds [Golden retriever (5), Boxer (3), Yorkshire terrier (2), and one each of the following breeds: Alaskan malamute, Dalmatian, GSD, Greyhound, Pointer, minature Poodle, Rough collie, Shih-tzu and Springer spaniel] having a bodyweight range of 3.5 - 57kg [M ± STDEV = 25.9±12] and an age between 1 and 13.3 years [M ± STDEV = 7.2±3.7].
2. **NAD-E:** No MRI abnormalities detected - idiopathic epilepsy. Fifty five dogs [19 female and 36 male] all had a history of seizures with no abnormalities besides the seizures detected on clinical and neurological examination, routine haematology and biochemistry and MRI of the brain. This group included 25 breeds [Labrador retriever (10), Border collie (6), Boxer (5), GSD (5), Springer spaniel (4), Dalmatian (2), Gordon setter (2), Husky (2), Miniature schnauzer (2), Yorkshire terrier (2), and one of the following: Alaskan malamute, Basset hound, Border terrier, Boston terrier, Chihuahua, Dobermann, English Springer spaniel, German shorthaired pointer, Hungarian vizsla, Lhasa apso, Mastiff, Pointer, Poodle, Shih-tzu and Staffordshire bull terrier]. These dogs had a range of bodyweight of 3.5 – 90kg [M ± STDEV = 25.2±14.23] and an age range of 1.1-17 years [M ±STDEV = 5.8±3.7].
3. **VM:** Conditions associated with gross pathological ventriculomegaly where this was considered to be the main MR imaging abnormality. Six dogs [equal females and males] diagnosed with congenital hydrocephalus, acquired hydrocephalus, quadrigeminal cyst with or without hydrocephalus or age-related ventriculomegaly with concurrent behaviour abnormalities]. Three Chihuahuas and one CKCS, Maltese terrier and Miniature poodle were included in this group. They had a bodyweight range of 1.8 - 5kg [M ±STDEV = 3.2±1.2] and were aged 0.4-19 years [M ±STDEV = 5.6±6.9].

4. **OBL:** Other brain lesions group. Dogs within this group were diagnosed with brain neoplasia, inflammation of the brain, granulomatous meningoencephalomyelitis and idiopathic cerebellitis (little white shaker disease). This group comprised seven dogs [5 female and 2 male] including Labrador retriever (2), Springer spaniel (2), and one Boxer, Maltese terrier and Poodle. The group had range of bodyweight from 2.7 - 32.8kg [M ±STDEV=18.4±11.3] and age of 0.5-9.8 years [M ±STDEV=4.4±3.03].

5. **CH-LMS:** Chiari-like malformation syndrome group. Thirteen CKCS were included with varying degrees of severity of caudal cerebellar herniation. The group comprised 6 female and 7 male, with an age range of 3.5 - 12.7 years [M±STDEV=7.2±2.8] and bodyweight of 4 - 8kg [M ±STDEV=6.2±2.1].

The areas of the structures of the middle fossa defined in section 2.12, were applied on all the above groups.

In addition to these groups, a further group was defined as the **Normal MRI Group** by combining the NAD and the NAD-E groups. The Normal MRI Group was used to define the normal descriptive appearance and midline area of the 3rd ventricle, interthalamic adhesion and quadrigeminal cistern after the comparison between the NAD and NAD-E groups demonstrated no statistical difference for these parameters (see Results, section 5.3.1).

5.2.2 The effect of head phenotype on the descriptive appearance and midline area of the 3rd ventricle, interthalamic adhesion and quadrigeminal cistern

Head phenotype was determined according to the olfactory bulb angle methods (Chapter 2) and dogs were classified as brachycephalic, mesaticephalic and dolichocephalic on the basis of these results. The effect of head phenotype on the descriptive appearance and area (expressed as a ratio relative to midline brain area) of the 3rd ventricle, interthalamic adhesion and quadrigeminal cistern was determined within the Normal MRI group after examining each area of these two groups (NAD and NAD-E groups) according to the statistical method described in Chapter 2.

5.2.3 The effect of bodyweight on the descriptive appearance and midline area of the 3rd ventricle, interthalamic adhesion and quadrigeminal cistern

Dogs were grouped according to bodyweight into the following three arbitrarily chosen groups:

1. <15 kilograms
2. 15-30 kilograms
3. >30 kilograms

The effect of bodyweight on the descriptive appearance and area (expressed as a ratio relative to midline brain area) of the 3rd ventricle, interthalamic adhesion and quadrigeminal cistern was determined within the Normal MRI group after examining each area of these two groups the (NAD and NAD-E groups) according to the statistical method described in Chapter 2.

5.2.4 The effect of age and gender on the descriptive appearance and midline area of the 3rd ventricle, interthalamic adhesion and quadrigeminal cistern

In this section, the Normal MRI group was used.

5.2.5 Effect of Chiari-like malformation syndrome (CH-LMS) on the descriptive appearance and midline area of the 3rd ventricle, interthalamic adhesion and quadrigeminal cistern

CKCSs within the CH-LMS group were classified as normal, mildly affected or severely affected on the basis of a previously published classification system (Lu et al. 2003). The classification was based on the position of the cerebellar vermis and its distance within the foramen magnum. When the cerebellar vermis was situated rostral to, or at the level of, the foramen magnum then dogs were assigned a score of 0 (normal). If the cerebellar vermis extended caudal to the foramen magnum for a distance of not more than 2 mm then dogs were assigned a score of 1 (mild). If the cerebellar vermis extended caudal to the foramen magnum for a distance of greater than 2 mm then dogs were assigned a score of 2 (severe) (Figure 5-2). The effect of CH-LMS on the descriptive appearance and area (expressed as a ratio relative to midline brain area) of the 3rd

ventricle, interthalamic adhesion and quadrigeminal cistern was determined within the CH-LMS group according to the statistical methods described in Chapter 2.

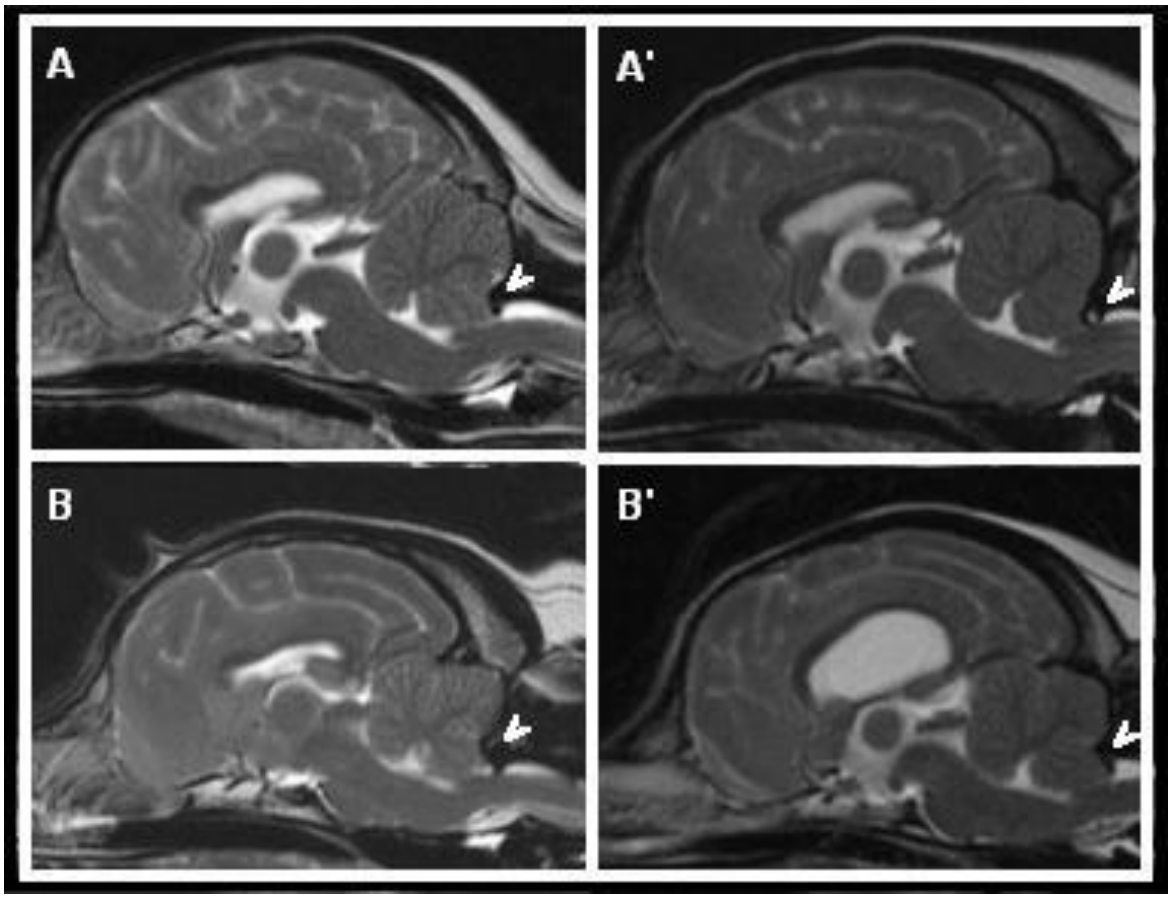

Figure 5-2: Examples of classification of CKCSs with CH-LMS on midline, sagittal plane T2-weighted MR images based on the methods used in a previous study (Lu et al. 2003). If the cerebellar vermis (arrow heads) extended caudal to the foramen magnum for a distance of not more than 2 mm then dogs were assigned a score of 1 (mild) (**A** and **A**'). If the cerebellar vermis extended caudal to the foramen magnum for a distance of greater than 2 mm then dogs were assigned a score of 2 (severe) (**B** and **B**')

5.3 Results

5.3.1 The normal descriptive appearance and midline area of the 3rd ventricle, interthalamic adhesion and quadrigeminal cistern

The descriptive appearance and the midline area (corrected for midline brain area) of the 3rd ventricle, interthalamic adhesion and quadrigeminal cistern in relation to olfactory bulb angle and bodyweight were similar for the NAD and the NAD-E groups (Figures 5-3 and 5-4). Head phenotype had a minimal effect in these two groups of dogs, with the effect being similar in the normal (NAD) and idiopathic epilepsy (NAD-E) groups. On the basis of these results the following description of the normal appearance of these structures was based on the merged sets of MRI studies for the two groups (Normal MRI group) in order to increase the animal numbers for the individual breeds.

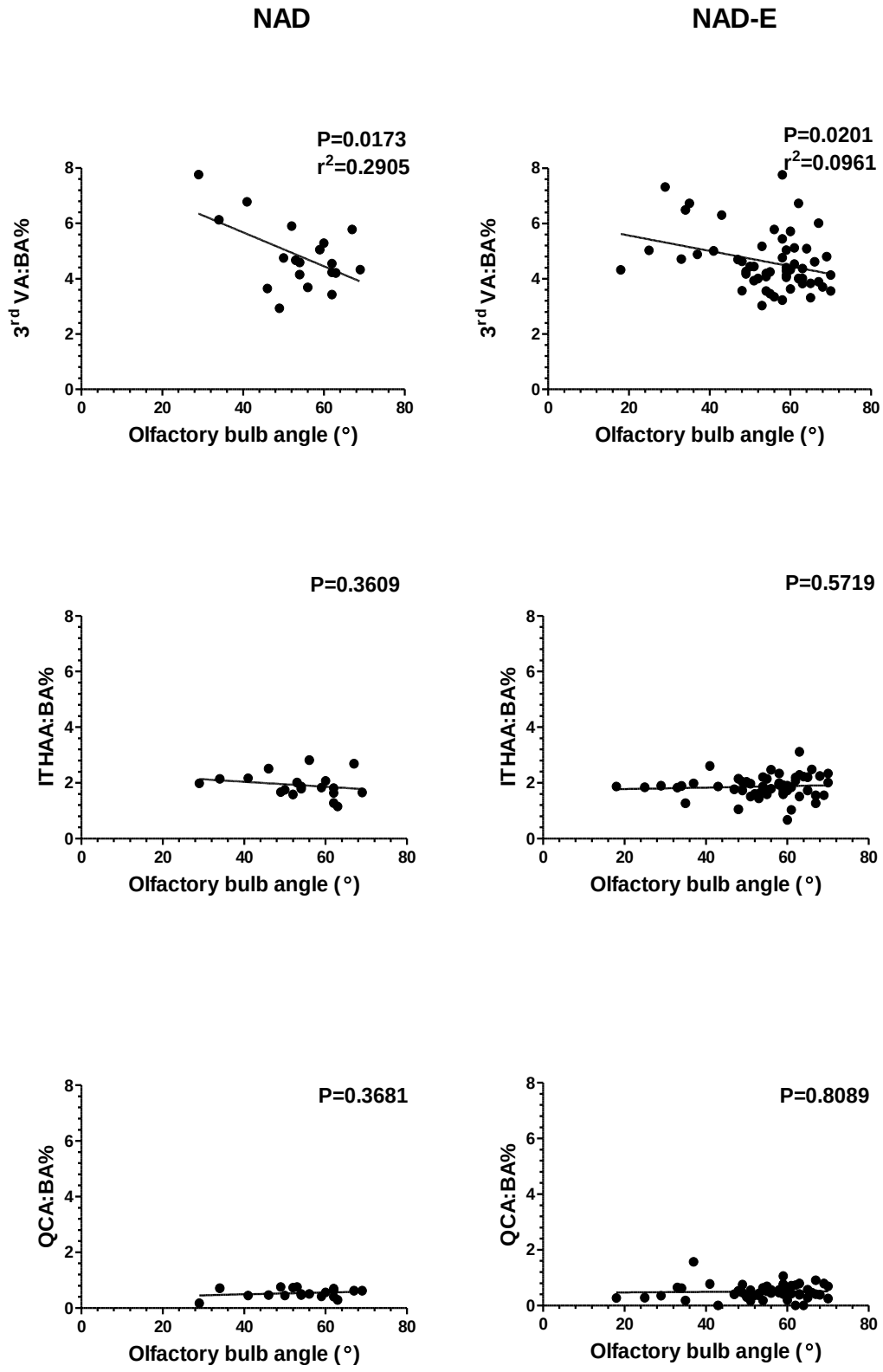

Figure 5-3: Linear regression analysis demonstrating the association between olfactory bulb angle and the corrected midline areas (relative to midline brain area) of the 3rd ventricle (3rd VA: BA %), interthalamic adhesion (ITHAA: BA %) and quadrigeminal cistern (QCA: BA %) on midline sagittal plane MR images of dog heads in the NAD & NAD-E groups

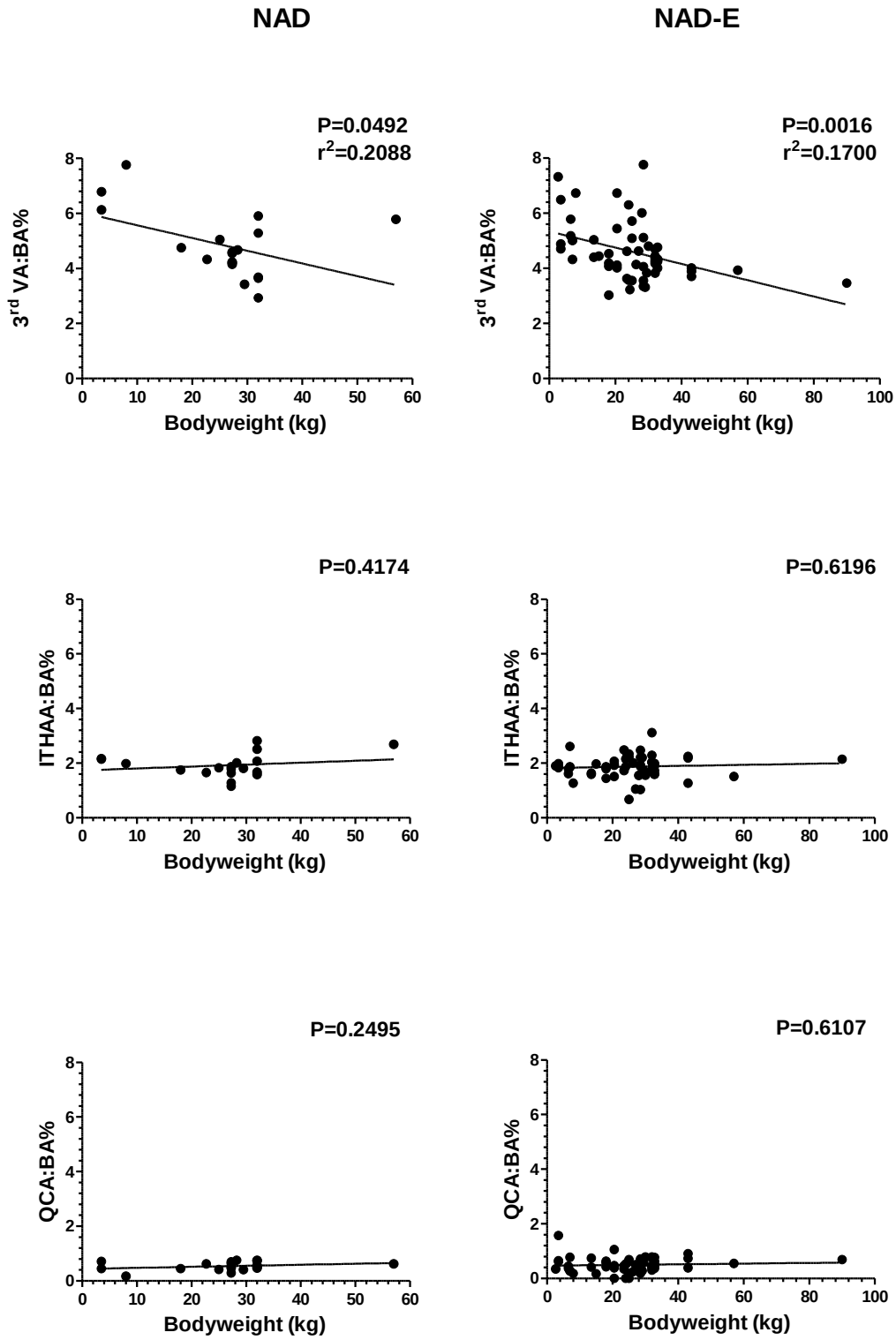

Figure 5-4: Linear regression analysis demonstrating the effect of bodyweight (in kg) on the corrected midline areas (relative to midline brain area) of the 3rd ventricle (3rd VA: BA %), interthalamic adhesion (ITHAA: BA %) and quadrigeminal cistern (QCA: BA %) on midline sagittal plane MR images of dog heads in the NAD & NAD-E groups

The 3rd ventricle and the interthalamic adhesion were situated within the middle fossa and on midline sagittal plane MR images (Figure 5-5). The body of the 3rd ventricle had a roughly parallelogram shape, with the interthalamic adhesion situated centrally.

Rostrally, the 3rd ventricle was bounded by the *lamina terminalis* (including the rostral commissure). The mesencephalon mass (including the caudal commissure and rostral colliculus), mammillary body, arachnoid membrane of the quadrigeminal cistern and the ependymal membrane of the suprapineal recess formed its caudal boundaries. The *tela chorioidae*, which was attached to the edges of the fornix, ventral aspect of the tubercle of the dentate gyrus and the callosal gyrus of the hippocampus, formed the dorsal border of the 3rd ventricle. The ventral border was bounded by the optic chiasm, pituitary gland, mammillary body and the arachnoid membrane of the subarachnoid space (Figures 5-6).

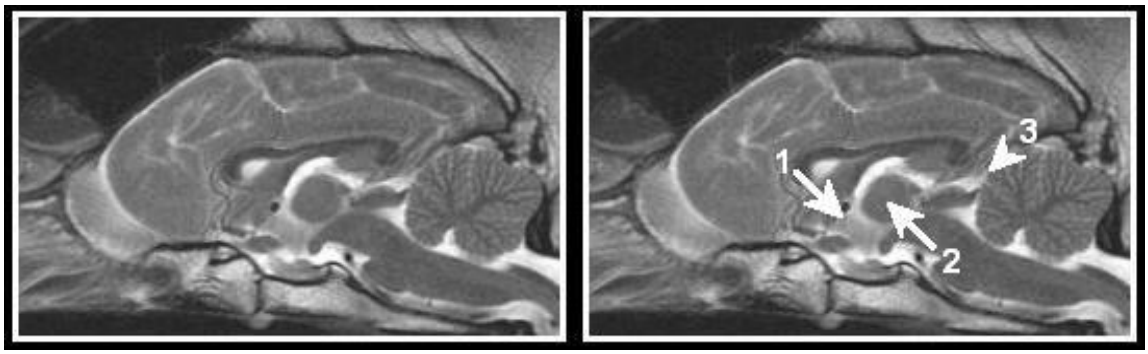

Figure 5-5: Midline, sagittal plane T2-weighted MR images of the dog brain detailing the location of the 3rd ventricle (1), the interthalamic adhesion (2) and the quadrigeminal cistern (3)

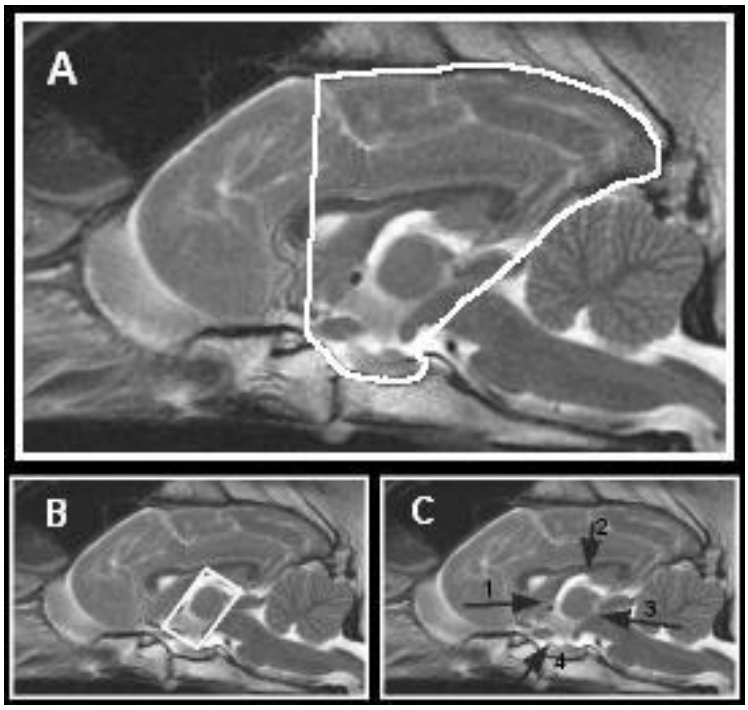

Figure 5-6: Three midline, sagittal plane T2-weighted MR images of a dog brain demonstrating the general features of the 3rd ventricle. The 3rd ventricle is situated within the middle fossa of the cranial fossae (A). The shape of the 3rd ventricle is roughly that of a parallelogram (B). The main borders of the 3rd ventricle (C) include: (1) the rostral border, which is comprised of the lamina terminalis; (2) the dorsal border, which is comprised of the *tela chorioidae* attached to the edges of the fornix, ventral surface of the tubercle of the denate gyrus and the callosal gyrus of the hippocampus; (3) the caudal border, which is comprised of the mesencephalon mass [including the caudal commissure and rostral colliculus], mammillary body, the arachnoid membrane of quadrigeminal cistern and the ependymal membrane of the suprapineal recess; and (4) the ventral border, which is comprised of the optic chiasm, pituitary gland, mammillary body and arachnoid membrane of the subarachnoid space

Three main 3rd ventricle recesses could be identified on MR images, the suprapineal, optic and infundibular (Figure 5-7). The optic recess was situated at the rostro-ventral angle of the 3rd ventricle and it resembled a small diverticulum. Caudal to the optic recess and at the level of the pituitary gland, the infundibular recess was lodged in the initial part of the pituitary gland.

The suprapineal recess had a roughly triangular shape and was evident within the dorsocaudal aspect of the 3rd ventricle. The pineal gland was rarely identified due to a combination of its small size and the fact that the MRI slices frequently failed to incorporate it. In the few animals where the gland was visible, the suprapineal recess was situated dorsal or dorso-caudal to the pineal gland. This recess extended for a variable distance caudally and was separated from the quadrigeminal cistern by a thin line of signal that was hypointense to CSF, and which was interpreted as the arachnoid membrane. It was difficult to identify the ependymal layer that separated the suprapineal

recess and the quadrigeminal cistern. However, the blood vessels which passed through the ependymal layer were detectable on MR images and best illustrated in Figure 5-8, corresponding to the rostrodorsal border of the quadrigeminal cistern. The caudo-ventral point of the 3rd ventricle abutted the pituitary gland. Identification of this point required examining two separate transverse MR images. The most rostroventral aspect of the floor of the 3rd ventricle was demarcated by the optic chiasm (Figure 5-9).

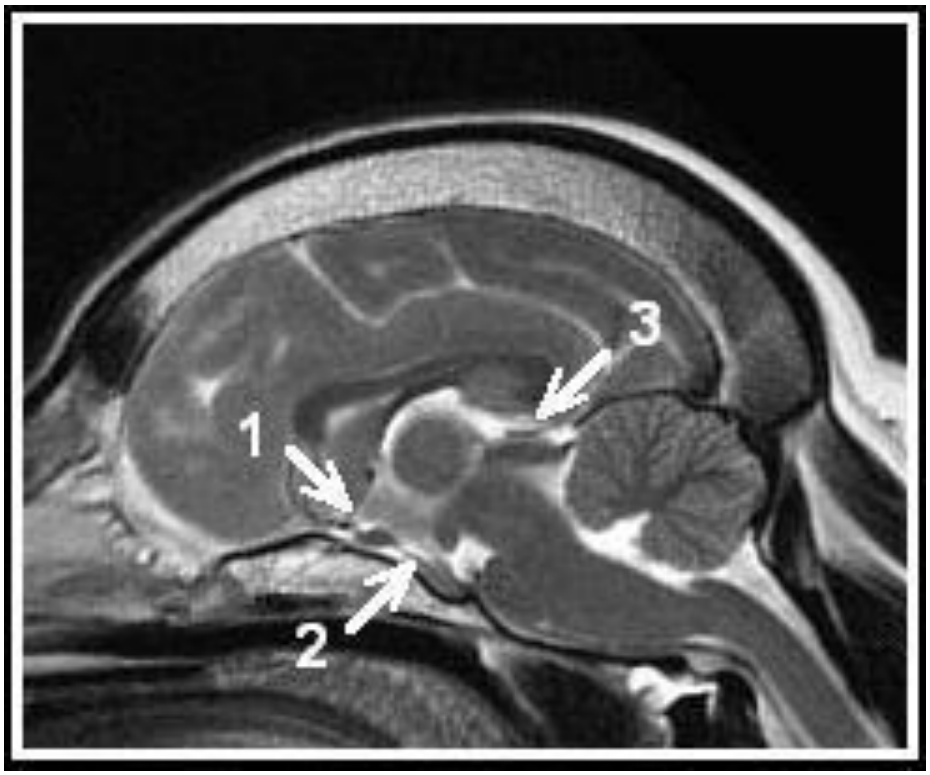

Figure 5-7: Midline, sagittal plane T2-weighted MR image of the dog brain demonstrating the three recesses of the 3rd ventricle: (1) optic, (2) infundibular and (3) suprapineal

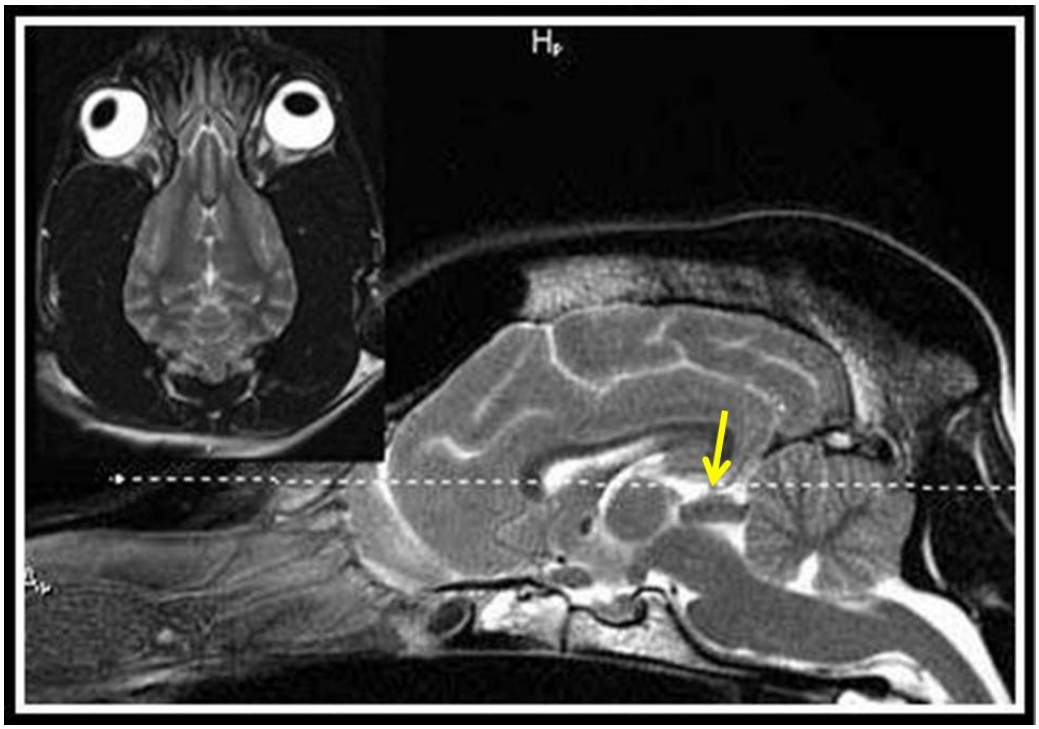

Figure 5-8: Midline, sagittal plane T2-weighted MR image with a reference line that indicates the level of the dorsal plane MR image that best demonstrates the separation of the quadrigeminal cistern from the suprapineal recess in the dog brain (yellow arrow)

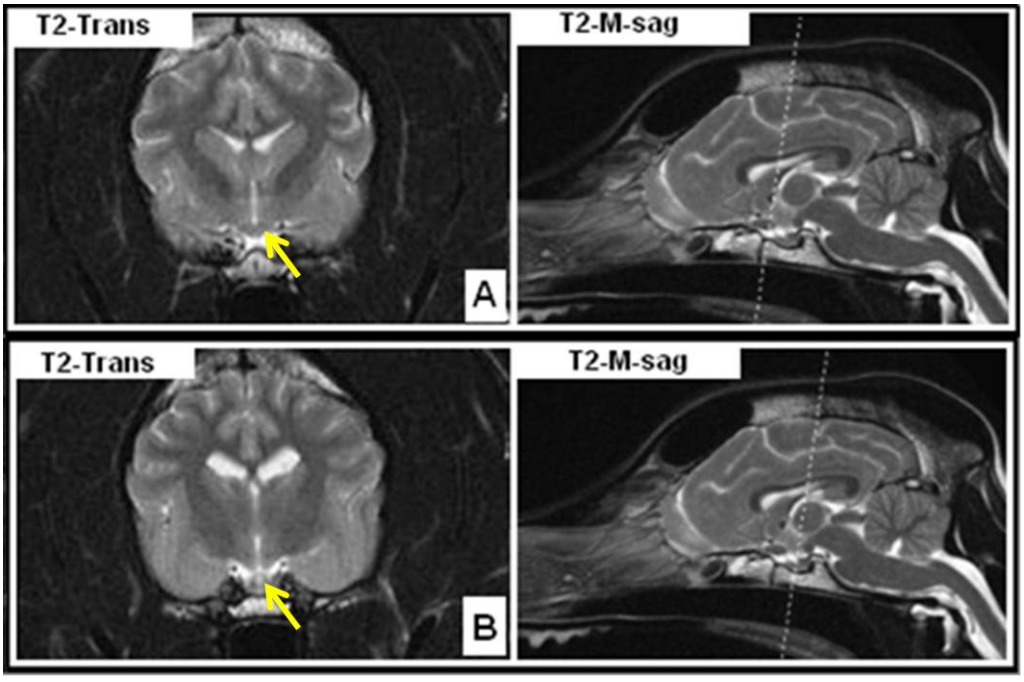

Figure 5-9: Transverse plane (left column) and midline sagittal plane (right column) T2-weighted MR images (with reference lines in the sagittal plane images corresponding to the level of the transverse plane images) showing the most ventro-rostral point of the 3rd ventricle, at the level of the optic chiasm (A), the most ventro-caudal point at the level of the pituitary gland (B)

A small ventral evagination within the roof of the 3rd ventricle was also recognised in all normal dogs between the fornix of the hippocampus and the splenium of the corpus callosum, the tubercle of the dentate gyrus and the callosal gyrus (Figure 5-10).

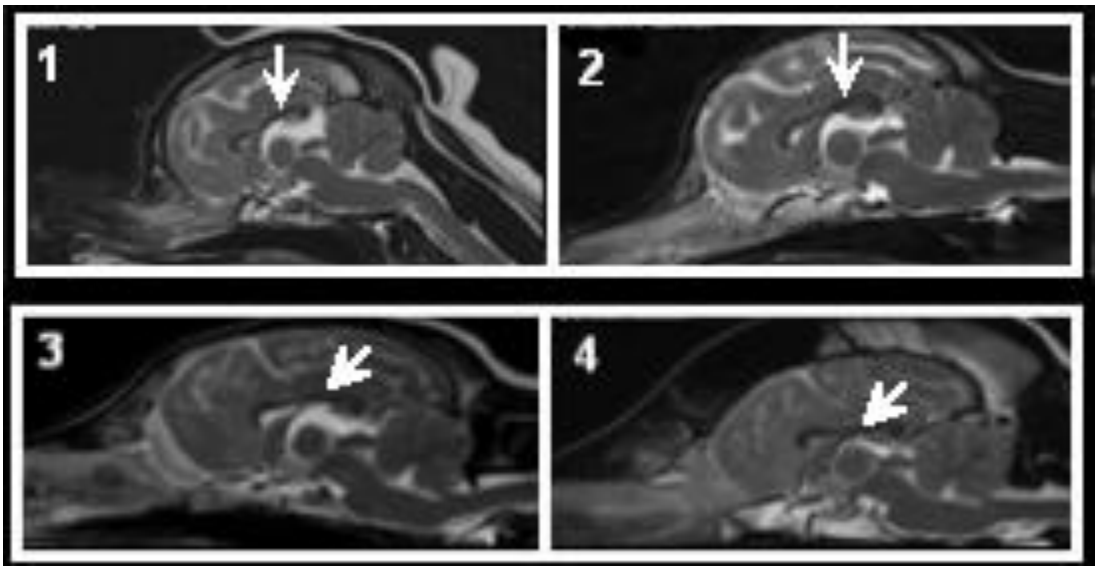

Figure 5-10: Midline, sagittal plane T2-weighted MR images from a representative spectrum of dog head phenotypes demonstrating the normal ventral evagination of the 3rd ventricle between the fornix of the hippocampus and the splenium of the corpus callosum, tubercle of the dentate gyrus and the callosal gyrus

5.3.1.1 Midline area of the 3rd ventricle

When the 3rd ventricle area was examined, the absolute 3rd ventricle area varied from 90.3 mm^2 in a Springer spaniel to 225.2 mm^2 in a Border collie, with a mean of 138.4 mm^2 (STDEV±24.34). When the corrected 3rd ventricle area was assessed (corrected relative to midline brain area), the 3rd ventricle was found to range from 2.9 mm^2 in a Boxer dog to 7.3 mm^2 in a Shih-tzu (M ± STDEV=4.57±0.98) (Table 5-1).

Dog breed	No	BW (Kg)	OBA (°)	3rd ventricle area (mm^2)	Corrected 3rd ventricle area [%]
English springer spaniel	1	24.4	58	95.5	3.2
German shorthaired pointer	1	29	65	113.1	3.3
Mastiff	1	90	55	124.3	3.5
Dobermann	1	38.5	70	133.4	3.6
Pointer	2	29.5	65	M±STDEV= 123±5.7 R= 119-127.1	M±STDEV= 3.6±0.3 R= 3.4-3.8
Boxer	8	31	47	M±STDEV= 140.5±19.2 R= 115-164.8	M±STDEV= 3.9±0.6 R= 2.9-4.7
Husky	2	23.5	63	M±STDEV= 123.3±17.3 R= 111-135.5	M±STDEV= 4.1±0.7 R=3.6-4.6
Springer spaniel	5	18	55	M±STDEV= 119.2±20.7 R= 90.3-142.3	M±STDEV= 4.1±0.7 R= 3.03-4.8
GSD	6	37.5	64	M±STDEV= 132.7±15.2 R= 111.9-156.3	M±STDEV= 4.2±0.6 R= 3.7-5.3
Boston terrier	1	7	18	110.5	4.3
Staffordshire terrier	1	15	51	134.4	4.4
Golden retriever	5	27.3	59	M±STDEV= 135.6±16.3 R= 107.2-148.5	M±STDEV= 4.4±0.2 R= 4.2-4.6
Basset hound	1	27	72	149.8	4.6
Labrador retriever	10	30.7	57	M±STDEV= 149.3±27.0 R= 99.2-182.1	M±STDEV= 4.6±1.2 R= 3.4-5.45
Greyhound	1	28.3	54	174.5	4.7
Hungarian Vizsla	1	30	69	150	4.8
Alaskan malamute	2	57	59	M±STDEV= 167.7±34.9 R= 143-192.3	M±STDEV= 4.9±1.3 R= 3.9-5.8
Border collie	6	13.5	58	M±STDEV= 151.7±40.0 R= 115.1-225.2	M±STDEV= 5.0±1.02 R= 4.02-6.7
Border terrier	1	7	41	136.3	5.01
Lhasa apso	1	7	25	107.5	5.03
Rough collie	1	25	59	134.03	5.1
Gordon setter	2	27.1	69	M±STDEV= 149.1±13.0 R= 139.9-158.3	M±STDEV= 5.1±1.3 R= 4.1-6.01
Dalmatian	3	24.2	64	M±STDEV= 159.5±2.4 R= 132.1-176.5	M±STDEV= 5.1±0.7 R= 4.3-5.7
Miniature schnauzer	2	6.5	55	M±STDEV= 132.9±1.0 R= 132.2-133.6	M±STDEV= 5.5±0.4 R= 5.2-5.8
Yorkshire terrier	4	3.5	36	M±STDEV= 118.2±26.8 R= 97.2-153.9	M±STDEV= 5.6±1.0 R= 4.7-6.8
Poodle	2	28	50	M±STDEV= 136.7±2.8 R= 133.9-139.4	M±STDEV= 6.1±0.3 R= 5.9-6.3
Chihuahua	1	3.5	34	130.5	6.5
Shih-tzu	2	8	3	M±STDEV= 163.2±6.3 R= 158.7-167.6	M±STDEV= 7.3±0.7 R= 6.7-7.8

Table 5-1: The absolute (mm^2) and corrected (relative to midline brain area) area of the 3rd ventricle, bodyweight and olfactory bulb angle for 74 dogs of 28 different breeds ordered according to corrected 3rd ventricle area (Normal MRI group)

5.3.1.2 Description and Midline area of the interthalamic adhesion

The interthalamic adhesion was identified by MR imaging (Figures 5-11). The interthalamic adhesion had a rounded shape and was situated within the centre of the 3rd ventricle. Due to the surrounding CSF appearing hyperintense on T2-weighted images, the margins of the interthalamic adhesion were more easily identified on T2-weighted MR images (Figure 5-11).

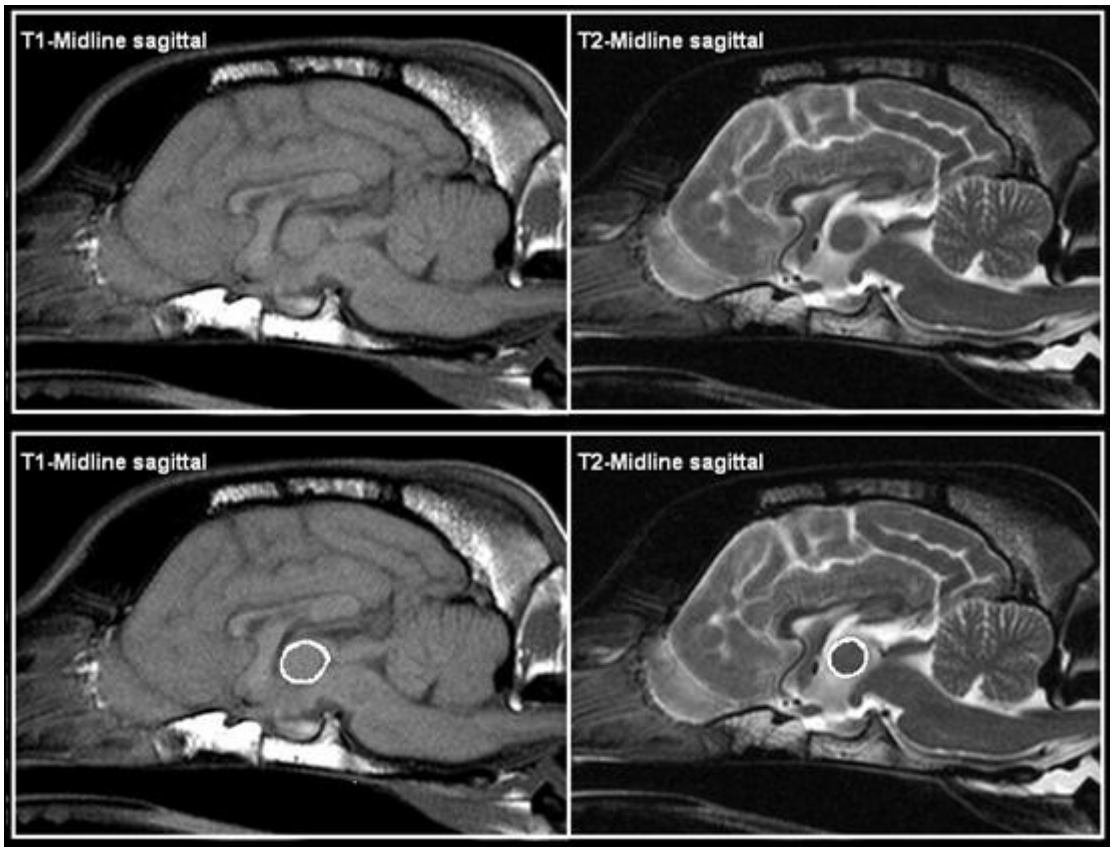

Figure 5-11: The interthalamic adhesion on T1- and T2-weighted midline, sagittal plane MR images. The borders of the interthalamic adhesion were better defined on T2-weighted images due to the surrounding CSF within the 3rd ventricle

The smallest absolute normal interthalamic adhesion area of 20.5 mm^2 was found in a Dalmatian and the largest of 102.7 mm^2 in a Boxer (M±STDEV=57.9 mm^2 ± 16.6 mm^2 for all dogs studied). The same Dalmatian had the smallest corrected area of the interthalamic adhesion (0.7%), while the largest was in a GSD at 3.1%. The average corrected area was 1.9±0.4. The absolute and corrected interthalamic adhesion areas for each breed are shown in Table 5-2.

Dog breed	No	BW (Kg)	OBA (°)	Interthalamic adhesion area (mm^2)	Corrected interthalamic adhesion area [%]
English springer spaniel	1	24.4	58	69.1	2.3
German shorthaired pointer	1	29	65	74.9	2.2
Mastiff	1	90	55	77.0	2.1
Dobermann	1	38.5	70	87.8	2.3
Pointer	2	29.5	65	M±STDEV= 60.1±4.0 R= 57.3-62.9	M±STDEV= 1.8±0.1 R= 1.7-1.8
Boxer	8	31	47	M±STDEV= 75.7±16.3 R= 54.4-102.7	M±STDEV= 2.1±0.4 R= 1.7-2.8
Husky	2	23.5	63	M±STDEV= 62.9±14.1 R= 52.9-72.8	M±STDEV= 2.1±0.5 R= 1.7-2.5
Springer spaniel	5	18	55	M±STDEV= 50.2±4.6 R= 42.9-55.03	M±STDEV= 1.7±0.2 R= 1.4-1.9
GSD	6	37.5	64	M±STDEV= 69.1±15.2 R= 45.9-91.00	M±STDEV= 2.2±0.6 R= 1.3-3.1
Boston terrier	1	7	18	47.8	1.9
Staffordshire terrier	1	15	51	59.7	2.0
Golden retriever	5	27.3	59	M±STDEV= 47.6±8.3 R= 38.1-58.3	M±STDEV= 1.6±0.3 R= 1.2-1.9
Basset hound	1	27	72	34.1	1.1
Labrador	10	30.7	57	M±STDEV= 61.2±15.6 R= 61.2-93.1	M±STDEV= 1.8±0.4 R= 1.03-2.5
Greyhound	1	28.3	54	72.2	2.01
Hungarian viszla	1	30	69	48.8	1.6
Alaskan malamute	2	57	59	M±STDEV= 72.3±24.4 R= 55-89.5	M±STDEV= 2.1±0.8 R= 1.5-2.7
Border collie	6	13.5	58	M±STDEV= 56.1±9.8 R= 42.7-69.3	M±STDEV= 1.8±0.2 R= 1.5-2.1
Border terrier	1	7	41	71.0	2.6
Lhasa apso	1	7	25	36.5	1.8
Rough collie	1	25	59	48.7	1.8
Gordon setter	2	27.1	69	M±STDEV= 57.5±14.7 R= 47.1-67.9	M±STDEV= 1.8±0.3 R= 1.6-2.01
Dalmatian	3	24.2	64	M±STDEV= 48.4±26.9 R=20.5-74.1	M±STDEV= 1.5±0.8 R= 0.7-2.2
Miniature schnauzer	2	6.5	55	M±STDEV= 41.2±0.4 R= 41.0-41.5	M±STDEV= 1.7±0.1 R= 1.6-1.8
Yorkshire terrier	4	3.5	36	M±STDEV= 42.5±5.0 R= 37.8-49.2	M±STDEV= 2.03±0.2 R= 1.8-2.2
Poodle	2	28	50	M±STDEV= 38.6±1.7 R= 37.4-39.8	M±STDEV= 1.7±0.2 R= 1.6-1.9
Chihuahua	1	3.5	34	38.01	1.9
Shih-tzu	2	8	3	M±STDEV=47.03 5.9 R= 42.8-51.2±	M±STDEV= 1.6±0.5 R= 1.3-2.0

Table 5-2: The absolute (mm^2) and corrected (relative to midline brain area) area of the interthalamic adhesion, bodyweight and olfactory bulb angle for 74 dogs of 28 different breeds ordered according to corrected 3rd ventricle area (Normal MRI group)

5.3.1.3 Description and midline area of the quadrigeminal cistern

The quadrigeminal cistern was predominantly triangular in shape in normal dogs (Figure 5-12). However, a large variation was evident in the midline area of the quadrigeminal cistern. It was found to be smaller in dogs with a relatively larger suprapineal recess.

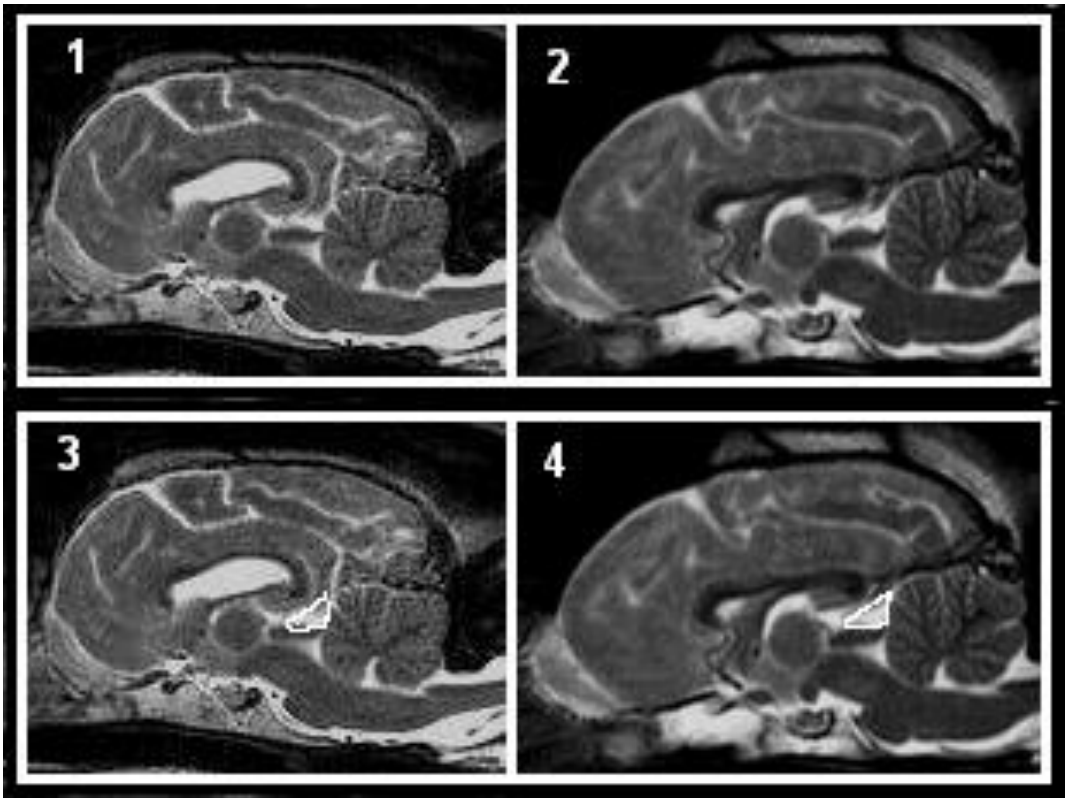

Figure 5-12: Midline, sagittal plane T2-weighted MR images from two normal dogs illustrating the shape of the quadrigeminal cistern

The quadrigeminal cistern was identifiable in all dogs on midline, sagittal plane T2-weighted MR images, except in two dogs: a Dalmatian and a poodle, both of which had a diagnosis of idiopathic epilepsy (Figure 5-13).

The midline quadrigeminal cistern absolute area ranged from 0 (as noted in the above 2 dogs) to a maximum of 33.9 mm^2 in a Border collie dog (M±STDEV=15.5 mm^2 ± 7.5), while the corrected area reached a maximum in a Yorkshire terrier of 1.6 (M±STDEV= 0.5 ± 0.3). The absolute and the corrected quadrigeminal cistern areas and for each breed are detailed in Table 5-3.

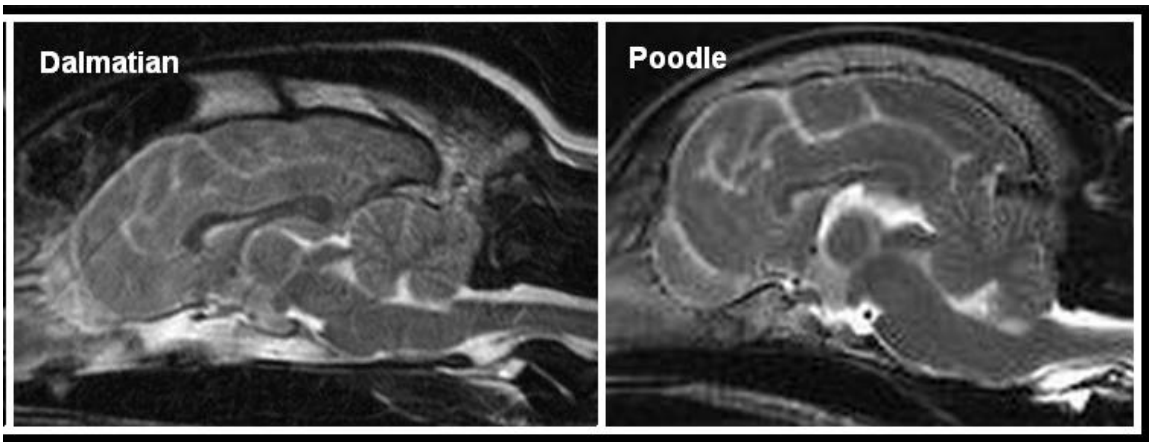

Figure 5-13: Midline, sagittal plane T2-weighted MR images from two dogs that lacked a visible quadrigeminal cistern

When the corrected area of the 3rd ventricle was compared with that of the interthalamic adhesion and the quadrigeminal cistern, no significant correlation was evident (P = 0.3093 and P = 0.1642 respectively) (Figure 5-14).

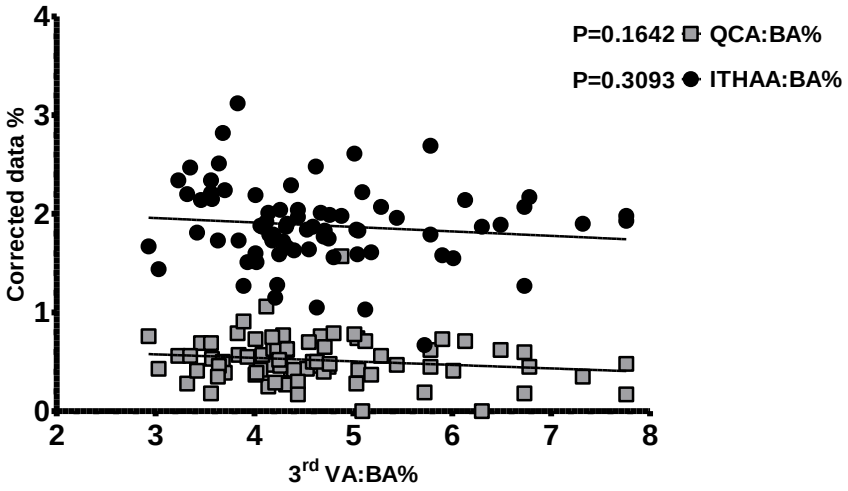

Figure 5-14: A horizontal scatter graph demonstrating the absence of any correlation between the corrected areas of the 3rd ventricle (3rd VA: BA%) and that of the interthalamic adhesion (ITHAA: BA%) and the quadrigeminal cistern (QCA: BA%)

Dog breed	No	Mean BW (Kg)	OBA (°)	Quadrigeminal cistern area (mm^2)	Corrected cistern area [%]
English springer spaniel	1	24.4	58	16.7	0.6
German shorthaired pointer	1	29	65	9.4	0.3
Mastiff	1	90	55	24.7	0.7
Dobermann	1	38.5	70	25.8	0.7
Pointer	2	29.5	65	M±STDEV= 16.5±3.2 R=14.2-18.8	M±STDEV= 0.5±0.1 R=0.4-0.6
Boxer	8	31	47	M±STDEV=17.6±3.9 R= 10.9-22.7	M±STDEV= 0.5±0.2 R=0.3-0.8
Husky	2	23.5	63	M±STDEV=12.04±2.1 R=10.6-13.5	M±STDEV=04±0.1 R= 0.4-0.5
Springer spaniel	5	18	55	M±STDEV=14.4±2.04 R=14.4-17.4	M±STDEV=0.5±0.1 R=0.4-0.6
GSD	6	37.5	64	M±STDEV=20.3±7.6 R= 13-32.9	M±STDEV=0.6±0.2 R= 0.4-0.9
Boston terrier	1	7	18	7.01	0.3
Staffordshire terrier	1	15	51	5.04	0.2
Golden retriever	5	27.3	59	M±STDEV=17.5±7.8 R= 9.7-29.1	M±STDEV=0.5±0.2 R= 0.3-0.7
Basset hound	1	27	72	16.3	0.5
Labrador	10	30.7	57	M±STDEV=17.3±6.1 R=5.0-25.2	M±STDEV=0.5±0.2 R= 0.2-0.8
Greyhound	1	28.3	54	28.3	0.8
Hungarian viszla	1	30	69	24.8	0.8
Alaskan malamute	2	57	59	M±STDEV=20.4±0.4 R= 20.1-20.6	M±STDEV=0.6±0.1 R=0.55-0.62
Border collie	6	13.5	58	M±STDEV=18.8±8.5 R= 10.9-33.4	M±STDEV=0.6±0.3 R=0.4-1.1
Border terrier	1	7	41	21.2	0.8
Lhasa apso	1	7	25	5.6	0.3
Rough collie	1	25	59	11.2	0.4
Gordon setter	2	27.1	69	M±STDEV=10.4±2.8 R= 8.4-12.4	M±STDEV=0.3±0.1 R= 0.3-0.4
Dalmatian	3	24.2	64	M±STDEV=8.3±9.7 R= 0-18.9	M±STDEV=0.3±0.3 R=0-0.6
Miniature schnauzer	2	6.5	55	M±STDEV=10.0±0.5 R= 9.7-10.3	M±STDEV=0.4±0.1 R=0.4-0.5
Yorkshire terrier	4	3.5	36	M±STDEV=17.4±9.6 R=10.2-31.6	M±STDEV=0.9±0.5 R= 0.5-1.6
Poodle	2	28	50	M±STDEV=8.6±12.2 R= 0-17.2	M±STDEV=0.4±0.5 R= 0-0.7
Chihuahua	1	3.5	34	12.4	0.6
Shih-tzu	2	8	3	M±STDEV=4.0±0.4 R= 3.7-4.3	M±STDEV=0.17±0.01 R= 0.17-0.18

Table 5-3: The absolute (mm^2) and corrected (relative to midline brain area) area of the quadrigeminal cistern, bodyweight and olfactory bulb angle for 74 dogs of 28 different breeds ordered according to corrected 3rd ventricle area (Normal MRI group)

5.3.2 The effect of brain lesions on the midline area of the 3rd ventricle

A significant difference (P<0.0001) was evident when the midline area of the 3rd ventricle (corrected for brain area) was compared between dogs in the normal MRI group (**NAD and NAD-E**) and dogs with an abnormal MRI (representing the VM, OBL & CH-LMS groups).

Dogs with an abnormal brain MRI had a significantly larger mean corrected 3rd ventricle area, than those in Normal MRI group (M±STDEV= 6.23 ±2.34) versus (M±STDEV=4.57±0.98) (Figure 5-15**).** The midline 3rd ventricle area was significantly larger in the abnormal MRI group (A), but this effect was due to inclusion of the VM group within the Abnormal MRI group (B).

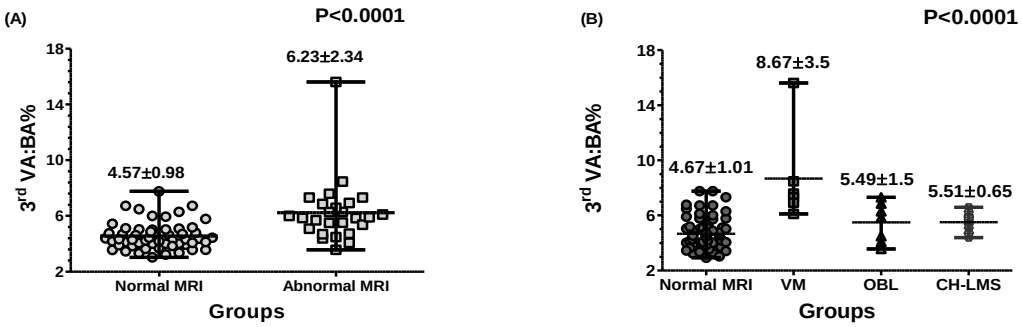

Figure 5-15: A vertical scatter plot (range, mean and standard deviation) representing the corrected area of the 3rd ventricle in (A) the Normal MRI vs. Abnormal MRI groups [the latter represents a merger of groups 3, 4 and 5] and (B) the Normal MRI group vs. each group of the abnormal separately [VM: gross pathological ventriculomegaly, OBL: other brain lesions and CH-LMS: Chiari-like malformation syndrome]

5.3.3 The effect of ventriculomegaly (VM) on the descriptive appearance and midline area of the 3rd ventricle, interthalamic adhesion and quadrigeminal cistern

The descriptive appearance of the 3rd ventricle, interthalamic adhesion and quadrigeminal cistern was altered in dogs in the **VM** group as compared to dogs in the Normal MRI group.

Enlargement of the 3rd ventricle in dogs with ventriculomegaly was found to be the result of marked dilation of both the lateral ventricles, which in some lacked a septum pellucidum, or due to obstruction of the CSF drainage pathways at the level of the mesencephalon aqueduct or 4th ventricle, leading to abnormal accumulation of CSF within the 3rd ventricle (Figures 5-16 and 15-17).

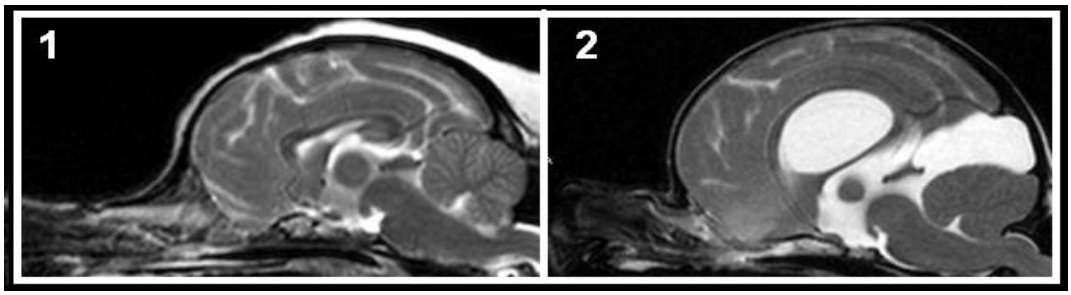

Figure 5-16: Midline, sagittal plane T2-weighted MR images of a normal Chihuahua (1), and an abnormal dog brain of a 6.7 year old male Chihuahua with obstructive hydrocephalus secondary to a quadrigeminal cistern cyst (2)

Figure 5-17: Dorsal (1-3) and midline sagittal (4) plane T-2 weighted MR images of the brain dog (2) of figure 5-16

There was also a change in shape of the corpus callosum in association with ventriculomegaly reflecting a reduction in the thickness of the fornix of the hippocampus, the splenium of the corpus callosum, the tubercle of dentate gyrus and, or,

the callosal gyrus (Figure 5-18), and this was apparent even if the area of the 3rd ventricle was not enlarged.

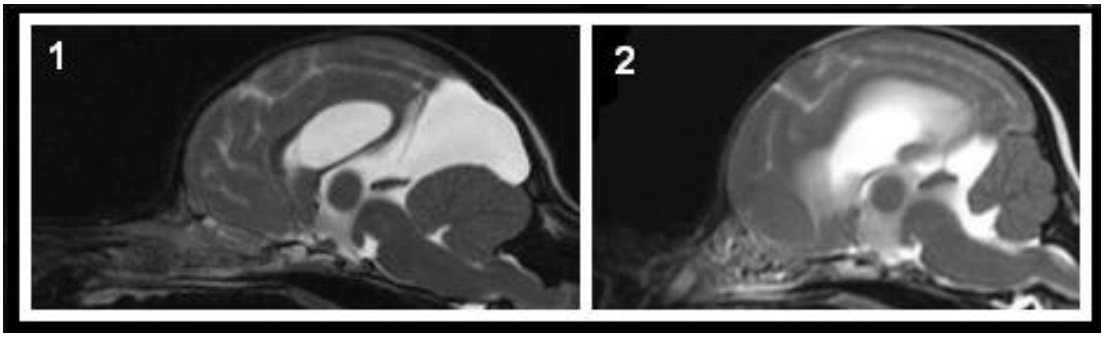

Figure 5-18: Midline sagittal plane T2-weighted MR images of 2 Chihuahuas with abnormal brains due to quadrigeminal cistern cysts. There is enlargement of the 3rd ventricle and the lateral ventricles, thinning of the fornix of the hippocampus and flattening of the ventral evagination between the fornix and the splenium of the corpus callosum

Enlargement of the 3rd ventricle also resulted in expansion of one or more of the three main 3rd ventricle recesses (Figures 5-17, 5-18 and 5-19). This was mainly evident on midline, sagittal plane T2-weighted MR images. The consequence of the expansion of these 3rd ventricle recesses were secondary changes to the adjacent brain tissues, in most cases compression of these tissues to a variable degree, and included the parenchymal brain tissue, optic chiasm and/or the pituitary gland. The pattern of involvement varied between cases, with some demonstrating more compression of the ventral structures, including the optic chiasm and pituitary gland (Figure 5-17), while in others there was a dorsal reduction in parenchymal tissue (Figure 5-18). The optic recess was also seen to extend rostrally to the optic chiasm or rostral commissure (Figure 5-16).

Reduction of parenchymal brain tissue may also cause hydrocephalus *ex vacuo*, best demonstrated in dogs with altered behaviour associated with age or senility and with generalised brain atrophy (Figure 5-19). Enlargement of the 3rd ventricle also resulted in variable thinning of the hippocampal fornix in this group (n=5), with flattening of the ventral evagination within the roof of the 3rd ventricle and expansion of the 3rd ventricle ventrally. Expansion of the infundibular recess occupied most of the pituitary fossa in some cases, leaving only a small space for the pituitary gland (Figure 5-17).

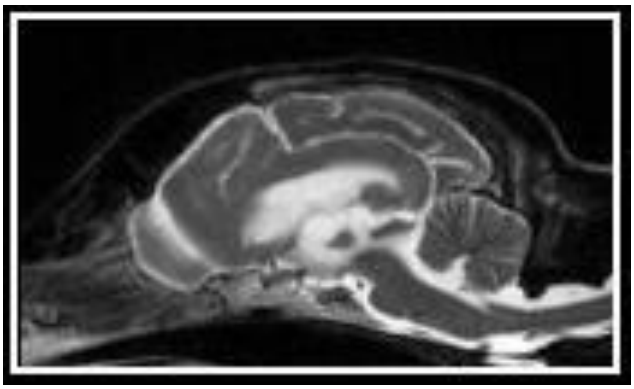

Figure 5-19: Midline sagittal plane T2-weighted MR image of the brain of a 19 year old Miniature poodle demonstrating altered behaviour associated with age-related brain changes (senility). There is diffuse brain atrophy resulting in widening the subarachnoid spaces and enlargement of the ventricular system due to hydrocephalus *ex-vacuo*

In the **VM** group, there was also an obvious increase in the absolute and corrected midline area of the 3rd ventricle (P=0.0002) (Figure 5-20A), but this effect was to be expected on the basis of the inclusion criteria of ventriculomegaly. This effect was maintained when the statistical analysis was repeated in a subpopulation of these dogs, to include only the brachycephalic (n=5) dogs in order to diminish the effect of head conformation (P=0.0066) (Figure 5-20B).

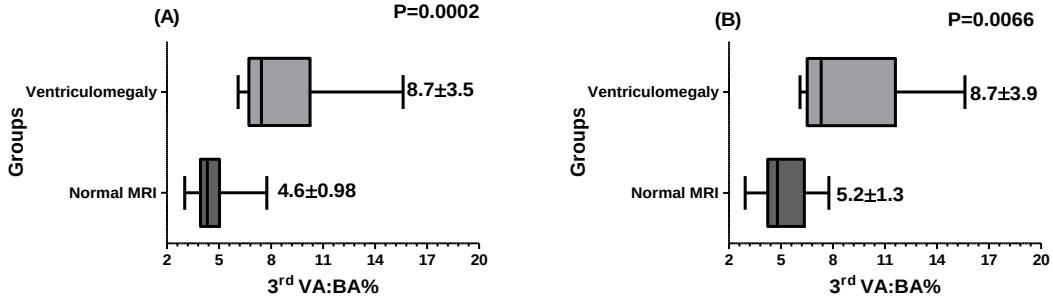

Figure 5-20: Whisker and box plot (range, mean and standard deviation) comparison of the corrected midline 3rd ventricle area in dogs of the **VM** group and the Normal MRI group (A). There was a significantly larger midline 3rd ventricular area in dogs with ventriculomegaly. The same analysis, but only including dogs with a brachycephalic head shape in order to diminish the effect of head conformation demonstrating the same effect (B)

The corrected midline interthalamic adhesion area was significantly larger in the Normal MRI versus the **VM** group (P=0.0004) (Figure 5-21A). Furthermore, when this analysis was restricted to only brachycephalic dogs from the Normal MRI and **VM** groups (Figure 5-21B), the corrected midline interthalamic adhesion area was still significantly

larger in the Normal MRI group (P=0.0016). When the ventriculomegaly was longstanding or severe then these differences were not only in terms of size, but also shape (Figure 5-19 and 5-22).

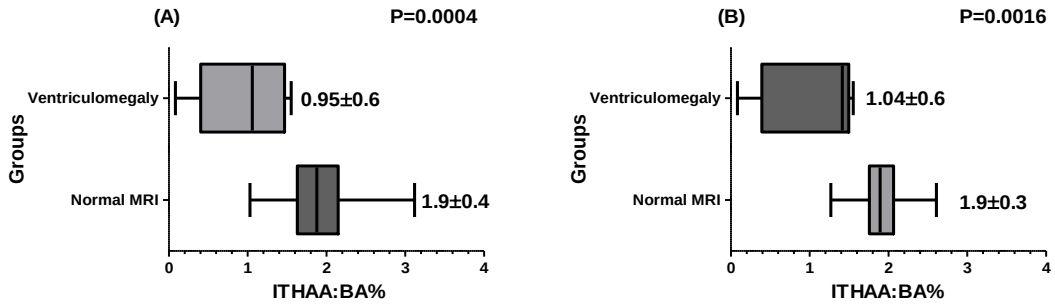

Figure 5-21: Whisker and box plot (range, mean and standard deviation) comparison of the corrected midline interthalamic adhesion area in dogs of **VM** group and dogs in the Normal MRI group. There was a significant reduction in the midline interthalamic adhesion area in dogs with pathological ventriculomegaly The same analysis, but only including dogs with a brachycephalic head shape in order to diminish the effect of head conformation demonstrating the same effect (B)

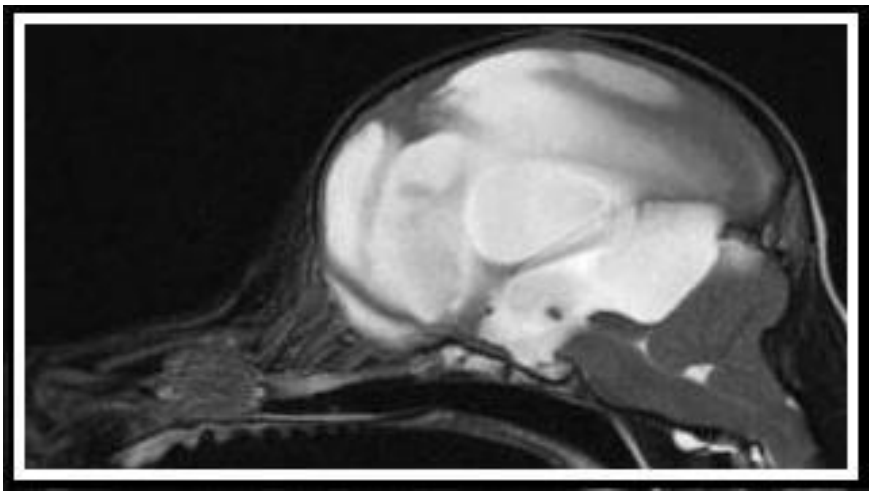

Figure 5-22: Midline, T2-weighted MR image from a CKCS with severe ventriculomegaly and obstructive hydrocephalus. This is severe compression and loss of parenchymal tissue and markedly reduced midline interthalamic adhesion area. The ventricles occupy most of the cranial cavity

In animals in the **VM** group, the shape of the quadrigeminal cistern was variable. However, most dogs within this group (n=5) had quadrigeminal cistern cysts leading to compression of the cerebellum, the caudal part of the cerebrum or both (Figure 5-18). In light of the occurrence of quadrigeminal cistern cysts in the **VM** group, there was therefore also a large and significant difference (P=0.0145) in midline quadrigeminal

cistern area between the Normal MRI and **VM** groups (with the **VM** group being substantially larger). This difference was also evident when only brachycephalic dogs were included for comparison (P=0.0025) (Figure 5-23).

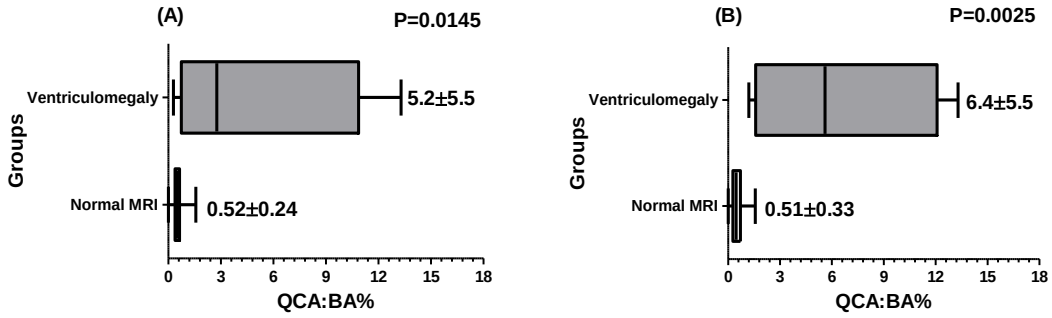

Figure 5-23: Whisker and box plot (range, mean and standard deviation) comparison of the corrected midline quadrigeminal cistern area in dogs of the **VM** group and the Normal MRI group (A). There was a large and significant increase in the midline quadrigeminal cistern area in dogs with pathological ventriculomegaly. The same analysis, but only including dogs with a brachycephalic head shape in order to diminish the effect of head conformation demonstrating the same effect (B)

5.3.4 The effect of other brain lesions (OBL) on the descriptive appearance and midline area of the 3rd ventricle, interthalamic adhesion and quadrigeminal cistern

Examination of the effect of other brain lesions (excluding the **VM** group) on the corrected 3rd ventricle area revealed that other brain lesions resulted in a significant increase in midline sagittal 3rd ventricle area (P=0.0011), as compared to the Normal MRI group (Figure 5-24A). However, when this analysis was repeated in only dogs with a brachycephalic head phenotype this effect was no longer significant (P=0.9679) (Figure 5-24B). When the corrected interthalamic adhesion and quadrigeminal cistern areas were compared between the Normal MRI group and the OBL group, neither of these demonstrated a significant difference when the entire population was examined or if the effect was only examined in brachycephalic dogs (Figure 5-25 and 5-26). No difference in 3rd ventricle shape was apparent either, when the Normal MRI group and OBL group were compared (Figure 5-27).

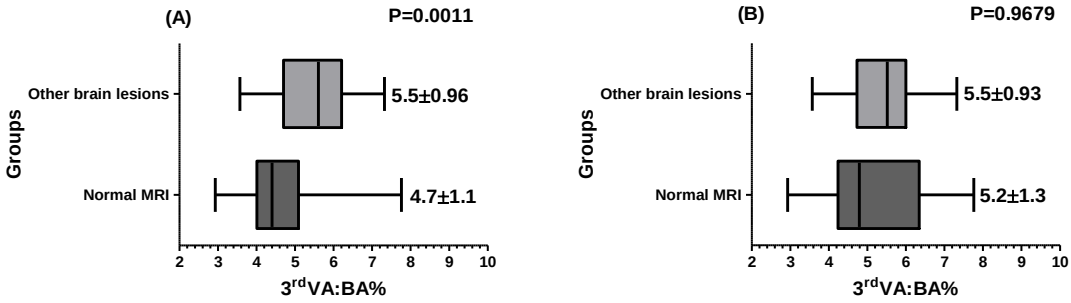

Figure 5-24: Whisker and box plots (with min-max and the mean & standard deviation) representing the comparison of the corrected midline 3rd ventricle area in the Normal and OBL groups (A), and in only dogs with a brachycephalic head phenotype (B). An increase in midline 3rd ventricle area was apparent in dogs with other brain lesions, when comparing the entire population, but not when the analysis was restricted to only dogs with a brachycephalic head phenotype.

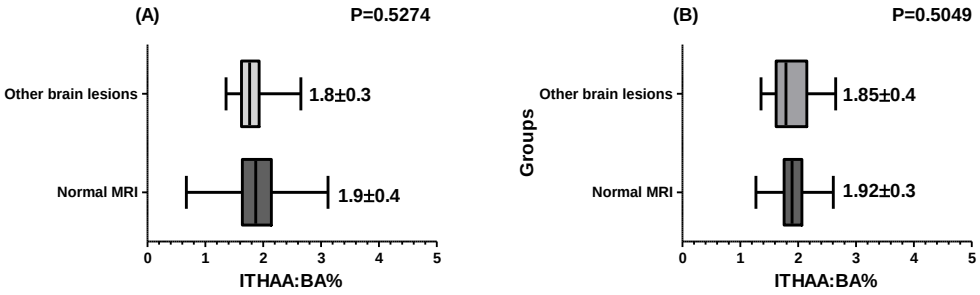

Figure 5-25: Whisker and box plots (with min-max and the mean & standard deviation) representing the comparison of the corrected midline interthalamic adhesion area in the Normal and OBL groups (A), and in only dogs with a brachycephalic head phenotype (B). No difference was apparent in either analysis

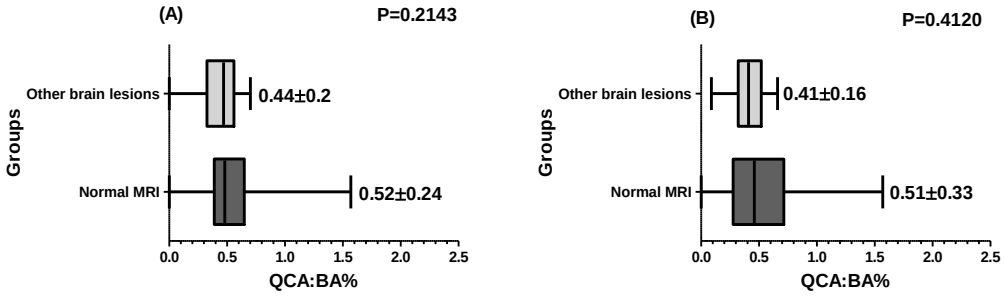

Figure 5-26: Whisker and box plots (with min-max and the mean & standard deviation) representing the comparison of the corrected midline quadrigeminal cistern area in the Normal and OBL groups (A), and in only dogs with a brachycephalic head phenotype (B). No difference was apparent in either analysis

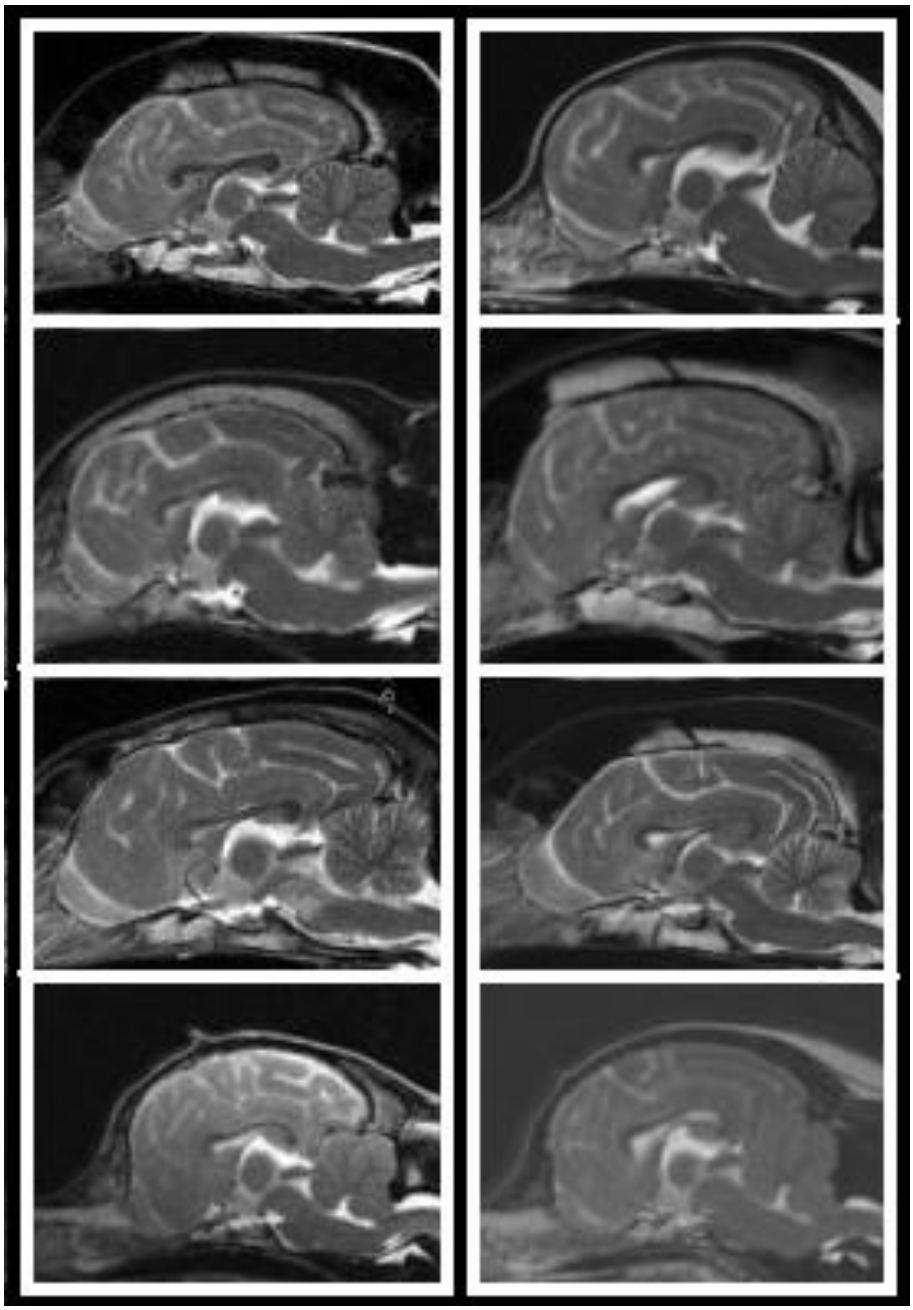

Figure 5-27: Midline, sagittal plane T2-weighted MR images from Normal MRI group (left column) and dogs in the **OBL** group (right column) demonstrating the 3rd ventricle appearance with no difference in the shape present between the two groups

5.3.5 The 3rd ventricle, interthalamic adhesion and the quadrigeminal cistern midline areas were not influenced by head phenotype

No significant differences were found in the corrected midline area of the 3rd ventricle in brachycephalic, mesaticephalic and dolichocephalic groups as defined using arbitrary group or olfactory bulb angle Method 2 (P= 0.2984, 0.0832 respectively) (Figure 5-28). Similarly, the corrected midline area of the interthalamic adhesion and quadrigeminal cistern showed no significant differences in these brachycephalic, mesaticephalic and dolichocephalic groups.

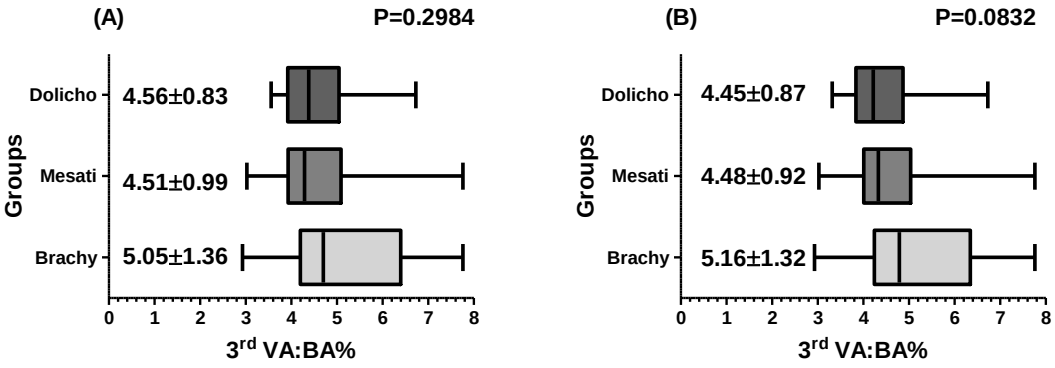

Figure 5-28: Comparisons of midline 3rd ventricle area (corrected for midline brain area) in three head phenotypes defined using two different methods: (A) arbitrary control, and (B) Method 2, the olfactory bulb angle. Head conformation does not influence midline 3rd ventricle area

5.3.6 Dogs with lower bodyweight had a relatively larger midline 3rd ventricle area, but bodyweight did not influence midline interthalamic adhesion or quadrigeminal cistern area

The corrected (relative to midline brain area) midline 3rd ventricle area was inversely correlated with bodyweight (Figure 5-29).

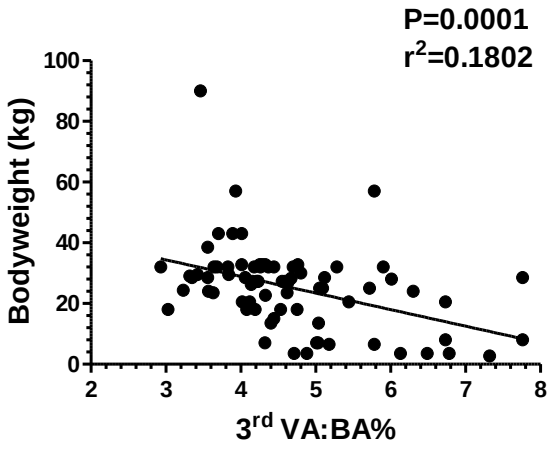

Figure 5-29: Linear regression analysis demonstrating a significant inverse correlation between the corrected 3rd ventricle area and bodyweight in the Normal MRI group

Once the dogs were assigned to bodyweight groups, a significant difference was found between the three different bodyweight groups (P=0.0001). However, the post comparison test demonstrated that the real difference was only between the lighter dogs (n=15) (<15 kg) and the others (15-30 (n=36) and >30 kg (24) groups) (Figure 5-30). No

significant effect was evident when the effect of bodyweight on the corrected midline area of the interthalamic adhesion or quadrigeminal cistern was examined (Figure 5-31).

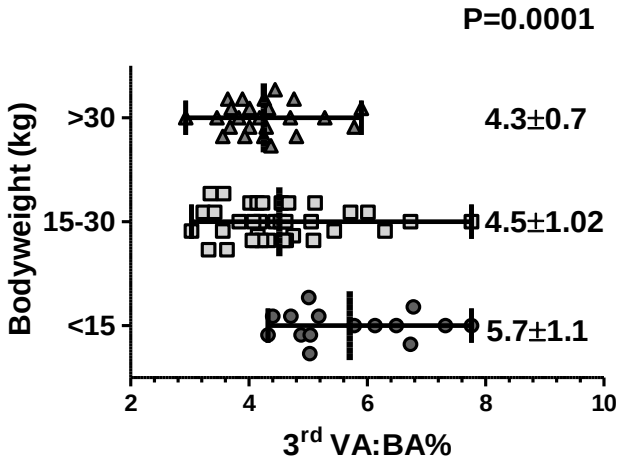

Figure 5-30: Horizontal scatter plot showing the corrected midline 3rd ventricle areas from three bodyweight groups. Midline 3rd ventricle area was significantly larger in dogs <15 kg bodyweight when compared to the higher bodyweight groups

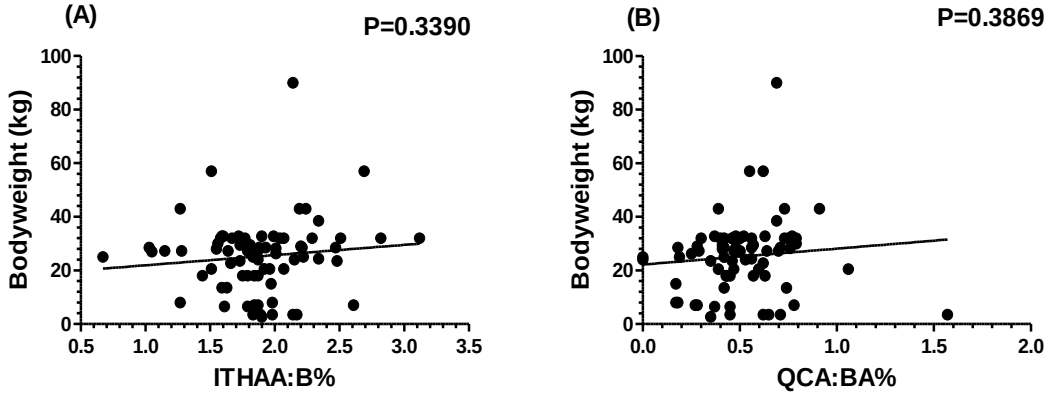

Figure 5-31: Linear regression graphs showing an absence of significant correlation between bodyweight and the corrected midline area of (A) the interthalamic adhesion and (B) quadrigeminal cistern in the Normal MRI group

5.3.7 The 3rd ventricle, interthalamic adhesion and the quadrigeminal cistern corrected midline areas were not influenced by age or gender

No significant effect of age or gender on the corrected midline area of the 3rd ventricle, interthalamic adhesion or quadrigeminal cistern was evident (P>0.05 in all) (Figures 5-32, 5-33 and 5-34).

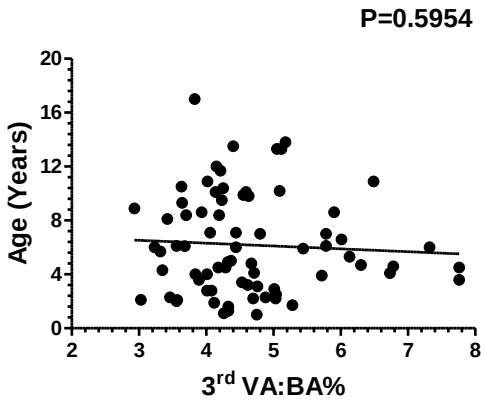

Figure 5-32: Linear regression plot showing that no significant effect was evident when the effect of age on the corrected midline area of the 3rd ventricle was examined in the Normal MRI group

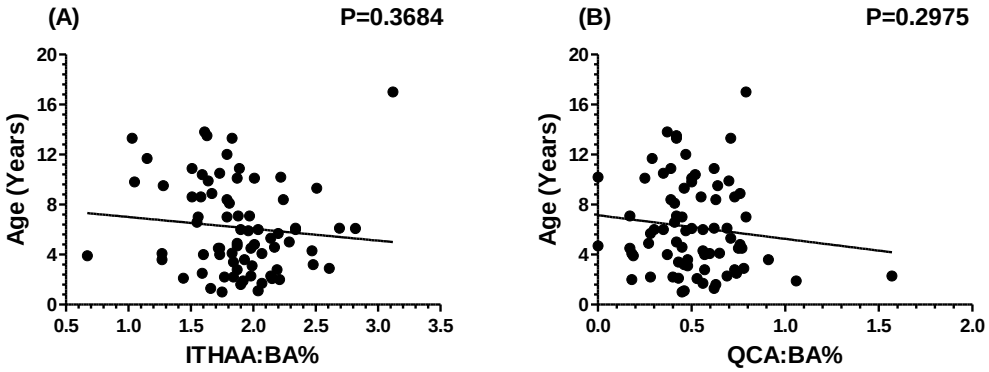

Figure 5-33: Linear regression plots showing that no significant effect was evident when the effect of age on the corrected midline area of the (A) interthalamic adhesion and (B) quadrigeminal cistern were examined in the Normal MRI group

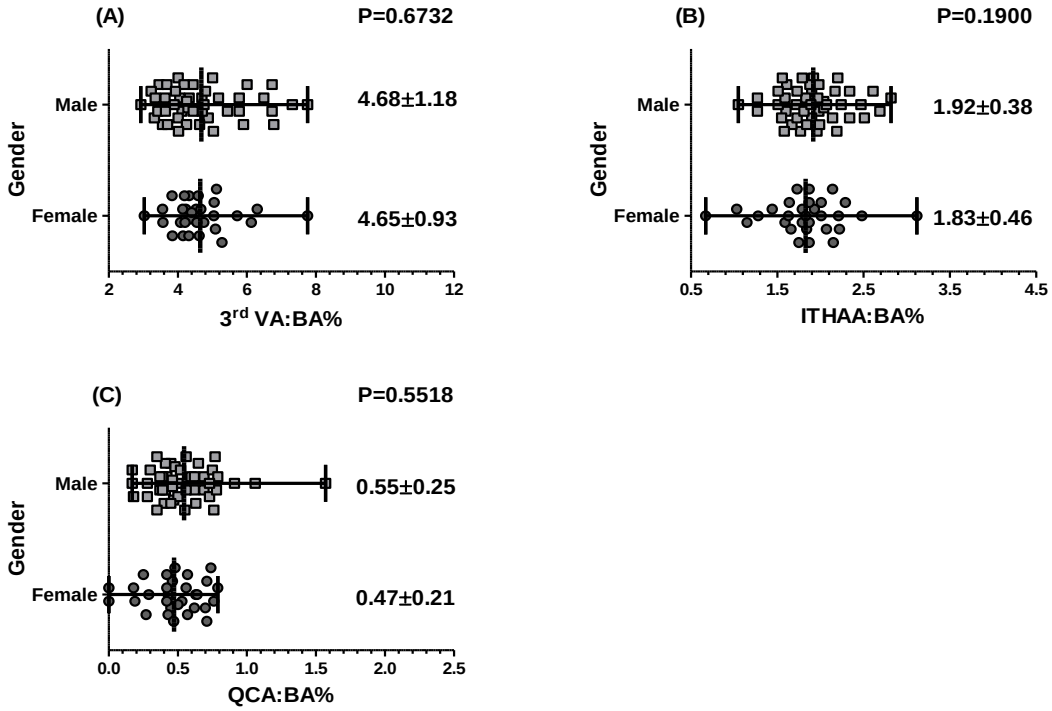

Figure 5-34: Horizontal scatter plots representing the corrected areas of the (A) 3rd ventricle, (B) interthalamic adhesion and (C) quadrigeminal cistern of female and male dogs in the Normal MRI group. No significant effect of gender on the corrected midline area of the 3rd ventricle, interthalamic adhesion or quadrigeminal cistern was evident

5.3.8 Chiari-like malformation syndrome (CH-LMS) demonstrated no significant effect on the corrected midline area of the 3rd ventricle, interthalamic adhesion and quadrigeminal cistern

Comparison of corrected midline 3rd ventricle area in CKCSs with (score 1) mild (n=8) and (score 2) severe (n=5) Chiari-like malformation syndrome revealed that absolute and corrected mean of the 3rd ventricle areas were slightly larger in the mild group (143.4 mm^2 and a corrected value of 5.63) than the severe group (139.44 mm^2 and a corrected value of 5.32), but this difference was not statistically significant (P = 1.000 and P = 0.5237 respectively) (Figure 5-35).

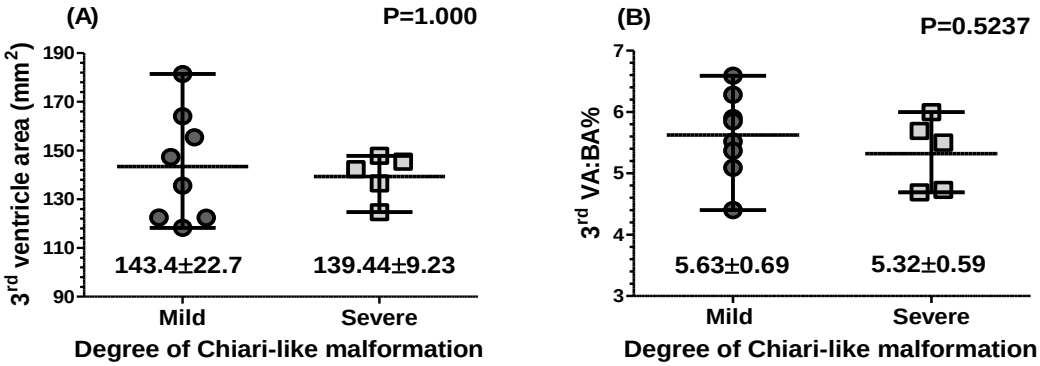

Figure 5-35: Vertical scatter plots (with range, mean and standard deviation) illustrating (A) absolute and (B) corrected 3rd ventricle area in dogs in the CH-LMS with mild and severe degrees of cerebellar herniation. The severity of cerebellar herniation did not have a significant effect on the midline area of the 3rd ventricle

Similarly, the midline areas of the interthalamic adhesion and quadrigeminal cistern, (absolute and corrected values) were not affected significantly by the severity of the cerebellar herniation occurring in association with Chiari-like malformation syndrome (Figures 5-36 and 5-37). Although not statistically significant, the results examined of the quadrigeminal cistern revealed that the mean midline area was slightly higher in the mild compared to the severe group which was similar to the results for the 3rd ventricle. In contrast the mean absolute and corrected midline interthalamic adhesion areas were slightly lower in dogs with mild cerebellar herniation although again this was not statistically significant than in dogs with severe cerebellar herniation.

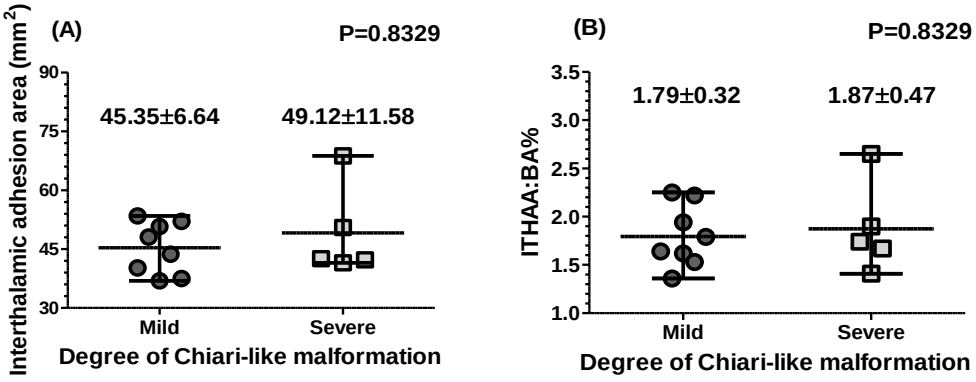

Figure 5-36: Vertical scatter plots (with range, mean and standard deviation) showing (A) absolute and (B) corrected midline interthalamic adhesion area in dogs in the CH-LMS group with mild and severe cerebellar herniation. The severity of cerebellar herniation did not have a significant effect on the midline area of the interthalamic adhesion

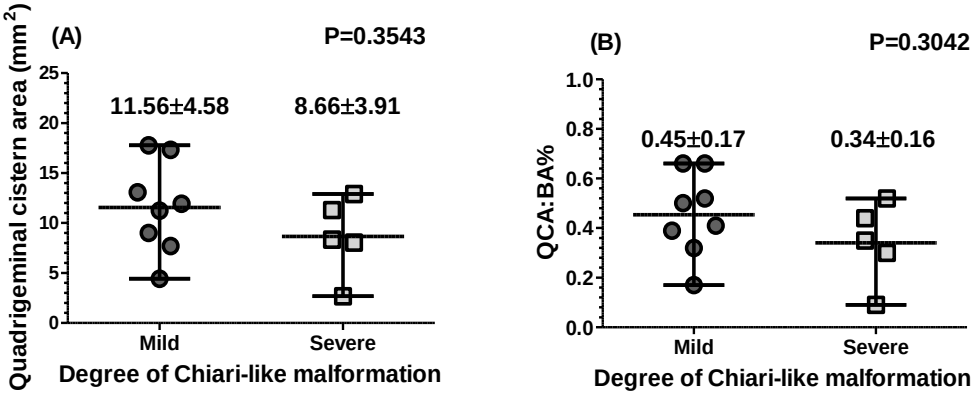

Figure 5-37: Vertical scatter plots (with range, mean and standard deviation) showing (A) absolute and (B) corrected midline area of the quadrigeminal cistern in dogs in the CH-LMS group with mild and severe cerebellar herniation. The severity of cerebellar herniation did not have a significant effect on the midline area of the quadrigeminal cistern

5.4 Discussion

The 3rd ventricle is a midline structure connecting the lateral ventricles with the 4th ventricle. It contains part of the choroid plexus, which contributes to the cerebrospinal fluid (CSF) of the ventricular system (Beitz and Fletcher, 1993; De Lahunta and Glass, 2009), and supplies the brain with hormones such as melatonin which is secreted from the pineal gland (Last and Tompsett, 1953). Using MR imaging, the body of the 3rd ventricle was found to have a consistent shape in normal dogs, comprising a roughly parallelogram shape with a central interthalamic adhesion. Fitzgerald (1961) showed using casts that the 3rd ventricle encircled the interthalamic adhesion (Fitzgerald, 1961), and appeared as a flattened ring (Horodyska and Kreiner, 1962). Evans described the 3rd ventricle as a narrow chamber that separated the left and right halves of the diencephalon, besides the junction of the diencephalon at the interthalamic adhesion (Evans, 1993). In cats, the 3rd ventricle consists of two arches surrounding the *massa intermedia* (Levinger and Edery, 1968). In man, the 3rd ventricle may display a variety of shapes, largely due to the absence of an interthalamic adhesion (Last and Tompsett, 1953)

The results of this study demonstrated that on MR images, the rostral border of the 3rd ventricle was defined by the *lamina terminalis* while the optic chiasm formed its rostroventral angle. In gross specimens in the dog, the *lamina terminalis* has been referred to as the rostral border of the 3rd ventricle (Horodyska and Kreiner, 1962). The optic chiasm was also found to form the very rostroventral point of the 3rd ventricle in man (McLone, 2004).

The mesencephalon mass has been reported to form the caudal boundary of the 3rd ventricle in dogs and man (Horodyska and Kreiner, 1962; McLone, 2004). Whilst, in a separate study, only two structures were identified as forming the caudal border of the 3rd ventricle - the pineal body and caudal commissure (Fitzgerald, 1961). All three of the above structures were identified as contributing to the caudal boundary of the 3rd ventricle on MRI in the present study. However, no previous MRI studies in the dog have mentioned the arachnoid membranes of the quadrigeminal cistern or the suprapineal recess that form the upper caudo-dorsal angle of the 3rd ventricle.

The roof of the 3rd ventricle was defined in this work by the edges of hippocampal fornix, its dentate tubercle and callosal gyri [the choroid plexus - *tela chorioidea,* attaches to these structures]. The roof of the 3rd ventricle also had a ventral evagination (Figure 5-10) that was formed by the above structures, and which appeared to be diminished in the presence of hydrocephalus (Figure 5-17 & 22). The roof of the 3rd ventricle was described as bulging dorsally and composed of a thin membrane with a pair of choroid plexuses (Beitz and Fletcher, 1993). This is supported by other workers who found the *tela chorioidea* formed the roof of the 3rd ventricle and consisted of a thin sheath called the ependymal layer and a folded pia mater (Fitzgerald, 1961; Horodyska and Kreiner, 1962).

Privous studies found that the floor of a 3rd ventricle cast was formed by the *basis hypothalamus* (Fitzgerald, 1961; Horodyska and Kreiner, 1962). In the present study using MRI, the optic chiasm and the pituitary gland formed the majority of the 3rd ventricle floor, with the mammillary body forming its caudo-ventral angle. Evans, referred to the hypothalamus (which included the ventro-caudally situated mammillary bodies), the optic chiasm rostrally, and a region located between these structures known as the *tuber cinereum,* as forming the wall and the floor of the 3rd ventricle (Beitz and Fletcher, 1993). In man, attempts at casting the ventricular system usually led to rupture of the roof or floor of the 3rd ventricle due to fragility (Last and Tompsett, 1953).

Three recesses were confirmed in the present study on the basis of the MRI appearance, the optic, the infundibular and the suprapineal. Fitzgerald (1961) and Horodyska & Kreiner (1962) defined the three recesses grossly. Hudson et al (1989) referred to the suprapineal recess as the caudal extent of the 3rd ventricle as described with ultrasonography. In contrast, a study of the clinical anatomical features of the brain using MRI described the 3rd ventricle as having two recesses, the optic and infundibular (Leigh et al. 2008). Horodyska & Kreiner (1962), described the above 3 recesses, but also defined further areas as diverticulae located under and above the rostral commissure

of the 3rd ventricle using casts. These diverticulae were not sufficiently identifiable or repeatable on MR images in the present study to be confident of their existence. Perhaps examination of the 3rd ventricle with higher Tesla MRI machines would allow their existence to be confirmed or excluded.

On MRI, the optic recess was found to lie just above the optic chiasm when examined in the present study (Figure 5-7). This was consistent with the gross anatomical appearance and location described by others (Fitzgerald, 1961; Horodyska and Kreiner, 1962). The enlargement of the 3rd ventricle had little effect on the area and position of the optic recess. In two dogs with hydrocephalus, the optic recess was found rostral to the optic chiasm (Figure 5-17) or the rostral commissure (Figure 5-22).

In one dog with age-related behavioural changes and generalised brain atrophy (senile changes), the 3rd ventricle increased in size on midline sagittal plane to exceed the level of the rostral commissure, though the optic recess apparently was unchanged in position. Milhorat et al (1970) found that one hour after inducing hydrocephalus in the dog and monkey, the anterior part the 3rd ventricle floor appeared normal with the exception of appearing slightly thinned. However by six hours the whole 3rd ventricle was affected (Milhorat et al. 1970). In man, hydrocephalus is reported to lead to rostral expansion of the optic recess (McLone, 2004), but only dilation in others studies (Corrales and Torrealba, 1976). The variable degree of ventriculomegaly found in a few animals in the present study might explain the alteration of the position and shape of the optic recess in some dogs, but not in others.

The infundibular recess was identified in the present study above the pituitary gland with a slight impinging extension into the pituitary gland itself, which was only clearly identifiable in some of the Normal brain MRI group (Figure 5-7). Horodyska and Kreiner (1962) also found on gross dissections that this recess was situated rostral to the mammillary body and dorsal to the pituitary gland, and Fitzgerald (1961) found that the infundibular recess extended cranial and ventral into the pituitary gland In the present study, when hydrocephalus was present this recess appeared to expand leading to compression of the underlying tissue (pituitary gland) and in some cases also merged with the optic recess rostrally (Figures 5-17 & 22). This change has also been recorded in man (Corrales and Torrealba, 1976; McLone, 2004).

The suprapineal recess in the present study was found to occupy the upper dorsocaudal aspect of the 3rd ventricle and had a generally triangular shape in MRI studies from dogs with normal brains (Figure 5-7). In addition, the size of this recess appeared to have an

inverse relationship with the quadrigeminal cistern. Within ventricular system moulds, this recess has been shown to be a diverticulum above the caudal border of the pineal gland and caudal commissure, and extended caudally (Fitzgerald, 1961). It had the largest area and most variable shape of all the recesses (Horodyska and Kreiner, 1962). This recess was not identified in a third of the human ventricular system moulds (Last and Tompsett, 1953). Following expansion of this recess it was seen to occupy the whole quadrigeminal cistern area on midline sagittal plane MR images in the present study in dogs with normal brain MRI studies (Figure 5-14). One possible explanation for the absence of the quadrigeminal cistern in these cases is early rupture of the membranes between the recess and the cistern or increasing suprapineal recess size, leaving no space for the quadrigeminal cistern on midline sagittal plane. Alternatively the quadrigeminal cistern may be laterally deviated from midline, but no evidence was identified to support this potential explanation.

The suprapineal recess was the only recess to demonstrate any real enlargement one hour after the induction of hydrocephalus in dogs and monkeys (Milhorat et al. 1970). Rupture of this recess into the subarachnoid space (as a spontaneous ventriculostomy) led to a reduction in the degree of the induced hydrocephalus in the rabbit (Wisniewski et al. 1969). It was also noted that this site may provide a safe and effective option for 3rd ventriculostomy, particularly if the suprapineal recess wall is thin and translucent (Daniel et al. 2004).

The corrected midline area of the 3rd ventricle in the Normal MRI group was shown to be significantly different from that found in the VM group (Figure 5-20). The results of the present study demonstrate that an increase in 3rd ventricle size is not usually seen in hydrocephalus with mild increasing in the ventricular system. For this reason, and based on the results of the present study, it is suggested that changes to the roof of the 3rd ventricle may be a useful guide for identifying early changes to the 3rd ventricle, and appeared to be more useful than the absolute or corrected 3rd ventricle area. Although there was a statistical difference between the corrected area of the 3rd ventricle in the Normal and Other Brain Lesions groups, this difference diminished if only the brachycephalic dogs from each group were compared. It is therefore likely that the difference in the corrected midline area of the 3rd ventricle in the Normal and Other Brain Lesions groups was due to other factors as well, rather than being the consequence of just the underlying brain disease.

In the majority of dogs within the present study with hydrocephalus the corpus callosum and fornix were clearly atrophied with an increased corrected and absolute 3rd ventricle

midline area. However, in some dogs with a clinical diagnosis of hydrocephalus, the corrected and absolute 3rd ventricle midline areas were within normal limits compared to dog within Normal MRI group which has a similar breed and bodyweight, but in these dogs the shape of the 3rd ventricle area was altered, as evidenced by the reduced ventral evagination in the roof (Figure 5-18). Supporting this finding, a dramatic increase in the 3rd ventricle was not found in a group of Beagles within six hours of induced hydrocephalus, even though these dogs had significant dilation of the lateral ventricles by this stage (Vullo et al. 1998). In mongrel dogs, the normal ventral angulation of the corpus callosum was absent in association with increased size of the lateral and 3rd ventricles, leading to elevation of the roof of the 3rd ventricle (Milhorat et al. 1970).

Two dogs in the present study showed expansion of the floor of the 3rd ventricle, suggesting rupture of the floor of the 3rd ventricle could potentially occur, thereby allowing CSF to drain into the ventral subarachnoid space. Scarff (1966) also suggested that by puncturing the *lamina terminalis* and the floor of the 3rd ventricle, hydrocephalus would be reduced due to CSF drainage into subarachnoid space (Scarff, 1966). In man, longstanding hydrocephalus and elevated intracranial pressure led to anatomical changes in the shape of the 3rd ventricle, which may be recognised by herniation of the rostro-ventral floor of the 3rd ventricle into the empty sella turcica (Hellwig et al. 2005).

Significant differences in the interthalamic adhesion midline areas were only evident when comparing the Normal and VM groups, but not when the OBLgroup was used for comparison. Increasing 3rd ventricle size most likely indicated more severe ventriculomegaly and it appeared that by the time increased 3rd ventricle size was evident that the parenchymal tissue of the brain had already started to be affected. In 2005, Hasegawa et al revealed a significant difference between the depth of the interthalamic adhesion in normal dogs and those with age-related abnormal behaviour (or what they termed dementia). They also found that enlargement of the ventricular system may result in decreased interthalamic adhesion thickness, reflecting the intracranial pressure changes caused by obstructive hydrocephalus.

Compression of the cerebellum as seen in some rabbits following the development of induced hydrocephalus was caused by expansion of the suprapineal recess, and additionally resulted in absence of an identifiable quadrigeminal cistern in these animals (Wisniewski et al. 1969). In the present study, the most common cause of cerebellar compression in obstructive hydrocephalus was due to the presence of a quadrigeminal cistern cyst (Figure 5-18). Absence of the quadrigeminal cistern in the present study in some clinically normal dogs may have been the result of rupture of the membrane

between the suprapineal recess and the quadrigeminal cistern, but this is speculation and the quadrigeminal cistern may just have been too small to identify. In one rabbit surviving for 20 days after the induction of hydrocephalus, rupture of the suprapineal recess was suggested as the reason for a reduction in the intracranial pressure, allowing CSF to escape into the subarachnoid space (Wisniewski et al. 1969).

As dogs with brachycephalic head phenotypes also tended to be dogs with a lower bodyweight, and dogs with lower bodyweight had a relatively larger midline 3rd ventricle area, it was essential to repeat the analysis in populations of dogs with a similar head phenotype. The Normal brain MRI group demonstrated a weak (but significant) correlation between midline 3rd ventricle area and head shape, however this correlation was no longer evident when the dogs were assigned into brachycephalic, mesaticephalic and dolichocephalic populations. All light dogs within this study were brachycephalics however, not all the brachycephalics were light dogs. It is therefore likely that head shape has less of an effect on 3rd ventricle size (increasing with more severe brachycephalia) than the bodyweight. In Normal human MRI studies, increased 3rd ventricle size was associated with larger head size when determined using CT (Gyldensted and Kosteljanetz, 1976).

It has been suggested that toy and brachycephalic breeds are at a higher risk of hydrocephalus than other breeds (Selby et al. 1979). It has also been suggested that there is an inverse relationship between bodyweight and the incidence of congenital hydrocephalus in dogs (Selby et al. 1979). However, in the absence of hydrocephalus the work reported here demonstrated that midline 3rd ventricle area was negatively correlated with bodyweight (P=0.0001) (Figure 5-29). Similarly, there appears to be an effect of breed on the size of the interthalamic adhesion, but this is reported to be due to the inherent smaller size of most brachycephalic breeds (Hasegawa et al. 2005). In the present study, comparing the absolute midline area of the interthalamic adhesion was considered to be inaccurate due to the different sizes of the different dog breeds, and therefore the midline sagittal interthalamic adhesion area was corrected according to a standard parameter (midline sagittal brain area). When Esteve-Ratsch et al (2001) examined the corrected area of the lateral ventricle on transverse section, they found that the lateral ventricle was affected by breed and discussed the difficulties of defining the normal area of the lateral ventricles for all breeds. These findings were based on two breeds: the GSD (large breed) and the Yorkshire terrier (small breed). While that study did not investigation age as a confounding factor, it is likely to have a significant effect on lateral ventricle size (Esteve-Ratsch et al. 2001). The results of the present study

demonstrated that smaller dogs had a larger midline sagittal 3rd ventricle area, relative to midline sagittal brain area (Figure 5-30).

Age (Figures 5-32 and 5-33) and gender (Figure 5-34) did not appear to exert a significant effect on midline sagittal 3rd ventricle, interthalamic adhesion or quadrigeminal cistern area. In human patients, head CT demonstrated a significant increase in the width of the 3rd ventricle on dorsal plane images in older people (Gyldensted and Kosteljanetz, 1976). A weak negative correlation between age and the size of the interthalamic adhesion has also been demonstrated in dogs using MRI, with the thickness of the interthalamic adhesion suggested to be a good marker for serially determining the degree of brain atrophy in dogs (Hasegawa et al. 2005). Supporting the findings of the present study, no difference was evident between male and female dogs in studies to examine the length of the 3rd ventricle in gross specimens (González-Soriano et al. 2001). However, one study has shown that the 3rd ventricle in man is significantly wider in men than women using CT (Gyldensted and Kosteljanetz, 1976).

Examination of the midline sagittal area of the 3rd ventricle also demonstrated no correlation with the severity of the cerebellar herniation (as a measure of the degree of Chiari-like malformation syndrome) in CKCS dogs. In human patients with Chiari Malformation II, it is reported that the 3rd ventricle is rarely enlarged but the angulation of the 3rd ventricle may change (Stevenson, 2004). In another human study, it was stated that the 3rd ventricle was different in Chiari II malformation compared to the normal, particularly the distance between the mammillary body and the pituitary recess which was shorter in affected patients than normal people (McLone, 2004). In the dog the incidence of primary hydrocephalus increased as a result of increased severity of occipital malformation and obstruction of the ventricular system drainage (Rusbridge, 2005).

In a summery the present study demonstrated that the MRI appearance and dimensions of the 3rd ventricle, interthalamic adhesion and the quadrigeminal cistern were different in normal dogs as compared to dogs with ventriculomegaly. The alteration in these regions may be evident as a change in their dimensions or shape. However, no changes were evident in these areas if there was no significant enlargement of the ventricular system. The appearance and dimensions of the 3rd ventricle, interthalamic adhesion and quadrigeminal cistern were also determined by the presence of other brain lesions, CH-LMS, head phenotype, age and gender however, only the area of the 3rd ventricle was related to bodyweight.

6 GENERAL DISCUSSION

Data presented in this study has provided further insight into the effect of head phenotype (brachycephalic, mesaticephalic and dolichocephalic) on the anatomy of the skull and brain, with particular emphasis on the olfactory system and the rostral and middle cranial fossae. Specifically, the study aimed to clarify the effect head phenotype had on the normal MRI appearance and dimensions of these regions. MRI was first used in the veterinary field in dogs towards the end of the last century (Kraft et al. 1989). MRI has proved to be useful for visualising the internal features of the head, with soft tissue providing the most detail, but with a signal void produced by air and compact bone (Gavin and Bagley, 2009). Despite a high air and compact bone content, MRI of the facial region in many cases still demonstrates sufficient differences between tissues, and tissue responses to disease, to allow accurate diagnosis (Assheuer and Sager, 1997; Rycke et al. 2003; Craven et al. 2007). However, it is particularly in imaging of the brain and CSF that MRI comes into its own, with an unparalleled ability to generate images with a high tissue contrast and spatial resolution, in a variety of different planes including the dorsal, sagittal and transverse (Leigh et al. 2008; Thames et al. 2010). MRI also allows the grey and white matter of the brain to be distinguished due to their differing inherent signal intensities in the normal and abnormal brains (Kraft et al. 1989).

6.1 Cephalic indices for determining head phenotype

Shortening of the skull-base of the head results from early fusion of one or more of the basicranial joints (Evans, 1993). The most obvious consequence of this is the difference in head shapes that are evident in different dog breeds, ranging from brachycephalic (e.g. the Boston terrier), through mesaticephalic (e.g. the Golden retriever), to dolichocephalic (e.g. the Scottish deerhound). These changes to overall head shape result from fundamental changes within individual regions of the head, but mainly to the bony structures including the facial, palatal and neural regions (Stockard, 1941; Evans, 1993; Drake and Klingenberg, 2010). Head shape in dogs has been measured using a variety of different cephalic indices, with those of Evans and Stockard being the most widely accepted. Although Evans and Stockard used more than one formula for the classification of dog heads, the commonly used ones are the Evans and Stockard skull indices. The index developed by Evans is widely regarded as the standard formula in order to define dogs as brachycephalic, mesaticephalic or dolichocephalic.

However, because Evans only published the average index values for each group, rather than individual ranges or cut-off points for each group, subjective judgments still have to be made for many individual dogs in order to decide whether they are truly brachycephalic, mesaticephalic or dolichocephalic. In light of this, the index has been expanded to incorporate a range for each group (Schwarz et al. 2000).

In an attempt to develop discrete ranges for each group, two methods were applied to the *arbitrary control* (Evans index). Method 1 showed a higher accuracy in defining each group from a statistical point of view. Method 2 was considered to define the best range for each group. So dogs having an index of 60.8 or less were more likely to be brachycephalic, while, those equal or less than 51.6 fell into the dolichocephalic group. A limitation of these divisions was the small number of available mesaticephalic and dolichocephalic dogs during the study period.

The Evans and Stockard skull indices require measurements to be made from an individual dog's skull, or from radiographs of the dog's head. MRI would represent an elegant way to determine the Evans and Stockard skull indices if the landmarks could accurately be determined. This study has demonstrated that the Evans and Stockard skull indices can be determined on the basis of MR images. In order to calculate the Evans and Stockard skull indices, MR images in two planes are required: the transverse plane at the level of the widest point of the zygomatic arch and the midline sagittal plane from the rostral aspect of the nose to the foramen magnum. Practically, the midline sagittal plane image is the easiest to obtain and identify (it is often used to plan all the other planes and has a unique combination of readily identifiable anatomical landmarks), but frequently the image does not extend to the rostral aspect of the nose (particularly in the longer-nosed breeds). Defining head shape on the basis of a single image and which did not require imaging of the whole midline sagittal head would be very useful in correlating head phenotype with the findings of a diagnostic head MRI study. The first part of the study was therefore proof of concept for the use of the olfactory bulb angle (relative to the rest of the brain) as a measure of head shape.

6.2 Nomenclature and descriptive anatomy of the olfactory bulb fissure

In order to define the position of the olfactory bulb, it was first necessary to be able to accurately identify its position. Correct identification of the olfactory bulbs, and their related ethmoidal turbinates, are also important in a number of neurological disorders, including neoplasia affecting the rostral skull fossa or caudal nasal cavity, hydrocephalus (with dilation of the olfactory bulb recess in obstructive hydrocephalus) and for harvesting of olfactory ensheathing cells from the nasal epithelium. A review of the anatomical literature from 1881 to 2010 identified a variety of terms for the grooves that separate the olfactory lobes from the rest of the brain; however there is no term to describe the groove separating the olfactory bulb from the brain. The study described the appearance of this groove on midline-sagittal plane MR images as a line sloping from rostro-dorsal to caudo-ventral, situated between the olfactory bulb and the neo- and allocortex, and on dorsal plane MR images as a line separating the olfactory bulb and neo- or allocortex, extending from rostro-medial to caudo-lateral. On the basis of the anatomical and MRI appearance, and in the absence of a suitable term in the literature, the olfactory bulb fissure was proposed as an appropriate descriptive term for this structure. In T1-weighted MR images the olfactory bulb fissure appeared as a hypointense line, while in T2-weighted images it appeared as a hyperintense line, confluent with the subarachnoid CSF filled spaces.

6.3 Olfactory bulb angulation and position as a measure of head phenotype

Data from this study demonstrated that olfactory bulb angulation is a feasible method of classifying head shape into brachycephalic, mesaticephalic and dolichocephalic in a similar manner to the Evans and Stockard indices. The advantage of this method is that it can be performed on a single midline sagittal plane MR image and does not need to include the entire head. Olfactory bulb angulation decreases with increasing brachycephalia. In addition, the position of the olfactory bulb is also influenced by shortening of the skull-base, with more ventral orientation of the olfactory bulb associated with increasing brachycephalia and vice versa. This concurs with the demonstration by Lyras (2009) that shortening of the skull-base during early embryological development results in the facial part of the skull being dragged ventro-caudally, and with it a more ventral position of the cribriform plate.

The range of the olfactory bulb angulation index values that corresponded to each head shape were determined using the same statistical methods as were used to determine the ranges for the Evans index. Although Method 1 showed higher accuracy in defining each group from a statistical perspective, this method was complicated by the fact that it resulted in a zone where individuals within some specific breeds did not fall into the range of either group. Method 2 defined, more satisfactorily, the best range for each group using either the Evans index values or the angulation of the olfactory bulb, as it engendered the least overlap. The final cut-off for brachycephalia was defined as an olfactory bulb angle of ≤51, while an angle of ≥62 degrees allowed a presumption of dolichocephalia, between these two values dogs would be classified as mesaticephalic. A limitation for defining these values in this study was the low number of mesaticephalic and dolichocephalic dogs having whole head MRI during the study period. The validation of olfactory bulb angulation as a measure of head phenotype may have implications for the selection of breeding dogs in order to exclude or ameliorate undesirable health traits correlated with head shape.

6.4 The classification of individual dog breeds as brachycephalic, mesaticephalic or dolichocephalic

Even though dogs can been classified according to the Evans index, interpretations as to the exact classification of different dog breeds as brachycephalic, mesaticephalic and dolichocephalic have varied between different studies. In part, this was due to the absence of an exact defined range for establishing each head shape. As an example, breeds including the Collie, GSD or Dobermann have been espoused in different studies as typical examples of mesaticephalic and dolichocephalic (Miller and Christensen, 1964; Hayes and Schiefer, 1969; Niebauer and Evans, 1988; Evans, 1993; Onar, 1999; Hasegawa et al. 2005). There is also debate as to whether the CKCS, Miniature poodle and the WHWTs are typical brachycephalic breeds or not. Even the Yorkshire terrier has been proposed to have a long skull shape (dolichocephalic features) and brachycephalic brain (Esteve-Ratsch et al. 2001). In the present study, breeds including the Scottish deerhound and German and Belgian shepherd dogs were classified as dolichocephalic, while the Shih-tzu, Pug, Bishon frise, Boston terrier and Chihuahua were classified as brachycephalic, on the basis of both skull index and olfactory bulb angulation index. Scottish deerhounds and German and Belgian shepherd dogs are generally considered long nosed or dolichocephalic (Stockard, 1941; Onar, 1999), but not by Evans (1993) who classified the GSD as mesaticephalic. Within the above studies, there is agreement

that the Pug, Boston terrier, Shih-tzu, Bishon frise, Chihuahua and Boxer dog are all brachycephalic. There is also agreement that the head shape of the Boxer dog is different to breeds like the Pug in terms of the degree of brachycephalia (Schmidt et al. 2011). This indicates that there are differences within dog breeds that are classified as brachycephalic, with some at the extreme end of the brachycephalic range and those that almost fall into the mesaticephalic group. The same also applies to mesaticephalic and dolichocephalic breeds.

Individual variation between the skull index values within the same breed has been reported (Onar, 1999; Schwarz et al. 2000). This is also the likely explanation for individual dogs within certain breeds falling across more than one classification in the present study. CKCSs and Boxer dogs had a range of both Evans skull index and olfactory bulb angulation values that placed them in both brachycephalic and mesaticephalic head types when the first statistical method was used, but not using Method 2. Although the Collie was defined as a typical dolichocephalic breed according to Evans, the results of this study seemed to demonstrate that the Border collie was more consistent with a mesaticephalic head shape. However, the use of the term *Collie* is rather imprecise as the UK and USA Kennel Clubs register a variety of types of Collie, including the Border, Bearded, Rough and Smooth collie.

6.5 The effect of head shape on the nasal cavity and the rostral and middle cranial fossae

The observations made in this study appear to have confirmed that the shape and size of the cranial fossae are influenced by both head shape and bodyweight. Evans (1993) believed that the cranial volume was mainly affected by bodyweight, but could not exclude head shape as another factor. The findings of this study demonstrated that although the fossae of the cranial cavity were generally affected by bodyweight, the ethmoidal fossa was predominately influenced by head shape.

Head shape not only impacted on the braincase portion of the skull, but also on the facial and palatal regions. Dragging the cribriform plate ventro-caudally as a result of shortening the skull-base in brachycephalic dogs reduced the midline and dorsal area of both the respiratory and the olfactory regions of the nose. Reducing the ethmoidal (olfactory) area may affect the acuity of smell in dogs, as it is well known that dogs used for hunting usually have a moderate to long nose, for example the Springer spaniel. Examination of the nasopharynx as part of this study revealed that the alteration in cross-

sectional shape of the nasopharynx with increasing brachycephalia was partly the result of the ventral orientation of the olfactory bulbs and the associated ethmoidal turbinates. In some cases, where the cross-sectional shape of the nasopharynx was as described *peanut* shape, this was associated with protrusion of the ethmoidal turbinates into the lumen of the nasopharynx. This abnormal shape to the bony nasopharynx is likely to be a contributory factor in brachycephalic obstructive airway syndrome.

When the components of the middle fossa were examined, particularly the 3rd ventricle, interthalamic adhesion and quadrigeminal cistern, the effect of head shape was less pronounced. The area of the 3rd ventricle tended to be larger in most brachycephalic breeds and inversely correlated with bodyweight. However, because brachycephalic breeds tended to be smaller breeds, the tendency for brachycephalic dogs to have a relatively larger midline 3rd ventricle area may be confounded by the effect of bodyweight. The shape of the 3rd ventricle was mainly characterised on midline sagittal plane images as a parallelogram, which had a small ventral evagination within its roof that was diminished in pathological ventriculomegaly, even if there was no visibly identifiable enlargement of the 3rd ventricle. Grossly three main recesses of the 3rd ventricle have previously been identified in dogs (Fitzgerald, 1961; Horodyska and Kreiner, 1962). These three recesses, the optic, infundibular and suprapineal, were also identified on MRI midline sagittal plane images in this study.

No reference to such recesses as being identifiable on MRI could be found in the veterinary literature. Although the interthalamic adhesion and the quadrigeminal cistern did not appear to be influenced by head shape or bodyweight, these structures may be altered in disease (Fitzgerald, 1961; Horodyska and Kreiner, 1962). In the present study, dogs with ventriculomegaly demonstrated significant changes, the area of the 3rd ventricle, interthalamic adhesion and quadrigeminal cistern but dogs with other brain lesions and CKCS with CH-LMS remained compared with the normal dogs.

Although it is difficult to determine whether bodyweight or the head shape has the greater effect, attempts were undertaken to reduce interference between the two factors by using a consistent correction factor. This was primarily midline brain area or on occasion bodyweight. Throughout all the studies, it is contended that this correction helped to reduce the multifactor effect.

6.6 Further studies

Any study invariably raises further questions and this study is no different. Having demonstrated a spectrum of head shapes within individual breeds, it would be interesting to perform genetic analysis to examine whether the genes responsible for modifying the brachycephalic head shape can be identified. This would allow breeding away from extreme brachycephalia, where this is associated with adverse health affects in specific populations of dogs. The demonstration that the midline and dorsal olfactory area of the nose is directly related to olfactory bulb area, and is influenced by head shape, would furthermore mean that genetic analysis would also be interesting in mesaticephalic and dolichocephalic breeds. The area of the olfactory turbinates gives an indirect measure of the ability to smell, and recognising the genes responsible for a larger or smaller olfactory area may allow selection for dogs with better olfactory acuity. Finally, better understanding the normal anatomy of the 3rd ventricle, in particular further studies to ascertain the factors responsible for the development of normal and pathological ventriculomegaly would be a clinical help. This study has characterised some of the abnormal changes occurring in the 3rd ventricle that allow recognition of pathological ventriculomegaly. Ideally these changes would be fully characterised in an induced model in a high field MRI unit.

In conclusion, MRI is able to provide detailed images of the components of the head and cranial fossae, including the ethmoturbinates, bony nasopharynx, brain, olfactory bulb, 3rd ventricle, quadrigeminal cistern and interthalamic adhesion. It also allows the dimensions of these structures to be determined. This study identified the fissure that separates the olfactory bulb from the rest of the brain, and suggested the term *olfactory bulb fissure* for this structure. For anatomical terms to be defined in authorised anatomical dictionaries such as *Nomina Anatomica Veterinaria* (Schaller, 1992), these terms should be named using an appropriate descriptive term and duplication or twin meaning should be avoided. This study has shown that MRI is a satisfactory technique for determining canine head shape anatomically, and using the one-dimensional olfactory bulb angulation index, instead of the classic two dimensional Evans index, is practicable and provides similar results to the conventional skull indices. The results of this study should provide a useful starting point for scoring the degree of brachycephalia in dogs having diagnostic MRI studies.

7 ABBREVIATIONS

ANOVA	Analysis of variance
BOAS	Brachycephalic obstructive airway syndrome
BNPH	Bony nasopharynx
CFA	Caudal fossa area
CH-LMS	Chiari-like malformation syndrome
CI	Confidence interval
CKCS	Cavalier King Charles Spaniel
CS	Cocker spaniel
CSF	Cerebrospinal fluid
CT	Computer tomography
DICOM	Digital imaging and communications in Medicine
EFA	Ethmoidal fossa area
Freq. dist.	Frequency distribution
GSD	German shepherd dog
ITHAA: BA	Interthalamic adhesion area: brain area
kg	Kilogram
L1	Length of the olfactory bulb measured on dorsal plane
L2	Length of the olfactory bulb measured on midline sagittal plane
L3	Length of the olfactory bulb measured on midline sagittal plane
M	Mean
MFA	Middle fossa area
Min & Max	Minimum and maximum
mm	Millimetre
MRI	Magnetic resonance image
n	Number within groups
NAD	No abnormalities detected

NAD-E	No abnormalities detected-Epileptic
OB	Olfactory bulb
OBH: BA	Olfactory bulb height: brain area
OBL	Other brain lesions
OBL1: BA	Olfactory bulb length1: brain area
OBL2: BA	Olfactory bulb length 2: brain area
OBL3: BA	Olfactory bulb length 3 : brain area
OBH:BA	Olfactory bulb height: brain area
OBI	Olfactory bulb index
OD	Olfactory dimension
OSAS	Obstructive sleep apnoea syndrome
PACS	Picture archiving and communication system
QCA: BA	Quadrigeminal cistern area: brain area
R	Range
RFA	Rostral fossa area
ROC	Receiver operating characteristics
STDEV	Standard deviation
T1	Spin-lattice relaxation time
T2	Spin-spin relaxation time
TE	Echo time
TR	Repetition time
VM	Ventriculomegaly
WHWT	West Highland white terrier
3^{rd} VA:BA	3^{rd} ventricle area: brain area
$\sqrt[3]{BW}$	Cube root of the bodyweight
$\sqrt[2]{CCA}$	Square root of the cranial cavity area
$\sqrt[2]{OBA}$	Square root of the olfactory bulb area

8 REFERENCES

Adams, D. (1972) Olfactory and non-olfactory epithelia in the nasal cavity of the mouse, peromyscus. *American Journal of Anatatomy* 133, 37-49.

Adams, D. (2004) *Canine anatomy: A systemic study*, Ames: Iowa State Press.

Allison, A. (1953) The morphology of the olfactory system in the vertebrates. *Biological Reviews* 28, 195-244.

Anderson, W.; Anderson, B. and Smith, B. (1994) *Atlas of canine anatomy*, Philadelphia: Lea and Febiger.

Asher, L.; Diesel, G.; Summers, J.; McGreevy, P. and Collins, L. (2009) Inherited defects in pedigree dogs. part 1: Disorders related to breed standards. *Veterinary Journal* 182, 402-411.

Assheuer, J. and Sager, M. (1997) *MRI and CT atlas of the dog*, Cambridge: Blackwell Scientific.

Bagley, W. (2005) *Fundamentals of veterinary clinical neurology*, Oxford: Blackwell.

Bang, B. and Cobb, S. (1968) The size of the olfactory bulb in 108 species of birds. *Auk* 85, 55-61.

Barr, M. (1948) Observations on the foramen of magendie in a series of human brains. *Brain* 71, 281-289.

Beitz, A. and Fletcher, TF. (1993) The brain 28. In: Miller, ME., (Ed.) *Miller's anatomy of the dog*, 3rd edn. pp. 894-952. Philadelphia: WB Saunders.

Bergland, O. (1963) The bony nasopharynx: A roentgen-craniometric study. *Acta Otodontal Scandanavia* 21, 1-137.

Bhatnagar, K. and Kallen, F. (1974a) Cribriform plate of ethmoid, olfactory bulb and olfactory acuity in forty species of bats. *Journal of Morphology* 142, 71-89.

Bhatnagar, K. and Kallen, F. (1974b) Morphology of the nasal cavities and associated structures in Artibeus jamaicensis and Myotis lucifugus. *American Journal of Anatatomy* 139, 167-189.

Bhatnagar, K.; Kennedy, R.; Baron, G. and Greenberg, R. (1987) Number of mitral cells and the bulb volume in the aging human olfactory bulb: A quantitative morphological study. *Anatomical Record* 218, 73-87.

Bianchi, L. (1895) *The functions of the frontal lobes*, London: Macmillan.

Billen, F.; Day, M. and Clercx, C. (2006) Diagnosis of pharyngeal disorders in dogs: a retrospective study of 67 cases. *Journal of Small Animal Practice* 47, 122-129.

Braund, K. (2003) Clinical neurology in small animal: localization, diagnosis and treatment. In: Braund, K., (Ed.) *International Veterinary Information Service*, Ithaca.

Budras, K.-D.; McCarthy, P.; Fricke, W. and Richter, R. (2002) *Anatomy of the dog*, Hannover: Schlütersche Verlagsbuchhandlung.

Cardoza, J.; Goldstein, R. and Filly, R. (1988) Exclusion of fetal ventriculomegaly with a single measurement: The width of the lateral ventricular atrium. *Radiology* 169, 711-714.

Carrera, I.; Dennis, R.; Mellor, D.; Penderis, J. and Sullivan, M. (2009) Use of magnetic resonance imaging for morphometric analysis of the caudal cranial fossa in Cavalier King Charles Spaniels. *American Journal of Veterinary Research* 70, 340-345.

Cinnamond, M. (1987) Congenital anomalies of the nose. In: Kerr, A. and Evans, J., (Eds.) *Scott-Brown's Otolaryngology: Paediatric Otolaryngology,* 5th edn. pp. 215-225. London: Butterworths.

Cistulla, P. (1996) Craniofacial abnormalities in obstructive sleep apnoea: implications for treatment. *Respirology* 1, 167-174.

Coben, L. (1967) Absence of a foramen of magendie in the dog, cat, rabbit, and goat. *Archives Neurology Journal* 16, 524-528.

Collins, LM; Asher, L; Summers, J and McGreevy, P. (2011) Getting priorities

straight: Risk assessment and decision-making in the improvement of inherited disorders in pedigree dogs. *Veterinary Journal* 189 147-154

Constantinescu, G. (2002) *Clinical anatomy for small animal practitioners*, Ames: Iowa State Press.

Cook, W. (1964) Observations on the upper respiratory tract of the dog and cat. *Journal of Small Animal Practice* 5, 309-329.

Corrales, M. and Torrealba, G. (1976) The third ventricle. normal anatomy and changes in some pathological conditions. *Neuroradiology* 11, 271-277.

Craven, B.; Neuberger, T.; Paterson, E.; Webb, A.; Josephson, E.; Morrison, E. and Settles, G. (2007) Reconstruction and morphometric analysis of the nasal airway of the dog (Canis familiaris) and implications regarding olfactory airflow. *Anatomical Record* 290, 1325-1340.

Craven, B.; Paterson, E. and Settles, G. (2010) The fluid dynamics of canine olfaction: unique nasal airflow patterns as an explanation of macrosmia. *Journal of the Royal Society Interface* 7, 933-943.

Daniel, R.; Lee, G. and Reilly, P. (2004) Suprapineal recess: An alternate site for third ventriculostomy? *Journal of Neurosurgery* 101, 518-520.

De Haan, C.; Kraft, S.; Gavin, P.; Wendling, L. and Griebenow, M. (1994) Normal variation in size of the lateral ventricles of the labrador retriever dog as assessed by magnetic resonance imaging. *Veterinary Radiology & Ultrasound* 35, 83-86.

De Lahunta, A. (1983) *Veterinary neuroanatomy and clinical neurology*, 2nd edn. London: WB Saunders.

De Lahunta, A. and Glass, E. (2009) *Veterinary neuroanatomy and clinical neurology*, 3rd edn. St. Louis: Elsevier Saunders.

Dhaliwal, R.; Barbara, E.; John, M.; Igor, V. and Clarkson, R. (2004) Subjective evaluation of computed tomography and magnetic resonance imaging detecting intracalvarial changes of canine nasal neoplasia. *International Journal of Applied Research in Veterinary Medicine* 2, 201-208.

Drake, A. and Klingenberg, C. (2010) Large-scale diversification of skull shape

in domestic dogs: Disparity and modularity. *American Naturalist* 175, 289-301.

Drees, R.; Forrest, L. and Chappell, R. (2009) Comparison of computed tomography and magnetic resonance imaging for the evaluation of canine intranasal neoplasia. *Journal of Small Animal Practice* 50, 334-340.

Duffner, F.; Schiffbauer, H.; Glemser, D.; Skalej, M. and Freudenstein, D. (2003) Anatomy of the cerebral ventricular system for endoscopic neurosurgery: A magnetic resonance study. *Acta Neurochirurgica* 145, 359-368.

Esteve-Ratsch, B.; Kneissl, S. and Gabler, C. (2001) Comparative evaluation of the ventricles in the yorkshire terrier and the shepherd dog using low-field MRI. *Veterinary Radiology & Ultrasound* 42, 410-413.

Evans, H. (1993) The skeleton. In: Miller, M., (Ed.) *Miller's anatomy of the dog*, 3rd edn. pp. 122-218. Philadelphia: WB Saunders.

Evans, H. and De Lahunta, A. (1996) *Miller's guide to the dissection of the dog*, 4th edn. Philadelphia: WB Saunders.

Evans, H. and De Lahunta, A. (2004) *Guide to the dissection of the dog*, 6th edn. St. Louis: Elsevier Saunders.

Farrow, C. (2003) Brain disease and injury (intracranial lesions). In: Farrow, C., (Ed.) *Veterinary diagnostic imaging: The dog and cat*, pp. 218-230. St. Louis: Mosby.

Fike, J.; Lecouteur, R.; Cann, C. and Pflugfelder, C. (1981) Computerized-tomography of brain-tumors of the rostral and middle fossas in the dog. *American Journal of Veterinary Research* 42, 275-281.

Fike, J.; Cann, C.; Turowski, R.; Hiffina, R.; Turrell, J. and Ax, L. (1986) Differentiation of neoplastic from non-neoplastic lesions in dogs brain using quantitative CT. *Veterinary Radiology* 27, 121-128.

Fitzgerald, T. (1961) Anatomy of the cerebral ventricles of domestic animals. *Veterinary Medicine* 56, 38-45.

Fletcher, TF. (1993) Spinal cord and meninges. In: Miller, M., (Ed.) *Miller's anatomy of the dog*, 3rd edn. pp. 800-828. Philadelphia: WB Saunders.

Fletcher, TF. (2011) Veterinary Anatomy web site. http://vanat.cvm.umn.edu/

Garcia-Real, I.; Kass ,P.; Sturges, B. and Wisner, E. (2004) Morphometric analysis of the cranial cavity and caudal cranial fossa in the dog: A computerized tomographic study. *Veterinary Radiology & Ultrasound* 45, 38-45.

Gavin, PR. and Bagley, RS. (2009) *Practical small animal MRI,* 1st edn. Ames: Wiley-Blackwell.

George, T. and Smallwood, J. (1992) Anatomic atlas for computed tomography in the mesaticephalic dog: Head and neck. *Veterinary Radiology & Ultrasound* 33, 217-240.

Giannini, N.; Wible, J. and Simmons, N. (2006) On the cranial osteology of Chiroptera. I. Pteropus (Megachiroptera: Pteropodidae). *Bulletin of the American Museum of Natural History* 1-134.

Ginn, J.; Kumar, M.; McKiernan, B. and Powers, B. (2008) Nasopharyngeal turbinates in brachycephalic dogs and cats. *Journal of American Animal Hospital Association* 44, 243-249.

Glass, E.; Kapatkin, A.; Vite, C. and Steinberg, S. (2000) A modified bilateral transfrontal sinus approach to the canine frontal lobe and olfactory bulb: surgical technique and five cases. *Journal of American Animal Hospital Association* 36, 43-50.

González-Soriano, J.; Contreras-Rodríguez, J.; Marín García, P.; Martínez-Sainz, P. and Rodríguez-Veiga, E. (2001) Age-related changes in the ventricular system of the dog brain. *Annals of Anatomy - Anatomischer Anzeiger* 183, 283-291.

Gottfried, J. and Zald, D. (2005) On the scent of human olfactory orbitofrontal cortex: meta-analysis and comparison to non-human primates. *Brain Research Reviews* 50, 287-304.

Gyldensted, C. and Kosteljanetz, M. (1976) Measurements of the normal ventricular system with computer tomography of the brain. A preliminary

study on 44 adults. *Neuroradiology* 10, 205-213.

Handelman, C. and Osborne, G. (1976) Growth of the nasopharynx and adenoid development from one to eighteen years. *Angle Orthodontist* 46, 243-259.

Hardy, W.; Brodey, R. and Riser, W. (1967) Osteosarcoma of the canine skull. *Veterinary Radiology* 8, 5-16.

Hasegawa, D.; Yayoshi, N.; Fujita, Y.; Fujita, M. and Orima, H. (2005) Measurement of interthalamic adhesion thickness as a criteria for brain atrophy in dogs with and without cognitive dysfunction (dementia). *Veterinary Radiology & Ultrasound* 46, 452-457.

Harvey, CE. (1989) Inherited and congenital airway conditions. *Small Animal Practice* 30, 184-187.

Hayes, K. and Schiefer, B. (1969) Primary tumors in the CNS of carnivores. *Pathologia Veterinaria Online* 6, 94-116.

Hedlund, CS. and Taboada, J. (2002) *Clinical atlas of ear, nose and throat diseases in small animals: The case-based approach*, Hannover: Schlütersche.

Hellwig, D.; Grotenhuis, J.; Tirakotai, W.; Riegel, T.; Schulte, D.; Bauer, B. and Bertalanffy, H. (2005) Endoscopic third ventriculostomy for obstructive hydrocephalus. *Neurosurgical Review* 28, 1-34.

Hendricks, J. (1992) Brachycephalic airway syndrome. *Veterinary Clinics of North America-Small Animal Practice* 22, 1145-1153.

Hinds, J. and McNelly, N. (1977) Aging of the rat olfactory bulb: growth and atrophy of constituent layers and changes in size and number of mitral cells. *Journal of Comparative Neurology* 171, 345-367.

Holland, GN.; Moore, WS. and Hawkes, RC. (1980) Nuclear magnetic-resonance tomography of the brain. *Journal of Computer Assisted Tomography* 4, 1-3.

Holmberg, H. and Linder-Aronson, S. (1979) Cephalometric radiographs as means of evaluating the capacity of the nasal and nasopharyngeal airway. *American Journal of Orthodontics* 76, 479-490.

Horodyska, M. and Kreiner, J. (1962) The brain ventricles in the dog. *Acta Biologiae Experimentalis* 22, 243-250.

Hudson, J.; Cartee, R.; Simpson, S. and Buxton, D. (1989) Ultrasonographic anatomy of the canine brain. *Veterinary Radiology* 30, 13-21.

Hudson, J.; Simpson, S.; Cox, N. and Buxton, D. (1991) Ultrasonographic examination of the normal canine neonatal brain. *Veterinary Radiology* 32, 50-59.

Isono, S.; Remmers, J.; Tanaka, A.; Sho, Y.; Sato, J. and Nishino, T. (1997) Anatomy of pharynx in patients with obstructive sleep apnea and in normal subjects. *Journal of Applied Physiology* 82, 1319-1326.

Johnson, C. (1986) Disorders of pregnancy. *Veterinary Clinics of North America-Small-Animal Practice* 16, 477-482.

Kaufman, HH.; Cohen, G.; Glass, TF.; Huchton, JD.; Pruessner, JL.; Ostrow, PT.; Andia-Waltenbaugh, A. and Dujovny, M. (1981) CT atlas of the dog brain. *Journal of Computer Assisted Tomography* 5, 529-537.

Kealy, J. and McAllister, H. (2005) The skull and vertebral column. In: *Diagnostic radiology and ultrasonography of the dog and cat,* 4th edn. pp. 387-476. St. Louis: Elsevier Saunders.

Kennel Club (1998) *Illustrated breed standards: the official guide to registered breeds,* London: Ebury.

Khoo, A.; Marchevsky, A.; Barrs, V. and Beatty, J. (2007) Choanal atresia in a himalayan cat-first reported case and successful treatment. *Journal of Feline Medicine & Surgery* 9, 346-349.

Kii, S.; Uzuka, Y.; Taura, Y.; Nakaichi, M.; Takeuchi, A.; Inokuma, H. and Onishi, T. (1997) Magnetic resonance imaging of the lateral ventricles in beagle-type dogs. *Veterinary Radiology & Ultrasound* 38, 430-433.

Kii, S.; Uzuka, Y.; Taura, Y.; Nakaichi, M.; Inokuma, H. and Onishi, T. (1998) Developmental change of lateral ventricular volume and ratio in beagle-type dgos up to 7 months of age. *Veterinary Radiology & Ultrasound* 39, 185-189.

Kim, J.; Jeon, H.; Woo, E. and Park, H. (2009) Dilation of the olfactory bulb cavity concurrent with hydrocephalus in four small breed dogs. *Journal of Veterinary Science* 10, 173-175.

König, H.; Koenig, H.; Liebich, H-G. and Bragulla, H. (2010) *Veterinary anatomy of domestic mammals: Textbook and colour atlas*, 4th edn. Stuttgart: Schattauer.

Kraft, SL.; Gavin, PR.; Wendling, LR. and Reddy, VK. (1989) Canine brain anatomy on magnetic resonance images. *Veterinary Radiology* 30, 147-158.

Langley, J. (1883) The structure of the dog's brain. *Journal of Physiology* 4, 248-326.

Last, R. and Tompsett, D. (1953) Casts of the cerebral ventricles. *British Journal of Surgery* 40, 525-543.

Laurikainen, E.; Erkinjuntti, M.; Alihanka, J.; Rikalainen, H. and Suonpää, J. (1987) Radiological parameters of the bony nasopharynx and the adenotonsillar size compared with sleep apnea episodes in children. *International Journal of Pediatric Otorhinolaryngology* 12, 303-310.

Lavin, L. (2003) *Radiography in veterinary technology* , 3rd edn. Philadelphia: WS Saunders.

Lee, D.; Cho, H. and Cho, Y. (2007) Typical carcinoid tumor of the nasal cavity. *Auris Nasus Larynx* 34, 537-539.

Leigh, E.; Mackillop, E.; Robertson, I. and Hudson, L. (2008) Clinical anatomy of the canine brain using magnetic resonance imaging. *Veterinary Radiology & Ultrasound* 49, 113-121.

Levinger, I. and Edery, H. (1968) Casts of the cat cerebro-ventricular system. *Brain Research* 11, 294-304.

Lieberman, D. (1998) Sphenoid shortening and the evolution of modern human cranial shape. *Nature* 393, 158-162.

Lu, D.; Lamb, C.; Pfeiffer, D. and Targett, M. (2003) Neurological signs and results of magnetic resonance imaging in 40 Cavalier King Charles

Spaniels with Chiari type 1-like malformations. *Veterinary Record* 153, 260-263.

Lyras, G. (2009) The evolution of the brain in canidae (mammalia: carnivora). *Scripta Geologica* 139, 1-39.

Martin-Garcia, P.; González-Soriano, J.; Corral-Gros, C. and Rodríguez-Veiga, E. (1995) Spinal cord central canal of the GSD: Morphological, histological, and ultrastructural considerations. *Journal of Morphology* 224, 205-212.

Maw, A.; Smith, I. and Lance, G. (1991) Lateral cephalometric analysis of children with otitis media with effusion: A comparison with age and sex matched controls. *Journal of Laryngology & Otology* 105, 71-77.

McLone, D. (2004) The anatomy of the ventricular system. *Neurosurgy Clinics of North America* 15, 33-38.

Milhorat, T.; Clark, R. and Hammock, M. (1970) Experimental hydrocephalus. *Journal of Neurosurgery* 32, 390-399.

Miller, M. and Christensen, G. (1964) *Anatomy of the dog*, 1st edn. London: WB Saunders.

Mirich, J.; Williams, N.; Berlau, D. and Brunjes, P. (2002) Comparative study of aging in the mouse olfactory bulb. *Journal of Comparative Neurology* 454, 361-372.

Mitten, R. (1988) Nasopharyngeal stenosis in four cats. *Journal of Small Animal Practice* 29, 341-345.

Mooney, M. and Siegel, M. (2002) *Understanding craniofacial anomalies: The etiopathogenesis of craniosynostoses and facial clefting*, New York: Wiley-Liss.

Moore, M.; Gavin, P.; Kraft, S.; DeHaan, C.; Leathers, C. and Dorn, R. (1991) MR, CT and clinical features from four dogs with nasal tumors involving the rostral cerebrum. *Veterinary Radiology* 32, 19-25.

Morgan, J.; Suter, P.; O'Brien, T. and Park, R. (1972) Tumors in the nasal cavity of the dog: A radiographic study. *Veterinary Radiology* 13, 18-26.

Negus, V. (1958) *The comparative anatomy and physiology of the nose and*

paranasal sinuses, Edinburgh: Livingstone.

Niebauer, G. and Evans, S. (1988) Transsphenoidal hypophysectomy in the dog. A new technique. *Veterinary Surgery* 17, 296-303.

Onar, V. (1999) A morphometric study on the skull of the GSD (Alsatian). *Anatomia, Histologia, Embryologia* 28, 253-256.

Ono, T.; Lowe, A.; Ferguson, K. and Fleetham, J. (1996) Associations among upper airway structure, body position, and obesity in skeletal Class I male patients with obstructive sleep apnea. *American Journal of Orthodontics and Dentofacial Orthopedics* 109, 625-634.

Pugliese, M.; Carrasco, J.; Gomez-Anson, B.; Andrade, C.; Zamora, A.; Rodriguez, M.; Mascort, J. and Mahy, N. (2010) Magnetic resonance imaging of cerebral involutional changes in dogs as markers of aging: An innovative tool adapted from a human visual rating scale. *Veterinary Journal* 186, 166-171.

Quignon, P.; Kirkness, E.; Cadieu, E.; Touleimat, N.; Guyon, R.; Renier, C.; Hitte, C.; André, C.; Fraser, C. and Galibert, F. (2003) Comparison of the canine and human olfactory receptor gene repertoires. *Genome Biology* 4, 1-9.

Rajtová, V. (2001) The adhesion and fusion of the ependyma and plexus chorioideus in the cerebral ventricles in sheep and goat. *Folia Veterinaria* 45, 72-75.

Reiter, R. (1981) The mammalian pineal gland: structure and function. *America Journal of Anatomy* 162, 287-313.

Renko, M.; Kristo, A.; Tapiainen, T.; Koivunen, P.; Ilkko, E.; Alho, O. and Uhari, M. (2007) Nasopharyngeal dimensions in magnetic resonance imaging and the risk of acute otitis media. *Journal of Laryngology & Otology* 121, 853-856.

Ricketts, R. (1960) A foundation for cephalometric communication. *American Journal of Orthodontics* 46, 330-357.

Roberts, T.; McGreevy, P. and Valenzuela, M. (2010) Human induced rotation and reorganization of the brain of domestic oogs. *PLoS ONE* 5, e11946.

Rusbridge, C. (2005) Neurological diseases of the Cavalier King Charles Spaniel. *Journal of Small Animal Practice* 46, 265-272.

Rycke, L.; Saunders, J.; Gielen, I.; Bree, H. and Simoens, P. (2003) Magnetic resonance imaging, computed tomography, and cross-sectional views of the anatomy of normal nasal cavities and paranasal sinuses in mesaticephalic dogs. *American Journal of Veterinary Research* 64, 1093-1098.

Saito, M.; Olby, N. and Spaulding, K. (2001) Identification of arachnoid cysts in the quadrigeminal cistern using ultrasonographay. *Veterinary Radiology & Ultrasound* 42, 435-439.

Satoh, K.; Wada, T.; Tachimura, T.; Sakoda, S. and Shiba, R. (1998) A cephalometric study by multivariate analysis of growth of the bony nasopharynx in patients with clefts and non-cleft controls. *Journal of Cranio-Maxillofacial Surgery* 26, 394-399.

Scarff, J. (1966) Third ventriculostomy by puncture of the *lamina terminalis* and the floor of third ventricle. *Journal of Neurosurgery* 24, 935-943.

Schaller, O. (1992) *Illustrated veterinary anatomical nomenclature*, Stuttgart: Verlag.

Schmidt, M.; Neumann, K.; Amort, K.; Failing, K. and Kramer, M. (2011) Cephalometric measurements and determination of general skull type of Cavalier King Charles Spaniels. *Veterinary Radiology & Ultrasound* 52, 436-440.

Schreider, J. and Raabe, O. (1981) Anatomy of the nasal-pharyngeal airway of experimental animals. *Anatomical Record* 200, 195-205.

Schwarz, T.; Sullivan, M. and Hartung, K. (2000) Radiographic anatomy of the cribriform plate (lamina cribrosa). *Veterinary Radiology & Ultrasound* 41, 220-225.

Selby, L.; Hayes, H. and Becker, S. (1979) Epizootiologic features of canine hydrocephalus. *American Journal of Veterinary Research* 40, 411-413.

Sisson, S. (1975) Carnivore osteology. In: Sisson, S. and Grossman, J., (Eds.) *The anatomy of domestic animals*, 5th edn. Philadelphia: WB Saunders.

Smith, B. (1999) *The brain and associated structures*, Nieginski, USA: Nieginski.

Smith, T. and Rossie, J. (2008) Nasal fossa of mouse and dwarf lemurs (primates, cheirogaleidae). *Anatomical Record* 291, 895-915.

Solow, B.; Siersbæk-Nielsen, S. and Greve, E. (1984) Airway adequacy, head posture, and craniofacial morphology. *American Journal of Orthodontics* 86, 214-223.

Sorensen, H.; Solow, B. and Greve, E. (1980) Assessment of the nasopharyngeal airway: a rhinomanometric and radiographic study in children with adenoids. *Acta Otolaryngol* 89, 227-232.

Stevenson, K. (2004) Chiari type II malformation: past, present, and future. *Neurosurgical Focus* 16, 1-7.

Stockard, G. (1941) *The genetic and endocrinic basis for differences in form and behavior*, Philadelphia: Wistar Institute.

Tacher, S.; Quignon, P.; Rimbault, M.; Dreano, S.; Andre, C. and Galibert, F. (2005) Olfactory receptor sequence polymorphism within and between breeds of dogs. *Journal of Heredity* 96, 812-816.

Tapp, P.; Siwak, C.; Gao, F.; Chiou, J.; Black, S.; Head, E.; Muggenburg, B.; Cotman, C.; Milgram, N. and Su, M. (2004) Frontal lobe volume, function, and ß-amyloid pathology in a canine model of aging. *Journal of Neuroscience* 24, 8205-8213.

Thames, RA.; Robtson, ID; Flegel, T.; Henke, D.; O'Brien, DP.; Coates, JR. and Olby, NJ. (2010) Development of a morphometric magnetic resonance image parameter suitable for distinguishing between normal dogs and dogs with cerebellar atrophy. *Veterinary Radiology & Ultrasound* 51, 246-253.

Trouth, C.; Winter, S.; Gupta, K.; Millis, R. and Holloway, J. (1977) Analysis of the sexual dimorphism in the basiocciptal portion of the dog-skull. *Cells Tissues Organs* 98, 469-473.

Venker-van-Haagen, A. (2005) *Ear, nose, throat, and tracheobronchial diseases in dogs and cats*, Hannover: Schlutersche Verlag.

Vullo, T.; Korenman, E.; Manzo, R.; Gomez, D.; Deck, M. and Cahill, P. (1997) Diagnosis of cerebral ventriculomegaly in normal adult beagles using quantitiative MRI. *Veterinary Radiology & Ultrasound* 38, 277-281.

Vullo, T.; Manzo, R.; Gomez, D.; Deck, M. and Cahill, P. (1998) A canine model of acute hydrocephalus with MR correlation. *American Journal of Neuroradiology* 19, 1123-1125.

Warwick, R. and Williams, P. (1973) *Gray's anatomy of the human body,* 29th edn. Philadelphia: Lea and Febiger.

Watson, A.; De Lahunta, A. and Evans, H. (1989) Dorsal notch of foramen magnum due to incomplete ossification of supraoccipital bone in dogs. *Journal of Small Animal Practice* 30, 666-673.

Weber, Z.; Preston, C. and Wright, P. (1981) Resistance to nasal airflow related to changes in head posture. *American Journal of Orthodontics* 80, 536-545.

Weidenreich, F. (1941) *The brain and its role in the phylogenetic transformation of the human skull,* Philadelphia: American Philosophical Society.

Wible, J. (2008) On the cranial osteology of the hispaniolan solenodon, solenodon paradoxus brandt, 1833 (mammalia, lipotyphla, solenodontidae). *Annals of Carnegie Museum* 77, 321-402.

Wilder, B. (1880) The cerebral fissures of the domestic cat. Felis domestica. *Science* 1, 49-51.

Wisniewski, H.; Weller, R. and Terry, R. (1969) Experimental hydrocephalus produced by the subarachnoid infusion of silicone oil. *Journal of Neurosurgery* 31, 10-14.

Wong, ML.; Sandham, A.; Ang, PK.; Wong, DC.; Tan, WC. and Huggare, J. (2005) Craniofacial morphology, head posture, and nasal respiratory resistance in obstructive sleep apnoea: an inter-ethnic comparison. *European Journal of Orthodontics* 27, 91-97.

Woodside, D. and Linder-Aronson, S. (1979) The channelization of upper and lower anterior face heights compared to population standard in males

between ages 6 to 20 years. *European Journal of Orthodontics* 1, 25-40.

Yu, X.; Fujimoto, K.; Urushibata, K.; Matsuzawa, Y. and Kubo, K. (2003) Cephalometric analysis in obese and nonobese patients with obstructive sleep apnea syndrome. *Chest* 124, 212-218.